Experimental and Theoretical Study of Biomass Pyrolysis and Product Characterization

THESIS

Submitted in partial fulfillment

of the requirements for the degree of

DOCTOR OF PHILOSOPHY

By

RAJEEV SHARMA

Under the supervision of

Prof. Pratik N Sheth

BITS Pilani

Pilani | Dubai | Goa | Hyderabad

BIRLA INSTITUTE OF TECHNOLOGY AND SCIENCE

PILANI (RAJASTHAN) INDIA

2018

ॐ सर्वे भवन्तु सुखिनः ।
सर्वे सन्तु निरामयाः ।।
सर्वे भद्राणी पश्यन्तु ।
मा कश्चित् दुःख भाग्भवेत् ।।
ॐ शान्तिः शान्तिः शान्तिः ।।

May all be prosperous and happy.
May all be free from illness.
May all see what is spiritually uplifting.
May no one suffer.
Om peace, peace, peace !

Dedicated to

My Grandparents
Parents
Wife
&
My Loving Daughters

ACKNOWLEDGEMENTS

This thesis is the culmination of five years of intensive work. It embodies the work carried out during this period as a PhD scholar. This thesis would not see the light of the day without the help that was available to me from various quarters. At the very outset I am pleased to express my deep sense of gratitude for my guide **Prof. Pratik N Sheth**, Associate Professor (Chemical Engineering Department) for his constant encouragement and valuable suggestions. He has been an immense moral support throughout the period of this research work. I have been truly privileged to have the opportunity to work under his valuable guidance.

I express my sincere thanks to the members of Doctoral Advisory Committee Prof. Suresh Gupta, Associate Professor and Prof. Smita Raghuvanshi, Associate Professor (Chemical Engineering Department) for their support and suggestions received by me during this period. I have been greatly benefited by their advice. Their experience only enriched my work and paved the way to carry the work ahead.

My sincere thanks go to Prof. Souvik Bhattacharyya, Vice-Chancellor, BITS Pilani for giving me the opportunity to carry out the PhD. work in BITS. I am thankful to Prof. Ashoke Kumar Sarkar, Director (Pilani Campus), Prof G Raghurama, Director (Goa Campus), Prof. G Sundar, Director (Hyderabad Campus), Prof.R.N.Saha, Director (Dubai Campus), Prof. Sanjay Kumar Verma, Dean (Administration), Prof. Srinivas Krishnaswamy, Dean, Academic – Graduate Studies & Research and Prof. Jitendra Panwar, Associate Dean, Academic – Graduate Studies & Research for providing the necessary facility and infrastructure to carry out this work.

I extend my special thanks to Prof. Harekrishna Mohanta, Head Chemical Engineering Department, Prof. Arvind Kumar Sharma, Dr Amit Jain, Dr Srinivas Appari, Dr Pradipta Chattopadhyay, Prof Banasri Roy, Dr Ajaya Kumar Pani and other members of Chemical Engineering Group for their valuable advice and moral support throughout the work.. I also like to thank Prof. B. V. Babu, Prof. B. Natarajan, Prof. Sushil Kumar, Dr. Nikhil Prakash, Dr. Ashish M Gujrathi, Dr Dipaloy Dutta for their continued support. My

special thanks and appreciation are due to Dr R. Roy for his help, suggestions, and encouragement throughout the work. My sincere thanks to Prof Arun Patil and Prof S. L. Kothari for their sincere concerns on the status of my PhD work. I would especially like to thank Prof Upendra Mishra, Dr Bornali Purkayastha, Dr Umesh Diwedi, Mr. Pankaj Sharma and Dr Sanyog Rawat for their help in getting scientific literature and constant support throughout the work. For paucity of space I am unable to name all my colleagues but the help rendered by them is sincerely acknowledged.

Besides all the faculty members and other friends, I would also take this opportunity to thank Mr. Ashok Saini and Mr. Jeevan Verma for the help extended by them for carrying out the experimental work. Thanks are also due to Mr. Babu Lal Saini and Shri Jangvir ji for the kind cooperation extended by them during my PhD work. I also wish to thank Mr. Vikas Sharma and Mr. Kamlesh Pipalwa for their help and cooperation. My thanks are also due to Prof K. S. Sangwan and his office personnel for their help in the fabrication of biomass pyrolyzer and getting the biomass sample holders of appropriate sizes ready.

I find myself short of words to express my gratitude for my parents, Shri Harish Chandra Sharma and Smt. Sharda Sharma for having stood by me through the thick and thin of every aspect of my life, this thesis being no exception. This body of work would not have seen the light of the day without their constant help and cooperation. My accomplishment would have been challenging without the encouragement of my in-laws Shri Rajkumar Sharma and Smt. Shashi Sharma.

Behind every successful man there is a woman and I do agree. My journey too would have been incomplete without my wife Yamini who has been my source of inspiration and motivation.

Last but not the least, I pray and thank to ALMIGHTY GOD for showering HIS blessings and giving me an inner strength and patience.

RAJEEV SHARMA

ABSTRACT

Biomass is considered as an important energy resource all over the world and is converted into useful forms of energy, including generating electricity, fuelling vehicles, and providing process heat for industrial facilities. It is the only renewable source of carbon that can be converted into convenient solid, liquid, and gaseous fuels. The choice of conversion process depends on the type and quantity of the biomass feedstock, the desired form of the energy, end user requirements, environmental standards, economic conditions etc. The conversion of biomass to energy is performed using two main process technologies: thermo-chemical and biochemical/biological. Pyrolysis is one of the primary thermo-chemical treatment methods to convert biomass into solid (char), liquid (bio-oil) and permanent gases.

In the present work, a multi reaction kinetic model is proposed for the decomposition of individual biomass constituents (*i.e.* cellulose, hemicellulose and lignin) with incorporation of moisture release phenomena. The model takes into account, the independent parallel reactions of n^{th} order for the production of volatiles and char from each of the biomass constituents. The model is simulated using finite difference method to predict the pyrolysis rate. The corresponding kinetic parameters of the developed model are estimated by minimizing the sum of the square of the error between the model predicted values of residual weight fraction and the experimental data of thermo-gravimetry using non-traditional optimization technique i.e. logarithmic differential evolution (LDE). The experimental results of thermo-gravimetric analysis (TGA) of *Jatropha curcas* de-oiled cakes are used. A researcher has reported the kinetic parameters for kinetic model based on the individual biomass constituent decomposition. Moreover, their model predicts incorrect order of biomass constituent degradation. However, in the present study, because of logarithmic DE algorithm, the range of kinetic parameters are chosen in such a way that the order in which biomass constituents degradation with time follow exactly reported sequence of biomass constituent degradation i.e. hemicellulose (150 ˚C to 350 ˚C), cellulose (300 ˚C to 450 ˚C), lignin (450 ˚C to 775 ˚C).

The applicability of the proposed kinetic model and those reported in litterature is limited and can be used only for small size (less than 1 mm) particles, which are undergoing kinetically controlled devolatilization. However the pyrolysis of large size particles is controlled by heat and mass transport within the particle. To predict the rate of devolatilization and yield of products for the pyrolysis of large size particles, there is a need to develop the particle model and incorporate it into the reactor model. The alternative to this approach is the development of apparent kinetic model for the pyrolysis process and use it without particle model development. In order to develop the apparent kinetic model, conventional thermo-gravimetric analysis (TGA) results of biomass pyrolysis cannot be used.

The pyrolysis of large size particle has to be carried out in a fixed bed reactor having the facility to monitor the weight reduction with respect to time. It is the same as TGA but at a macro level. Hence, the term “macro-TGA” is used for this kind of pyrolysis reactor. In the present study, macro thermogravimetric analysis (TGA) of *Jatropha curcas* de-oiled cake is performed using a laboratory scale macro TGA. The weight loss of the biomass, product yields and composition of non-condensable gases are measured. These experimental results are used to develop the apparent kinetic model. The apparent kinetic model is developed considering one step multi reaction apparent kinetic scheme to represent the thermal degradation of biomass. The degradation of biomass is expressed as parallel production of volatiles, gases and char by n^{th} order reaction. The model is simulated using finite difference method to predict the pyrolysis rate. The corresponding global kinetic parameters activation energy and frequency factor are estimated by minimizing the sum of the square of the error between the models predicted values of residual weight fraction and the corresponding experimental data of macro TGA.

The present work also presents a 2D (*r, z*) dynamic combined transport and kinetic model for the cylindrical fixed bed pyrolyzer. It is developed to understand the dynamic temperature variation and porosity variation in the fixed bed. The model consists of partial differential equations of heat and volatile transport and ordinary differential equations of biomass decomposition and char generation. The model takes into account the heat transfer from the reactor wall to biomass bed both by radiation as well as by convection mode. Due to incorporation of radiation boundary conditions, model equations become nonlinear; hence Jacobian iterative method is used to solve the set of nonlinear algebraic equations developed by applying the implicit finite difference method.

The pyrolysis experiments are carried out using *Jatropha curcas* de-oiled cake at different reactor temperatures and varying particle sizes of biomass. The bio-oil produced from pyrolysis process is characterized using FTIR, TGA and GC-MS. The result obtained from GC-MS confirms the presence of acids, alkanes, aromatics, aldehydes and ketones. The reactor temperature is varied from 350 ˚C to 750 ˚C. The variation of product yield with temperature is estimated and the maximum yield of bio-oil is found to be 31.1 wt % at 550 ˚C. Thermo-gravimetric analysis of biomass and bio-oil are performed and from the results it is found that the most of the compound volatilized in the range of 100 ˚C to 300 ˚C.

Keywords: *Bioenergy; Biomass; Jatropha curcas de-oiled cake; Pyrolysis; Fixed bed pyrolyzer; Macro TGA; Bio-oil: Reaction kinetics; Mathematical model; Apparent kinetic model; Kinetic parameter estimation; Simulation; Logarithmic differential evolution.*

TABLE OF CONTENTS

Acknowledgements		i
Abstract		iii
Table of Contents		v
List of Tables		viii
List of Figures		ix
Nomenclature		xii
1	**Introduction**	**1**
	1.1 Biomass energy	2
	1.1.1 Biomass	2
	1.1.1.1 Cellulose	4
	1.1.1.2 Hemicellulose	5
	1.1.1.3 Lignin	6
	1.1.1.4 *Jatropha curcas* as biomass	7
	1.1.2 Thermochemical conversion of biomass	9
	1.1.2.1 Gasification	9
	1.1.2.2 Pyrolysis	10
	1.1.2.3 Liquefaction	10
	1.2 Biomass pyrolysis	11
	1.2.1 Types of pyrolysis	12
	1.2.1.1 Slow pyrolysis	12
	1.2.1.2 Fast pyrolysis	12
	1.2.1.3 Flash pyrolysis	12
	1.2.2 Pyrolysis products	13
	1.2.2.1 Bio-oil	13
	1.2.2.2 Char	14
	1.3 Modeling of biomass pyrolysis	14
	1.3.1 Kinetic model development	15
	1.3.1.1 One step global models	15
	1.3.1.2 One step multi reaction models	16
	1.3.1.3 Two step semi-global models	16
	1.3.2 Apparent kinetic model development	18
	1.3.3 Fixed bed model development	19
	1.4 Objectives of proposed research	20
2	**Literature Review**	**23**
	2.1 Theoretical studies on biomass pyrolysis	23
	2.2 Experimental studies on biomass pyrolysis	32
	2.3 Existing gaps of research	45
	2.4 Scope of work	48
3	**Mathematical Model Development and Simulation**	**50**
	3.1 Model development for biomass pyrolysis	50

3.1.1 Kinetic model development 50
3.1.2 Apparent kinetic model development 54
3.1.3 Fixed bed model development 56
3.2 Simulation of biomass pyrolysis models 59
3.2.1 Numerical methods and optimization technique 59
3.2.1.1 Optimization technique 60
3.2.1.1.1 Logarithmic DE (LDE) 61
3.2.2 Simulation of kinetic model 62
3.2.2.1 Kinetic parameter estimation 62
3.2.2.2 Apparent kinetic parameter estimation 64
3.2.2.3 Simulation of fixed bed model 66

4 Experimental Studies 70
4.1 Experimental setup and analytical equipments 71
4.1.1 Pyrolysis experimental set up 71
4.1.2 Analytical instruments 74
4.1.2.1 Thermo-gravimetric analyzer (TGA) 74
4.1.2.2 Liquid column chromatography 74
4.1.2.3 Rotary evaporator 75
4.1.2.4 Fourier transform infra-red spectroscopy (FTIR) 75
4.1.2.5 Gas chromatography (GC) 75
4.1.2.6 Gas chromatography mass spectrometry (GC-MS) 77
4.2 Materials 77
4.3 Experimental procedure 78
4.3.1 Pyrolysis of biomass 79
4.3.1.1 Pyrolysis of biomass in TGA 79
4.3.1.2 Pyrolysis of biomass in macro TGA 80
4.3.2 Product analysis 82
4.3.2.1 Liquid product (bio-oil) analysis 82
4.3.2.1.1 Liquid column chromatography analysis 82
4.3.2.1.2 Fourier transform infra-red spectroscopy (FTIR) analysis 82
4.3.2.1.3 Gas chromatography mass spectrometry (GC-MS) analysis 83
4.3.2.1.4 Thermo-gravimetric analyzer (TGA) 83
4.3.2.2 Gas product analysis using gas chromatography 84

5 Results and Discussion 86
5.1 Experimental studies 86
5.1.1 Thermo-gravimetric analyzer experimental studies 86
5.1.2 Macro Thermo-gravimetric analyzer experimental studies 94
5.1.2.1 Effect of reactor temperature 94
5.1.2.2 Effect of particle size 95
5.1.2.3 Gas composition 101
5.1.2.4 Bio-oil analysis 102
5.1.2.4.1 FTIR analysis 102
5.1.2.4.2 TGA analysis 105
5.1.2.4.3 GC-MS analysis 106

5.1.2.4.3.1 GC-MS analysis of aliphatic fraction of bio-oil 109
5.1.2.4.3.2 GC-MS analysis of aromatic fraction of bio-oil 111
5.1.2.4.3.3 GC-MS analysis of polar fraction of bio-oil 113
5.2 Mathematical Modeling and Simulation 115
5.2.1 Kinetic parameter estimation 115
5.2.1.1 Kinetic parameters estimation for kinetic model 115
5.2.1.2 Global kinetic parameters estimation for apparent kinetic mode 124
5.2.2 Modeling and simulation of fixed bed model 132
5.2.2.1 Temperature profiles in the bed at different time intervals 132
5.2.2.2 Biomass decomposition profiles in the bed at different time intervals 141
5.2.2.3 Porosity profiles in the bed at different time intervals 142
5.2.2.4 Char profiles in the bed at different time intervals 143

6 Concluding Remarks 146
6.1 Summary 147
6.1.1 Introduction 147
6.1.2 Gaps in literature 148
6.1.3 Scope of work 150
6.1.4 Mathematical modeling and simulation 151
6.1.4.1 Component based decomposition kinetic model development 151
6.1.4.2 Apparent kinetic model development 152
6.1.4.3 Fixed bed model development 153
6.1.5 Experimental studies 153
6.1.6 Results and discussion 154
6.1.6.1 Mathematical modeling and simulation 154
6.1.6.2 Experimental studies 155
6.2 Conclusions 157
6.3 Future Scope of Research 159

References 156
List of Publications 172
Biography 174
Appendix I 176
Appendix II 181
Appendix III 188
Appendix IV 191
Appendix V 198
Appendix VI 199

LIST OF TABLES

Table No	Title	Page No
1.1	Process conditions for pyrolysis	13
2.1	Kinetic parameters of various types of kinetic schemes	33
3.1	Properties of correlation	68
3.2	Constants used in the simulation	69
4.1	Chemical composition of Jatropha curcas de-oiled cake	78
4.2	Ultimate analysis of Jatropha curcas de-oiled cake	78
4.3	Details of the biomass pyrolysis experiments using TGA	79
4.4	Details of the biomass pyrolysis experiments using macro TGA	81
4.5	Details of the gaseous product analysis of *Jatropha curcas* de-oiled cake	84
5.1	FTIR analysis of *Jatropha curcas* de-oiled cake pyrolysis oil	105
5.2	Chemical compounds in bio-oil (GC-MS Analysis)	107
5.3	Chemical compounds in aliphatic fraction of bio-oil	109
5.4	Chemical compounds in aromatic fraction of bio-oil	111
5.5	Chemical compounds in polar fraction of bio-oil	113
5.6	Kinetic parameters of reaction 1 for Heating rate of 10 ˚C /min to 60 ˚C /min	116
5.7	Kinetic parameters of reaction 2 & 3 for Heating rate of 10 ˚C /min to 60 ˚C /min	117
5.8	Kinetic parameters reported by Sricharoenchaikul and Atong	120
5.9	Estimated kinetic parameters for small size biomass pyrolysis	124
5.10	Estimated kinetic parameters for large size biomass pyrolysis	126
5.11	Nominal values of parameters	133

LIST OF FIGURES

Figure No	Title	Page No
1.1	Sources of biomass	4
1.2	Molecular structure of cellulose	5
1.3	Molecular structure of softwood hemicellulose	6
1.4	Molecular structure of the three main components of lignin	7
1.5	*Jatropha curcas:* (a) plant (b) fruit (c) seeds	8
1.6	De-oiled *Jatropha curcas* cake	9
1.7	Process steps for biomass pyrolysis	11
1.8	Single step multi-reactions model	16
1.9	Two-step semi-global models	17
3.1	(a) Schematic of biomass bed (b) Computational domain	57
3.2	Algorithm for kinetic parameter estimation for kinetic model	64
3.3	Algorithm for kinetic parameter estimation for apparent kinetic mode	65
3.4	Computational domain showing different algebraic equations	67
4.1	Schematic of the pyrolysis experimental setup	73
5.1	Thermo-gravimetric analysis of *Jatropha curcas* de-oiled cake at various heating rates with temperature	88
5.2	Thermo-gravimetric analysis of *Jatropha curcas* de-oiled cake at various heating rates time	88
5.3	DTG plot of *Jatropha curcas* de-oiled cake at heating rate 10 ˚C/min	90
5.4	DTG plot of *Jatropha curcas* de-oiled cake at heating rate 20 ˚C/min	90
5.5	DTG plot of *Jatropha curcas* de-oiled cake at heating rate 30 ˚C/min	91
5.6	DTG plot of *Jatropha curcas* de-oiled cake at heating rate 40 ˚C/min	91
5.7	DTG plot of *Jatropha curcas* de-oiled cake at heating rate 50 ˚C/min	92
5.8	DTG plot of *Jatropha curcas* de-oiled cake at heating rate 60 ˚C/min	92
5.9	DTG plot of *Jatropha curcas* de-oiled cake at various heating rate with time.	93
5.10	DTG plot of *Jatropha curcas* de-oiled cake at various heating rate with temperature.	93
5.11	Product yield distribution of pyrolysis of *Jatropha* curcas de-oiled cake	95
5.12	Bio-oil yield distribution of pyrolysis of *Jatropha curcas* de-oiled cake	96
5.13	Charcoal yield distribution of pyrolysis of *Jatropha curcas* de-oiled	97

	cake	
5.14	Gas yield distribution of pyrolysis of *Jatropha curcas* de-oiled cake	97
5.15	Macro thermogravimetric analysis of *Jatropha curcas* de-oiled cake at 400 ˚C for different particle size	99
5.16	Macro thermogravimetric analysis of *Jatropha curcas* de-oiled cake at 550 ˚C for different particle size	100
5.17	Macro thermogravimetric analysis of *Jatropha curcas* de-oiled cake at 700 ˚C for different particle size	100
5.18	Gas chromatographic analysis of nitrogen free non-condensable gas	101
5.19	FTIR analysis of bio-oil sample at 700 ˚C temperature	103
5.20	FTIR analysis of char sample at 700 ˚C temperature	103
5.21	FTIR spectra of bio-oil for 350 ˚C, 400 ˚C, 450 ˚C, 500 ˚C, 550 ˚C, 600 ˚C, 650 ˚C and 700 ˚C	104
5.22	Thermo-gravimetric analysis of bio-oil at heating rate 60 ˚C/min	106
5.23	Comparison of experimental and simulated residual weight fraction for heating rate (a)10 ˚C/min (b) 20 ˚C/min (c) 30 ˚C/min (d) 40 ˚C/min (e) 50 ˚C/min (f) 60 ˚C/min	119
5.24	Predicted thermal degradation order of Sricharoenchaikul and Atong for biomass constituents for heating rate (a) 5 ˚C/min (b) 15 ˚C/min (c) 30 ˚C/min (d) 90 ˚C/min	121
5.25	Predicted thermal degradation order of biomass constituents for heating rate (a)10 ˚C /min (b) 20 ˚C/min (c) 30 ˚C/min (d) 40 ˚C/min (e) 50 ˚C/min (f) 60 ˚C/min	123
5.26	Comparison of experimental and simulated residual weight fraction at 400 ˚C temperature for particle size (a)1 inch (b) 0.5 inch (c) 10-14 mesh (1.4 to 2.0 mm) (d) 52-60 mesh (0.25 to 0.3 mm)	127
5.27	Comparison of experimental and simulated residual weight fraction at 550 ˚C temperature for particle size (a)1 inch (b) 0.5 inch (c) 10-14 mesh (1.4 to 2.0 mm) (d) 52-60 mesh (0.25 to 0.3 mm)	128
5.28	Comparison of experimental and simulated residual weight fraction at 700 ˚C temperature for particle size (a)1 inch (b) 0.5 inch (c) 10-14 mesh (1.4 to 2.0 mm) (d) 52-60 mesh (0.25 to 0.3 mm)	129
5.29	Comparison of experimental and simulated oil yield at different reactor temperatures for particle size 0.5 inch and 1 inch	130
5.30	Comparison of experimental and simulated charcoal yield at different reactor temperatures for particle size 0.5 inch and 1 inch	130
5.31	Comparison of experimental and simulated gas yield at different reactor temperatures for particle size 0.5 inch and 1 inch	131

5.32	Temperature profiles plotted against radial and axial direction at initial time and t=1 s	134
5.33	Temperature profiles plotted against radial and axial direction at t=10 s and t=60 s	136
5.34	Temperature profiles plotted against radial and axial direction at t=180 s and t=600 s	137
5.35	Temperature profiles plotted against radial and axial direction at t=1200 s and t=1500 s	138
5.36	Temperature profiles plotted against radial and axial direction at t=2400 s and t=2700 s	139
5.37	Temperature profiles plotted against radial and axial direction at t=3500 s and t=3600 s	140
5.38	Biomass decomposition profiles plotted against radial and axial direction at different time	141
5.39	Porosity profiles plotted against radial and axial direction at different time	142
5.40	Char profiles plotted against radial and axial direction at different time	142
5.41	Volatile flux with pyrolysis time	144
5.42	Char average concentration in the bed with time	144
I.1	Photograph of laboratory pyrolyzer setup	175
I.2	Photograph of pyrolysis reactor	175
I.3	Photograph of sample holder and inside view of reactor	176
I.4	Thermo-gravimetric analyzer (TGA) setup	176
I.5	Liquid column chromatography setup	177
I.6	Rotary evaporator setup	177
I.7	Fourier Transform Infra-Red Spectroscopy (FTIR) setup	178
I.8	Gas chromatography setup	178
I.9	Gas chromatography mass spectrometry (GC-MS) setup	179

NOMENCLATURE

A_1	Arrhenius constant of reaction 1
A_{2i}	Arrhenius constant of reaction 2 for i^{th} component
A_{3i}	Arrhenius constant of reaction 3 for i^{th} component
A_{p1}	Frequency factor below temperature 300 ˚C, 1/s
A_{p2}	Frequency factor above temperature 300 ˚C, 1/s
B	Concentration of biomass
B_M	Concentration of moisture of biomass
B_i	Concentration of i^{th} component of biomass
C	Concentration of charcoal
C_{1i}	Concentration of charcoal 1 for i^{th} component
C_p	Specific heat capacity, J/kg. ˚C
D_{AB}	Mass transfer diffusivity, m^2/s
E_1	Activation energy of reaction 1
E_{2i}	Activation energy of reaction 2 for i^{th} component
E_{3i}	Activation energy of reaction 3 for i^{th} component
E_{p1}	Activation energy below temperature 300 ˚C, J/mol
E_{p2}	Activation energy above temperature 300 ˚C, J/mol
G	Concentration of non-condensable gases
G_{1i}	Concentration of volatile component 1 for i^{th} component
HR	Heating rate
ΔH	Heat of reaction, J/kg
i	Biomass component: cellulose, hemicellulose, lignin, bio-oil, non-condensable gases and charcoal
k	Thermal conductivity, W/m˚C

K_p	Rate constant, 1/s
k_g	Mass transfer coefficient, m/s
k_i	Kinetic constant of reaction for i^{th} component
k_{2i}	Kinetic constant of reaction 2 for i^{th} component
k_{3i}	Kinetic constant of reaction 3 for i^{th} component
k_{4i}	Kinetic constant of reaction 4 for i^{th} component
L	Length of cylinder, m
n_i	Order of reaction for i^{th} component
r	Radial distance in biomass bed, m
r_i	Rate of reaction for ith component
r_{2i}	Rate of reaction 2 for i^{th} component
r_{3i}	Rate of reaction 3 for i^{th} component
r_{4i}	Rate of reaction 4 for i^{th} component
r_p	Rate of pyrolysis reaction, 1/s
R	Radius of cylindrical biomass sample, m
R_g	Universal gas constant, 8.3144×10^{-3} kJ/mol.K
t	Time, s
T	Temperature, K
T_0	Initial temperature
T_{rs}	Reactor surface temperature, K
T_{rz}	Temperature at specific grid point (At r and z)
V	Concentration of bio-oil
$W_{total,exp}$	Experimental value of the residual weight fraction
$W_{total,cal}$	Calculated value of the residual weight fraction (predicted from model)
z	Axial distance in biomass bed, m

Greek letters

ε	Emissivity coefficient
ρ_c	Char mass concentration, kg/m^3
ρ_b	Biomass mass concentration, kg/m^3
ρ_v	Volatile mass concentration, kg/m^3
σ	Stefan Boltzmann constant, 5.67x10^{-8} Watt/m^2.K^4
ν_i	Stoichiometric coefficient of i

Subscripts

AB	Diffusion of gas *A* in *B*
b	Biomass
c	Char
g	Gas
i	H_2, CH_4, CO_2, CO
P	Pyrolysis primary reaction
rz	Components of position vector
rs	Reactor surface
v	Volatiles

CHAPTER – 1

INTRODUCTION

1. Introduction

The need of the twenty first century is environment friendly, economically feasible and renewable fuel to replace the shrinking conventional fuel resource. The prolonged time constraints for the formation of conventional fossil fuel sources present us with the problem of rapid depletion of these resources. The alarming population levels, urbanization and industrialization have increased the global energy demand. Conventional fuels being a good source of energy are at a verge of extinction [1]. Prior to industrial revolution, the energy requirements were achieved from the natural resources and forest produce [2-4]. Extensive research is carried out to reduce dependence on the conventional fossil fuels and to replace sizeable portion of conventional fuels with alternative fuels. The challenge of our times is to partly switch back to natural resources like biomass for the energy requirements which are sustainable. One of the major renewable sources is biomass waste. It can replace conventional fuels and provides solutions to the global warming situation by reducing greenhouse gases emissions [5]. It is composed of organic carbonaceous materials such as woody and lignocellulosic

materials, various types of herbage, especially grasses and legumes, and crop residues. Biomass can be converted to various forms of energy by numerous technical processes, depending upon the raw material characteristics and the type of energy desired. It is used to meet a variety of energy needs, such as generating electricity, heating homes, fuelling vehicles, and providing process heat for industrial facilities [6]. Biomass power plants have advantages over fossil-fuel plants, because their pollution emissions are less. There is no addition of carbon dioxide to the atmosphere because it absorbs the same amount of carbon dioxide in growing as it releases when consumed as a fuel [7]. The CO_2 emissions from the use of fossil fuels that provide about 85 % of the total world demand for primary energy, cause the observed increase of the CO_2 concentration in the atmosphere[8]. Using biomass fuels in the form of a closed carbon cycle, as a substitute for fossil fuels, is one of the few most promising ways for halting the increase of the CO_2 concentration [9].

1.1. Biomass energy

Energy generated from biomass is known as biomass energy. Biomass energy can be generated through thermochemical conversion of biomass. The details of biomass and thermochemical conversion technologies are discussed in section 1.1.1 and 1.1.2, respectively.

1.1.1. Biomass

Biomass can be classified into two categories namely algal biomass and lignocellulosic biomass. Algal biomass is rich in nutrients, especially nitrogen and phosphorus. Therefore a process to recycle algal waste after lipid extraction is desirable [10]. Lignocellulosic biomass is inclusive of a wide range of traditional fuels such as wood;

agricultural crops which are especially cultivated for energetic purpose, forest and agricultural residues and are closely related to other fuels such as waste from both industries and households, and peat. Figure 1.1 shows the pictorial presentation of various biomass resources. The use of biomass offers the advantage, such as, its availability in every country in various forms and thus assures supply of raw material to the energy system. The socio-economic benefits are the creation of new employment opportunities in rural districts [11].

Biomass is a polymer that is made of three major components; cellulose, hemicellulose and lignin. Cellulose and hemicellulose, which consist of long chains of sugars, are surrounded by lignin, a complex polymer of alcohols, which joins them and provide rigidity to the biomass. This makes it difficult to breakdown. It is necessary to destruct lignin and weaken its makeup [12]. The compositions of these groups usually depend on the type of wood, but normally mass fractions ranging from 40 to 50% for cellulose, from 15 to 25% for hemicelluloses and between 20 and 30% for lignin. Together these three groups from 90 to 95% of wood. The other 5 to 10% consists of mineral matter and a few other organic compounds [13]. The next sections describe the three groups in more detail.

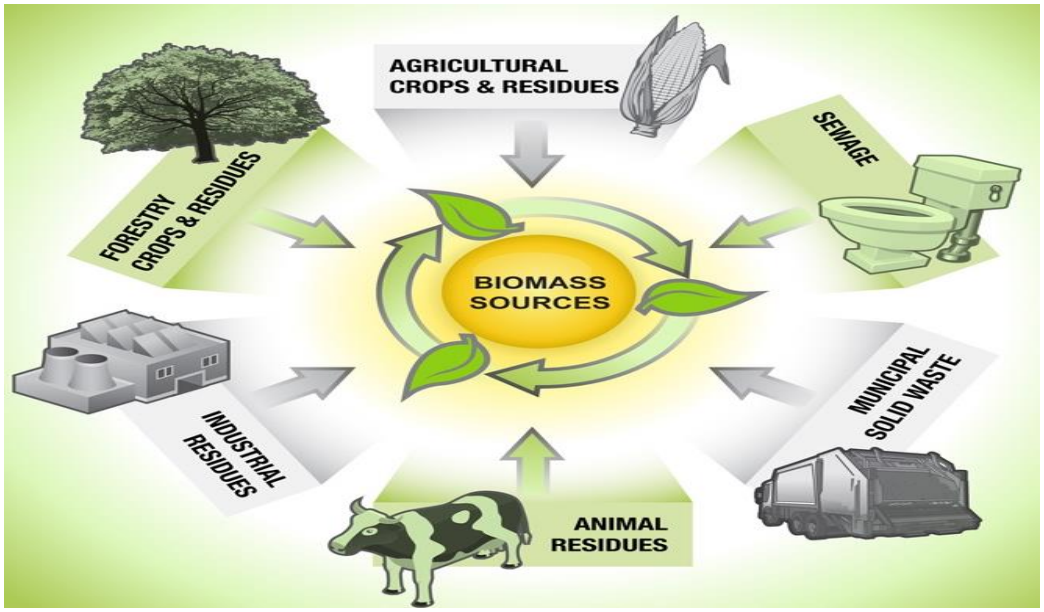

Figure 1.1 Sources of biomass

Source: https://www.bioenergyconsult.com/biomass-resources/

1.1.1.1. Cellulose

Cellulose is the main component of lignocellulosic biomass. Cellulose consists of long polymers built with a C_6 monomer as base structure. Figure 1.2 shows the molecular structure of cellulose. The glucose units in cellulose are combined in a way that results in the formation of very linear flat molecules that possess extensive networks of hydrogen bonds. The presence of hydroxyl groups allow H-bonding, for instance to available positions in neighboring cellulose molecules, and also chemical bonding with lignin and other phenolics [14]. As a result of these bonds, cellulose are particularly strong a property critical to the function of plant cell walls. Cellulose shows a variable degree of polymerization, with anywhere from 1,000 to 14,000 glucose residues comprising a single cellulose polymer. Because of its high molecular weight and crystalline structure, cellulose is insoluble in water and has a poor ability to absorb water. Thermal degradation of cellulose normally starts around 350 ˚C. This temperature depends on the

presence of side groups and branches along the chains. During pyrolysis the polymer chains can be broken down into smaller polymers, but also in gas species that are much smaller than one monomer.

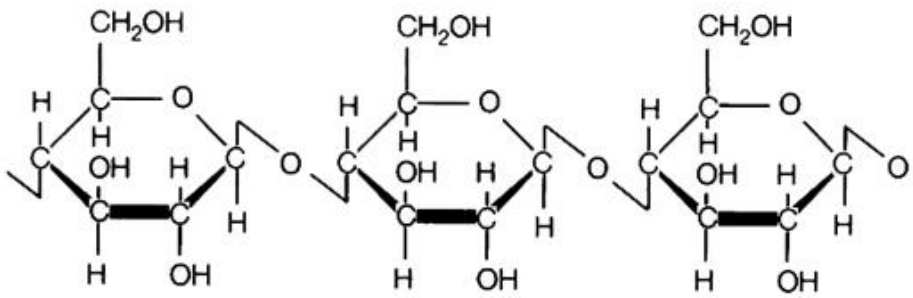

Figure 1.2 Molecular structure of cellulose

1.1.1.2. Hemicellulose

Hemicellulose is in most aspect similar to cellulose. The hemicellulose polymers form a crystalline structure and the same types of chemical bonds are present. Hemicellulose is a branched polymer of pentose (xylose and arabinose), hexoses (mannose, glucose, and galactose), and sugar acids [15, 16]. The base structure of hemicellulose, as shown in Figure 1.3, consists of C_5 monomers and the polymerization grade is in the order of 100. Compared to cellulose, hemicellulose is a more branched polymer. This result in a lower thermal stability and thermal degradation of hemicellulose starts around 270 ˚C. The monomers having C_6 and C_5 structure give chains either a hexagonal or a pentagonal shape.

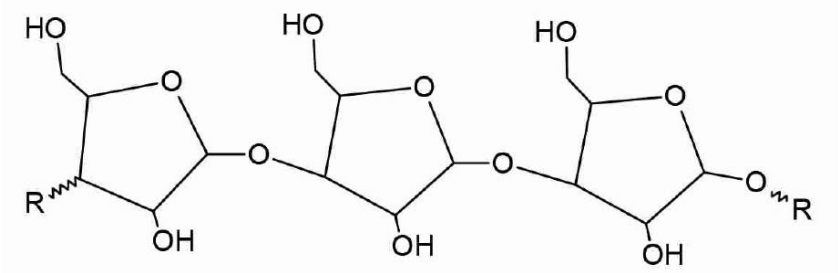

Figure 1.3 Molecular structure of softwood hemicellulose

1.1.1.3. Lignin

Lignin is complex and heterogeneous polymer that is predominantly present in the walls of secondary thickened cells and consists of many different chemical structures as shown in Figure 1.4 [17]. It is mainly derived from three cinnamyl alcohol units, the monolignols *p*-coumaryl alcohol, coniferyl alcohol and sinapyl alcohol. When incorporated into lignin, these form the *p*-hydroxyphenyl (H), guaiacyl (G) and syringyl (S) units, respectively. The complex of these components is cross-linked together through carbon–carbon, ester and ether bonds [18]. It has the highest energy content amongst three fractions. It has relatively high carbon content compared to cellulose and hemicellulose, and as a result it is the most charring biomass component. Lignin does not have a well-defined crystalline structure such as cellulose and hemicellulose, but is amorphous and highly cross-linked, meaning that the polymer chains are highly interconnected. Thermal degradation of lignin, which starts around 390 ˚C, takes place over a wide temperature range, due to the many different chemical structures present in it. Lignin can be subdivided into three different groups of lignin. These structures are indicated with Lig-C, Lig-O and Lig-H.

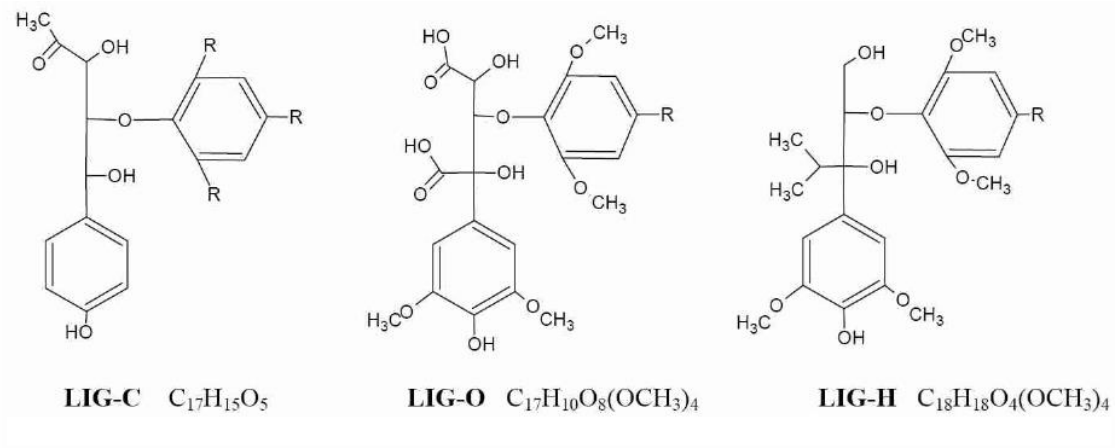

Figure 1.4 Molecular structure of the three main components of lignin

1.1.1.4. *Jatropha curcas* as biomass

Jatropha curcas grows almost anywhere, even on gravelly, sandy and saline soils. It can thrive on the poorest stony soil. It is a small tree or shrub with smooth gray bark, which exudes whitish colored, watery latex when cut. Regarding climate, *Jatropha curcas* is found in the tropics and subtropics and likes heat, although it does well even in lower temperatures and can withstand a light frost. Its water requirement is extremely low and it can stand long periods of drought by shedding most of its leaves to reduce transpiration loss. *Jatropha curcas* is also suitable for preventing soil erosion and shifting of sand dunes [19]. Fruits of *Jatropha curcas* are produced in winter when the shrub is leafless, or it may produce several crops during the year if soil moisture is good and temperatures are sufficiently high. Each inflorescence yields a bunch of approximately 10 or more ovoid fruits [20]. *Jatropha curcas* grows wild in many areas of India and even thrives on infertile soil [21]. A good crop can be obtained with little effort. The annual nut yield ranges from 0.5 to 12 tons [22]. The seed material comprises of 41 wt % shell and 59 wt% kernel. The kernel consists of 40 wt % to 50 wt % of oil [23]. The oil can be processed to generate the bio diesel, which can be combusted as fuel. Although the oil is

an excellent biodiesel feedstock, potential utilization or safe disposal of huge amounts of seed cake by-product needs to be addressed. Additionally due to continuous increasing demand of biodiesel, production of oil cakes have increased immensely and about 2 tons of oil cake is dumped as a waste for every tons of biodiesel production [24]. The press cake contains about 9 wt % -12% oil whose gross energy value is 18.2 MJ/kg [25]. De-oiled *Jatropha curcas* seed cake is shown in Figure 1.6. The average chemical composition of deoiled seed cake is 60 wt % protein, 0.6 % fat, 9% ash, 4% fiber and 26% carbohydrates [26]. *Jatropha curcas* seed cake cannot be used as cattle feed, unlike other oil seeds mainly due to the presence of toxic phorbol esters in it. Phorbol esters have been identified as main toxicants in cake which could not be destroyed even by heating at 160°C for 30 min [27].

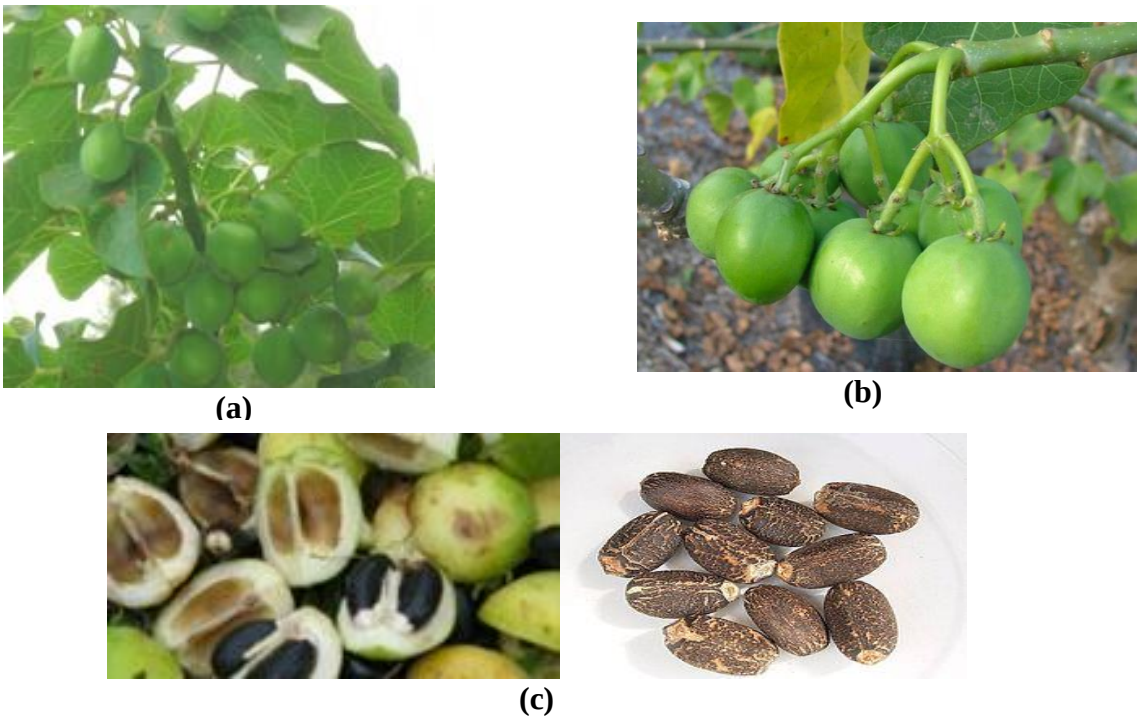

Figure 1.5 ***Jatropha curcas:*** **(a) plant (b) fruit (c) seeds**

Source: http://bulkagro.com/product/jatropha-curcas-seeds/

Figure 1.6 De-oiled *Jatropha curcas* cake

1.1.2. Thermochemical conversion of biomass

Thermochemical conversion processes involve treating biomass at high temperature and moderate or atmospheric pressure. The basic approaches include gasification, high-temperature pyrolysis, and high-pressure liquefaction. Various thermochemical conversion processes are described as below.

1.1.2.1. Gasification

Gasification is the process of converting the biomass into a combustible gas mixture by partial oxidation of the biomass at high temperature, in the range of 800 ˚C to 1000 ˚C. The essence of gasification process is the conversion of solid carbon rich fuels into carbon monoxide and hydrogen. The following reactions take place in the reactor during the gasification process.

$$C + H_2O \longrightarrow CO + H_2$$

$$CO + H_2O \longrightarrow CO_2 + H_2$$

$$CO_2 + C \longrightarrow 2\,CO$$

Gasification generally involves pyrolysis as well as combustion to provide heat for the endothermic pyrolysis and reduction reactions.

1.1.2.2. Pyrolysis

Pyrolysis is thermal decomposition of biomass fuels in the absence of oxygen. The process involves release of all three phases of products: solid, liquid and gases. The ratio of products is influenced by the chemical composition of biomass fuels and operating conditions [28]. The heating value of gas produced during the pyrolysis process is low (3.5 - 8.9 MJ/m ^{3}). Pyrolysis generally starts at 300 ˚C and continues up to 500 ˚C –800 ˚C.

1.1.2.3. Liquefaction

The conversion of biomass from its natural solid form to liquid fuels is not a spontaneous process. Liquefaction is a low-temperature, high-pressure process using a catalyst with the addition of hydrogen producing a liquid product. In other words, hydrothermal liquefaction of biomass is the thermochemical conversion of biomass into liquid fuels by processing in a hot, pressurized water environment for sufficient time to break down the solid bio polymeric structure to mainly liquid components. This process is synonym of hydrous pyrolysis, but compared to pyrolysis hydrothermal liquefaction is carried at lower temperatures and heating rates. High pressure is maintained to ensure good heat transfer, or to maintain a liquid-phase system at high temperatures. Typical hydrothermal processing conditions are 250 ˚C to 375 ˚C of temperature and operating pressures from 4 MPa to 22 MPa. Liquefaction is unfavourable because the reactors and fuel feeding systems are more complex and more expensive than for the pyrolysis and gasification processes [29].

1.2. Biomass pyrolysis

Pyrolysis is thermal degradation in complete absence of oxidizing agent or a limited supply such that gasification does not occur to an appreciable extent. As shown in Figure 1.7, pyrolysis of biomass generates char, oils and gases in different quantities. Their relative proportion depends on the pyrolysis method, characteristics of the biomass and the operating conditions of pyrolysis reactor [30]. This is carried out at temperatures of 300 ˚C to 800 ˚C.

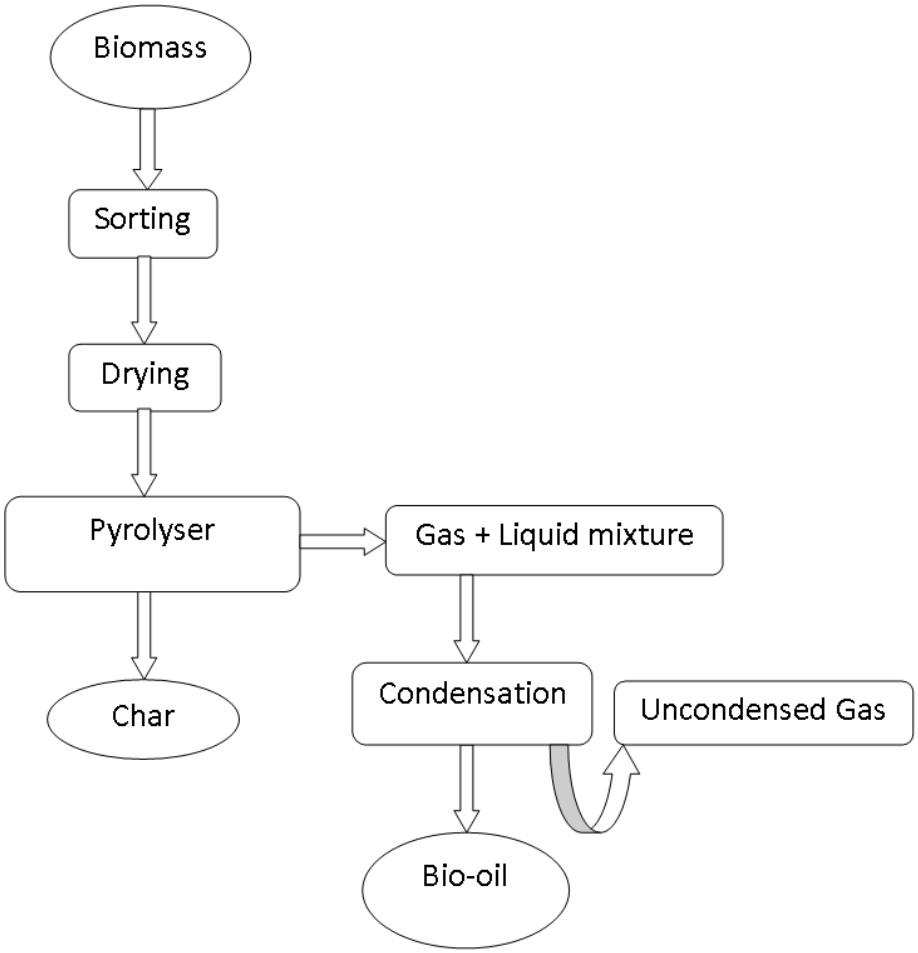

Figure 1.7 Process steps for biomass pyrolysis

The biomass pyrolysis is one of the sought after methods; both in terms of efficiency wise and cost-wise because solid biomass and wastes are difficult and costly to manage. The biomass can be readily converted into liquid products. These liquids, as crude bio-oil or slurry of char or water or oil, have advantages in transport, storage, combustion, retrofitting and flexibility in production and marketing. The most interesting temperature range for the production of the pyrolysis products from biomass is between 350 ˚C and 500 ˚C. The char yield decreases as the temperature increases. The production of liquid products has maximum yield at temperatures between 350 ˚C and 550 ˚C.

1.2.1. Types of biomass pyrolysis

1.2.1.1. Slow pyrolysis

This is a conventional process whereby the heating rate is kept slow (approximately 5 ˚C/min –7 ˚C/min) and slow heating rate leads to higher char yields than the liquid and gaseous products. Different kinds of biomass, such as wood samples, safflower seeds, sugarcane bagasse, sunflower seeds, municipal wastes, etc., are generally subjected to slow pyrolysis [28].

1.2.1.2. Fast pyrolysis

Fast pyrolysis is considered a better process than conventional one. In this, the heating rates are kept higher, about 300 ˚C/min to 500 ˚C/min and the obtained liquid product yield is higher. High oxygen and water content of pyrolysis liquids during the process makes a process inferior to traditionally used hydrocarbon fuels [31].

1.2.1.3. Flash pyrolysis

Flash pyrolysis is a process in which organic materials are rapidly heated to a temperature of 500 ˚C -700 ˚C. Under these conditions, organic vapours, pyrolysis gases and char are

produced. The vapours are condensed to bio-oil. Typically 60-75 wt % of the feedstock is converted into gaseous product. The process conditions for all the processes are shown in table 1.1.

Table 1.1 Process conditions for pyrolysis [28]

Parameters	**Conventional Pyrolysis**	**Fast Pyrolysis**	**Flash Pyrolysis**
Pyrolysis Temperature (˚C)	275-675	575-975	775-1025
Particle size (mm)	5-50	<1	<0.2
Heating rate (˚C/s)	0.1-1.0	10-200	>1000
Solid residence time (s)	450-550	0.5 -10	<0.5

1.2.2. Pyrolysis products

Much research is done to determine product yields in terms of char, bio-oil and gas. Detected yields range for biomass from 2 wt % - 25 wt % for char, 10 wt % - 30 wt % for gasses and 45 wt % - 90 wt % for bio-oil. These differences result from diversity in biomass origin and experimental setups and procedures. Especially variations in heating rate and temperatures lead to large changes in observed yields [32].

1.2.2.1. Bio-oil

The liquid, or bio-oil, or bio-crude is a micro-emulsion containing many reactive species, which contribute to its unusual properties. It is composed of a complex mixture of oxygenated compounds that provides for potential and challenges for its utilization. Depending on the type of biomass and the mode of pyrolysis, the color can be almost black through dark red-brown to dark green. The liquid has an acrid, smoky, irritating smell due to the presence of low-molecular-weight aldehydes and acids. Bio-oil is immiscible with water but soluble in polar solvents such as methanol, acetone, etc. It is

totally immiscible with petroleum-derived fuels [33]. The density of the liquid is very high at around 1.2 kg/L compared to light fuel oil at around 0.85 kg/L. It has potential for multiple applications. It is used as a substitute for hydrocarbon fuels to produce electricity or generates steam. This is primarily due to lower cost of bio-oils compared to petroleum based fuels. This has been used as fuel for combustion, power generation and the production of chemicals [34].

1.2.2.2. Char

Char is produced as product of biomass pyrolysis process along with bio-oil and non-condensable gases. Char produced from pyrolysis contains high energy comparable to the coal used as feedstocks for fuel [35]. It is used for several industrial applications because of its micro porous structure and high carbon content. In agriculture, it is useful in upgradation of the soil quality. Rate of carbon sequestration in soil can be enhanced by mixing the soil with char. It also increases the soil quality by reducing the rate of decay of nutrients from soil [36]. In refinement industry, char is used to remove heavy metals such as Cr [37], Cd [38], Ni [39], Hg [40] and Pb [41] . Apart from heavy metals, it is also a low-cost means to remove different hazardous chemical like tetracycline [42], phenol [43], etc. char is also economically and successfully used in textile industries to remove different kinds of dyes and pigments which otherwise pollutes the water and is harmful to human being [44]. Char contains a high carbon percentage hence it is used as fuel in power generation plants as well.

1.3. Modeling of biomass pyrolysis

Mathematical modeling, simulation and optimization are the best tools for analyzing and developing any complex process. Mathematical modeling can also provide greater inputs to thermochemical conversion of biomass such as pyrolysis and gasification, which involves the chemical and physical phenomena. Economic and efficient pyrolysis reactors can be developed only through better understanding of the phenomena. Biomass pyrolysis involves numerous extremely complex reactions with large number of intermediates and end products. Since devising an exact reaction mechanism for biomass pyrolysis is extremely difficult. Inside the pyrolyzing particle, heat is transferred by all modes of heat transfer. At the surface, it receives the heat via convection and radiation both. Heat gets diffused inside the solid particle by conduction and inside the pore by convection. Design of pyrolyzer requires prediction of the rate of biomass devolatilization and yield of pyrolysis products. The modeling and simulation of the pyrolysis process largely involves two approaches: (1) kinetic model development using thermal degradation experimental data and (2) reactor modeling to predict the yields of pyrolysis products.

1.3.1. Kinetic model development

Different kinetics or models predicts the biomass decomposition differently. The models are classified into three categories: one-step global models, one-step multi-reaction models, and two-step semi-global models [28].

1.3.1.1. One-step global models

The one-step global model is the simplest kinetic model which assumes that the

decomposition rate of the pyrolysis process depends on an arbitrary reaction order [33]. The physical significance of one-step global reaction scheme is that it describes the overall devolatilization rate from the biomass. In this model, the overall reaction is considered as conversion of biomass to volatiles and char. The reaction scheme can be represented by following pyrolysis reaction (Equation 1.1).

$$\text{Biomass} \xrightarrow{K_i} \text{volatiles} + \text{char} \qquad (1.1)$$

1.3.1.2. One-step multi-reaction models

In one step multi-reaction mechanism, biomass gets pyrolyzed into gas, bio-oil and char as per three parallel reactions as shown in Fig. 1.8.

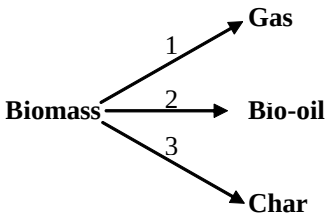

Figure 1.8 Single stage multi-reactions model

1.3.1.3. Two-step semi-global models

The limitation of one step global kinetic and multi reaction model is that they predict the continuous increase in the yield of liquid, gas and char with temperature as the rate of reaction increases. However, the yield of liquid product increases with temperature to a certain maximum value and beyond that it decreases due to the cracking of liquid product at high temperature. Figures 1.9 (a) and (b) represents the different types of two-step semi-global models.

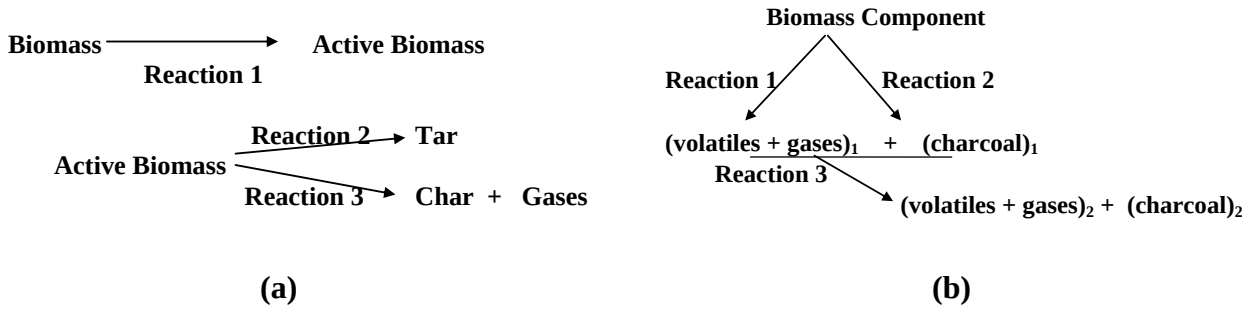

Figure 1.9 Two-stage semi-global models

In two-step semi global reaction mechanism, the decomposition of biomass can also be described by three independent parallel reactions, each analogous to the decomposition of the intermediate constituent of biomass. Overall rate of pyrolysis is the sum of the corresponding rates of all the main biomass components (cellulose, hemicellulose and lignin) [6]. The kinetic scheme based on decomposition of each biomass constituent into intermediate and subsequently further decomposition into volatiles and char [45]. Sricharoenchaikul and Atong [25] estimated the kinetic parameters using the scheme based on biomass constituent decomposition and it is represented by Eqs. (1.2) to (1.4).

$$\text{Raw material} \xrightarrow{k} \text{Volatile}_1 + \text{Volatile}_2 + \text{Volatile}_3 + \text{Char} \qquad (1.2)$$

$$M_i \xrightarrow{k_i} \text{Volatile}_i + \text{Char} \qquad i = 1, 2, 3 \qquad (1.3)$$

where, M_1, M_2, and M_3 represent hemicellulose, cellulose and lignin, respectively. They independently decompose at a different rate constants of k_1, k_2, and k_3. The rate of decomposition is expressed by Eq. (1.4).

$$\frac{d\alpha}{dt} = A\exp\left(-\frac{E}{RT}\right)(1-\alpha)^n \qquad (1.4)$$

Where, n is the order of the reaction; A is a pre-exponential factor; E is the activation energy; R is the gas constant; t is time; and α is the normalized fractional

conversion. In general, while developing the kinetic model, the experimental results of thermo-gravimetric analysis (TGA) are used and kinetic parameters are estimated. The applicability of this kind of model is limited and can be used only for small size (less than 1 mm) particles, which are undergoing kinetically controlled devolatilization. The pyrolysis of large size particles is controlled by heat and mass transport within the particle. To predict the rate of devolatilization and yield of products for the pyrolysis of large size particles, there is a need to develop the particle model and incorporate it into the reactor model [46]. Alternatively, an apparent kinetic model can be developed which can be used in the reactor modeling without developing the particle model.

1.3.2. Apparent kinetic model development

The apparent kinetic model can be developed by utilizing the experimental results of pyrolysis of large size biomass particles. However, its applicability is limited for a particular temperature range and also for a particular size. Eq. (1.5) represent the apparent kinetic model developed by Di blasi [46, 47]

$$\text{Biomass} \xrightarrow{K_P} \nu_C\ \text{Char} + \nu_{CO}\ \text{CO} + \nu_{CO_2}\text{CO}_2 + n_{H_2}\text{H}_2 + n_{CH_4}\text{CH}_4 + n_{H_2O}\ \text{H}_2\text{O} + n_T\ \text{Bio-oil} \tag{1.5}$$

Essentially each kinetic model employs a rate law and the kinetic constant obeys the fundamental Arrhenius rate expression [8]:

$$r_p = A_p \exp\left(\frac{-E_p}{R_g T}\right)\rho_b \tag{1.6}$$

Where K_p is kinetic constant and is given by Eq. (1.7):

$$K_p = A_p \exp\left(\frac{-E_p}{R_g T}\right) \tag{1.7}$$

Where T is the absolute temperature in K, R is the universal gas constant in $Jmol^{-1}K^{-1}$, K_p is temperature dependent reaction rate constant, A_p is frequency factor, or pre-exponential, and E_p is the activation energy of the reaction. The temperature dependency of Arrhenius equation is mainly from the exponential term, the frequency factor A_p, also depends slightly on temperature.

1.3.3. Fixed bed model development

Heating rate, particle size, final temperature of the furnace, are important parameters which have control over the product yield of the pyrolysis process, hence the heat and mass transfer also play an important role for describing the thermal degradation process of biomass. The fixed bed model represents both mass and energy balances for the solid phase (biomass and char) and gas phase (bio-oil and permanent gases) [48-54]. The rate of degradation of biomass with incorporation of mass transfer in biomass is given by Eqs. (1.8) to (1.11).

$$\frac{\partial \rho_{\mathrm{b}}}{\partial t} = -r_{\mathrm{biomass}} \tag{1.8}$$

$$\frac{\partial \rho_{\mathrm{v}}}{\partial t} = D_{\mathrm{AB}}\left(\frac{\partial^2 \rho_{\mathrm{v}}}{\partial z^2}\right) + r_{\mathrm{volatiles}} \tag{1.9}$$

$$\frac{\partial \rho_{\mathrm{c}}}{\partial t} = r_{\mathrm{char}} \tag{1.10}$$

Where,

$$r_{\mathrm{biomass}} = A_{\mathrm{p}} \exp\left(\frac{-E_{\mathrm{p}}}{R_{\mathrm{g}} T_{\mathrm{s}}}\right)\rho_{\mathrm{b}} \tag{1.11}$$

Eq. (1.11) represents the apparent kinetic model scheme if regular kinetic model is used instead there is a need to develop particle model. The temperature of biomass is same as the volatiles and char, the biomass balance is as follows which is same for char and volatiles and given by Eq. (1.12)

$$\frac{\rho_b C_P}{k}\left(\frac{\partial T}{\partial t}\right)=\frac{1}{r}\left(\frac{\partial T}{\partial r}\right)+\frac{\partial^2 T}{\partial r^2}+\frac{\partial^2 T}{\partial z^2}+\frac{\partial \rho_b}{\partial t}\left(\frac{\Delta H - TC_p}{k}\right) \quad (1.12)$$

The model consists of two partial differential equations (heat and volatile transport) and two ordinary differential equations (biomass decomposition and char generation). The heat transport equation includes the conductive heat transport in both directions along with accumulation term. The volatile transport equation includes the molecular diffusion of volatiles with accumulation term. The model includes heat transfer from the reactor wall to biomass bed both by radiation as well as convection mode.

1.4. Objectives of the proposed research

i. To study various kinetic models of biomass pyrolysis and improve existing kinetic model by incorporating moisture release phenomena and develop multi reaction apparent kinetic model for large size biomass particles.

ii. To carry out the thermo-gravimetric analysis of biomass and perform experimental study using fixed bed pyrolyzer for identifying the effects of pyrolysis temperature and particle size of biomass on yield of pyrolysis products.

iii. To characterize the produced bio-oil using GC-MS, FTIR, TGA and liquid column chromatography for understanding its composition.

The above mentioned objectives are achieved by initially carrying out an exhaustive literature survey in Chapter-2 followed by comprehensive modeling & simulation studies and detailed experimental study. In the present study, in modeling and simulation study, two different kinetic models and one transport and kinetic model of fixed bed is developed and simulated. The first kinetic model involves multi reaction individual biomass constituent (*i.e.* cellulose, hemicellulose and lignin) decomposition based kinetic scheme with incorporation of moisture release phenomena for thermal decomposition. Apart from this, one step multi reaction apparent kinetic model is also proposed. To find the kinetic parameters for the kinetic model and apparent kinetic model, the experimental studies are carried out covering a wide range of operating parameters using TGA and macro TGA. The combined transport and kinetic model is 2D and dynamic in nature. It takes into account of the kinetics of chemical reactions, heat and mass transfer between solid and gaseous phases and transport of volatiles produced. It is developed to understand the dynamic temperature variation and porosity variation in the fixed bed. As far as experimental studies is concerned, pyrolysis of biomass is carried out in a fixed bed reactor having facility to monitor the weight reduction with time. It is the same as TGA but at a macro level. Hence, the term “macro-TGA” is used for this kind of pyrolysis reactor. TGA of the biomass at different heating rates is also performed. Experimental study with macro TGA is carried out using *Jatropha curcas* de-oiled cake as biomass to generate bio-oil, char and non-condensable gases. The bio-oil produced is characterized using FTIR, TGA and GC-MS.

As far modeling and simulation study is concerned, two different kinetic models and one transport and kinetic model of fixed bed is developed and discussed in Chapter-

3. It also includes simulation methodology for the proposed models. To produce the products of pyrolysis for characterization, experiments are carried out and the details of experimental setup and its procedures are elaborated in Chapter-4. The obtained experimental data are discussed and analyzed in detail in Chapter-5. It also includes the validation of proposed mathematical model with the obtained experimental data and the data available in the literature. Chapter-6 deals with the summary of the work and important conclusions drawn from the present study.

CHAPTER – 2

LITERATURE REVIEW

2 Literature Review

Various studies reported in literature on theoretical and experimental investigations of biomass pyrolysis are discussed in detail in section 2.1 and 2.2 respectively.

2.1 Theoretical studies on biomass pyrolysis

In modeling of the biomass particle pyrolysis, it is common to employ a kinetic model, whether it is a simple lumped kinetic model or a complex multiple reactions one, to form the base of the model for describing pyrolysis reactions.

The various types of models are presented here with their experimental proof that enriches the model suggested by Bamford *et. al.* [55] . In his model, he assumed first order kinetics and combined heat generation equation with the heat conduction equation in pyrolyzing solid However, the effect of change in density of biomass with time was not given enough emphasis. In continuation, in 1977, Fan *et. al*. developed a model for

pyrolysis process, which includes heat and mass transfer in the particle [56]. The reaction is considered to be first order with respect to initial particle concentration, but product concentrations cannot be analyzed from the above model because the secondary reactions were not considered. Researchers developed new model overcoming drawbacks of previously developed models. Miyanami *et. al.* [57] and Fan *et. al.* [56] incorporated the effect of heat of reaction in the above model. The model developed by Bamford *et. al.* [58] was used by Tinney [59], Roberts *et. al.* [60] which further modified by Kung *et. al.* [61]. They incorporated the effects of internal convection and variable transport properties. However, the model was insufficient to determine the concentration of various product components due to negligence of specific kinetic mechanism. Kansa *et. al.* included the momentum equation for the motion of pyrolysis gases within the solid [62]. A suitable kinetic mechanism has not been utilized and the solution to the heat and momentum balance equation is based on arbitrary boundary conditions.

Physical processes that involve physical changes, heat transfer and mass transfer, additional elements such as secondary reaction, particle shrinkage, and heat of pyrolysis reaction, vapor residence time and interaction with the reactor environment are usually considered and studied. Studies have been carried out on pyrolysis of biomass and other substances by Di Blasi [63, 64], Jalan *et. al.* [65, 66] and Bamford *et. al.* [58]. Some researchers considered only primary reactions, there were few which involved both primary and secondary reactions in chemical kinetics. Kansa *et. al.* pointed out that secondary reactions are essential to match fully the experimental observations [62]. Keeping in view the drawbacks of the existing models, Babu and Chaurasia presented the kinetic model, which considered the secondary reactions in pyrolysis kinetics [50].

This kinetic model was developed for pyrolysis of a single biomass particle, which includes kinetics and heat transfer effects in the particle. The temperature profiles obtained by Babu and Chaurasia were compared with predicted value of Pyle and Zaror in which Baby and Chaurasia utilized Bamford's model [67, 68]. The simulated results obtained by Babu and Chaurasia's model was in excellent agreement with the experimental data and infact better than the models proposed by Jalan and Srivastava and Bamford *et. al.* [50].

Roberts observed that permeability for flow along the grains is 104 times higher than across the grain. The chemical pathways of the pyrolysis reactions are very complex. In computational models, global reaction rates have been extensively used for simplifying the process to reproduce the levels of char, light hydrocarbons, and tars produced in laboratory experiments. Smaller particles tend to produce endothermic values while larger samples produce exothermic values [69]. Kung *et.al.* and Fan *et. al.* in their model incorporated effects of internal heat convection and other transport properties. They considered the effect of endothermicity, variable density, specific heat, thermal conductivity but ignored moisture removal and possibility of secondary reactions [56, 61]. Kansa *et. al.* included the momentum calculation for the motion of pyrolysis gases within the solid and solved the heat and momentum balance equation which was based on capricious boundary conditions. Secondary reactions were not considered [62].

Thurner *et. al.* investigated the kinetics for wood pyrolysis for the products char, tar and gas in the temperature range of 300 ˚C to 400 ˚C at the atmospheric pressure. In the kinetic model the single-step three reactions in parallel i.e. decomposition of biomass

in char, tar and gas has considered to determine the values of activation energy and frequency factors from the experiments data [70, 71].

Pyle and Zaror [67] and Chan *et. al.* [72] defined various simplified models using the Bamford model. Using the different values of Biot Number, they determined the internal and external heat transfer and 1st order Pyrolysis (intrinsic). In the model proposed by Koufopanos *et. al.* the effect of density as a function of time is not appraised while solving the heat transfer equation. They also pointed out that it is very difficult to define physically the components or composition of the intermediates, and accordingly it is not possible to measure their concentration experimentally in order to test the model rigorously [48].

Di Blasi developed different kinetic models of different complexity for charring (solid fuels) and non-charring materials. For charring materials one step primary to semi-global kinetics and secondary degradation has considered and after coupling these in kinetics with transport model simulations has done. For non-charring materials the effect of bubbling of volatiles while thermal degradation has reported through the global single-step kinetics has proposed. Density of Biomass significantly influences the final product composition and yield. For conversion in the thermally thick regime (intra particle heat transfer control) biomass density mainly affect the activity of secondary reactions of tar vapors and conversion time. In thermal thin regime (external heat transfer control), they only affect the conversion [73, 74]. They also compared the semi-global models of different literatures, for kinetically controlled primary pyrolysis of cellulose and biomass for the formation of char, tar and gases. Product yields and conversion times are reported at different temperature and heating rates. Author has reported that overall cellulose also

behave same as biomass that is the tar yield increases and char and gas yields decreases as final temperature and heating rate increases [75].

In the model of Liliedahl *et. al.* and Jalan & Srivastava, the thermal conductivity and the specific heat capacity of biomass were considered constants [76] [65]. Di Blasi pointed out that a detailed transport model integrating the kinetics, heat, and mass transfer effects is necessary to predict the effects of the widely variable corporeal properties (density, thermal conductivity, specific heat capacity) in the pyrolysis of biomass. However, different kinetic scheme wherein the agile cellulose was considered to be formed as an intermediate product [74, 75, 77].

Chen *et. al.* developed a kinetic model for fixed bed pyrolyzer in which the virgin biomass decomposes in primary products (char, tar and semi-char), secondary decomposition of the production as well as this followed by simultaneous interaction of primary char and gas. The scheme was reported to be pretty good for high temperatures i.e. 900 ˚C for pine sawdust and validated with different kinetic schemes in literature. [78]

Williams *et. al.* suggested that low char yield at low heating rates high char yield at high heating rates is obtained because of the larger residence time of primary products within the solid matrix whereas the yield of volatiles increases markedly at fast heating rates, as secondary reactions would be expected to dominate yielding small quantity of char. Higher heating rate favors release of hydrocarbon gases like CO, CO_2, CH_4, C_2H_6, etc. [79]. Miller remarked that the increase in the mass-transfer resistance results in the decrease of condensable fraction because a longer vapor residence time in the reacting region induces more severe secondary reaction [80]. The variation in the wood specific

heat capacity does not affect the primary product yields. However conversion time is found to increase with this parameter [81]. The activity of secondary reactions appears to be significantly influenced by the specific heat capacity of the biomass. Intra-particle residence times become longer and secondary tar cracking occurs to an even greater extent. Consequently the final tar yield continuously decreases. The combined impact of char shrinkage and particle moisture on pyrolysis products and time is a function of pyrolysis regime [82]. Shrinkage has negligible effect in the thermally thin regime ($Bi<0.2$), in the thermally thick regime ($0.2 < Bi < 10$) it reduces the pyrolysis times by 5-30%. In thermal wave regime ($Bi>10$) it affects both the pyrolysis time and products [83]. In general coupling both shrinkage and moisture result in longer pyrolysis times, increased tar yield and decreased light hydro carbon yield than if they were considered separately.

Babu and Chaurasia observed in their study of heat of devolatilization is of great importance in modeling thermal effect during a pyrolysis process. The issue of whether pyrolysis reactions are endothermic or exothermic plays an important role in modeling considering heat-transfer controlled reaction and self-sustaining reaction [50, 52]. They observed the production of (char) is favored by the endothermic reactions while the production of (volatile and gases) is favored by the exothermic reactions. Thermal conductivity varies with temperature. It is possible to get the same extent of conversion of biomass with lesser pyrolysis time under controlled conditions by increasing convective heat transfer at much lower operating temperatures which are much safer than at higher operating temperatures leading to combined convective and radioactive heat transfer mechanisms which are not safe [49]. Onwubolu *et. al.* reported that the pyrolysis

is faster for zero order as compared to first order of primary reaction as the rates are independent of initial biomass concentration for zero order [84]. Pettersson *et. al.* reported that emissivity has almost no effect on the pyrolysis rate, whereas initial wood density, specific heat and thermal conductivity affect the heat transfer and the pyrolysis rate as they define thermal diffusivity [85]. It was observed that the effect of emissivity on the concentration of products becomes significant at higher values of emissivity by Babu and Chaurasia, where the activities of both the primary and secondary pyrolysis reactions are changing significantly. They found that in thermally thick regime [51]

- the most dominant properties are emissivity and thermal conductivity
- The least sensitive parameter is the convective heat transfer coefficient.

They found conversion time becomes successively longer as the thermal conductivity of the biomass increases and/or emissivity decreases. The yield of volatiles and gases is a maximum for sphere and is least for slab, while the other yields are more for slab and is least for sphere. Thunman *et. al.* derived a model to calculate the effective thermal conductivity applied to different stages of combustion of wood. They also developed two principle models of thermal conductivity and validated by a comparison with direct numerical simulation of the fibre structure. The effective thermal conductivity is estimated from temperature, density, moisture content and shrinkage of solid material [86].

Marias *et. al.* developed kinetic model as well as further char oxidation is reported [87]. Degradation of biomass with time has modeled and validated with the experimental results of Tabare *et. al.* [88].

Di Blasi developed a kinetic and mass, momentum and energy transport model for thermal degradation of wood slab which is being heated radioactively. The kinetic scheme proposed has different zones first is virgin biomass region where slow flow of pyrolysis takes place second in which primary decomposition is considered as the reaction temperature was relatively low and third the char undergoes to secondary decomposition and temperature being high in this region. The effect of kinetic data and activation energies of primary and secondary reactions were also analyzed. Author has reported the values of all kinetic parameters as well as the heat of reaction for each reaction [77].

Sadhukhan *et. al*. proposed transient heat transfer model with kinetic model. FVM with implicit scheme for temporal equations has been used for discretization and simplified equations have been solved using TDMA [89]. They also developed a transient model for large biomass particles as well as a kinetic model with primary and secondary reactions [90]. Simulation has carried out to see the effect of final reactor temperature and particle size on pyrolysis time and char yield. It is reported that by increasing the final temperature char yields decreases and volatile yield increases and at the same final temperature. Park *et. al.* found the dependency of product concentration (Char, Gas, tar) on the heating rate. The pyrolysis mechanism is modified when the heating rate changes. They also studied on the effect of final pyrolysis temperature on the yield distribution and found that with the increase in temperature char yield reduces and increase in the yields of the other fractions [91].

Sun *et. al.* employed a first order kinetic model to describe biomass flash pyrolysis characteristics and the pertinent kinetic parameters were determined. Numerical

simulation of pyrolysis process was carried out, the predicted yields of produced gases agreed reasonably with the investigational data [92].

Csukás *et. al.* studied a dynamic simulation model has developed based on a four-step degradation scheme, considering four cracking product fractions (gas, naphtha, middle distillate and heavy oil) and their hydrocarbon conformation (paraffin, olefin and aromatic). Genetic algorithm was used for the estimation of kinetic and stoichiometric model parameters [93].

Meng *et. al.* developed an unsteady state 1-D model of pyrolysis of sawdust in a packed bed. The model consists of mass, energy and momentum balance of solid and gas in the bed. Primary pyrolysis cracking is assumed in the kinetic model. Implicit FVM method has been used to discretization and RK fourth order method has been adopted to solve the algebraic equations. It is suggested by the author to consider secondary reactions to analyze the insight of the process the volatile flow in the void. It is reported that by increasing the gas temperature pyrolysis rate can be increased that is the time of decomposition decreases significantly [94]. Olaleye *et. al.* developed a 2D dynamic model in a two stage fixed bed pyrolyzer and reported that experimentally hydrogen, char and tar yield [95]. Chowdhury R. estimated kinetic parameters for fixed bed pyrolysis of jute wastes in the temperature range of 400 ˚C - 900 ˚C [96]. Chen *et. al.* in performed slow pyrolysis experiments in fixed bed pyrolyzer to determine effect of heating rate (at 700 ˚C), to estimate kinetic parameter and also to characterize the products of moso-bamboo [97]. It is reported that as heating rate increases the activation energy, phenolic content in the bio-oil and also increases. Pozzobon *et. al.* modelled a 2D unsteady state model for pyrolyzer for biomass (beech wood particles). It is reported that

the high temperature char forces steam out of the sample bed which makes the char steam gasification possible. Experiments for thermally thick biomass with certain specifications are reported [98]. Boriouchkine *et. al.* developed a dynamic model of pyrolysis to comprises energy, mass, momentum as well as the kinetics equations for both primary and secondary pyrolysis reactions of spruce debarking residue. Simulation results shows that by increasing particle size and nitrogen flow rate increase the liquid yield as well these parameters increase the amount of untreated biomass because of the cooling effect of the nitrogen [99].

2.2 Experimental Studies on Biomass pyrolysis

Nelson *et. al.* observed the pyrolysis of polyethylene and polypropylene in an exploratory fashion. Analysis of gas products formed was done by GC. The analysis showed the presence of hydrogen, air, carbon monoxide and methane [100]. Fujimaki *et. al.* observed the pyrolysis of sulphur and cysteine containing amino acids resulted in the identification of 7-8 volatile compounds including methyl-thiazolidine. From the pyrolysis of methionine eleven volatiles were identified with degradation schemes [101].

Tran and Charanjit found that biomass is a mixture of structural constituents (hemicelluloses, cellulose, and lignin) and minor amounts of extractives each constituent pyrolyze at different rates and by different mechanisms and pathways. It is reported that as the reaction progresses the carbon becomes less reactive and forms stable chemical structures, and consequently the activation energy increases as the conversion level of biomass increases [102].

Table 2.1 Kinetic parameters of various types of kinetic schemes

Sr no.	Type of kinetic scheme	Kinetic model	Kinetic parameters		Reference
			K_i (s^{-1})	E (kJ/mol)	
1	One-step global models	$\text{Solid} \rightarrow \text{Products}$	0.0000283 $(T \leq 563K)$	-	Bilbao *et. al.* [103]
			8.31 x 10^5 $(563 < T \leq 673K)$	24.21	
			$0.0113\,(T > 673K)$	-	
2	one-step multi-reaction models	$\text{Solid} \rightarrow (\text{products})_i$ where i = gases, tars and char	8.607×10^5	88.6	Thurner *et. al.*[71]
			2.475×10^8	112.7	
			4.426×10^7	106.5	
3	two-step semi-global models	$\text{Solid} \rightarrow \text{Gases}_1$	1.3×10^8	140	Chan *et. al.* [72]
		$\text{Solid} \rightarrow \text{Tars}_1$	2.0×10^8	133	
		$\text{Solid} \rightarrow \text{Char}_1$	1.08×10^7	121	
		$\text{Moisture} \rightarrow \text{Water}$	5.13×10^6	87.9	
		$\text{Tars}_1 \rightarrow \text{Gases}_2 + \text{Char}_2$	1.48×10^6	144	
		Biomass —Reaction 1→ **Active Biomass**	2.8×10^{19}	242.4	Di Blasi [63, 104]
			1.3×10^{10}	150.5	
		Active Biomass —Reaction 2→ **Tar**; —Reaction 3→ **Char + Gases**	3.28×10^{16}	196.5	

		Biomass Component Reaction 1 Reaction 2 (volatiles + gases)$_1$ + (charcoal)$_1$ Reaction 3 (volatiles + gases)$_2$ + (charcoal)$_2$	$K_1(s^{-1}) = A_1 \exp[(-D_1/T) + (L_1/T^2)]$ $A_1=3.28\times10^{-5}$, $D_1=17254.4$ K and $L_1=-9061227$ K^2		Babu and Chaurasia [49-54]
			$K_2(s^{-1}) = A_2 \exp[(-D_2/T) + (L_2/T^2)]$ $A_2=1.068\times10^{-3}$, $D_2=10224.4$ K $L_2=-6123081$ K^2		
			$K_3(s^{-1}) = A_3 \exp(-E_3/RT)$ $A_3=5.7\times10^5$, $E_3=81$ kJ/ mol		
			168.4	51.965	Sadhukhan *et. al.* [89, 90]
			13.2	45.96	
			5.7×10^6	92.4	
4	One step apparent global kinetic model	$\text{Solid} \rightarrow (\text{Tars})_1 + \text{Char} + \text{CO} + \text{CO}_2 + \text{H}_2 + \text{CH}_4$ $\text{Tars}_2 \rightarrow (\text{Tars})_1 + \text{H}_2\text{O} + \text{CO} + \text{CO}_2 + \text{H}_2 + \text{CH}_4$	1.516×10^3	105	Di blasi [46, 77, 105] and Patra *et. al.* [106]
			4.28×10^6	107	
		$\text{Solid} \rightarrow \text{Products}$	5×10^6	120	Bonnefoy *et. al.*[107]
		$\text{Solid} \rightarrow \text{Products}$	1.2×10^8	108.78	Roberts [69]

Sakuma *et. al.* observed the pyrolysis of cellulose under various conditions like pyrolysis in the presence of nitrogen and air separately. Maximum products were found to be more in nitrogen [108]. Shafizadeh defined that the conventional pyrolysis is a process that occurs at slow heating rate. This condition permits the production of solid, liquid, and gaseous pyrolysis products in significant proportions [109]. Corte *et. al.* observed the pyrolysis of woody biomass at a heating rate of 250 ˚C/s, 300 ˚C/s and vapor residence time of less than one second. Characterization and weight contents were found. Result of gas species distribution could be controlled by water content, catalyst and temperature [110].

Beaumont described the qualitative and quantitative composition of the most volatile part of pyrolytic oil from flash pyrolysis [111]. Rocha *et. al.* [112] and Barth [113].found that hydro-pyrolysis (pyrolysis in a hydrogen atmosphere) is also considered to have a potential application in the conversion of biomass to liquids enriched in hydrocarbons

Degroot *et. al.* observed the heating of wood at 250 ˚C on a thermal balance and characterization of gasses formed was carried out by FTIR. 60% of weight loss is accounted by five compounds water, carbon dioxide, methanol, acetic acid and formic acid. The decomposition of uronic acids is easily achieved leading to formation of these products [114]. Avenell *et. al.* concluded the pyrolysis of peat in a 200 kW pyrolyzer for 70 min. The maximum temperature was attained after 40min and carbon monoxide emission level rose with increasing temperature [115]. Sipila *et. al.* observed the characterization of pyrolysis oil from flash pyrolysis of straw, pine and hardwood. Co-

relation between physical properties and chemical compositions were drawn. Water soluble fractions were extracted by diethyl ether [116].

Bridgwater *et. al.* found that lignin decomposes over a wider temperature range compared to cellulose and hemicelluloses, which rapidly degrade over narrower temperature ranges. Thermal degradation properties of hemicelluloses, cellulose, and lignin can be summarized as follows [31]

Thermal degradation of hemicelluloses > cellulose > lignin.

Sensoz *et. al.* performed the pyrolysis of rape seed (brassica napus L) in a pyrolysis reactor at 500 ˚C and heating rate of 30 ˚C/min. Effects of particle size on yields were investigated. The HHV of pyrolysis oil was found to be 38.4 MJ/kg. FTIR analysis showed that the pyrolysis oil was highly dominant with oxygenated species [117].

Williams and Nugranad carried out the pyrolysis of Rice husks in a fluidized bed reactor at 400 ˚C, 450 ˚C, 500 ˚C, 550 ˚C and 600 ˚C in presence of catalyst zeolite ZSM 5. Molecular weight distribution of oils were decreased after catalysis and kept decreasing with increase in temperature [118].

Koçkar *et. al.* conducted experiments on the fixed bed fast pyrolysis of hazelnut shell circa. The results showed that in a fixed bed heinze the maximum oil yield was of 22.5 wt % at optimum temperature of 550 ˚C and at a heating rate of 5 ˚C/min. Chemical class composition of oil was determined by liquid column chromatographic fractionation and the column was successfully eluted with pentane, toluene and methanol to produce aliphatic, aromatic and polar fractions [119]. Yorgun *et. al.* conducted the pyrolysis of sunflower under flash pyrolysis in a tubular transport reactor. They investigated that

pyrolysis temperature, particle size and sweep gas flow rate on yield of bio-oil. Maximum bio-oil yield was 45 wt % [120].

Demirbas observed the conversion of biomass into liquid, charcoal, non-condensable gasses, acetic acid by heating to 475 ˚C. He observed maximum liquid yield at low temperatures, higher heating rate and short residence time for gasses [11]. Sansoz *et. al.* experimented on pyrolysis of pine in a fixed bed reactor. The parameters measured the effects of heating rate and pyrolysis temperature. They observed increase in pyrolysis conversion from 450 ˚C to 500 ˚C is due to volatilization of cellulose and hemicellulose [121]. Thermal de-polymerization and degradation of biomass, cellulose, hemicelluloses, and products were formed as well as a solid residue of charcoal. The mechanism of the pyrolytic degradation of structural components of the biomass samples were separately studied [122]. The hemicelluloses break down first, at temperatures of 200 ˚C to 300 ˚C, and cellulose follows in the temperature range 240 ˚C to 375 ˚C, with lignin being the last component to pyrolyze at 375 ˚C to 500 ˚C. Lignin gives higher yields of char and tar from wood, although lignin has higher methoxyl content than wood. Demirbas *et. al.* conducted flash pyrolysis of tobacco stalk and yellow pine. They found that on increasing the temperature from 400 ˚C to 750 ˚C the char yield decreased from 33.9 wt % to 23 wt % and 29.2 wt % to 17 wt % for tobacco stalk and yellow pine respectively. He also found that the liquid yield increased till 400 ˚C then decrease. The maximum yields were 43% and 48.7% for tobacco and yellow pine [122]. Demirbas carried out pyrolysis (conventional, fast and flash) of coal and found parameters affecting yield of bio-oil based on different temperatures [33]. Demirbas also observed the pyrolysis of beech trunk bark [123].

Chen *et. al.* conducted pyrolysis using an atmospheric pressure TGA apparatus and a fixed bed reactor. They found TGA results pyrolysis can be identified as three phase's- moisture evaporation, main de-volatilization and continuous de-volatilization whereas fixed bed pyrolysis results show that producer gas is an important product up to 60 wt % and is a high quality gas source with low tar concentration [78].

Miao *et. al.* and Hasan *et. al.* carried out the pyrolysis of euphorbia macrolada in a laboratory scale fixed bed reactor. They summarized the highest yield of bio-oil was 24.1 wt % at a temperature of 550 ˚C with heating rate of 10 ˚C/min. The highest conversion of 78 wt % was obtained at 700 ˚C at heating rate 30 ˚C/min [124] [125].

Ozlem *et. al.* summarized that the pyrolysis of walnut shell in a fixed bed reactor (fast pyrolysis). The oil yield increased up to a temperature of 500 ˚C after which it decreased. Maximum oil yield of 31.2 wt % was achieved at 500 ˚C and a heating rate of 300 ˚C/min [126]. Zhang *et. al.* observed pyrolysis of waste paper in a tubular furnace reactor at different temperatures, heating rates. They observed that the maximum bio-oil yield was of 49.13 wt % at 420 ˚C with heating rate of 30 ˚C/min. Through characterization by spectroscopy four different main components found were anhydro sugars, carboxyl compounds, carbonyl compounds and aromatic compounds [127].

Putun *et. al.* observed pyrolysis on cotton seed cake in static, nitrogen and steam atmosphere was carried out to check the influence of different atmospheres on the yield. They noticed that pyrolysis under water vapour give a rising yield as opposed to pyrolysis under nitrogen and under steam atmosphere. They found that steam inhibits the secondary cracking reaction at higher temperatures and registers a higher yield of bio-oil at high temperatures [128]. Demiral and Sensoz conducted pyrolysis using hazelnut

extracted bagasse in a fixed bed reactor under static, nitrogen atmospheres. The highest yield of bio-oil was 34.40 wt % at a temperature of 500 ˚C with heating rate 10 ˚C/min [129]. Tian *et. al.* carried out pyrolysis on corn stalk in a TGA apparatus. They observed that the pyrolysis of corn stalk reduced a volatiles precipitated more easily resulting in pyrolysis rate gradually increasing [130].

Xiaoya *et. al.* carried out pyrolysis of fir sawdust. They concluded that on the addition of microwave absorption medium, the size reduction of feed particles was not required as particle size doesn't affect rate of pyrolysis and bio-oil yield [131] [132].

Bologa *et. al.* found volatiles namely oil mist by electrostatic precipitator Carola. It operates on the principle of unipolar particle charging in the Corona discharge and particle precipitation under the field of space change. The operating voltage of the precipitator was 10-12 KV and Corona current of 1mA. Efficiency was 97-99.5% [133]. Aho *et. al.* found that softwood carbohydrates were pyrolyzed in fluidized bed reactor. They observed that on increasing temperature at the rate of 278 ˚C /min until 480 ˚C was achieved after which at constant temperature the release of non-condensable gasses [134].

Ateş & Işıkdağ characterised bio-oil using liquid column chromatographic technique to determine the chemical class compositions of the oil, and used NMR, GC and MS to determine different constituents of the oil. He also studied the influence of temperature on the composition of oil [135].

Garcia-Perez *et. al.* studied the water content of bio-oil is determined with Karl Fisher titration, which showed a minimum at 450 ˚C at which the bio-oil yield peaked. The chemical compounds such as furans, phenols, carboxylic acids, alcohols, aldehydes, ketones, and sugars of about 35 compounds are identified using GC-MS which was

accounted up to 34 wt % of the compounds present in the studied bio-oils . Thermo-gravimetric analysis and UV-fluorescence spectroscopy were performed to obtain the content of lignin-derived oligomers [136].

Mullen *et. al.* analyzed water content in bio-oil. Calorific values of the feedstock, bio-oil, and bio charcoal were determined. Elemental analyses (C, H, N, S) of the feed stocks and products were determined. Oxygen was then determined by difference after accounting for C, H, N, S and ash. Ash was determined as the percentage remaining after heating a sample in a muffle furnace in air to 650 ˚C for 6 hour. Bio-oil viscosity and pH were measured [137].

Demirbas carried out LC-MS on different biomass feed stocks to show the main constituents of biomass were aromatic, aliphatic, naphthenic hydrocarbons and oxygenated compounds such as phenols, furans, alcohols, acids, ethers, ketones and aldehydes. He observed hemicellulose degradation followed by cellulose and ending with lignin from 200 ˚C to 500 ˚C [133]. Demirbas pyrolysis was carried out on hazelnut shell, beech wood, spruce wood and organic fraction of MSW. The observed samples were pyrolyzed to produce char, liquid, vapor at different temperatures. Char yield decreased as the temperature was increased highest liquid yield was observed between 375 ˚C and 525 ˚C. Char yield at 225 ˚C [139].

Haykiri *et. al.* conducted pyrolysis of different feedstock (sunflower shell, colza seed, cotton refuse and olive refuse) in a TG apparatus (Non-Isothermal) to obtain pyrolysis oil. They stated the lowest char yield was observed for sunflower shell due to low ash content of the feed whereas olive refuse observed the highest amount of char because of highest ash content [140]. Leite *et. al* perfomed trans-esterification using

Jatropha gossypiifolia and *Jatropha Curcas*. Result showed the oil content of *curcas* is 32 mass% and *gossypiifolia* 24 wt % are relatively higher than soya bean, cotton seed and other commercial oil sources indicating a fuel similar to diesel [141].

Xinbao *et. al.* reported the results of characterization of bio-oil by GC-MS and its mix with iso-paraffin and ethanol, respectively. They found that iso-paraffin increases the yield of bio-oil significantly. Xiqiang *et. al.* [142] in 2009 reported pyrolysis of straw in a microwave TG analyser. Volatile Components were released in highest percentage between the range of 210 ˚C and 480 ˚C. After 480 ˚C 80-93% of volatiles were released [143].

Wu *et. al.* conducted pyrolysis of rice straw, corn stalk in macro TG analyser. They observed that biomass physical properties such as biomass type, particle size and ash content are influential in biomass isothermal pyrolysis characteristics, large particle size needs more pyrolysis time leading to more char yield [144]. Demirbas summarized the results of pyrolysis of biomass. Between 350 ˚C and 500 ˚C the charcoal yield decreases with increasing temperature and maximum liquid yield is obtained between 350 ˚C and 450 ˚C [145].

Liu *et. al.* performed the pyrolysis of corn straw in fluidized bed reactor. The maximum bio-oil yield noted was 42 wt % at 520 ˚C to the vapour residence time of 0.8 s. The characterization by GC/MS showed a large presence of oxygen [146]. Li *et. al.* observed fast pyrolysis of biomass. They concluded volatile, ash and oxygen content in chars per higher than that of activated carbon and hence activation pre-treatments were required for char to equally achieve activity of active carbons [147]. They, also reported the study on the pyrolysis of shattered wood and maize straw in a rotating cone reactor

and observed the highest yield of bio-oil was 54.83 wt % and 48.3 wt % respectively. The char, bio-oil, vapors were separated by fractionation [148].

Bahri *et. al.* found that pyrolysis of palm oil industry solid waste in a tube reactor. The production of bio-oil increases as temperature is increased and char production decreases with increase in temperature. Maximum bio-oil yield of 58.75 wt % was achieved at 600 ˚C [149]. Xinbao *et. al.* found that the pyrolysis of pine saw dust in a vacuum pyrolyzer. At 200 ˚C carbon dioxide and carbon monoxide were the only gasses present in the off gas. Below 300 ˚C there were more volatiles and large presence of organic acids. Maximum bio-oil yield obtained was 47.81 wt % between 300 ˚C and 400 ˚C. The presence of large molecules like aromatic compounds increased and volatile compounds decreased [150].

Demirbas conducted pyrolysis of various feed stocks (hazelnut shell, beech wood, spruce wood and organic fraction of MSW). Higher heating value varies from 22.5 to 25.7 MJ/kg. With increase of lignin content the HHV of pyrolysis oil increases [151]. Gozde Duman and Cagdas Okutucu observed the pyrolysis (slow and fast) of pungam oil cake in an electrically heated fluidized bed reactor at different temperatures. Fast pyrolysis maximum bio-oil yield was 44 wt % at 500 ˚C whereas from slow pyrolysis maximum yield was 21 wt % at 500 ˚C. Results show that fluidized bed reactors are most suitable for fast pyrolysis [152].

Montes *et. al.* combusted *Jatropha curcas* seeds in a muffle furnace and characterize the composition of products by GC. The end product formed is bio-diesel. HHV of *Jatropha* was similar to diesel [153]. Keles *et. al.* [8] published that the pyrolysis of hazelnut cupula in a fast pyrolysis fixed bed reactor. The optimum temperature of 600

˚C was found over a range of temperatures to be best suited for maximum oil yield of hazelnut cupula. As the particle size was increased an initial increase in bio-oil was noticed but then gradually decreased.

Amutio *et. al.* carried out product analysis by analyzing the reactor outlet stream by means of a gas chromatograph equipped with a flame ionization detector (FID). To avoid the condensation of heavy oxygenated compounds, the line from the reactor outlet to the chromatograph is heated to a temperature of 280 ˚C. Non-condensable products were monitored using a micro gas chromatograph. This micro-GC has also been used to measure the water yield [154]. Dengxiang *et. al.* were compiled that the pyrolysis of saw dust in a laboratory scale reactor. The experiment found with increased feeding rate of saw dust, the char yield increase gradually and maximum yield of bio-oil and gasses were attained at feeding rates of 1.36 g/min [155].

Li *et. al.* conducted experiments on pyrolysis of populous tomentosa black liquor. The bio-oil produced was characterized by GC/MS. Liquid products increased with the temperature. The product characterized was 16-phenolics, 6-ketones and 2-olefinic matter at a temperature of 500 ˚C [156]. Longchao, Fengwen found that the pyrolysis of soybean oil in a continuous fixed bed reactor. Maximum yield of the bio-oil was noted at 450 ˚C to be 76 wt %. In the presence of CaO catalyst soybean had increased behaviour similar to diesel [157].

Sijin *et. al.* stated that the pyrolysis of biomass lignin, cellulose and hemicellulose was pyrolized in TGA. The results show that the weight loss occurred in following order- hemicellulose, cellulose and lignin. The introduction of UF resin inhabited the decomposition of cellulose and spurred decomposition of lignin with little

effect on hemicellulose [158]. Li *et. al.* conducted pyrolysis in a tubular furnace pyrolysis reactor. Effect of temperature and heating rate on yield parameters were measured. It was observed that the maximum yield of bio-oil was 44.85 wt % at 450 ˚C with the heating rate of 30 ˚C/min. Characterization was conducted by spectroscopy methods and chromatographic methods [156].

Engr *et. al.* found that the report on the pyrolysis of seeds of wheat crop in a fixed bed reactor. They summarized that the bio-oil produced was has a calorific value near the calorific value of furnace oil (35.7 kJ/kg) [159].

Günay *et. al.* quantified that the pyrolysis of beech wood in presence of acid catalyst in a fixed bed pyrolysis reactor. The introduction of the catalyst ($FeCl_3$) increased yield of aldehydes and conversely decrease the yield of alcohols and phenols [160]. Punsuwan *et. al.* found that coking coal, and woody biomass yellow poplar. TG & TBR analysis were conducted under non-isothermal and isothermal conditions. The coking coal pore development mechanism can be explained by- formation of new pores through gas evolution to pore growth by bubble expansion. This paper found that weak coking blend has a micro pore structure, whereas the high coking blend has a macro pore structure [161].

Poddar *et. al.* found that the pyrolysis of castor seeds in a semi-batch reactor. The bio-oil yield was maximum 62.45 wt % at 450 ˚C with a calorific value of 36.5 MJ/kg similar to HHV of diesel [162]. Jeong *et. al.* observed that the pyrolysis of newspaper waste in a packed bed pyrolyzer. The effects of pyrolysis temperature on HHV is directly proportional to HHV of char increases from 30-34 MJ/kg over a temperature range of 300

˚C -500 ˚C, beyond which the HHV decreases to 23 MJ/kg as temperature reaches 900 ˚C [163].

Xie *et. al.* found that the pyrolysis of biomass in a three-zone free-fall reactor. Cassava pulp residue gives higher volatiles and lesser char than residues of palm kernel and palm shells. The char calorific value hit a peak of 29.87 MJ/kg [164].

Ates *et. al.* found that the pyrolysis of waste jute sacks and sesame oil cake in a long tubular type semi-batch reactor. It was observed that tar yield increased over the range of 300 ˚C to 500 ˚C after which it gradually decrease. The char yield decreased up to 600 ˚C after which it increase, whereas gas yield increased from 300 ˚C to 900 ˚C. They found maximum oil-yield 31.9 wt % at 500 ˚C from the pyrolysis of wheat straw with mesoporous materials as catalyst in a nitrogen atmosphere [165]. Murugan and Gu researched the contributions of the Indian scientific community on the research of pyrolysis over the last three decades. In their work they concluded that India has got infinite potential for biomass [166]. Gorlistsky *et. al.* observed the yield of switch grass in fall harvesting period over the period of September to November for improving quality without reduction in biomass yield. Observation showed October at the highest yield [167].

Bhaskar *et. al.* found that the pyrolysis of cow manure in a fluidized bed reactor give a maximum yield of 53.75 wt % at 400 ˚C. It was observed that the higher water content existed in bio-oil extracted from cow manure as opposed to other biomasses [12].

2.3 Research gaps

The kinetics of thermal decomposition of biomass material is complicated, as it involves a large number of reactions in parallel and series. Different classes of mechanisms are reported for the pyrolysis of wood and other ligno-cellulosic materials. The models are classified into three categories: one-step global models; one-stage multi-reaction models; and two-stage semi-global models. The second category of models discuss those mechanisms, which consider simultaneous and competing first order reactions in which virgin biomass decomposes into different constituents of pyrolysis products, namely, tar, char, and volatile gases. The third class of models consider pyrolysis to be a two-stage reaction, in which the products of the first stage break up further in the presence of each other to produce secondary pyrolysis products [28]. These reported kinetic studies are limited to use for certain species of biomass only for which kinetic data is available. Limited work has been done to describe the pyrolysis process by the independent parallel first order reactions model. Also, the degradation of biomass is described as the decomposition of its components *i.e.* cellulose, hemicellulose and lignin. However, they have not incorporated individual biomass constituent's decomposition in their kinetic model. Biomass constituent's decomposition with moisture release phenomenon and order of degradation of biomass constituents are also not reported in the literature yet. Hence, it is necessary to incorporate the moisture release phenomena in the kinetic scheme itself to predict the pyrolysis process accurately and prediction of order of degradation of biomass constituents.

As far as apparent kinetic model is concerned, the limitation of one step single reaction global apparent kinetic model is the false prediction of product yields variation

with increase in the temperature. It predicts the continuous increase in the yields of bio oil, gas and char with temperature, which is not observed experimentally. It is observed that the yield of bio oil increases as the temperature increase till 550 ˚C - 600 ˚C and after that it decreases as the cracking of volatile products takes place increasing the yield of gaseous products. Hence, to predict the correct value of yield for various products, one or more step multi reaction global kinetic model is needed.

It is evident that the applicability of TGA study based kinetic models are limited and can be used only for small size (less than 1 mm) particles, which are undergoing kinetically controlled devolatilization. The pyrolysis of large size particles is controlled by heat and mass transport within the particle. To predict the rate of devolatilization and yield of products for the pyrolysis of large size particles, one has to develop the particle model and incorporate it into the reactor model. The alternative to this approach is the development of apparent kinetic model for the pyrolysis process and use it without particle model development. To understand the pyrolysis process it is must to develop the apparent kinetic model and fixed bed model, conventional thermo-gravimetric analysis (TGA) results of biomass cannot be used.

Many of the researchers worked on characterization of bio-oil generated from the pyrolysis of various biomass resources such as wood, rice husk, mustard cake and other de-oiled cakes. However, very limited work has been done on the characterization of bio-oil collected from pyrolysis of *Jatropha curcas* de-oiled cake. It has been observed that the characterization of whole bio-oil leads to difficulty in identifying the exact components even with GC-MS. Very few researchers have used liquid column chromatographic technique to separate out the aliphatic, aromatic and polar compounds

followed by GC-MS to determine different constituents of each fraction [135]. Based on the literature survey carried out, it is suggested to separate the bio-oil compounds using liquid column chromatography. The results of FTIR, GPC, and H-NMR can be better understood if bio-oil is separated into various fractions in comparison to whole bio-oil. For identifying the compounds, the aliphatic, aromatic portions and polar fraction can be analyzed with GC-MS.

2.4 Scope of work

The use of abundant biomass waste is a big concern to the society. Thermo-chemical conversion is most prominent route to produce valuables from the biomass. There is a need of biomass pyrolysis is to be carried out to produce the bio-oil. To understand the pyrolysis of biomass a generalized mathematical model for fixed bed pyrolyzer (macro TGA) is to be developed which takes into account of the limitations of the earlier studies. For the successful operation of the pyrolyzer, prediction of the rate of biomass devolatilization and yield of pyrolysis products is crucial. In general, the kinetics of biomass pyrolysis is developed by conducting the thermo-gravimetric analysis (TGA) experiments but still limited work is done on prediction of order of degradation of biomass constituents with incorporation moisture release phenomena. Hence there is need to develop a kinetic model with moisture release inclusion to predict the order of degradation of biomass constituents as well as yield of products. To validate this type of model TGA experiments is to be carried out.

The applicability of this kinetic of model is limited and can be used only for small size particles, which controlled by kinetically devolatilization. For large size particles the

heat and mass transport within the particle played an important role. To predict the rate of devolatilization and yield of products for the pyrolysis of large size particles, there is a need of development of apparent kinetic model for fixed bed pyrolizer. This developed model could be an important contribution in the scientific literature to predict the pyrolysis process behavior and their product yields either for an independent operation or as a step/zone in the pyrolysis process operation. It can be further utilized for dynamic optimization for improving the performance of the system on a continuous basis. To validate this, pyrolysis experiments of large particle size biomass is to be carried out in laboratory fixed bed pyrolyzer.

For maximum utilization of the bio-oil by extracting the valuable chemical compounds presents in bio-oil, it is necessary to understand its composition and properties. Based on the gaps in literature, it is suggested to separate the bio-oil compounds in aliphatic, aromatic and polar compounds using liquid column chromatography. The analysis of oil requires various spectroscopic and chromatographic methods due to the limitations of the individual analytical techniques. The functional groups of bio-oil can be detected by Fourier transform infrared (FTIR) spectroscopy and components are identified by gas chromatography and mass spectroscopy (GC-MS).

CHAPTER – 3

MATHEMATICAL MODEL DEVELOPMENT AND SIMULATION

3 Mathematical Model Development and Simulation

In this chapter, the mathematical model development and simulation is described in two sections 3.1 Model development for biomass pyrolysis and section 3.2 Simulation of biomass pyrolysis. In the section 3.1, model development of pyrolysis is divided in to three sections i.e. section 3.1.1 kinetic model development, section 3.1.2 apparent kinetic model development and section 3.1.3 fixed bed model development**.** In the section 3.2, simulation methodology of all the models is discussed.

3.1 Model development for biomass pyrolysis

3.1.1 Kinetic model development

In the present study, the multi reaction individual biomass constituent (*i.e.* cellulose, hemicellulose and lignin) decomposition based kinetic model with incorporation of moisture release phenomena is proposed for pyrolysis of biomass. Each biomass constituent, i.e. cellulose, hemi-cellulose and lignin get decomposed by two parallel

independent first-order reaction producing volatiles & gases and char. The volatiles and gases may further react with char to produce different types of volatiles, gases and char where the compositions are distinct. Hence, products of the primary pyrolysis undergo secondary interactions, producing a modified final product distribution. The moisture evaporation is also included in the model.

The kinetic model is described below by Eqs. (3.1) and (3.2):

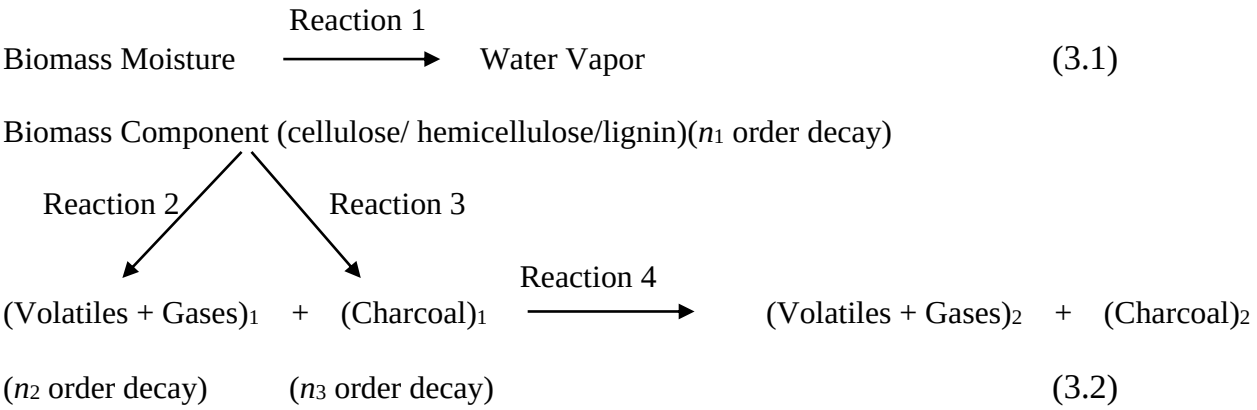

The kinetic equation for the moisture evaporation is described in Eq. (3.3).

$$r_1 = k_1 B_M \tag{3.3}$$

The kinetic equations for the mechanism, shown above are represented by Eqs. (3.3) to (3.6).

$$r_{2i} = k_{2i} B_i^{n_1} \tag{3.4}$$

$$r_{3i} = k_{3i} B_i^{n_1} \tag{3.5}$$

$$r_{4i} = k_{4i} G_{1i}^{n_2} C_{1i}^{n_3} \tag{3.6}$$

To find the kinetic parameters of the above-mentioned reactions, the square of the error between the experimental data of thermo-gravimetry of *Jatropha curcas* de-oiled cake and model predicted values of residual weight fraction are minimized. The residual weight fraction is defined as given in Eq. (3.7)

$$\text{Residual Weight Fraction}(W) = \frac{(\text{Residual Weight})}{(\text{Initial Weight})} \tag{3.7}$$

To find the residual weight fraction theoretically, net rate of production of different species by reaction 2 & 3 of the proposed kinetic model in terms of rate of reactions are found. Due to small size (1.84 mm) of the *Jatropha curcas* de-oiled cake taken in the TGA experiments, the secondary reaction (reaction 4) is neglected. The residual weight fraction is calculated using Eq. (3.8).

$$W_{\text{total}} = B_{\text{M}} + W_{\text{C}} + W_{\text{HC}} + W_{\text{L}} \tag{3.8}$$

$$W_{\text{i}} = B_{\text{i}} + C_{1\text{i}} \qquad \text{for i = cellulose (C), hemi-cellulose (HC) and lignin (L)} \tag{3.9}$$

Using Eq. (3.3), the rate of change of biomass moisture is given by Eq. (3.10).

$$\frac{dB_{\text{M}}}{dt} = -k_1 B_{\text{M}} \tag{3.10}$$

Using Eqs. (3.4) & (3.5), rate of change of biomass constituents are given by Eq. (3.11) and rate of production of char is given by Eq. (3.12).

$$\frac{dB_{\text{i}}}{dt} = -\left(k_{2\text{i}} + k_{3\text{i}}\right) B_{\text{i}}^{n_i} \tag{3.11}$$

$$\frac{dC_{1\text{i}}}{dt} = k_{3\text{i}} B_{\text{i}}^{n_i} \tag{3.12}$$

Hence, change of residual weight fraction with time [Eq. (3.13)] is obtained by addition of Eq. (3.11) & Eq. (3.12).

$$\frac{dW_{\text{i}}}{dt} = -k_{2\text{i}} B_{\text{i}}^{n_1} \tag{3.13}$$

To find temperature (T) at a particular time (t), following equation [Eq. (3.14)] is used

$$T = (HR)t + T_0 \tag{3.14}$$

Differentiating Eq. (3.14) would result in Eq. (3.15)

$$dT = (HR)dt \tag{3.15}$$

Using Eq. (3.13) and Eq. (3.15), the relations of change of residual weight fraction with temperature is found and given by Eq. (3.16).

$$\frac{dW_{\mathrm{i}}}{dT} = -k_{2\mathrm{i}} B_{\mathrm{i}}^{n_i} \frac{1}{HR} \tag{3.16}$$

Using Eq. (3.11) and Eq. (3.15), the relation of change of biomass weight fraction with temperature is found and given by Eq. (3.17).

$$\frac{dB_{\mathrm{i}}}{dT} = -\left(k_{2\mathrm{i}} + k_{3\mathrm{i}}\right) B_{\mathrm{i}}^{n_i} \frac{1}{HR} \tag{3.17}$$

Arrhenius relation of kinetic constants with temperature is given by Eqs. (3.18 – 3.20) respectively for reaction 1, reaction 2 and reaction 3.

$$k_1 = A_1 \exp\left(\frac{-E_1}{RT}\right) \tag{3.18}$$

$$k_{2i} = A_{2i} \exp\left(\frac{-E_{2i}}{RT}\right) \tag{3.19}$$

$$k_{3i} = A_{3i} \exp\left(\frac{-E_{3i}}{RT}\right) \tag{3.20}$$

The values of the frequency factor and activation energy of all reactions are found by minimizing the objective function as given by Eq. (3.21). For the minimization, all data points (n) of a particular heating rate (10 ˚C/min to 60 ˚C/min) are considered to determine the kinetic parameters.

$$F\left(A_1, E_1, A_{2\mathrm{i}}, E_{2\mathrm{i}}, A_{3\mathrm{i}}, E_{3\mathrm{i}}, n_{\mathrm{i}}\right) = \sum_{\mathrm{j}=1}^{n} \left(W_{\mathrm{total,exp,j}} - W_{\mathrm{total,\ cal,j}}\right)^2 \tag{3.21}$$

3.1.2 Apparent kinetic model development

The kinetic model based on biomass degradation is proposed. Biomass gets decomposed by three parallel independent n^{th} order reaction producing volatiles & gases and char. The kinetic model is described by Eq. (3.22).

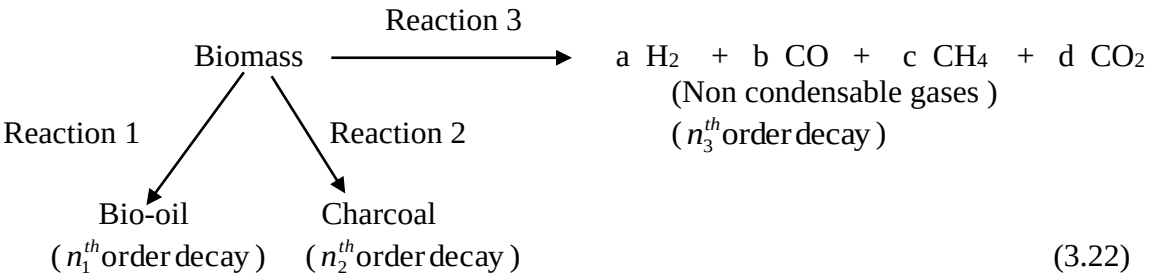

(3.22)

The kinetic equations for the mechanism, shown above are represented by Eq. (3.23).

$$r_i = k_i B^{n_i} \tag{3.23}$$

To find the residual weight fraction theoretically, net rate of production of charcoal by reaction 2 & next rate of consumption of biomass by both reactions 1 & 2 are found. The residual weight fraction is calculated using Eq. (3.24).

$$W = B + C \tag{3.24}$$

Using Eq. (3.23) & (3.24), rate of change of biomass constituents are given by Eq. (3.25) and rate of production of char is given by Eq. (3.27).

$$\frac{dV}{dt} = \left(k_V\right) B^{n_i} \tag{3.25}$$

$$\frac{dG}{dt} = \left(k_G\right) B^{n_i} \tag{3.26}$$

$$\frac{dC}{dt} = \left(k_C\right) B^{n_i} \tag{3.27}$$

$$\frac{dB}{dt} = -\left(k_G + k_V + k_C\right) B^{n_i} \tag{3.28}$$

Change of residual weight fraction with time [Eq. (3.29)] is obtained by addition of Eq. (3.30) & Eq. (3.31).

$$\frac{dW}{dt} = -\left(k_G + k_V\right) B^{n_i} \tag{3.29}$$

To find temperature (T) at a particular time (t), following equation [Eq. (3.30)] is used

$$T = (HR)t + T_0 \tag{3.30}$$

Differentiating Eq. (3.31) would result in

$$dT = (HR)dt \tag{3.31}$$

Using Eq. (3.29) and Eq. (3.31), the relations of change of residual weight fraction with temperature is found and given by Eq. (3.32).

$$\frac{dW}{dT} = -\left(k_G + k_V\right) B^{n_i} \frac{1}{HR} \tag{3.32}$$

Using Eq. (3.28) and Eq. (3.31), the relation of change of biomass weight fraction with temperature is found and given by Eq. (3.33).

$$\frac{dB}{dT} = -\left(k_G + k_V + k_C\right) B^{n} \frac{1}{HR} \tag{3.33}$$

Arrhenius relation of kinetic constants with temperature is given by Eqs. (3.34 – 3.36) respectively for reaction 1, reaction 2 and reaction 3.

$$k_G = A_G \exp\left(\frac{-E_G}{RT}\right) \tag{3.34}$$

$$k_V = A_V \exp\left(\frac{-E_V}{RT}\right) \tag{3.35}$$

$$k_C = A_C \exp\left(\frac{-E_C}{RT}\right) \tag{3.36}$$

The values of the frequency factor and activation energy of all reactions are found by minimizing the objective function as given by Eq. (3.37). For the minimization, all data points (*n*) of a particular heating rate are considered to determine the kinetic parameters.

$$F\left(A_{\mathrm{G}}, E_{\mathrm{G}}, A_{\mathrm{V}}, E_{\mathrm{V}}, A_{\mathrm{C}}, E_{\mathrm{C}}, n_{\mathrm{i}}\right) = \sum_{\mathrm{j}=1}^{n}\left(W_{\mathrm{total,exp,j}} - W_{\mathrm{total,\ cal,j}}\right)^2 \tag{3.37}$$

3.1.3 Fixed bed model development

A 2D (r, z) dynamic combined transport and kinetic model for the cylindrical fixed bed pyrolyzer is developed to understand the dynamic temperature variation and porosity variation in the fixed bed. The model consists of two partial differential equations (heat and volatile transport) and two ordinary differential equations (biomass decomposition and char generation). The model includes heat transfer from the reactor wall to biomass bed both by radiation as well as convection mode.

The bed made of *Jatropha curcas* de-oiled cake is assumed to be continuous (closely packed), and is in cylindrical shape. It is also assumed that there is a symmetry along the angular direction of the cylindrical reactor. The holder surface of the bed is heated directly by conduction, and the exposed area is heated indirectly via radiation which is facilitated by creating inert environment using nitrogen. Heating rate, particle size, final temperature of the furnace, are important parameters which has control over the product yield of the pyrolysis process, one of the objectives of current study was to study these parameters. The model presented is based on both mass and energy balances for the solid phase (biomass and char) and gas phase (tar and permanent gases). The assumptions taken to model the process are listed below:

1. Unsteady state two-dimensional system.
2. The bed is considered continuous hence spatial intra-particle gradients of temperature and concentration does not exists.
3. Particles are of the same size and shape.
4. The diffusion of volatiles in the bed is assumed to take place only in axial direction.
5. Biomass does not move at all and the velocity is considered zero.
6. At any given location, the temperature of the solids and volatiles is same

The schematic of fixed bed and the computation domain is shown in Figure 3.1 (a) and (b), respectively. The Figure 3.1 (b) represents the domain of interest discretized in M grids in *r* direction and N in *z* direction.

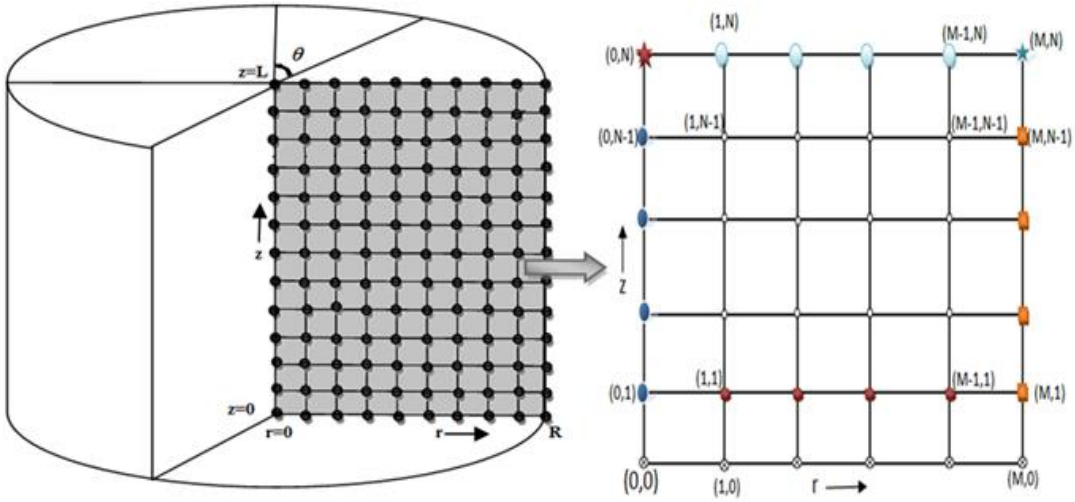

Figure 3.1 (a) Schematic of biomass bed (b) Computational domain

The energy balance equation is given by Eq. (3.38)

$$\frac{\rho_b C_P}{k}\left(\frac{\partial T}{\partial t}\right)=\frac{1}{r}\left(\frac{\partial T}{\partial r}\right)+\frac{\partial^2 T}{\partial r^2}+\frac{\partial^2 T}{\partial z^2}+\frac{\partial \rho_b}{\partial t}\left(\frac{\Delta H - TC_p}{k}\right) \tag{3.38}$$

Boundary Conditions are represented by Eqs. (3.39) to (3.42)

1.) At $r = 0$ $$\frac{\partial T}{\partial r} = 0 \tag{3.39}$$

2.) At $z = 0$ $$T_{rz} = T_{hs} \tag{3.40}$$

3.) At $r = R$ $$\sigma A\left(T_{\mathrm{rs}}{}^4 - T_{\mathrm{rz}}{}^4\right) = kA\left(\frac{\partial T}{\partial r}\right) \tag{3.41}$$

4.) At $z = L$ $$\sigma A\left(T_{\mathrm{rs}}{}^4 - T_{\mathrm{rz}}{}^4\right) = kA\left(\frac{\partial T}{\partial z}\right) \tag{3.42}$$

Initial Condition represented by Eq. (3.43)

$$T_{\mathrm{rs}} = 30\ ^\circ\mathrm{C} \tag{3.43}$$

Where T_{hs} is a function of T_{rs} which was derived from calibration curve plotted using experimental data are given by Eq. (3.44) and Eq. (3.45), respectively.

$$T_{\mathrm{hs}} = 1.001101 \times T_{\mathrm{rs}} + 5.50375 \tag{3.44}$$

And T_{rs} is a function of time as

$$T_{\mathrm{rs}} = 303.15 + 0.13056 \times t \tag{3.45}$$

Biomass and char are stationary and volatiles are diffusing in z direction hence the balances are given by Eqs. (3.46) to (3.51).

$$\frac{\partial \rho_{\mathrm{b}}}{\partial t} = -r_{\mathrm{biomass}} \tag{3.46}$$

$$\frac{\partial \rho_{\mathrm{v}}}{\partial t} = D_{\mathrm{AB}}\left(\frac{\partial^2 \rho_{\mathrm{v}}}{\partial z^2}\right) + r_{\mathrm{volatiles}} \tag{3.47}$$

$$\frac{\partial \rho_{\mathrm{c}}}{\partial t} = r_{\mathrm{char}} \tag{3.48}$$

Where,

$$r_{\text{biomass}} = A_{\text{p}} \exp\left(\frac{-E_{\text{p}}}{R_{\text{g}} T_{\text{s}}}\right) \rho_{\text{b}} \tag{3.49}$$

$$r_{\text{volatiles}} = 0.68 r_{\text{biomass}} \tag{3.50}$$

$$r_{\text{char}} = 0.32 r_{\text{biomass}} \tag{3.51}$$

Boundary conditions represented by Eqs. (3.52) to (3.55)

1. At $z = L$ $\qquad \dfrac{\partial \rho_{\text{v}}}{\partial z} = 0$ (3.52)

2. At $z = 0$ $\qquad -D_{\text{AB}} \dfrac{\partial \rho_{\text{v}}}{\partial z} = K(\rho_{\text{v}} - \rho_{\text{vb}})$ (3.53)

Initial condition represented by Eq. (3.54) to (3.55)

$$\rho_{\text{b}} = 601.2 \text{ kg/m}^3 \tag{3.54}$$

$$\rho_{\text{v}} = 0.0 \text{ kg/m}^3 \tag{3.55}$$

3.2 Simulation of biomass pyrolysis models

Simulation of biomass pyrolysis models is divided into 2 sections. In section 3.2.1 numerical methods and optimization schemes are discussed and in section 3.2.2 logarithmic differential evaluation (LDE) is discussed which is used to optimize the kinetic parameters is in. The simulation methodology of kinetic model, apparent kinetic model and fixed bed model is described in section 3.2.3.

3.2.1 Numerical methods and optimization technique

In energy balance equation, the heat is diffusing in radial and axial direction hence both the terms has discretized using central difference (FDM). The first order derivative has

handled using backward difference method because of stability issues. Boundary conditions have discretized using image point technique for convection terms and central difference for radiation boundaries.In mass balance equations only volatiles are diffusing as earlier mentioned which is again discretized using central difference method.

3.2.1.1 Optimization technique

It is reported that the kinetic parameter estimation of the non-isothermal pyrolysis of hazelnut shell is highly nonlinear and complex in nature [168]. Most of the gradient based traditional optimization algorithms may get trapped at local optimum based on the initial guess. Differential evolution (DE) is applied to find the global optimum set of kinetic parameters. The details of DE algorithm and pseudo code are available in the literature [2, 84, 169]. However, DE gives poor population distribution for cases where the range of limits is very wide (more than three orders of magnitude). In the present case of kinetic parameter estimation, lower and upper limits of frequency factors are 10^{10} and 10^{18} respectively. Hence, simple DE is modified first by including the logarithmic initialization (LIDE). The algorithm is further improved by incorporating the logarithmic mutation also and named as logarithmic DE (LDE). Optimum kinetic parameters are found by minimizing the objective function using simple DE, LIDE and LDE and obtained results are compared [170]. The key parameters of logarithmic DE are number of population (NP), crossover constant (CR) and scaling factor (F). The values used in the present case are: NP – 200, CR – 0.9 and F – 0.5. The limits of the frequency factors and activation energies are given below, which is chosen based on the available literature for kinetic modeling of different biomasses.

Limits of frequency factors (A_1, A_{2i} & A_{3i}) = (1.0e+2, 1.0e+18)

Limits of activation energy (E_1) = (1.0e+04, 2.5e+05)

Limits of activation energy (E_{2i}) = (1.0e+05, 2.5e+05)

Limits of activation energy (E_{3i}) = (1.0e+05, 2.5e+05)

3.2.1.1.1 Logarithmic DE (LDE)

To overcome the problem of population distribution, logarithmic mapping rule is used for initialization of normalized population and given by Eq. (3.56)

Variable value = AntiLog {Log(minimum value) + (random number) [Log(maximum value) - Log(minimum value)]} (3.56)

New variables are found using Eq. (3.56) with a minimum value of 10^{10} and maximum value of 10^{18} for different values of random numbers ranging from 0.1 to 1.0. In comparison with simple DE, DE with logarithmic initialization (LIDE) gives better population distribution for A_1, A_{2i}, A_{3i}, E_1, E_{2i} and E_{3i}. In the mutation operation of the DE, weighted difference vector is calculated by difference of two randomly chosen vectors. Noisy random vector is calculated by adding weighted difference vector and the randomly chosen target vector. Mathematically, it is written as given by Eq. (3.57).

Noisy Random Vector = Target Vector + Scaling Factor (difference of two randomly chosen vectors) (3.57)

It is observed that population distribution problem still persists even after using LIDE. Because of this linear operation, all the members of the mutant population would be of highest order among the three randomly selected vectors (irrespective of their numerical values) and after few generations, the entire population of points lies near the upper limit of the variable.

To overcome the problem of population distribution generation after generation, logarithmic mutation is used and given by Eq. (3.58).

Noisy Random Vector = AntiLog {log(variable[c]) + F(log(variable[a])

- log(variable[b]))} (3.58)

Where a, b and c are randomly chosen number from the population size. By implementation of logarithmic mutation in DE, better mutant population in terms of wide population distribution is expected and hence better chances to get the global optimum values. This logarithmic initialization and logarithmic mutation of DE are termed as Logarithmic DE (LDE) [170].

3.2.2 Simulation of kinetic model

3.2.2.1 Kinetic Parameter estimation

Pyrolysis of *Jatropha curcas* de-oiled cake (biomass used in the present study) is performed using TGA. The weight loss of the biomass is measured. These results are used to develop the kinetic model. The model is simulated and corresponding kinetic parameters are found. To find the theoretical value of residual weight fraction (W_{total}), finite difference technique [171] is applied to Eqs. (3.16) to (3.20) and Eqs. (3.32) to (3.36) with the following initial conditions.

At time t=0

T_0 = 30 ˚C; B = 1.0; C = 0.0; W = 1.0,

B_{HC}= 0.166; C_{HC}=0.0; W_{HC}=0.166;

B_C= 0.535; C_C=0.0; W_C=0.535;

B_L= 0.249; C_L=0.0; W_L=0.249;

B_M= 0.05; C_M=0.0; W_M=0.05;

Eqs. (3.16) to (3.20) are discretized by a finite difference method using a pure implicit scheme. The pure implicit scheme is an unconditionally stable scheme, i.e. there is no restriction on time step in sharp contrast with the Euler and Crank-Nicholson method discussed by Ghoshdastidar (1998). The initial and boundary conditions are applied to solve them numerically. Eqs. (3.16 – 3.20) are solved simultaneously. The kinetic parameters are established by minimizing the square of the error between experimental and theoretical residual weight fractions using logarithmic differential evolution (LDE). LDE provides set of optimum kinetic parameters with minimum value of the objective function.

Algorithm to find the kinetic parameters

1) Specify the value of *R, hr and T*.
2) Assume the values of A_1, A_{2i}, A_{3i}, E_1, E_{2i} and E_{3i}.
3) Find the values of k_1, k_{2i}, k_{3i} using Eq. (3.18) and Eq. (3.20)
4) Find the values of residual weight fraction W_i using Eq. (3.16) discretized by a finite difference method using a pure implicit scheme.
5) Compare the square of experimental and calculated values of residual weight fraction.
6) Repeat steps 2-5 (again apply finite difference method using a pure implicit scheme with new set of values), until the square of experimental and calculated values of residual weight fraction is less than 0.001.
7) New values of A_1, A_{2i}, A_{3i}, E_1, E_{2i} and E_{3i} are found. These kinetic parameters are used to predict the weight degradation with temperature.
8) By using new values of A_1, A_{2i}, A_{3i}, E_1, E_{2i} and E_{3i} find the W_i using Eq. (3.16).

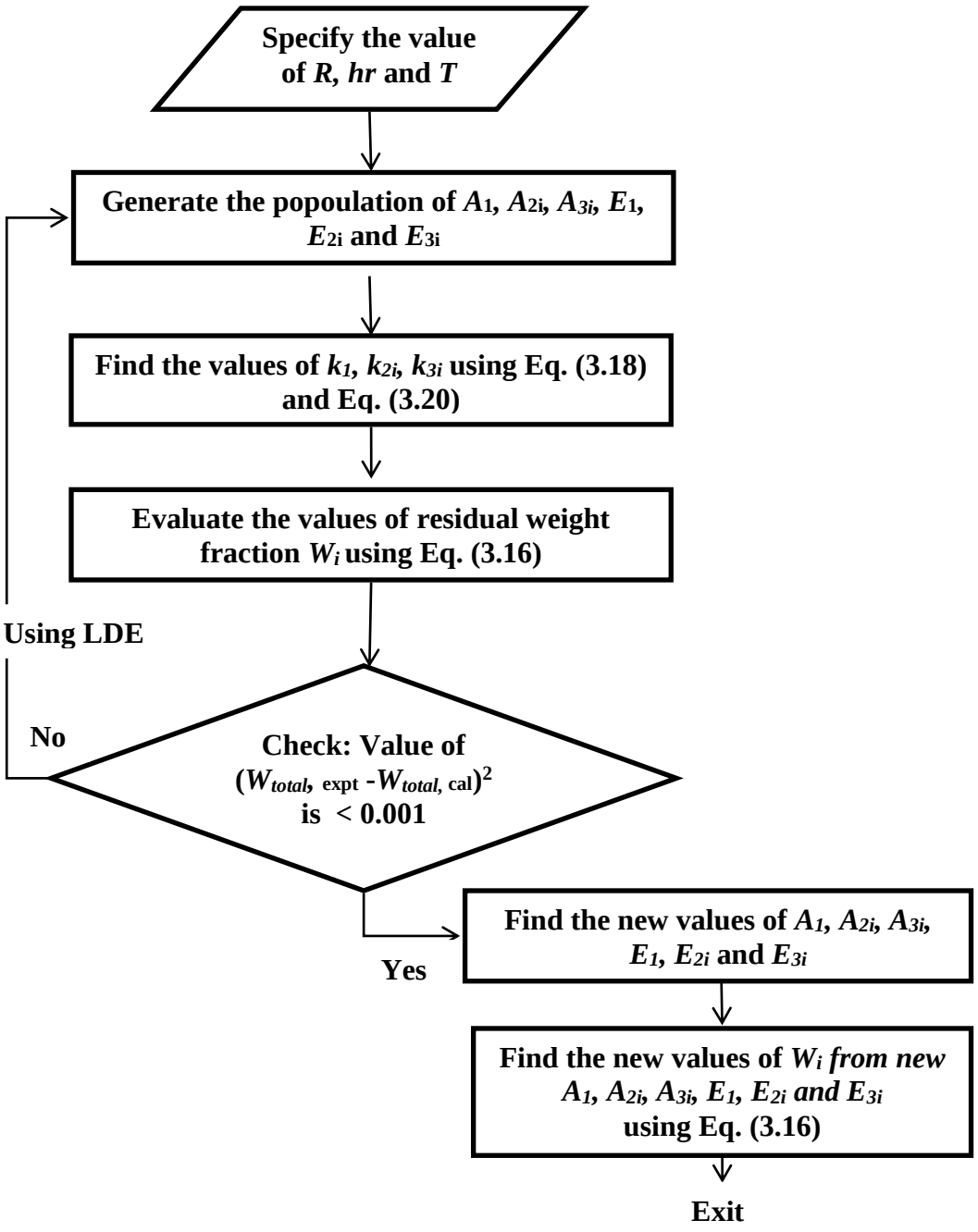

Figure 3.2 Algorithm for kinetic parameter estimation for kinetic model

3.2.2.2 Apparent kinetic parameter estimation

Macro thermo-gravimetric analysis (TGA) of *Jatropha curcas* de-oiled cake (biomass used in the present study) is performed using laboratory macro TGA. The weight loss of the biomass, product yields and composition of non-condensable gases are measured.

These results are used to develop the apparent kinetic model. The model is simulated and corresponding global kinetic parameters are found. To find the theoretical value of residual weight fraction (W_{total}), finite difference technique is applied to Eq. (3.33) to Eq. (3.37) with the following initial conditions.

At time t=0

T_0 = 30 ˚C; B = 1.0; C = 0.0; G=0; V=0; W = 1.0

Algorithm to find the kinetic parameters

1) Specify the value of *R, hr and T*.
2) Assume the values of A_G, A_V, A_C, E_G, E_V, E_C and n.
3) Find the values of k_G, k_V, k_C using Eq. (4.31) to Eq. (4.33)
4) Find the values of residual weight fraction W_i using Eq. (4.29) discretized by a finite difference method using a pure implicit scheme.
5) Compare the square of experimental and calculated values of residual weight fraction.
6) Repeat steps 2-5 (again apply finite difference method using a pure implicit scheme with new set of values), until the square of experimental and calculated values of residual weight fraction is less than 0.001.
7) New values of A_G, A_V, A_C, E_G, E_V, E_C and n.are found. These kinetic parameters are used to predict the weight degradation with temperature.
8) By using new values of A_G, A_V, A_C, E_G, E_V, E_C and n find the W_i using Eq. (4.29).

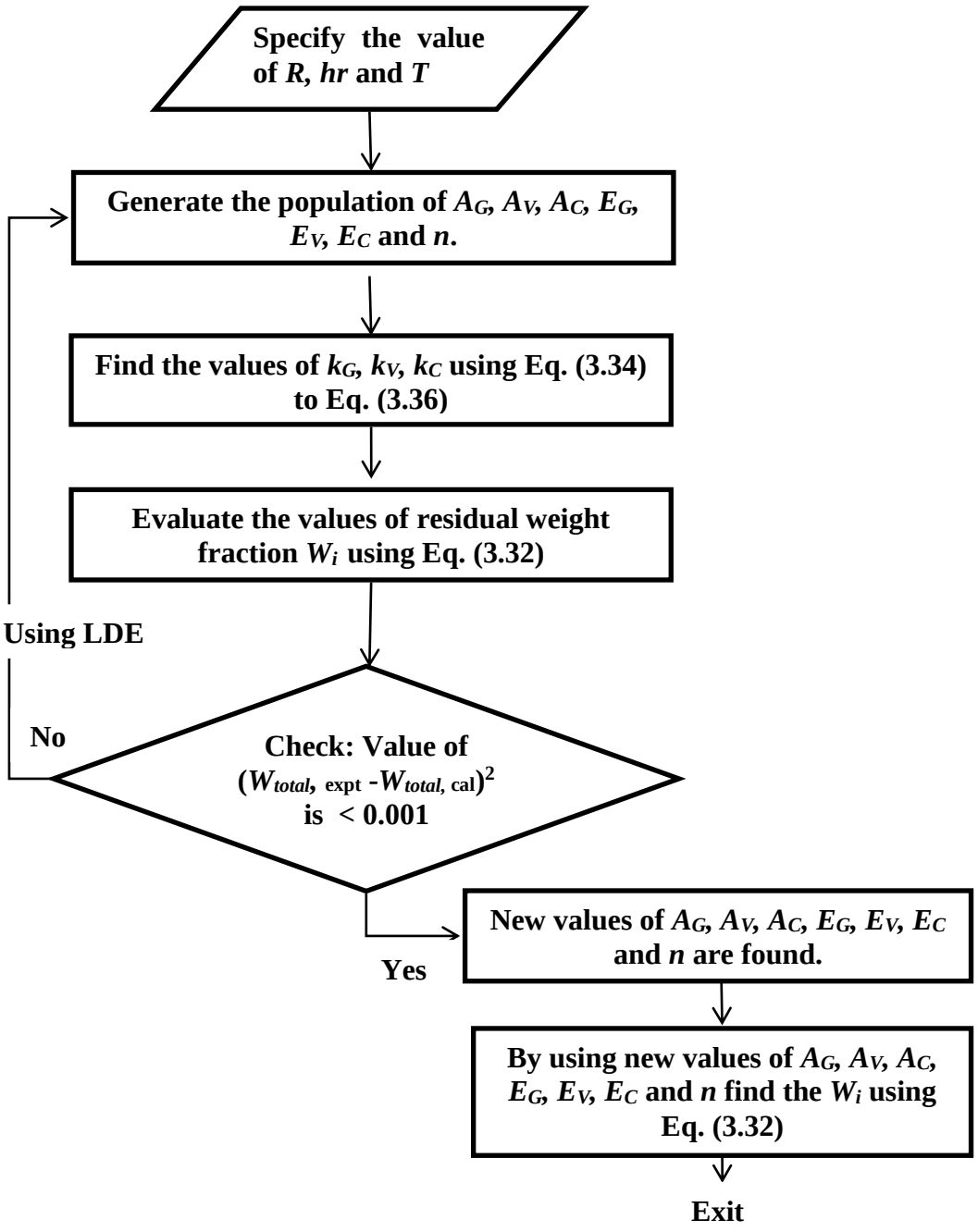

Figure 3.3 Algorithm for kinetic parameter estimation for apparent kinetic model

3.2.2.3 Simulation of Fixed bed model

Finite difference method (FDM) is used for spatial discretization of the set of partial differential equations as well as boundary and time dependent initial conditions (Eqs. 3.38 – 3.45). As the problem mentioned is 2-dimensional and also does not involve much

complexity; FDM involves lesser complexity and lesser computations with almost same accuracy as other methods by considering small grid size. For temporal discretization pure implicit scheme is used as it is unconditionally stable and it does not involve any restriction on step size and time step ($\Delta r, \Delta z, \Delta t$). The simplified system of non-linear algebraic equations is solved using Jacobian iterative method to obtain the temperature distribution throughout the bed, same results (temperature value) at each grid shown in Figure 3.4 were used every time to determine the mass concentration distribution by solving mass balance equations with boundary and initial conditions (Eqs. 3.46 – 3.55). The values of various correlations and parameters are tabulated in Table 3.1 and Table 3.2, respectively.

After discretization PDE's has simplified into set of non-linear algebraic equations (Non-linearity is due to radiation boundary condition). That is computational domain has one equation for each grid point.

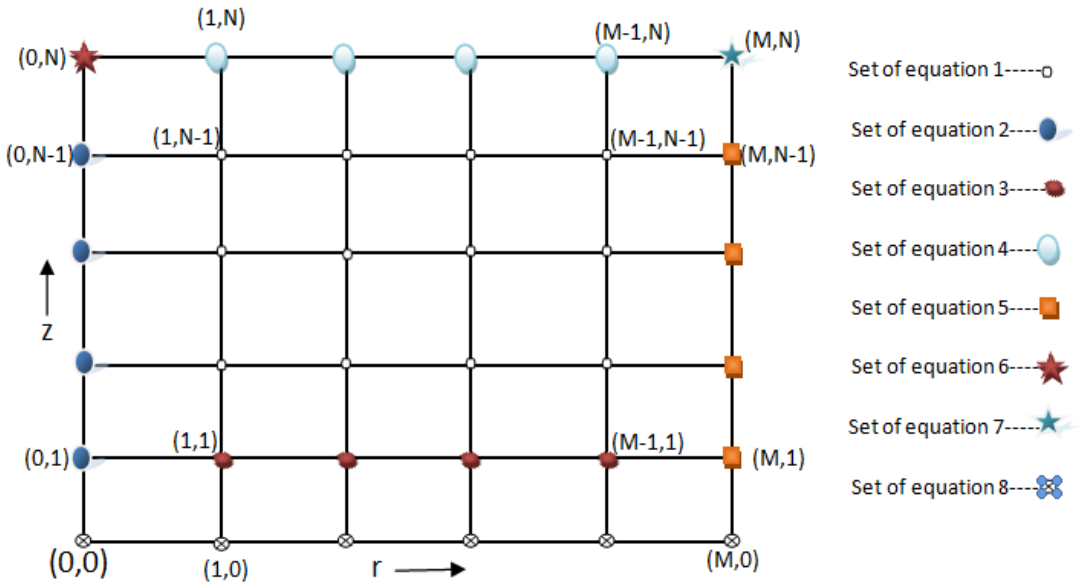

Figure 3.4 Computational domain showing different algebraic equations

Set of algebraic equations has solved using Jacobian iteration method. In which all the non-linear terms has calculated at initial point and taken on right hand side as constant value. Then simultaneous equations have solved using iterative method until the tolerable limit reaches. The optimum value of time step is 1 s that is after increasing the value of Δt after this point, the temperature values will not change. Simulation specifications are below:

1. MSVC (Microsoft visual C++) has used to solve the set of simultaneous algebraic equations.
2. Number of grid points taken in radial direction M=50, and step size 0.06
3. Number of grid points taken in axial direction N=25, and step size 0.01
4. Time step- 1 s (35 minutes runtime)
5. Temperature of reactor surface (T_{rs}) =550 ˚C
6. Temperature of holding surface (T_{hs}) =500 ˚C
7. All the constant values were taken as stated in the literature.

Table 3.1 Properties of correlation

Property	Correlation/value	Unit	Reference
Wood specific heat capacity	C_{Pb}= 1112.0 + 4.85(T − 273)	J/kg˚C	[13]
Char specific heat capacity	C_{Pc} = 1003.2 + 2.09(T − 273)	J/kg˚C	[13]
Wood thermal conductivity	k_b = 0.13 + 0.0003(T − 273)	W/m˚C	[13]
Char thermal conductivity	k_c = 0.08 – 0.0001(T − 273)	W/m˚C	[13]
Gas thermal conductivity	k_g = 25.77 × 10^{-3}	W/m˚C	[42]
Emissivity coefficient	$\varepsilon = 0.95$	___	[43]

Porosity (ε)	$\varepsilon = a + b\rho_b$		[44]
Effective diffusivity of (volatiles and gases)	$D_{ab}=0.2\times 10^{-4}$	m^2/s	[45]
Effective diffusivity of (volatiles and gases)	$\frac{D_{G1}}{D_{G0}} = \theta^{P_1} \exp\left(p_2 \left(1 - \frac{C_B}{C_{B0}} \right) \right)$	m^2/s	[46]
Rate constant	$k_p = A_p \exp\left(\frac{-E_p}{R_g T_s} \right)$ $A_p = 1.52\times 10^3$ $E_p = 62.8\times 10^3$	s^{-1} J/mol	[47]
Pore diameter	d	M	[46]
Effective thermal conductivity	$k_{eff} = \eta k_b + (1-\eta)k_c + \phi k_g + 13.5\sigma T^3 \frac{d}{\varepsilon}$	W/m˚C	[45]
Mass Transfer co-efficient (k)	$k_c = 0.00005$	m/s	[47]

Table 3.2 Constants used in the simulation

Constant	Value	unit
A_p	1.52 x10^3	s^{-1}
E_p	62.8x10^3	J/mol
R_g	8.314	J/mol˚C
D_{AB}	2.52 x10^{-9}	m^2/s
ρ_b	601.20	kg/m^3
C_p	2800	J/mol˚C
σ	5.67x10^{-8}	$J/m^2s˚C^4$
h	8.40	$J/m^2s˚C$

CHAPTER – 4

EXPERIMENTAL STUDIES

In this chapter, the detailed description of the experimental work and the procedure followed for carrying out the effective utilization of *Jatropha curcas* de-oiled cake waste as a biomass in a fixed bed pyrolyzer is described. It also describes the details of the analytical equipments used and methodology followed for the analysis of pyrolysis products.

4 Experimental Studies

The description of the experimental work for the pyrolysis of the *Jatropha curcas* deoiled residue cake and the pyrolysis products analysis is reported in three parts:

1. Details of the experimental set and analytical instruments used
2. Physical and chemical properties of the *Jatropha curcas* deoiled residue cake
3. Methodology followed and operating conditions used

4.1 Experimental setup and analytical equipments

The pyrolysis experimental study was carried out using the custom designed pyrolysis reactor with volatiles condensing units. The analytical instruments used are thermogravimetric analyzer (TGA), fourier transform infra-red spectroscopy (FTIR), gas chromatography (GC), gas chromatography mass spectroscopy (GCMS), rotavapor, and column chromatography set ups.

4.1.1. Pyrolysis experimental set up

The experimental set up consisted of mainly six parts: furnace, pyrolysis reactor, condensers, sample holder, weighing balance, and inert gas supply system. The pyrolysis was conducted in the reactor as shown in Figure 4.1. The weight loss was monitored for a specific heating rate. It was same as TGA but at a macro level. Hence, the term "macro-TGA" is used for the pyrolysis reactor [47, 172-175]. The macro TGA (pyrolysis reactor) was designed in lab and fabrication was carried out by Indfurr Superheat Furnaces, Tamilnadu, India. The main part of the setup was a macro TGA (pyrolysis reactor), which was made of stainless steel (SS - 310). The cylindrical reactor had a diameter of 15.5 cm and a height of 30 cm, and was placed in an electric furnace and heated externally. The furnace can achieve maximum temperature upto 1100 ˚C and temperatures of different locations were measured by thermocouples. The temperature controller unit (M/N: FY 400-301000) was connected to the furnace, which controlled the reactor temperature and the heating rates. The reactor was purged with nitrogen gas to provide inert environment in the reactor from two different positions. As shown in Figure 4.1 one from top of the reactor and another was from bottom of the setup which insure the complete inert environment inside the pyrolyzer. The biomass was placed on the

sample holder, which was resting above the digital weighing balance in a closed air tight chamber. Digital weighing balance was connected to the computer system to record the weight readings continuously in the interval of 0.5 second. Upon increasing the temperature, the biomass sample gets pyrolyzed and releases the volatiles. The volatiles along with inert nitrogen exits from the top of the reactor and were cooled in a two-stage condenser assembly followed by an ice trap. The condenser assembly is consisted of hot water condenser and atmospheric condenser. Hot water condenser is made from stainless steel and hot water (80 ˚C) was flown through the hot water bath with the help of pump. Atmospheric condenser was made of glass and tap water at atmospheric temperature was used to condense the volatiles. The series of condensers were used to trap all volatiles. The schematic drawing of the experimental setup and actual laboratory pyrolysis set up are shown in Figure 4.1 and Figure I.1 of appendix 1.

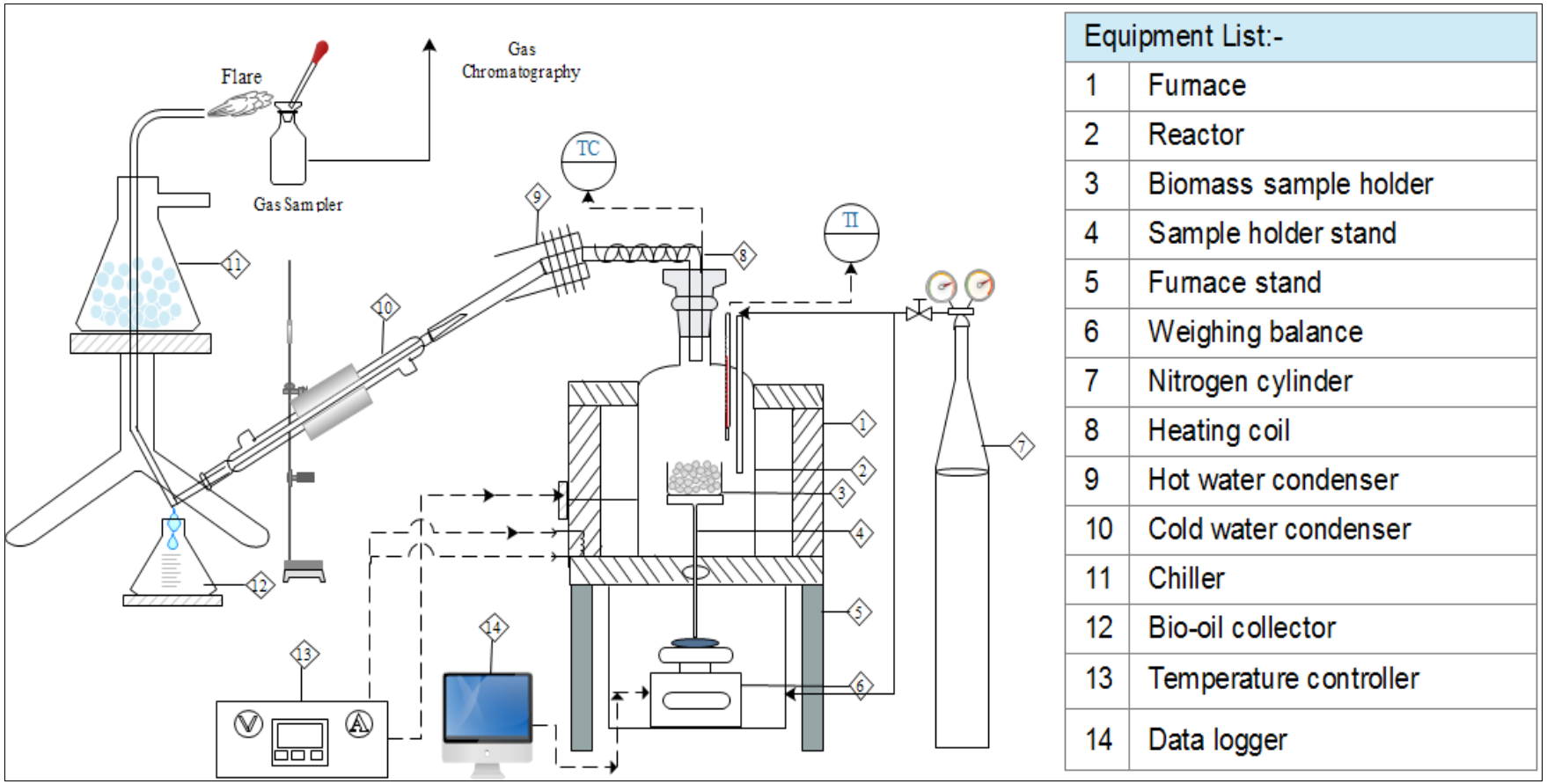

Equipment List:-	
1	Furnace
2	Reactor
3	Biomass sample holder
4	Sample holder stand
5	Furnace stand
6	Weighing balance
7	Nitrogen cylinder
8	Heating coil
9	Hot water condenser
10	Cold water condenser
11	Chiller
12	Bio-oil collector
13	Temperature controller
14	Data logger

Figure 4.1 Schematic of the pyrolysis experimental setup

4.1.2 Analytical Instruments

The descriptions of analytical instruments which were used in the analysis of pyrolysis products are described in sub-sections.

4.1.2.1 Thermo-Gravimetric Analyzer (TGA)

Thermo-gravimetric analysis (TGA) is one of the most widely used techniques for the investigation of thermal degradation and their kinetics during the pyrolysis of solid raw materials such as coal, biomass, and plastic. This instrument is also used to find the proximate analysis data for different types of biomass or coal. The main purpose of this analysis is to observe the thermal behavior of the sample subjected to controlled heating and cooling inside the TGA furnace. The weighing balance of accuracy ± 0.2 % with sensitivity of 1 µg provides the sample weight change with time instantaneously as a function of temperature and/or time. . In the present study, the TGA of Perkin Elmer make (model no: TGA 4000) was used for studying the thermal degradation characteristic of *Jatropha curcas* deoiled cake as shown in Figure I.4 of appendix 1.

4.1.2.2 Liquid column Chromatography

Column chromatography is a preparative technique used to purify compounds depending on their polarity or hydrophobicity. In a column chromatography, a mixture of molecules is separated based on their differentials partitioning between a mobile phase and a stationary phase. In column chromatography as shown in Figure I.5 of appendix 1, initially the chromatography column was cleaned and dried column packed with silica gel (stationary phase) while the mobile phase comprised of the solvent and the fraction sample. The continuous flow of different mobile phase and solvents causes the separation of desired fractions.

4.1.2.3 Rotary evaporator

The purpose of the rotary evaporator is to remove the low boiling organic chemicals, usually solvents, from a mixture of compounds. The rotary evaporator is the method of choice for solvent removal in the modern organic laboratory. In this study bio-oil faction samples *i.e.* aliphatic, aromatic and polar fractions are being separated from their solvents n-hexane, toluene and methanol respectively. The separation was done using rotavapor of Butchi make (model R-210) as shown in Figure I.6 of appendix 1.

4.1.2.4 Fourier Transform Infra-Red Spectroscopy (FTIR)

Fourier transform infrared spectroscopy, also known as FTIR Analysis or FTIR spectroscopy, is an analytical technique used to identify organic, polymeric, and, in some cases, inorganic materials. The FTIR analysis method uses infrared light to scan test samples and observe functional groups of chemical compounds. The FTIR analysis of whole bio-oil was done using Perkin Elmer- Frontier model as shown in Figure I.7 of appendix 1.

4.1.2.5 Gas Chromatography

Chromatography is a technique for separating the components of a mixture on the basis of differences in their affinity towards stationary and mobile phase. Gas chromatography (GC) is a type of chromatography in which there is a mobile phase and a stationary phase. The mobile phase is a carrier gas, usually an inert gas such as helium or an unreactive gas such as nitrogen. The stationary phase is a microscopic layer of liquid or polymer on an inert solid support, inside glass or metal tubing, called a column. The comparison of retention times is the analytical power of GC.

In a GC analysis, a known volume of gaseous or liquid analyte is injected at the entrance (head) of the column, usually using a micro-syringe or solid phase micro-extraction fibers or a gas source switching system. As the carrier gas sweeps the analyze molecules through the column, this motion is inhibited by the adsorption of the analyte molecules either onto the column walls or onto packing materials in the column. The rate at which the molecules progress along the column depends on the strength of adsorption, which in turn depends on the type of molecule and on the materials of stationary phase. Since each type of molecule has a different rate of progression, the various components of the analyze mixture are separated as they progress along the column and reach the end of the column at different times (retention time). A detector is used to monitor the outlet stream from the column; thus, the time at which each component reaches the outlet and the amount of that component can be determined. Generally, substances are identified (qualitatively) by the order in which they emerge (elute) from the column and by the retention time of the analyte in the column.

The purpose of a detector is to monitor the carrier gas as it emerges from the column and to generate a signal in response to variation in its composition due to eluted components. Detection devices for GC must respond rapidly to minute concentration of solutes as they exit the column. The speed of response decides the sensitivity of detection device. Other desirable properties of a detector are linear response, good stability, ease of operation, and uniform response to a wide variety of chemical species or, alternately predictable and selective response to one or more classes of solutes. The thermal conductivity detector (TCD) is a nondestructive universal detector. It is widely used in gas chromatography for its high reliability, simplicity and ease of operation. The TCD

measures the difference in thermal conductivity between the carrier gas flowing through a reference and a sample component mixture flowing through a measuring cell.

In this study the exhaust gas samples are analyzed by using gas chromatography of Simadzu make (model GC 2014). Figure I.8 of appendix 1 shows the picture of the gas chromatography.

4.1.2.6 Gas chromatography mass spectrometry (GC-MS)

The GC-MS instrument is made up of two parts. Gas chromatography mass spectrometry (GC-MS) is an instrumental technique, comprising a gas chromatograph (GC) coupled to a mass spectrometer (MS), by which complex mixtures of chemicals may be separated, identified and quantified. For the qualitative identification of volatile and semi-volatile organic compounds in bio-oil, GC-MS-QP 2010 SHIMADZU, equipped with flame ionization and mass spectrometry detection (GC-FID-MS) is used.

4.2 Materials

The biomass (*Jatropha curcas* de-oiled cake) used in the present study is the waste generated in *Jatropha curcas* oil extraction industries. It is purchased from the supplier based at Gujrat, India. *Jatropha curcas* de-oiled cake is pyrolyzed in a macro TGA experimental set up at different temperatures ranging from 400 ˚C – 800 ˚C for particle size varying from 0.25 mm to 25.4 mm. The physical characteristics and chemical composition of *Jatropha curcas* deoiled cake is given in Table 4.1. The chemical analysis of *Jatropha curcas* deoiled cake is taken from literature [21].

Table 4.1 Chemical Composition of *Jatropha curcas* deoiled cake

Physical properties			
Size (Equivalent Diameter)	**Absolute density (kg/m^3)**	**Bulk density (kg/m^3)**	
1.84 mm	1170	505	
Proximate analysis (% by wt. dry basis)			
Fixed carbon (FC)	**Volatile matter (VM)**	**ASH**	**Moisture**
18.86	79.20	1.5	0.44
Ultimate analysis (% by wt. dry basis)			
Carbon	**Hydrogen**	**Oxygen**	**Nitrogen**	**Others**
52.30	6.50	26.8	5.20	9.2
Chemical analysis (% by wt.)*			
Cellulose	**Hemi cellulose**	**Lignin**	**Extractives**
53.5	16.6	24.9	5.00

*[21, 25]

Table 4.2 Ultimate analysis of *Jatropha curcas* De-oiled Cake

Property	
C (% by mass)	53.39
H (% by mass)	6.81
O (% by mass)	29.27
N (% by mass)	0.45
S (% by mass)	0.12
H/C Ratio	1.53
Empirical Formula	$CH_{1.53}O_{0.4}N_{0.007}S_{0.0008}$

4.3 Experimental procedure

The procedure followed for carrying out the biomass pyrolysis experiments and for analysing the products obtained are reported in this section. The operating parameters such as final temperature and size of the biomass are varied to study their effects on the product yield distribution. The experimental procedure is divided in two parts: (1)

pyrolysis of biomass, and (2) product analysis. Both processes are discussed in sections 4.3.1 and 4.3.2 respectively.

4.3.1 Pyrolysis of biomass

Biomass pyrolysis experiments are carried out in TGA and Macro TGA. The experimental procedure of biomass is divided in two parts: (1) Pyrolysis of biomass in TGA, and (2) Pyrolysis of biomass in macro TGA. Both processes are discussed in sections 4.3.1.1 and 4.3.1.2, respectively.

4.3.1.1 Pyrolysis of biomass in TGA

The thermal degradation characteristic of *Jatropha curcas* deoiled cake is studied using the thermo-gravimetric analyzer (TGA 4000, Perkin Elmer) as shown in Figure 4.5. A ceramic crucible (volume 180 μl) loaded with biomass sample was placed inside the analyzer. The sample weight was continuously measured and recorded together with the time and temperature profile inside the TGA.

Table 4.3 Details of the biomass pyrolysis experiments using TGA

Biomass species	**Heating rate (˚C/min)**
Jaropha de-oiled cake	10
	20
	30
	40
	50
	60

In the present work, TGA experiments were carried out in an inert gas (N_2) environment with flow rate of 80 ml/min. Heating in TGA experiment was started after allowing inert purging for 20 min. As per table 4.3 experiments were performed at various heating rates from 10 ˚C/min to 60 ˚C/min with an increment of 10 ˚C /min. In all the experiments, heating was applied to the biomass sample at a constant heating rate from ambient temperature to 800 ˚C.

4.3.1.2 Pyrolysis of biomass in macro TGA

The thermal degradation characteristic of *Jatropha curcas* deoiled cake macro TGA experiments are performed with variation particle size of biomass and reactor temperature. The schematic diagram and real photograph of macro TGA are shown in Figure 4.1 and Figure I.1 of appendix 1, respectively.

In the macro TGA experiments, a known amount of biomass sample with specific particle size is placed on the sample holder, and made sure that the weight of sample shown in balance is same as measured initially and the box is closed. The reactor is placed inside the furnace, over the holder such that it does not touch any part of holder as shown in Figure I.2 and Figure I.3 of appendix 1. The weighing balance is also kept inside the air tight box hence as to obtain stable readings. Nitrogen is continuously flushed inside the box and the reactor for around 20 minutes hence as to create inert environment for pyrolysis to take place. The data logger was started to record the weight of the sample. Before switching on the heater, the controller was set for the desired temperature and heating rate. As heat passes from the furnace through the reactor to the holder, sample gets heated and after particular temperature the pyrolysis starts. Biomass decomposes into solid and vapor products and reduction in weight of sample was

recorded on the logger. The reactor outlet was connected to a two stage condenser followed by an ice trap for the volatiles to get condensed. The volatile products exits the reactor and the temperature of the volatiles drops after passing through the hot water condenser, which was passed through the cold water condenser and bio-oil was collected at the outlet. The stream of volatiles which was not condensed and passed through the chillers, where all the condensable volatiles get condensed and non-condensable flue gases was sent out through vent and was collected at the outlet. There was no change in the sample weight & hence it was assumed that reaction went till completion and whatever left was assumed to be char.

Table 4.4 Details of the biomass pyrolysis experiments using macro TGA

Biomass species	**Final temp of pyrolysis reactor (˚C)**	**Particle size of Biomass**
Jaropha de-oiled cake	400	52-60 mesh (0.25 to 0.3 mm)
		10-14 mesh (1.4 to 2.0 mm)
		0.5 inch
		1.0 inch
	550	52-60 mesh (0.25 to 0.3 mm)
		10-14 mesh (1.4 to 2.0 mm)
		0.5 inch
		1.0 inch
	700	52-60 mesh (0.25 to 0.3 mm)
		10-14 mesh (1.4 to 2.0 mm)
		0.5 inch
		1.0 inch

4.3.2 Product analysis

4.3.2.1 Liquid product (bio-oil) analysis

The liquid produced from pyrolysis was blackish dark oily matter (pyrolytic oil or bio-oil). The produced liquid was separated from heavier impurities by using the separating funnel as shown in Figure I.5 of appendix 1. The bio-oil produced from the biomass pyrolysis was first mixed with pentane, from which two phases were obtained. The two phases are soluble n-pentane and insoluble n-pentane. This solution was filtered to remove the solid particles which settled at the bottom.

4.3.2.1.1 Liquid column Chromatography

After removal of the solid particles soluble pentane fraction got separated into aliphatic, aromatic and polar fractions by column chromatography. The separation of aliphatic, aromatic and polar fractions are separated using solvents such as n-hexane, toluene and methanol, respectively. The pentane soluble fraction were added to the column and then the column was sequentially eluted with pentane, toluene and methanol to obtain aliphatic, aromatic, and polar fractions. The boiling point of pentane, toluene and methanol are 68 ˚C, 110.6 ˚C and 64.7 ˚C, respectively at STP. Each fraction was collected in different flask and dried in rotary evaporator as shown in Figure I.7 of appendix 1. The remnants after solvent drying from the above fractions are tested with FTIR spectroscopy for detection of various types of compounds present in the individual fractions.

4.3.2.1.2 Fourier Transform Infra-Red Spectroscopy (FTIR)

This analysis was carried out for detection of different types of compounds present in the sample. Firstly a KBr pellet was made and it was used to obtain a reference curve. A

small amount of liquid was mixed with KBr (mixed in a ratio of 1:50) and a pellet was made which was analyzed. The bio-oil sample was placed in the sample holder & FTIR was carried out. The results obtained from FTIR studies were analyzed, to understand different type of functional groups present in a particular fraction.

4.3.2.1.3 Gas chromatography mass spectrometry (GCMS)

Bio-oil fractions are analysed using gas chromatograph mass spectrometry (GCMS) with split injection at 290 ˚C. The DB5 fused silica capillary column with 0.25 μm film thickness was used & having 0.25 mm ID & 30 m length. Helium was used as carrier gas with a flow rate of about 1 ml /min. The GC oven temperature was initially maintained at 50 ˚C for 2 min, and programmed to increase to 100 ˚C at 30 ˚C/min and then to 290 ˚C at 5 ˚C/min. The oven temperature was then held at 290 ˚C for 20 min. The end of the column was introduced directly into the ion source of a mass selective detector. The transfer line was set at 270 ˚C and the mass spectrometer ion source was at 250 ˚C with ionization potential of 70 eV. Data acquisition is carried out with the NIST library database. The mass range of m/z = 30 - 500 Daltons.

4.3.2.1.4 Thermo-Gravimetric Analyzer (TGA)

The thermal degradation characteristic of bio-oil was studied using the TGA (TGA 4000, Perkin Elmer) (Figure I.4 of appendix 1). TGA shows the change in weight with respect to temperature. The TGA of bio-oil was conducted in a nitrogen environment with a purge flow rate of 80 ml/min. A fixed amount of biomass was placed in the reactor. Initially the temperature is kept at 30 ˚C for 20 min. The sample was then heated from 30 ˚C to 800 ˚C at 10 ˚C/min, 20 ˚C/min and 60 ˚C/min.

4.3.2.2 Gaseous product analysis using gas Chromatography

The gas chromatographic analysis of non-condensable gas was done using Shimadzu GC-2014 gas chromatography. The GC analysis shows the composition of gases (H_2, CH_4, CO and CO_2) at different time and at different temperature of reactor. The carbosphere column was used and Argon was used as a carrier gas with flow rate of 8 ml/min. The operating conditions for GC were injection temperature, column temperature and thermal conductivity detector temperature are kept at 100 ˚C, 45 ˚C and 100 ˚C respectively. The gas samples were taken at every 50 ˚C interval and analyzed using GC.

Table 4.5 Details of the gaseous product analysis of *Jatropha curcas* de-oiled cake

Particle size of Biomass	Final temperature of pyrolysis reactor (°C)	Gas Sample taken at temperature (°C)
52-60 mesh (0.25 to 0.3 mm)	400	350
		400
	550	350
		400
		450
		500
		550
	700	350
		400
		450
		500
		550
		600
		650
		700
10-14 mesh (1.4 to 2.0 mm)	400	350
		400
	550	350
		450
		500

		550
	700	350
		400
		450
		500
		550
		600
		650
		700
0.5 inch	400	350
		400
	550	350
		450
		500
		550
	700	350
		400
		450
		500
		550
		600
		650
		700
1.0 inch	400	350
		400
	550	350
		450
		500
		550
	700	350
		400
		450
		500
		550
		600
		650
		700

CHAPTER – 5

RESULTS AND DISCUSSION

This chapter presents the experimental and simulation results obtained for the pyrolysis of *Jatropha curcas* de-oiled cake. The results of the experimental study are discussed in Section 5.1 and the simulation results of the mathematical models are presented and discussed in Section 5.2.

5 Results and Discussion

5.1 Experimental studies

5.1.1 Thermo-gravimetric analyzer

The thermal degradation of *Jatropha curcas* de-oiled cake was carried out using TGA under inert environment. Nitrogen gas was continuously purged at the flow rate of 2 L/min while conducting the experiments. The results of experimental runs performed at distinct heating rates (10 ˚C/min to 60 ˚C/min) are collectively represented in Figure 5.1 and 5.2. The residual weight fraction represents the ratio of residual weight to initial weight of biomass. The stepwise degradation pathway corresponding to the thermal decomposition of the different biomass constituents (cellulose, hemicellulose and lignin). Figure 5.1 shows, the first steep weight loss is followed by the second and third gentle carbonization step. The initial devolatilization step (50 ˚C to 200 ˚C) was attributed to the

moisture vaporization. The maximum devolatilization occurs in the range of temperature 200 ˚C to 450 ˚C. The hemicellulose is the easiest to be pyrolyzed due to its linear polymer structure with short side chains. The cellulose is constructed of semi crystalline array chains associated with one another, which makes it thermally more stable. The lignin is a complicated structure of phenolic polymers encasing the polysaccharides of the cell walls that produces strong and durable composite materials [176]. The second devolatilization step (200 ˚C to 450 ˚C) is attributed to the decomposition of carbohydrate components such as hemi cellulose and cellulose while the small third step at 450 ˚C to 800 ˚C represents the degradation of lignin. Figure 5.2 shows that the time required for final weight loss is higher for lower heating rate. The yield of char is increasing with increase in the heating rate. This may be due to high residence time at lower heating rate which allows biomass sample to get exposed for longer duration at high temperature. It provides the opportunity to get released the maximum amount of volatiles from biomass. Hence the heating rate alone does not define the product yield. The residence time of the reactant in the reactor is also important [177]. The char yield is found 20 wt % and 28 wt % for heating rate 10 ˚C/min and 60 ˚C/min, respectively. The similar results of char yield with heating rate variation are reported by Seo *et. al.* [176], Sricharoenchaikul and Atong [25] Vikranth & Singh [178] and El-Sayed *et. al.* [179].

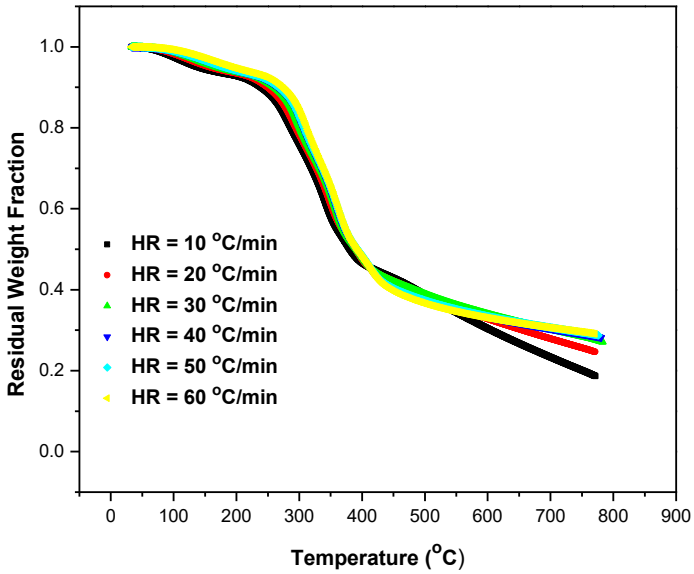

Figure 5.1 Thermo-gravimetric Analysis of *Jatropha curcas* de-oiled cake at various heating rates with temperature.

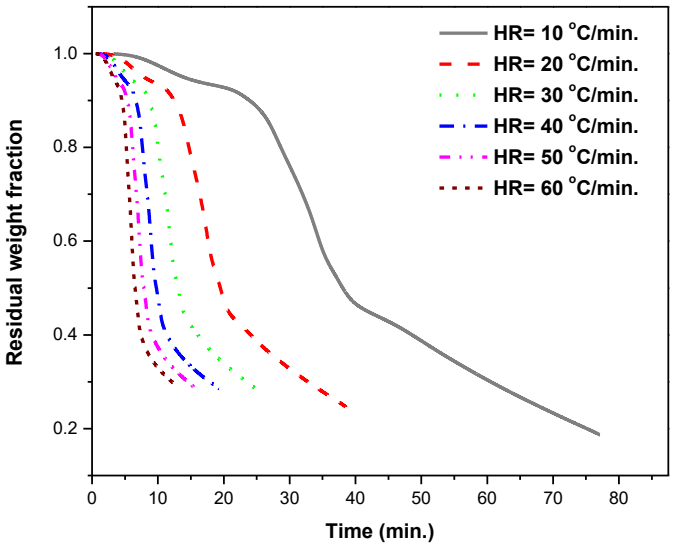

Figure 5.2 Thermo-gravimetric Analysis of *Jatropha curcas* de-oiled cake at various heating rates with time.

Derivative weight analysis helps to understand the rate of change of biomass weight upon thermal treatment. Figures 5.3 to 5.10 show the obtained results presented as the corresponding first derivative (DTG curves) weight percent remaining or residual weight fraction. Generally, the TGA curves shows sigmoidal shape and DTG curves exhibits two or three major peaks. Figures 5.3 to 5.10 shows the DTG curve obtained from the pyrolysis of *Jatropha curcas* de-oiled cake at heating rate 10 ˚C/min to 60 ˚C/min, respectively. It is evident from Figures 5.3 that the main pyrolysis decomposition occurs predominantly in the range of 200 ˚C -450 ˚C. The thermal decomposition of biomass will result from contributions of their lignocellulosic components (hemicellulose, cellulose and lignin), which generally decompose over the temperature range of 200 ˚C - 450 ˚C. Lignin usually starts decomposing at 450 ˚C temperature and continues up to the temperature around 800 ˚C. The same trends were obtained at different heating rates of 10 ˚C/min -60 ˚C/min. The curves have the typical appearance of pyrolysis of lignocellulose materials. Four separate peaks are distinguished clearly in all the DTG curves. The first peak, which occurs at lower temperatures at 100 ˚C –150 ˚C, is related to the moisture release. The second peak, which occurs at temperatures in the range of 200 ˚C –350 ˚C, corresponds to the hemicellulose decomposition. The third peak, which occurs at temperatures in the range of 300 ˚C –450 ˚C, corresponds to the cellulose decomposition and lignin, as the fourth major component in the *Jatropha curcas* de-oiled cake, decomposes slowly in a broader range. Figure 5.9 and 5.10 represent the derivative weight fraction at various heating rate with time and temperature, respectively. It is observed that the peak intensity is increasing as the heating rate increases and shown a

shift in derivative weight fraction curve because the pyrolysis time is less for high heating rate.

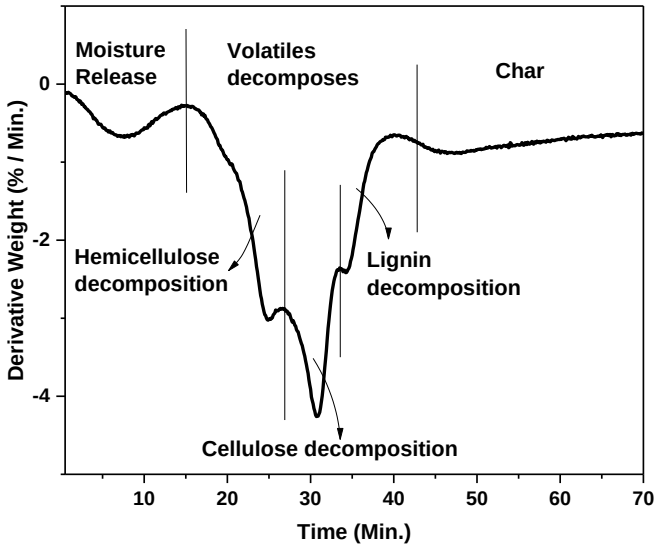

Figure 5.3 DTG plot of *Jatropha curcas* de-oiled cake at heating rate 10 ˚C/min.

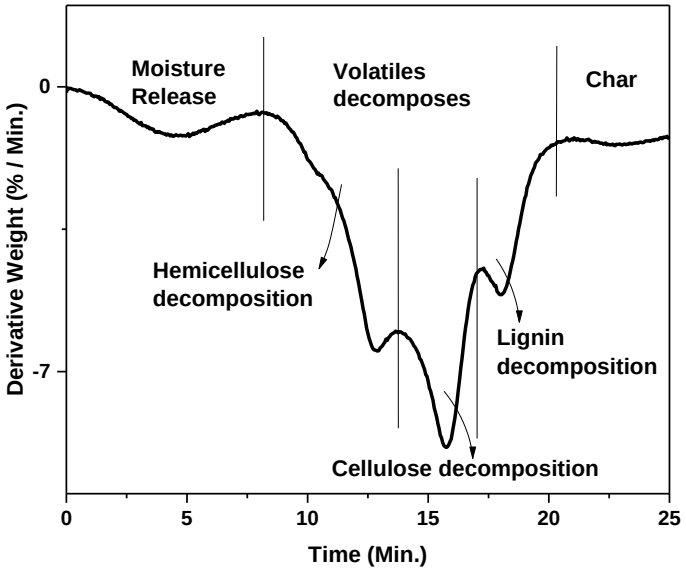

Figure 5.4 DTG plot of *Jatropha curcas* de-oiled cake at heating rate 20 ˚C/min.

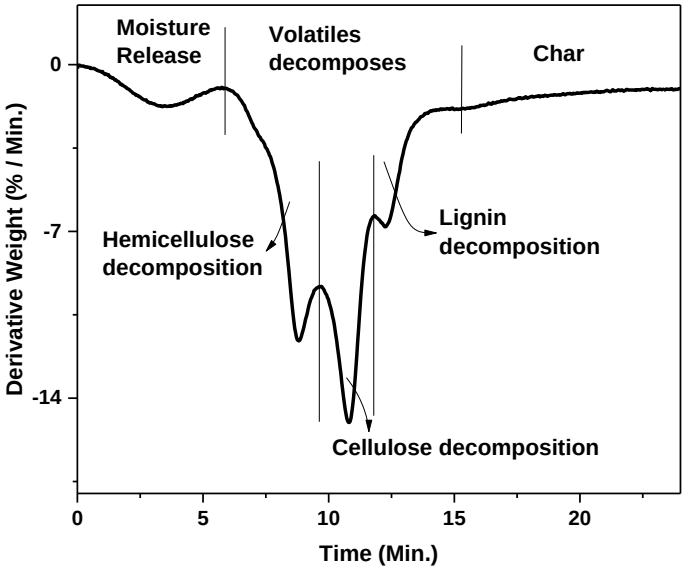

Figure 5.5 DTG plot of *Jatropha curcas* de-oiled cake at heating rate 30 ˚C/min.

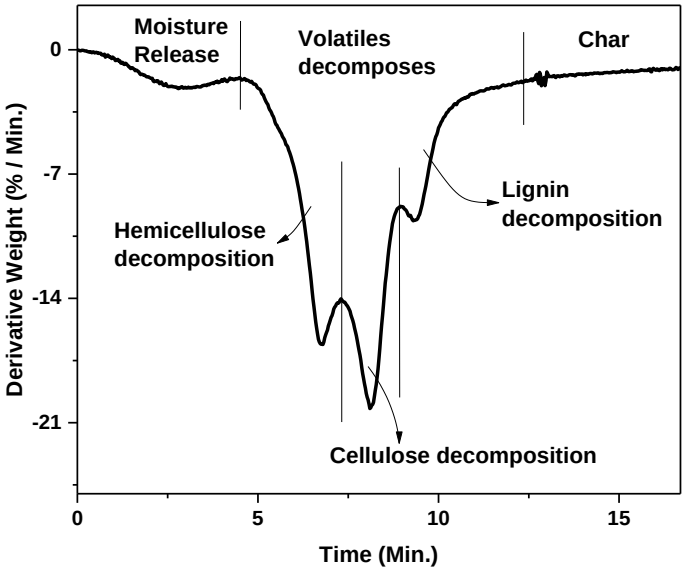

Figure 5.6 DTG plot of *Jatropha curcas* de-oiled cake at heating rate 40 ˚C/min.

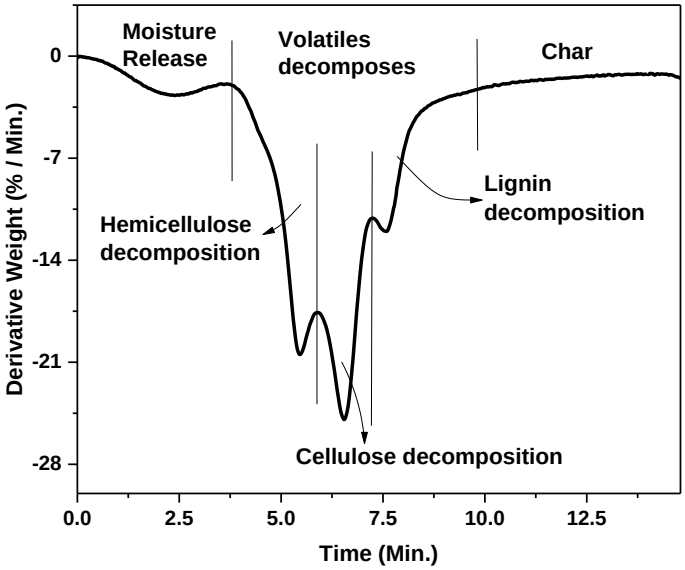

Figure 5.7 DTG plot of *Jatropha curcas* de-oiled cake at heating rate 50 ˚C/min.

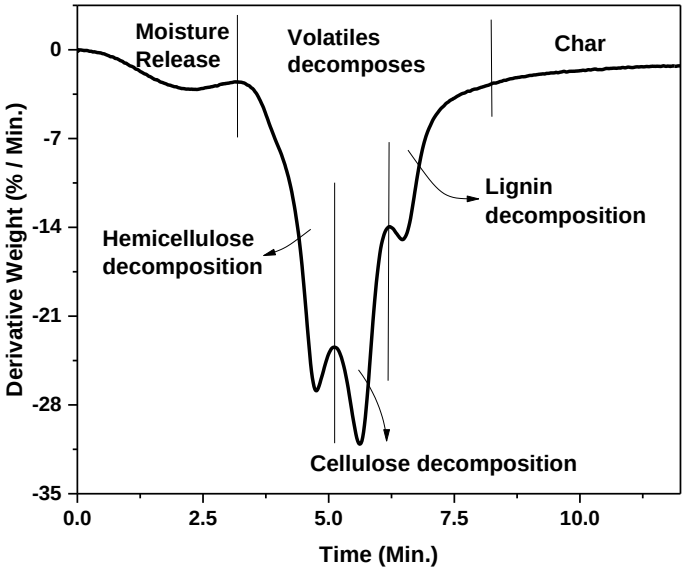

Figure 5.8 DTG plot of *Jatropha curcas* de-oiled cake at heating rate 60 ˚C/min.

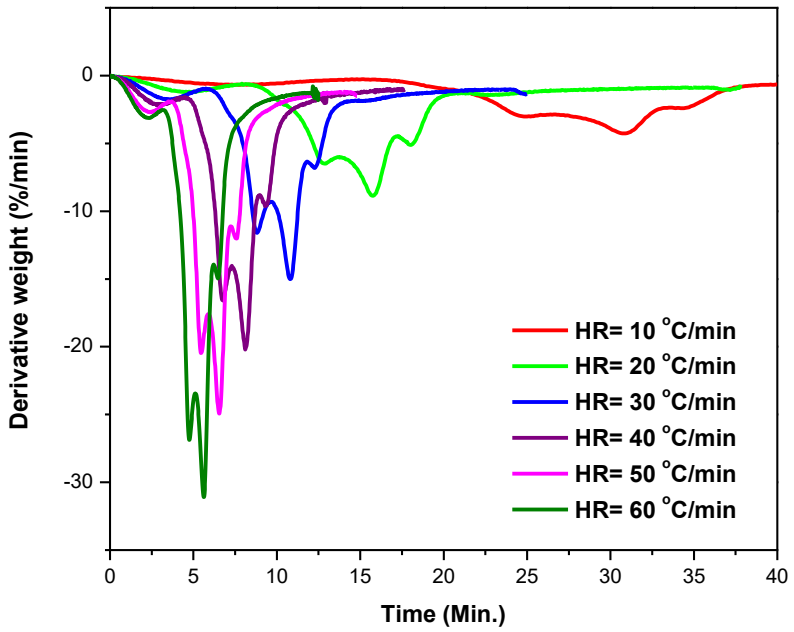

Figure 5.9 DTG plot of *Jatropha curcas* de-oiled cake at various heating rate with time.

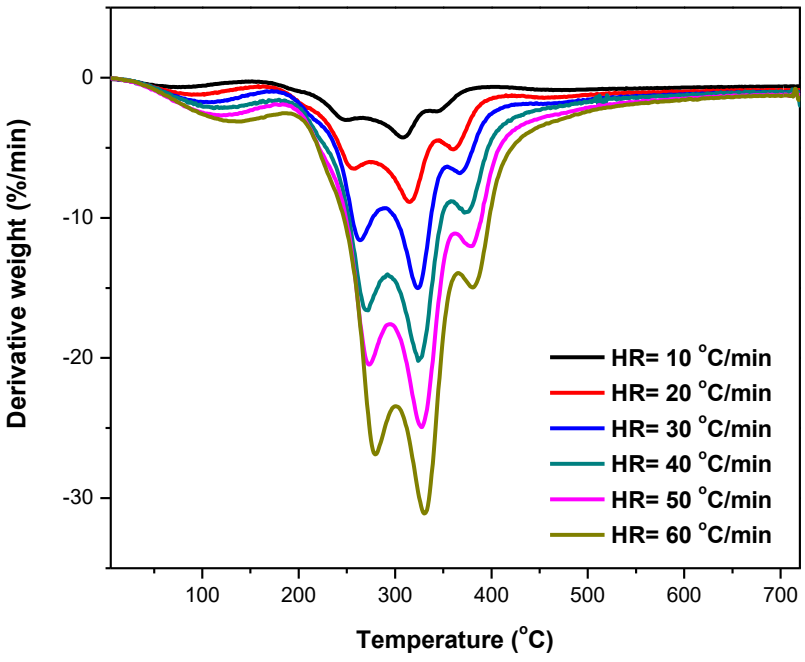

Figure 5.10 DTG plot of *Jatropha curcas* de-oiled cake at various heating rate with temperature.

5.1.2 Macro thermo-gravimetric analyzer

The macro thermo-gravimetric analysis of biomass was carried out using laboratory fixed bed pyrolyzer to study the effect various operating parameter such as reactor final temperature and particle size of biomass. The effect of rector temperature is described in section 5.1.2.1. The effect of change is described in section 5.1.2.2.

5.1.2.1 Effect of reactor temperature

Figure 5.11 shows the product yield distribution for the pyrolysis of *Jatropha curcas* de-oiled cake carried out at different final temperatures. The liquid product obtained has a reddish-brown colour with an irritant odour. The liquid yield is found to be 18 wt %, 25 wt %, 29 wt % at pyrolysis temperatures of 350 ˚C, 400 ˚C and 550 ˚C, respectively. The maximum liquid yield is found to be 31.2 wt % at the final reactor temperature of 500 ˚C, this further decreased with an increase in temperature. The char yield gradually decreases to 31.8 wt % from 48.25 wt % with the increase in temperature. At higher temperature the secondary degradation of the products lead to decrease in solid product yield with the increase in temperature [180]. The gaseous product yield remain constant initially and increased with increase in temperature. This may be certainly due to the secondary cracking of the pyrolysis vapours and char at high temperatures, which may also lead to formation of some non- condensable gaseous products.

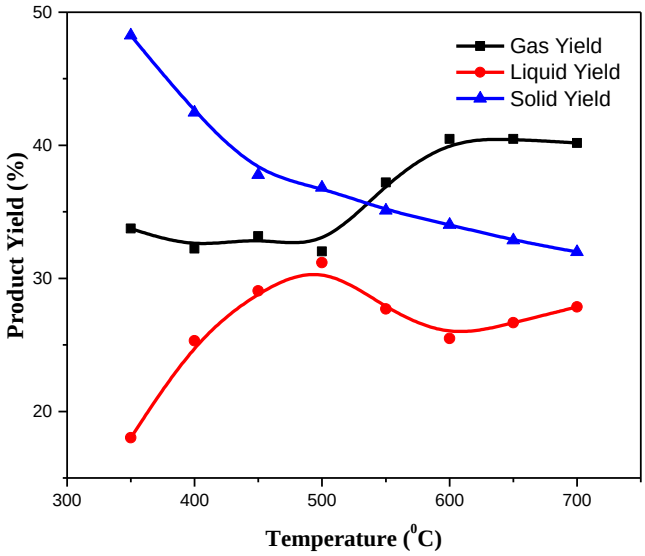

Figure 5.11 Product yield distribution of pyrolysis of *Jatropha curcas* de-oiled cake

5.1.2.2 Effect of particle size

Figures 5.12 to 5.14 show of the product yield distribution for the pyrolysis of different particle size (0.25 mm to 25.4 mm) *Jatropha curcas* de-oiled cake at different temperatures. Figure 5.13 show that char yield was more for large particle size than the small size particle for the same final temperature of reactor. It was due to the fact that for the large particle size, the temperature within the particle would be much lower than that of the reactor. Hence, the lower temperature in the core of the particle leads to low temp pyrolysis producing more char and lesser yield of bio-oil and non-condensable gases. As the final temperature increases, the char yield is reduced for the same particle size. At the same time the yield of non-condensable gases (shown in Figure 5.14) increases with increase in the final temperature of the reactor. However, for the bio-oil yield shown in Figure 5.12, increment in the yield is observed for 550 ˚C and reduction in yield is observed at 700 ˚C. It is due to the secondary cracking of the volatiles into the permanent

gases. It can be seen from Figures 5.12 to 5.14, the difference between the char yield, bio-oil yield and yield of non-condensable gases of 52-60 mesh size and 10-14 mesh size particle is small and same observation is made for 0.5 and 1 inch particle size. However, there is a huge difference (13.3 wt %) in char yield of 52-60 mesh size and 1 inch size particle at 400 ˚C of reactor temperature. As the final temperature of reactor got increased, this difference in the yield is reduced up to a value of 3.5 wt %. The yield of non-condensable gases varied from 35.9 wt % to 41.4 wt % and 25.6 wt % to 41 wt % for 52-60 mesh size and 1 inch particle size respectively.

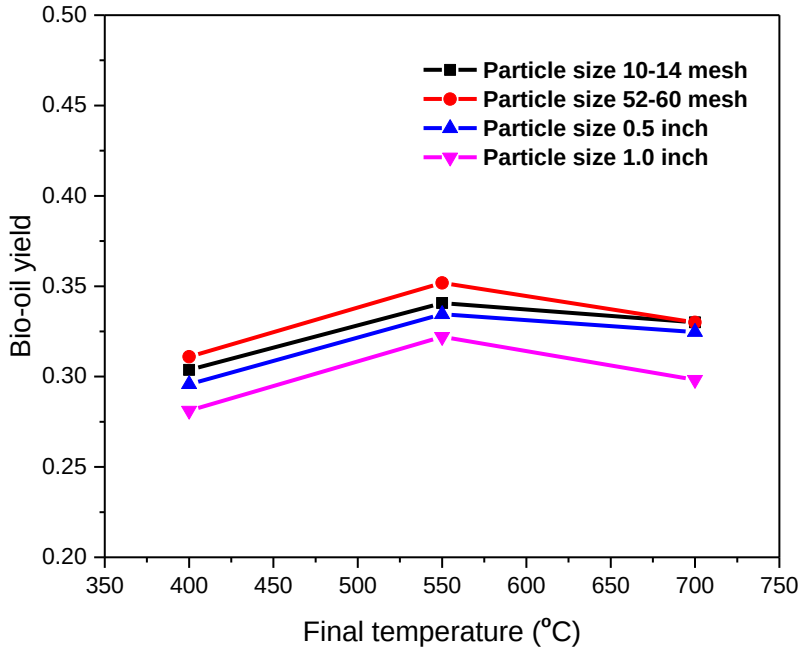

Figure 5.12 Bio-oil yield distribution of pyrolysis of *Jatropha curcas* de-oiled cake

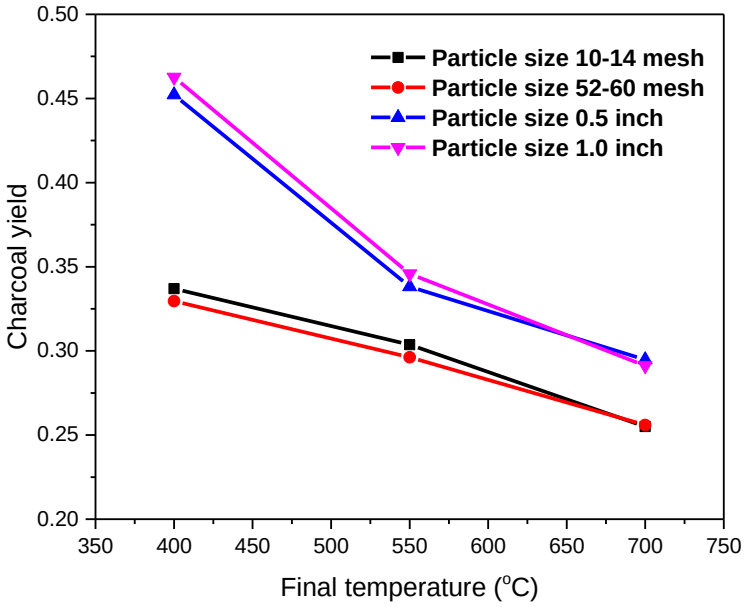

Figure 5.13 Char yield distribution of pyrolysis of *Jatropha curcas* de-oiled cake

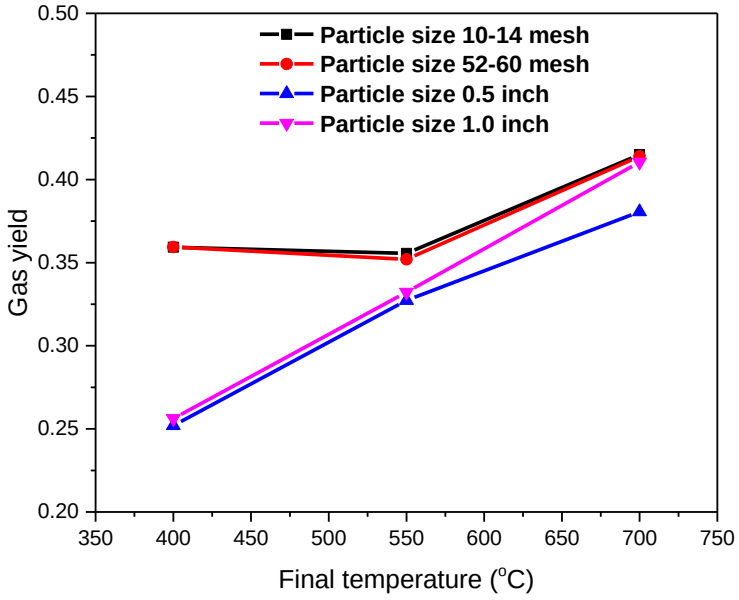

Figure 5.14 Gas yield distribution of pyrolysis of *Jatropha curcas* de-oiled cake

Figures 5.15 to 5.17 show the macro TGA of *Jatropha curcas* de-oiled cake at final reactor temperature of 400 ˚C, 550 ˚C and 700 ˚C, respectively. Three stages are observed for the pyrolysis of de-oiled cake. The first stage was a pre-pyrolysis which occurs between 120 ˚C and 220 ˚C with a small weight loss. This may be due to some internal rearrangements, such as breakage of bond and formation of free radicals & carbonyl groups. The larger size particle heat has to penetrate in the particle and it takes time to diffuse till core of the particle. The mode of transfer of heat is diffusion but it is slow due to lower thermal diffusivity and larger size particles. As the particle gets heated, the volatile releases and the onset of drop in weight fraction are observed. The second stage displays main pyrolysis process, during which a significant weight loss from initially fed biomass is observed. This maximum weight loss takes place from 250 ˚C to 500 ˚C. In this stage, the weaker chemical bonds and intermolecular associations are destroyed [181]. The further cleavage of C–H and C–O bonds occur at the last stage, which is continuous char devolatilization [182]. Figure 5.14 shows the weight reduction with temperature for four different particle sizes of biomass for the final reactor temperature of 700 ˚C. Similar trends are observed for 400 ˚C and 550 ˚C.

It can be seen that the weight reduction till 300 ˚C was appreciable for larger size particles (0.5 and 1 inch size) in comparison to the smaller size particles (10-14 mesh and 52-60 mesh). The larger size particles have shown early weight reduction in comparison to the smaller size particles. It is due to the heat transfer effects in the reactor. The particles are placed in the cylindrical pan in the reactor and get heated by radiation from top and by conduction through bottom and through circular periphery. Due to high porosity of larger size particle bed, it receives the large amount of heat through radiation.

Hence, its temperature gets increased and achieves higher weight reduction at lower reactor temperature in comparison to the low porosity of smaller size particle bed.

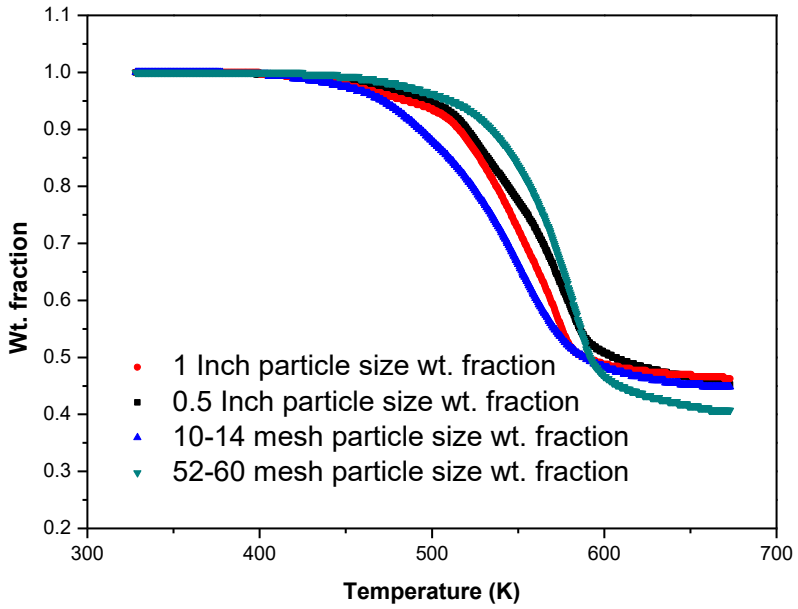

Figure 5.15 Macro Thermogravimetric Analysis of *Jatropha curcas* de-oiled cake at 400 ˚C for different particle size

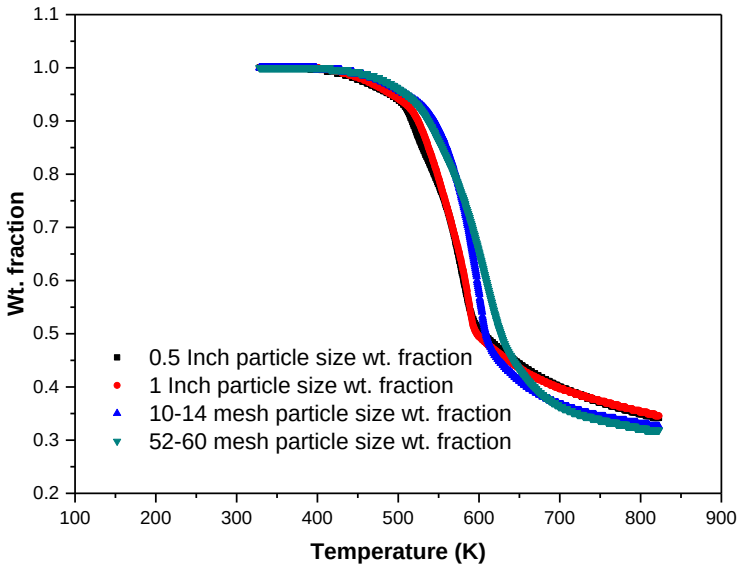

Figure 5.16 Macro Thermogravimetric Analysis of *Jatropha curcas* de-oiled cake at 550 ˚C for different particle size

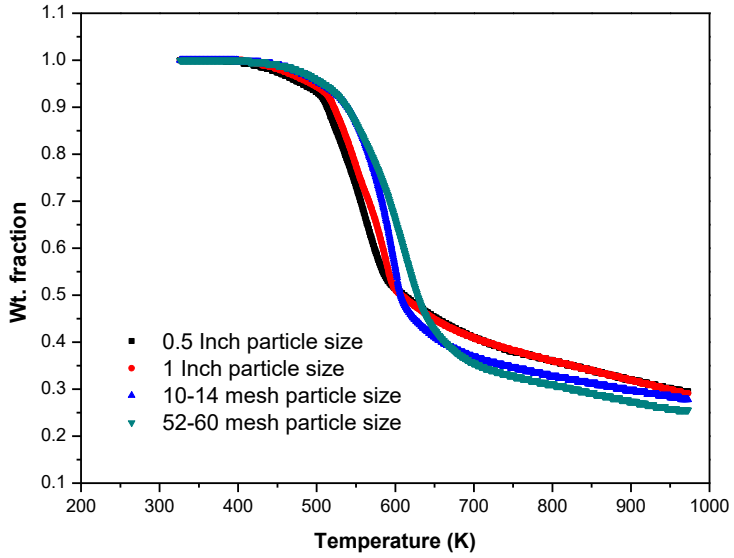

Figure 5.17 Macro Thermogravimetric Analysis of *Jatropha curcas* de-oiled cake at 700 ˚C for different particle size.

5.1.2.3 Gas composition

Gas chromatography of the gas sample (collected at final temperature 700 ˚C as it covers the entire range of reactor temperature) has been done and is plotted for different temperatures in Figure 5.18. The major compounds characterized by GC analysis of non-condensable gas are H_2, N_2, CH_4, CO and CO_2. N_2 is used as inert gas so major composition of N_2 is observed in non-condensable gases. Hence, the N_2 free compositions of different gases are shown in Figure 5.15 for precise analysis of other compounds. Here we found that in non-condensable gases the maximum composition is CO_2 (70 vol %) and minimum composition of CH_4 was obtained (2 vol % to 5 vol %).

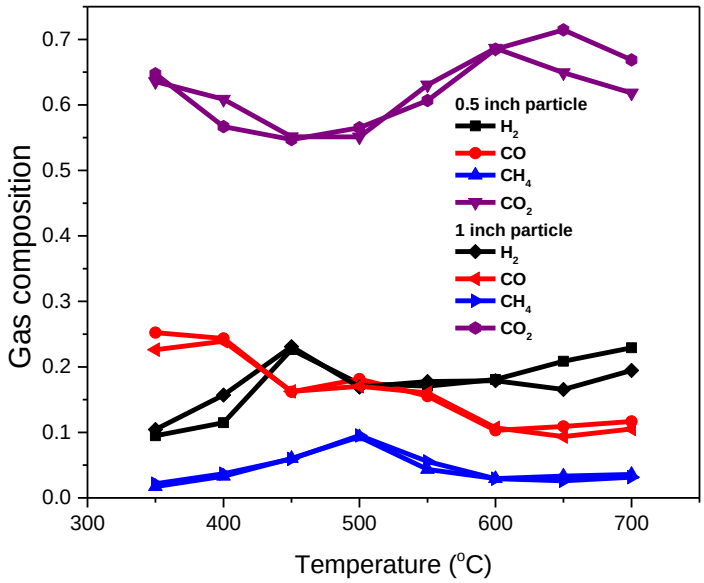

Figure 5.18 Gas chromatographic analysis of nitrogen free non-condensable gas

The composition of CO_2 is decreasing with increase in temperature till 500 ˚C and then slightly increased till maximum at 600 ˚C after that starts decreasing. CH_4 concentration was least and was almost constant for all temperatures. It was observed that H_2 concentration varied from 0.1 to 0.22 and slightly increases with increase in temperature.

CO concentration was decreasing with increase in temperature and varied from 0.25 to 0.12. CO concentration was decreasing due to water shift gas reaction and formed CO_2 and H_2 at high temperature.

5.1.2.4 Bio-oil analysis

Section 5.1.3.1 describe FTIR analysis of bio-oil at different reactor temperatures. As shown in Figure 5.21 we have not found significant difference in functional group in bio-oil collected from different reactor temperature. Hence detailed TGA and GC-MS analysis of bio-oil collected from pyrolysis of biomass at 700 $^{\circ}$C reactor temperature were carried out and described in section 5.1.3.2 and 5.1.3.3 respectively

5.1.2.4.1 FTIR analysis

Figures 5.19 and 5.20 show the FTIR analysis of bio-oil and char. Peaks at 2800 cm^{-1} and 2900 cm^{-1} assures the presence of single bond with hydrogen that is (C-H, N-H etc), peaks at 1700 cm^{-1} ensures double bond with carbon (C=C, C=N, C=O etc) and peaks between 1100 to 1200 cm^{-1} ensures single bond with carbon (C-O, C-H, C-N, C-X).

Figure 5.21 shows the Fourier transform infrared (FTIR) spectra, representing functional group analysis for the pyrolysis oil prepared at various temperatures. The presence of O-H vibrations between 3050 cm^{-1} and 3600 cm^{-1} indicate the presence of water, alcohol and acid, together with the presence of C=O stretching vibrations between 1650 cm^{-1} and 1850 cm^{-1} indicates the presence of carboxylic acids and their derivatives [183]. Monocyclic, polycyclic and substituted aromatic groups are indicated by the absorption peaks between 800 cm^{-1} - 1000 cm^{-1} and 1550 cm^{-1} - 1700 cm^{-1}. Single ring aromatic compounds and polycyclic compounds are also present in the pyrolysis oil [79]. The presence of the C=O stretching vibrations between 1650 cm^{-1} and 1850 cm^{-1} may

also indicate the presence of ketones and aldehydes. Table 5.1 shows the FTIR analysis of the bio-oil produced.

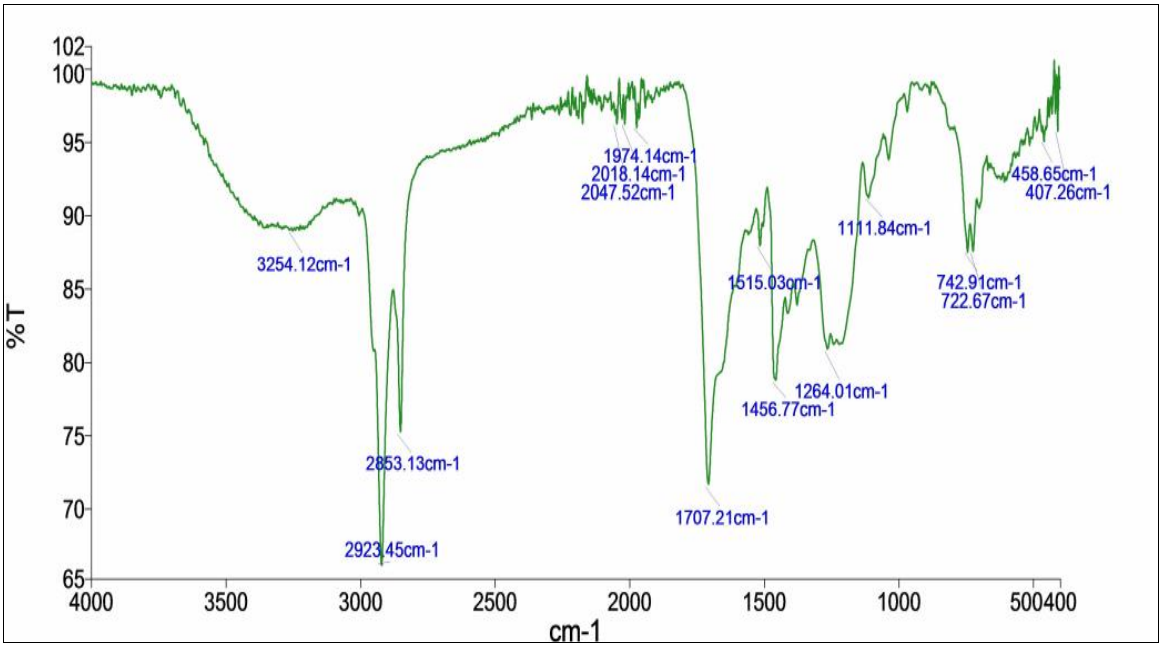

Figure 5.19 FTIR analysis of bio-oil sample at 700 ˚C temperature

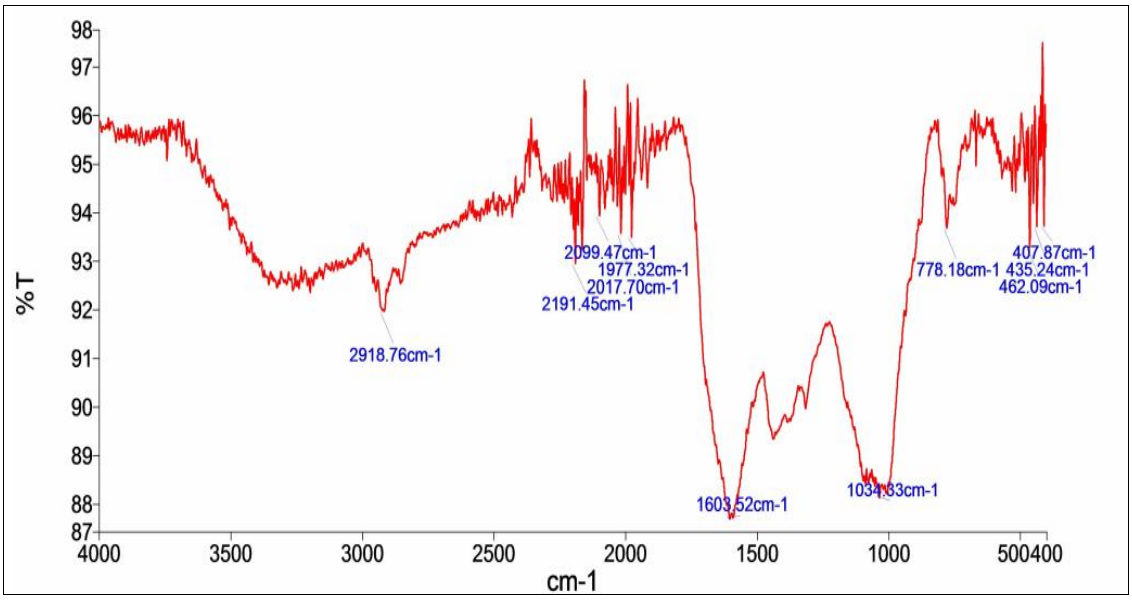

Figure 5.20 FTIR analysis of char sample at 700 ˚C temperature

An increase in temperature indicates changes in the peak intensities and therefore, composition of the oils. The peak intensity has increased in the 1400 cm^{-1}-1600 cm^{-1}

band, representing an increase in mono-aromatic, poly-aromatic and substituted aromatic compounds.

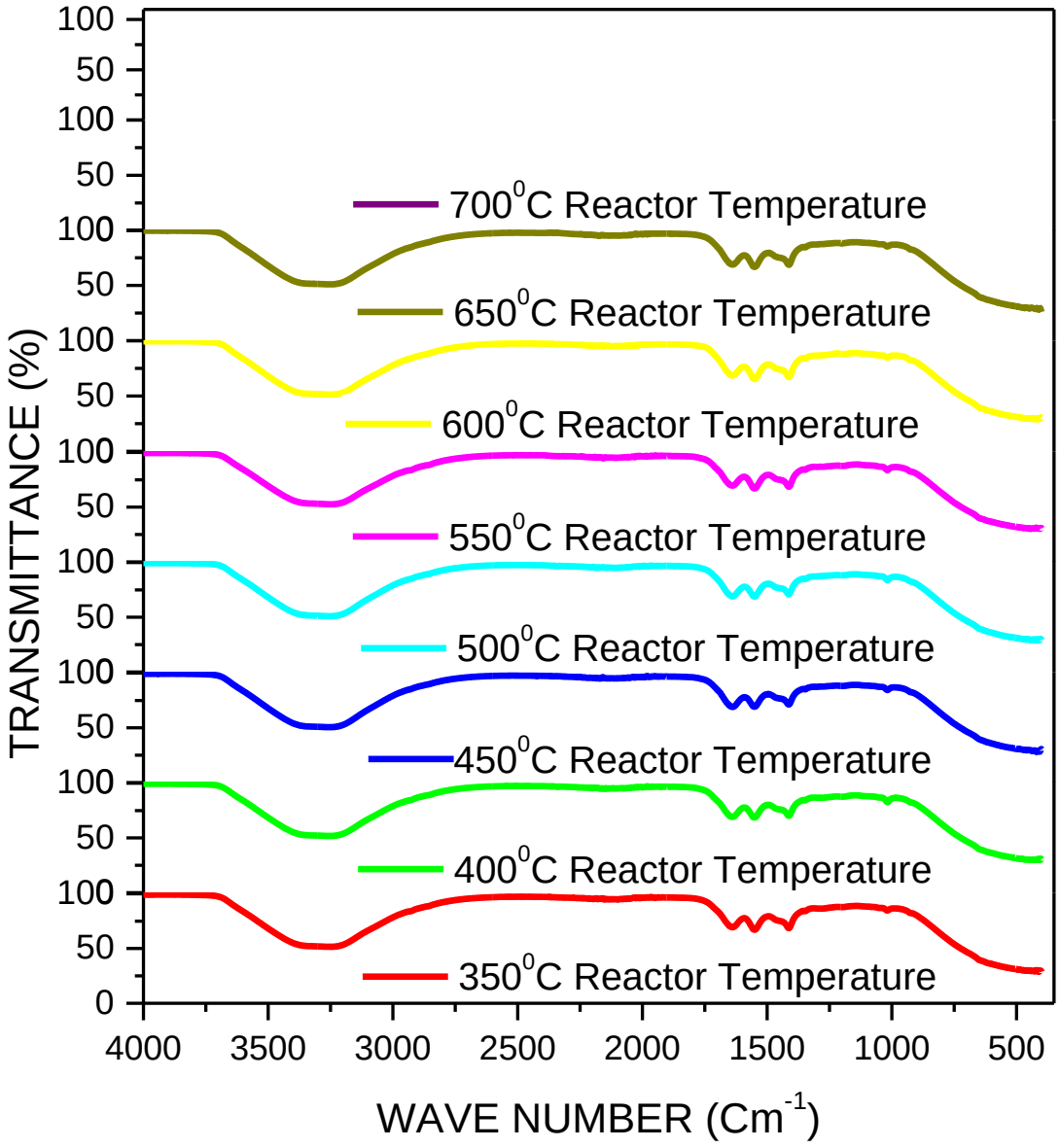

Figure 5.21 FTIR spectra of bio-oil for 350 ˚C, 400 ˚C, 450 ˚C, 500 ˚C, 550 ˚C, 600 ˚C, 650 ˚C and 700 ˚C

Table 5.1 FTIR analysis of *Jatropha curcas* de-oiled cake pyrolysis oil

Frequency (cm^{-1})	Type of Vibration	Name of Functional Group/ Compound representation
3600-3300	O-H stretch	Alcohol, acid, water
2850-2960	C-H stretch	Alkanes
2220-2260	C=N stretch	Nitriles
2100-2260	C=C stretch	Alkynes
1670-1760	C=O stretch	Aldehydes, carboxylic acids, ketones, esters
1620-1680	C=C stretch	Alkenes
1580-1650	N-H bend	Amines
1500-1660	NO_2 asymmetric stretch	Nitro Compounds
1400-1600	C=C stretch	Aromatic rings

5.1.2.4.2 TGA analysis

Figure 5.22 shows the TGA analysis of bio-oil which was carried out with nitrogen as purge gas and at heating rates of 60 ˚C/min. The analysis shows maximum weight reduction of the bio-oil which takes place from 100 ˚C to 300 ˚C indicating large portion of bio-oil being vaporized in this range of temperature, and presence of compounds with a boiling point in this range.

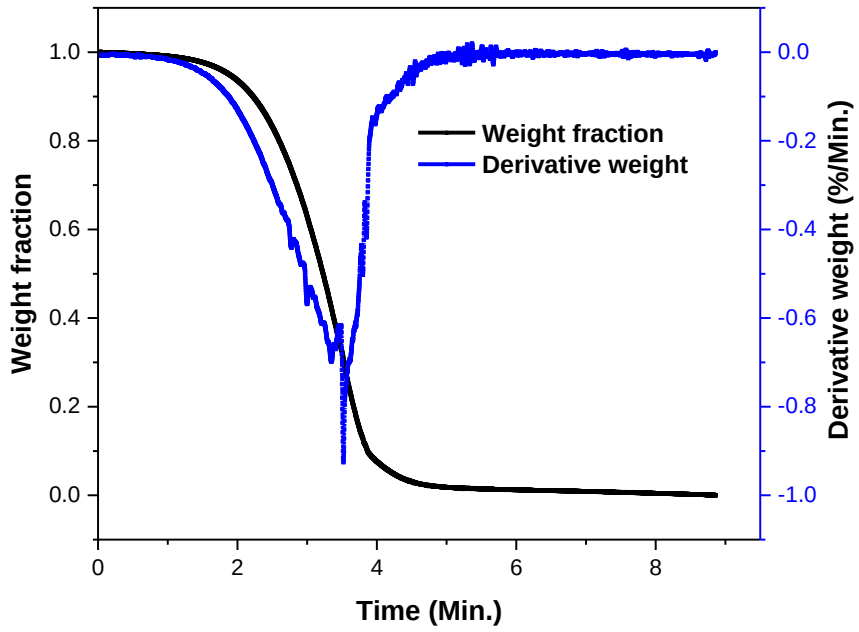

Figure 5.22 Thermo-gravimetric analysis of bio-oil at heating rate 60 ˚C /min

5.1.2.4.3 GC-MS analysis

The major compounds characterized by GC MS in the pentane soluble fraction of bio-oil are given in Table 5.2. Various compounds such as normal alkanes, alkenes, phenols, saturated fatty acids and their derivatives such as esters, acid amides and nitriles were identified. Three major compounds were observed at 28.142, 28.672 and 27.656 retention times with area percent of 19.03, 6.91 and 9.12, respectively. These compounds were identified as 12-Nonadecatriene-5, 14-diol, Octadecanoic acid, methyl ester and (E)-9-Octadecenoic acid, respectively. It was seen in the chromatograms that most compounds were polar in nature. Few aromatics could be seen in the bio-oil, among which some phenol and benzene compounds are confirmed.

Table 5.2 Chemical compounds in bio-oil (GC-MS Analysis)

No.	RT (min)	Name of Compound	% Area
1	4.081	Pyridine, 3-methyl-	0.3
2	4.496	2-Cyclopenten-1-one, 2-methyl-	0.25
3	4.535	Ethanone, 1-(2-furanyl)-	0.33
4	4.786	Pyridine, 2,5-dimethyl-	0.26
5	5.266	Phenol	0.85
6	5.561	Pyridine, 3-methoxy-	0.41
7	6.032	2-Cyclopenten-1-one, 2,3-dimethyl-	0.24
8	6.219	Phenol, 2-methyl-	0.49
9	6.514	Phenol, 4-methyl-	1.14
10	6.763	Phenol, 2-methoxy-	0.34
11	7.581	Benzyl nitrile	0.28
12	7.945	Benzene, pentyl-	0.32
13	7.987	Phenol, 3-ethyl-	0.6
14	8.503	1-Tridecene	0.79
15	9.156	6-Dodecyne	0.42
16	9.431	Benzene propane nitrile	0.24
17	9.671	Benzene, 1,3-bis(1,1-dimethylethyl)-	0.27
18	10.523	1-Tetradecene	0.47
19	10.607	Indole	0.4
20	12.444	1,3-Benzenediol, 4-ethyl-	0.34
21	12.744	1-Pentadecene	1

22	15.213	Heptadecane	0.26
23	15.336	Phenol, 2,4-bis(1,1-dimethylethyl)-	0.43
24	17.311	1-Nonadecene	0.38
25	19.693	Heneicosane	0.25
26	24.323	Hexadecanoic acid	0.64
27	27.355	cis-9-Hexadecenal	2.53
28	27.656	9-Octadecenoic acid	9.12
29	28.142	Octadecanoic acid	6.91
30	28.672	12-Nonadecatriene-5, 14-diol	19.03
31	29.21	Hexadecanamide	2.56
32	29.722	N-Methyldodecanamide	0.36
33	32.162	9-Octadecenamide, (Z)-	3.23
34	32.583	Octadecanamide	0.63
35	42.796	Stigmast-5-en-3-ol, oleate	0.89
36	46.675	.gamma.-Sitosterol	0.45

It has been observed that the characterization of whole bio-oil lead to difficulty in identification of the exact components with GC-MS. Very few researchers have used liquid column chromatographic technique to separate out the aliphatic, aromatic and polar compounds followed by GC and MS to determine different constituents of each fraction [135]. The results of FTIR and GC-MS can be better understood if bio-oil is separated into various fractions (such as aliphatic, aromatic and polar) in comparison to whole bio-oil. Based on the literature survey carried out, separation of the bio-oil compounds into

aliphatic, aromatic and polar compounds was done using liquid column chromatography. The aliphatic, aromatic and polar fraction were analyzed with GC-MS and discussed in sections 5.1.2.4.3.1, 5.1.2.4.3.2 and 5.1.2.4.3.3, respectively.

5.1.2.4.3.1 GC-MS analysis of aliphatic fraction of bio-oil

The major compounds characterized by GC-MS are given in Table 5.3, which were identified in the n-hexane soluble fraction of bio-oil from liquid column chromatography. Various compounds such as normal alkanes, alkenes and alkynes were identified. Three major compounds are observed at 2.541, 2.590 and 2.645 min of retention times with area percent of 29.06, 7.09 and 4.28, respectively. These compounds were n- Hexane, 1, 3-Dithiane and 2-Pentadecen identified, respectively.

Table 5.3 Chemical compounds in aliphatic fraction of bio-oil

No.	RT (min)	Name	% Area
1	2.098	Dotriacontane	0.44
2	2.541	n-Hexane	29.06
3	2.565	Carbon Tetrachloride	4.27
4	2.590	1,3-Dithiane	7.09
5	2.645	2-Pentadecen	4.28
6	9.680	Dotriacontane	0.43
7	10.532	Methane	0.43
8	12.770	1-Tetradecene	2.59
9	12.940	Tetradecane	0.72
10	15.057	1-Pentadecene	2.05
11	15.236	Heptadecane	1.32

12	15.335	Acetic acid	0.83
13	16.495	1-octene	0.57
14	16.895	5-Tetradecen-1-ol	2.11
15	16.983	1,13-Tetradecadiene	1.81
16	17.150	1,16-Hexadecanediol	0.58
17	17.348	Dodecane	2.80
18	17.506	Heptadecane	1.17
19	19.043	Octadecane	0.81
20	19.208	7-Tetradecene	1.86
21	19.336	Tetracosane	1.43
22	19.550	n-Nonadecanol-1	1.30
23	19.711	Heneicosane	1.20
24	21.687	1-Nonadecene	1.22
25	21.833	Ergost-5-en-3-ol, (3.beta.)-	0.55
26	23.736	1-Nonadecene	0.76
27	25.704	9-Tricosene	1.02
28	25.827	Stigmast-5-en-3-ol, oleate	0.48
29	27.579	1-Heptacosanol	0.49
30	29.388	Eicosane	1.05
31	29.491	1-Heptacosanol	0.53
32	31.209	trifluoroacetate	0.44
33	32.773	Trichloromethane	0.45
34	41.578	Heneicosane	0.53

35	41.953	Cyclopentene, 1-octyl-	0.69
36	42.746	Stigmast-5	2.54

5.1.2.4.3.2 GC-MS analysis of aromatic fraction of bio-oil

The major compounds characterized by GC-MS analysis of toluene soluble fraction of bio-oil (aromatic fraction of bio-oil) are given in table 5.4, the table shows compounds identified in the toluene soluble fraction of bio-oil from liquid column chromatography are mostly aromatic compounds. The three major compounds are observed at 2.508, 27.704 and 28.808 min of retention times with area percent of 20.78, 4.14 and 3.18, respectively. These compounds were identified as toluene, phenol and pentyl-Benzene, respectively.

Table 5.4 Chemical compounds in aromatic fraction of bio-oil

No.	RT (min)	Name	% Area
1	2.508	Toluene	20.78
2	3.446	Carbon Tetrachloride	1.71
3	3.636	1H-Indene, 1-methyl-	0.52
4	3.679	Cyclohexane	0.62
5	3.807	Pyrrole	0.59
6	3.876	Octane	0.99
7	4.139	Ethylbenzene	1.48
8	4.232	p-Xylene	2.25
9	4.432	N-Methyl-3,5-	0.74

		dihydroxyaniline	
10	5.569	Undecane	1.09
11	6.947	Benzofuran	0.74
12	7.888	1-methyldecyl-Benzene	0.50
13	7.961	2-methyl-Naphthalene	0.54
14	8.676	Camphor-10	0.49
15	10.654	Indole	2.08
16	12.680	Isoquinoline	1.07
17	12.760	1-Tetradecene	0.96
18	12.941	1,3-bis(1,1-dimethylethyl)-Benzene	0.57
19	15.345	p-Xylene	0.89
20	16.892	5-Eicosyne	0.80
21	17.330	n-Pentadecanol	0.80
22	17.500	Butyl- Benzene	0.49
23	19.203	propyl-Benzene	0.50
24	21.690	Benzoic acid	0.53
25	23.827	Naphthalene	1.01
26	24.365	Styrene	2.33
27	27.298	Oleanitrile	2.30
28	27.377	1-ethenyl-2-methyl-Benzene	1.44
29	27.530	Benzyl nitrile	0.59

30	27.704	Phenol	4.14
31	27.808	Pentyl-Benzene	3.19
32	28.173	1H-Indole	2.01
33	30.321	Bibenzyl	0.89
34	41.967	Eicosyl trifluoroacetate	0.63
35	42.434	Styrene	0.60
36	42.847	Stigmast-5	2.50

5.1.2.4.3.3 GC-MS analysis of polar fraction of bio-oil

The major compounds characterized by GC-MS are given in Table 5.5, which shows compounds identified in the methanol soluble fraction of bio-oil from liquid column chromatography. Three major compounds are observed at 4.1, 5.27 and 10.11 min of retention times with area percent of 20.25, 6.49 and 5.46, respectively. These compounds were identified as methanol, phenol and 1,2-benzenediol, respectively.

Table 5.5 Chemical compounds in polar fraction of bio-oil

No.	RT (min)	Name	% Area
1	4.100	Methanol	20.25
2	4.143	o-Xylene	1.44
3	4.196	2-Cyclopenten-1-one	1.04
4	4.532	Butyrolactone	1.02
5	4.804	1H-Pyrazole-1-carbothioamide	0.92
6	5.270	Phenol	6.49

7	5.398	3-methyl-Pyridine	1.71
8	5.493	3-methoxy-Pyridine	0.63
9	5.702	Pentanamide	0.63
11	6.103	2-methyl-Phenol	3.13
12	6.298	4-methyl-Phenol	4.89
13	6.692	2-methoxy-Phenol	1.14
14	6.811	2,4-Imidazolidinedione	0.64
15	7.118	Benzyl nitrile	0.83
16	7.633	2,4-dimethyl-Phenol	0.77
17	7.793	2,3-dimethyl-Phenol	0.70
18	7.878	N-Ethyl-4-pyridinemethylamine	0.79
19	8.008	4-ethyl-Phenol	2.10
20	8.666	1,2-Benzenediol	0.80
21	8.930	Ethyl (phenylacetoxy)acetate	1.08
22	8.975	1H-Imidazole	2.04
23	9.158	2,3,5-trimethyl-Phenol	0.75
24	9.286	2H-Pyrazole-3-carboxylic acid	1.83
25	9.450	Benzenepropanenitrile	1.86
26	9.571	2-Dimethylamino-3-methylpyridine	0.76
27	10.115	1,2-Benzenediol	5.46
28	11.244	Propylphosphonic acid	0.96
29	12.740	1,3-Benzenediol, 4-ethyl-	2.53

30	15.124	9-Octadecenoic acid	2.20
31	28.152	Octadecanoic acid, methyl ester	0.72
32	28.713	Hexadecanamide	1.58
33	29.245	p-Tetradecylaniline	0.74
34	29.564	9-Octadecenamide	2.16
35	32.348	Octadecanamide	1.75
36	32.658	gamma-Sitosterol	1.20

5.2 Mathematical modeling and simulation

Kinetic and fixed bed models are proposed for biomass pyrolysis. The kinetic parameters were found using TGA and macro TGA results and were discussed in section 5.2.1. The details of fixed bed model are described in section 5.2.2.

5.2.1 Kinetic parameter estimation

The estimation of kinetic parameters for kinetic model was done using TGA & the results are discussed in section 5.2.1.1. The estimation of global kinetic parameters for apparent model is described in section 5.2.1.2.

5.2.1.1 Kinetic parameters estimation for kinetic model

The kinetic parameters are found by minimizing the square of the error between experimental and theoretical residual weight fractions at heating rate of 10 °C/min to 60 °C/min using logarithmic differential evolution (LDE). LDE gives set of optimum kinetic parameters with minimum value of the objective function. Tables-5.6 & 5.7 show the kinetic parameters of reaction 1 (A_1 and E_1), reaction 2 and reaction 3 (A_{2i}, E_{2i} and A_{3i}, E_{3i}) of decomposition of biomass constituents, and reaction orders for the heating rate of

10 ˚C/min to 60 ˚C/min. The biomass is a multi-constituents complex species of hemicellulose, cellulose and lignin hence the different values of activation energy and order of reaction for a particular biomass constituents for different heating rate are observed. These diverse values are accepted as the model predictions using these kinetic parameters are fitting well with the experimental data. The similar results are also reported by Tran *et. al.* [184], Sricharoenchaikul and Atong [25], El-Sayed *et.al.* [179] Figures 5.23 (a)-(f) shows that the model predicted values of residual weight fractions are matching very well with the TGA experimental data for all heating rates.

Table-5.6 Kinetic parameters of reaction 1 for heating rates of 10 ˚C/min to 60 ˚C/min

Heating rate (°C /min)	**Moisture**	
	A_1 **(min^{-1})**	E_1 **(J/mol)**
10	1.72E+02	5.31E+04
20	1.01E+03	5.86E+04
30	5.39E+03	6.50E+04
40	1.04E+04	6.78E+04
50	6.42E+03	6.49E+04
60	1.17E+04	6.76E+04

Table-5.7 Kinetic parameters of reaction 2 & 3 for heating rates of 10 ˚C/min to 60 ˚C/min

Heating rate (°C /min)	Hemicellulose				
	$A_{2,1}$ (min^{-1})	$E_{2,1}$ (J/mol)	$A_{3,1}$ (min^{-1})	$E_{3,1}$ (J/mol)	Reaction order
10	1.00E+02	7.00E+04	3.66E+13	1.80E+05	5.00E-01
20	1.00E+02	7.00E+04	4.67E+13	1.80E+05	5.00E-01
30	1.00E+02	7.00E+04	5.37E+13	1.80E+05	5.00E-01
40	3.30E+04	9.00E+04	3.51E+13	1.80E+05	5.00E-01
50	2.28E+05	9.99E+04	4.06E+13	1.80E+05	5.00E-01
60	1.00E+02	1.00E+05	5.50E+13	1.80E+05	5.00E-01
Heating rate (°C /min)	**Cellulose**				
	$A_{2,1}$ (min^{-1})	$E_{2,1}$ (J/mol)	$A_{3,1}$ (min^{-1})	$E_{3,1}$ (J/mol)	Reaction order
10	1.95E+13	1.80E+05	5.20E+02	8.00E+04	2.50E+00
20	2.53E+13	1.80E+05	3.15E+03	8.00E+04	2.50E+00
30	2.82E+13	1.80E+05	4.60E+03	8.00E+04	2.50E+00
40	4.06E+13	1.80E+05	2.40E+03	6.00E+04	2.04E+00
50	4.86E+13	1.80E+05	3.28E+03	6.00E+04	2.12E+00
60	6.11E+13	1.80E+05	5.00E+03	6.00E+04	2.31E+00

Heating rate (°C /min)	**Lignin**				
	$A_{2,1}$ **(min^{-1})**	$E_{2,1}$ **(J/mol)**	$A_{3,1}$ **(min^{-1})**	$E_{3,1}$ **(J/mol)**	**Reaction order**
10	1.00E+02	1.50E+05	1.75E+03	3.97E+04	1.82E+00
20	6.48E+02	8.00E+04	8.67E+02	3.71E+04	2.50E+00
30	2.34E+03	8.00E+04	1.10E+03	3.75E+04	2.50E+00
40	1.00E+02	1.50E+05	5.04E+02	3.54E+04	2.50E+00
50	3.45E+02	1.51E+05	6.11E+02	3.52E+04	2.50E+00
60	1.00E+02	1.60E+05	3.49E+02	3.37E+04	2.50E+00

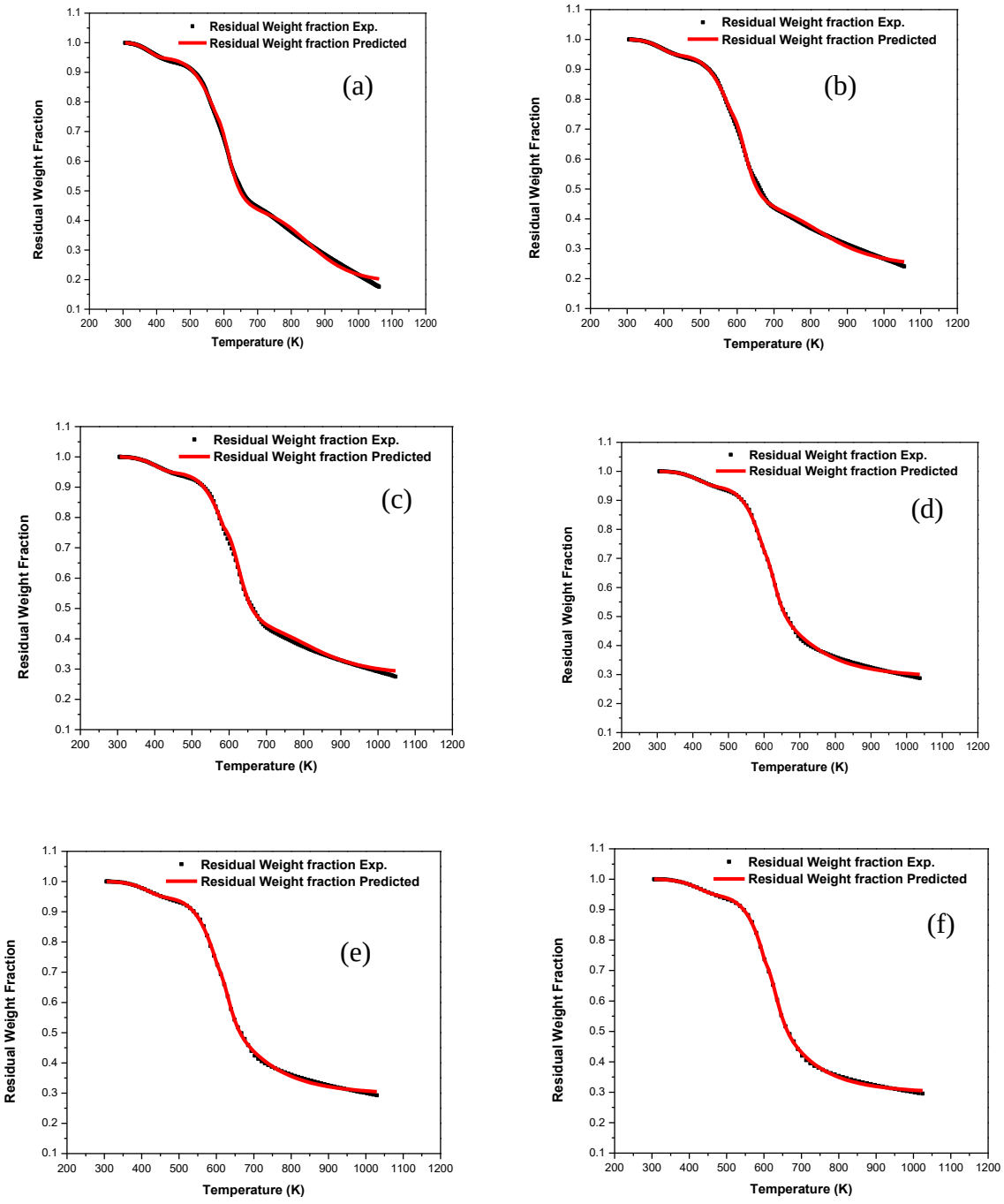

Figure 5.23 Comparison of Experimental and simulated residual weight fraction for heating Rate (a) 10 ˚C/min (b) 20 ˚C/min (c) 30 ˚C/min (d) 40 ˚C/min (e) 50 ˚C/min. (f) 60 ˚C/min

Sricharoenchaikul and Atong [25] estimated the kinetic parameters for the model similar to the one developed in the present study except moisture release. The kinetic parameters reported in their article [25] for different heating rates are given in Table-5.8.

Table-5.8 Kinetic parameters reported by Sricharoenchaikul and Atong [25]

Kinetic Parameter	**Heating Rate**			
	5 °C/min.	**15 °C/min.**	**30 °C/min.**	**90 °C/min.**
A_1 (min^{-1})	5.93×10^{3}	4.32×10	1.76×10	2.06×10
E_1 (kJ/mol)	68.0	49.3	45.7	40.9
A_2 (min^{-1})	8.35×10^{14}	2.56×10^{14}	2.78×10^{15}	1.92×10^{15}
E_2 (kJ/mol)	235.3	227.4	218.5	186.5
A_3 (min^{-1})	5.81×10^{16}	4.92×10^{14}	2.21×10^{14}	1.56×10^{14}
E_3 (kJ/mol)	149.5	143.2	98.7	97.3
N	3.24	3.05	2.37	2.46

The model simulations using kinetic parameters reported in Table 5.8 matches very well with the experimental data of total biomass degradation. However, it is interesting to find that Sricharoenchaikul and Atong [25] have not reported fractional conversion of individual biomass constituents with temperature in their article. To find the fractional conversion of each biomass constituent, we attempted to simulate the kinetic model proposed by Sricharoenchaikul and Atong [25] using the kinetic parameters reported in their article. Figure 5.24 (a) to (d) shows the fractional conversion of the cellulose, hemicellulose and lignin with temperature. It clearly shows that lignin decomposes in the temperature range of 50 °C to 323 °C and hemicellulose decompose in the temperature range of 523 °C to 823 °C whereas the cellulose decomposes over the large temperature range, *i.e.* 177 °C to 923 °C. These results suggested that kinetic parameters found are not truly representing the actual process in which cellulose and hemicellulose

decompose early and over a narrow temperature range in comparison to lignin. To represent the process with kinetic model consisting of biomass constituents' decomposition, not only total biomass decomposition data matching with experimental data, but degradation profile of individual biomass constituent should also be justifiable.

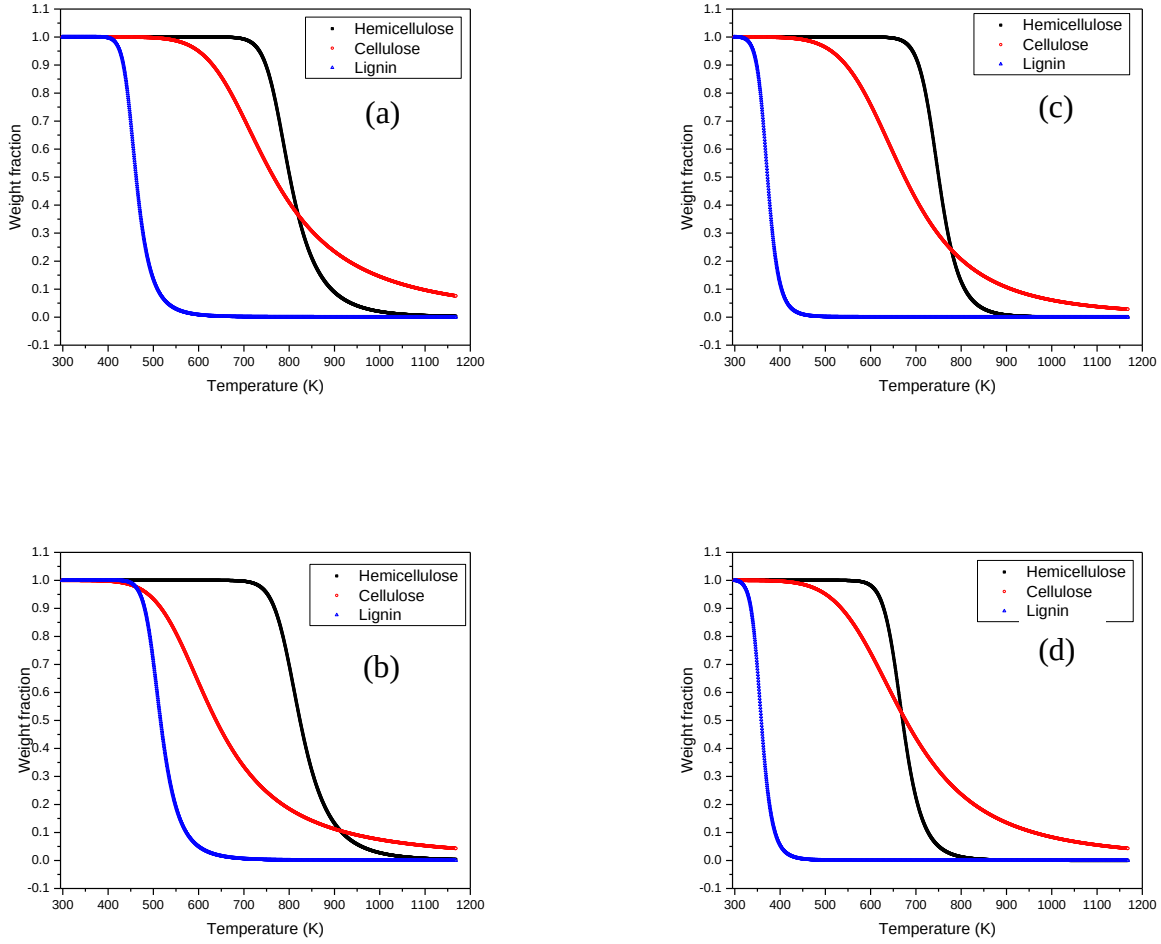

Figure 5.24 Predicted thermal degradation order of Sricharoenchaikul and Atong [25] for Biomass constituents for Heating Rate (a) 5 ˚C/min (b) 15 ˚C/min (c) 30 ˚C/min (d) 90 ˚C/min

Based on these observations, in the present study, along with comparison of experimental and simulated residual weight fraction, the individual biomass component

decomposition along with moisture is also reported (Figure 5.25). Figure 5.25 shows the predicted thermal degradation order of biomass constituents at heating rate of 10°C/min to 60 °C/min. It clearly shows that the moisture is released first followed by hemicellulose and cellulose decomposition. Lignin is the last constituent to get decomposed. The moisture release predictions are observed until 150 °C for heating rate of 10 °C/min. As heating rate increased the span of temperature, in which moisture release phenomenon is observed, also increased from 30 °C - 150 °C for 10 °C/min heating rate to 30 °C - 150 °C for 60 °C/min. It is because the fast increase in temperature does not allow all the moisture to get released. The predicted hemicellulose decomposition occurred in the range of 150 °C to 350 °C. It can be clearly seen from the Figures 5.25 (a) to (f), as heating rate is found to increase the lower value of the simulated temperature span of the hemicellulose decomposition also increased. The temperature span of the hemicellulose degradation is found to decrease as heating rate increased. The temperature span of the simulated cellulose decomposition is 300 °C to 450 °C for all heating rates. Figures 5.25 (c) and (d) shows that the char production from cellulose is increased by 1.5 times upon the increment of heating rate from 30 °C/min to 40 °C/min. The simulated profiles of the cellulose decomposition has shown that there is no further increase in char production beyond heating rate of 40 °C/min. The lignin decomposition took place over a wide temperature range (450 °C to 775 °C for mostly all heating rate values. The thermal decomposition characteristics of biomass constituents are matching qualitatively with the results reported in the literature. Vamvuka *et. al.*[185] proposed a kinetic scheme based on parallel first-order decomposition of biomass components. They reported simulated temperature span of biomass constituent

decomposition in their article. For agricultural residue biomass, their predicted hemicellulose decomposition is at a low temperature (160 ˚C to 360 ˚C), and cellulose is happening over a narrow range of temperature (240 ˚C to 390 ˚C). The simulated lignin decomposition is predicted to occur over a wide range of temperature (400 ˚C to 775 ˚C).

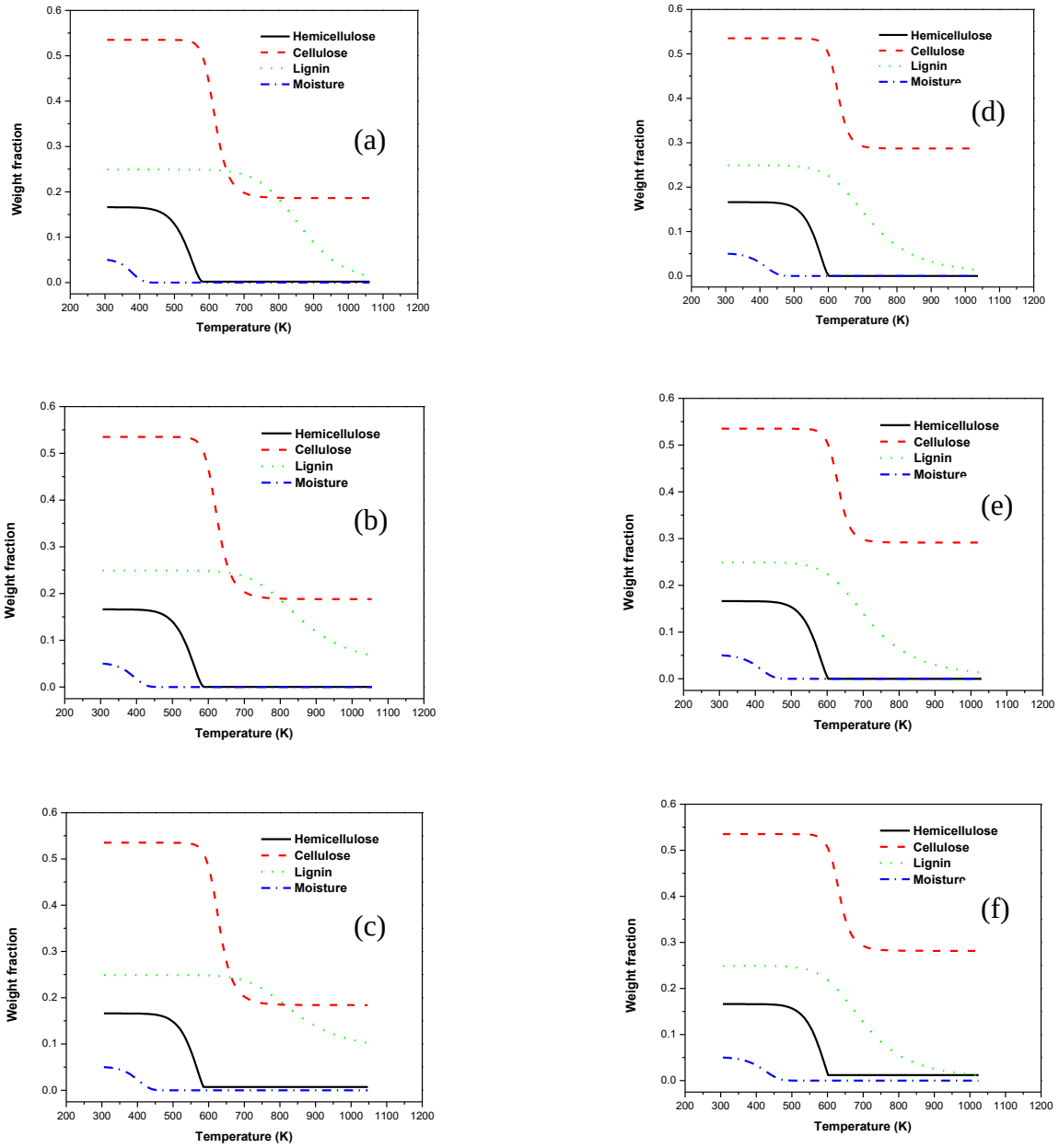

Figure 5.25 Predicted thermal degradation order of Biomass constituents for heating Rate (a) 10 ˚C/min. (b) 20 ˚C/min. (c) 30 ˚C/min. (d) 40 ˚C/min. (e) 50 ˚C/min. (f) 60 ˚C/min.

5.2.1.2 Global kinetic parameters estimation for apparent kinetic model

The global kinetic parameters are established by minimizing the square of the error between experimental and theoretical residual weight fractions at different reactor temperature using logarithmic differential evolution (LDE). LDE provides set of optimum kinetic parameters with minimum value of the objective function. Tables-5.9 and 5.10 has shown the estimated kinetic parameters for small size biomass pyrolysis and large size biomass pyrolysis, respectively, The different values of activation energy and reaction order are accepted as the model predictions using these kinetic parameters are fitting well with the experimental data. Figures 5.26, 5.28 and (a)-(d) shows that the model predicted values of residual weight fractions are matching very well with the experimental data for all reactor temperature. Figures 5.29- 5.31 show the comparison of the predicted yield of oil, non-condensable gases and char with experimental product yields for large particle of biomass (0.5 inch and 1.0 inch particle size) and is found in good agreement with experimental product yield.

Table-5.9 Estimated kinetic parameters for small size biomass pyrolysis.

Particle size		**10-14 mesh (1.4 to 2.0 mm)**			**52-60 mesh (0.25 to 0.3 mm)**		
Reactor temp. (^{0}C)		**400**	**550**	**700**	**400**	**550**	**700**
Kinetic data for volatiles	A_0 **(min^{-1})**	4.34E+02	3.72E+11	4.14E+04	1.02E+02	1.00E+02	4.53E+02
	E_V **(J/mol)**	6.42E+04	1.63E+05	8.64E+04	5.27E+04	5.80E+04	6.69E+04
	Order of reaction	1.55E+00	2.00E+00	2.00E+00	1.85E+00	2.00E+00	2.00E+00
Kinetic	A_0	1.00E+18	7.52E+09	5.93E+03	1.24E+07	3.35E+05	4.56E+02

data for char	**(min^{-1})**						
	E_C **(J/mol)**	2.30E+05	1.44E+05	7.69E+04	1.01E+05	9.77E+04	6.76E+04
	Order of reaction	1.55E+00	2.00E+00	2.00E+00	1.85E+00	2.00E+00	2.00E+00
Kinetic data for gas	A_0 **(min^{-1})**	1.00E+18	1.00E+02	4.97E+04	5.32E+15	1.55E+08	2.62E+03
	E_G **(J/mol)**	2.32E+05	5.87E+04	1.94E+05	1.94E+05	1.29E+05	7.46E+04
	Order of reaction	1.55E+00	2.00E+00	2.00E+00	1.85E+00	2.00E+00	2.00E+00
	a	0.2193			0.2206		
	b	0.1743			0.1637		
	c	0.0445			0.0412		
	d	0.5619			0.5745		

Table-5.10 Estimated kinetic parameters for large size biomass pyrolysis.

Particle size		**1 inch**			**0.5 inch**		
Reactor temp. (^{0}C)		400	550	700	400	550	700
Kinetic data for volatiles	A_0 **(min^{-1})**	1.00E+02	1.23E+03	3.60E+02	7.08E+17	9.80E+03	1.21E+02
	E_V **(J/mol)**	5.48E+04	6.71E+04	5.95E+04	4.23E+04	7.62E+04	5.38E+04
	Order of reaction	1.74E+00	2.00E+00	2.00E+00	1.87E+00	2.00E+00	2.00E+00
Kinetic data for char	A_0 **(min^{-1})**	6.14E+15	1.13E+05	3.89E+02	9.60E+11	1.17E+03	1.00E+02
	E_C **(J/mol)**	1.96E+05	8.71E+04	6.29E+04	1.57E+05	6.58E+04	5.60E+04
	Order of reaction	1.74E+00	2.00E+00	2.00E+00	1.87E+00	2.00E+00	2.00E+00
Kinetic data for gas	A_0 **(min^{-1})**	1.91E+17	2.46E+06	4.46E+15	1.01E+02	2.01E+03	3.64E+15
	E_G **(J/mol)**	2.15E+05	1.02E+05	2.50E+05	5.55E+04	6.89E+04	2.50E+05
	Order of reaction	1.74E+00	2.00E+00	2.00E+00	1.87E+00	2.00E+00	2.00E+00
	a	0.1722			0.1749		
	b	0.1580			0.1654		
	c	0.0445			0.0432		
	d	0.6252			0.6164		

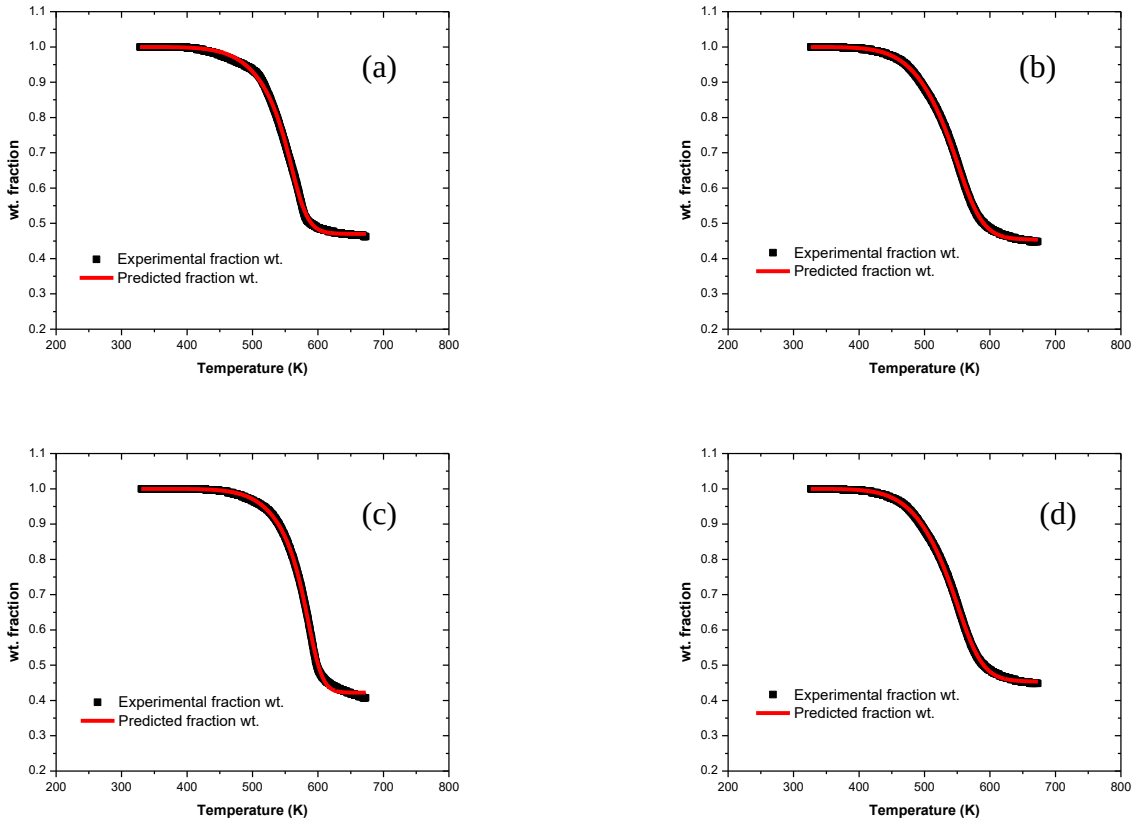

Figure 5.26 Comparison of Experimental and simulated residual weight fraction at 400 °C temperature for particle size (a)1 inch (b) 0.5 inch (c) 10-14 mesh (1.4 to 2.0 mm) (d) 52-60 mesh (0.25 to 0.3 mm)

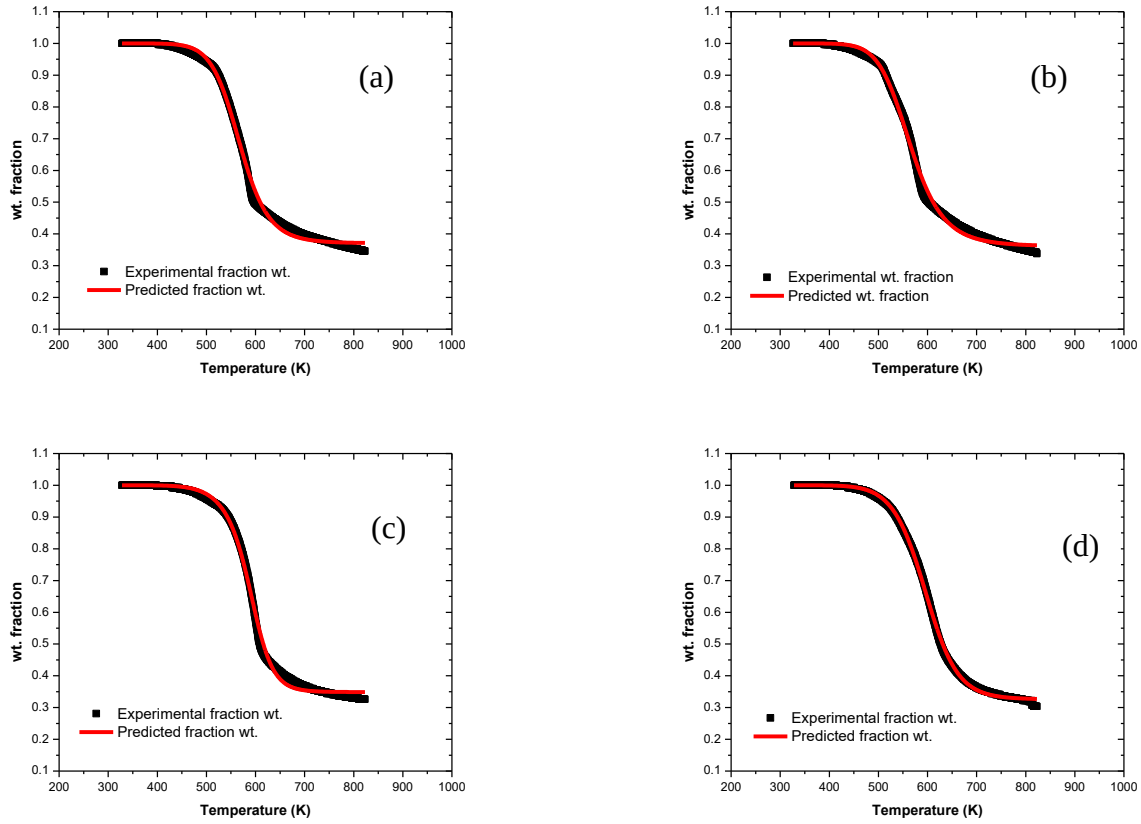

Figure 5.27 Comparison of Experimental and simulated residual weight fraction at 550 °C temperature for particle size (a)1 inch (b) 0.5 inch (c) 10-14 mesh (1.4 to 2.0 mm) (d) 52-60 mesh (0.25 to 0.3 mm)

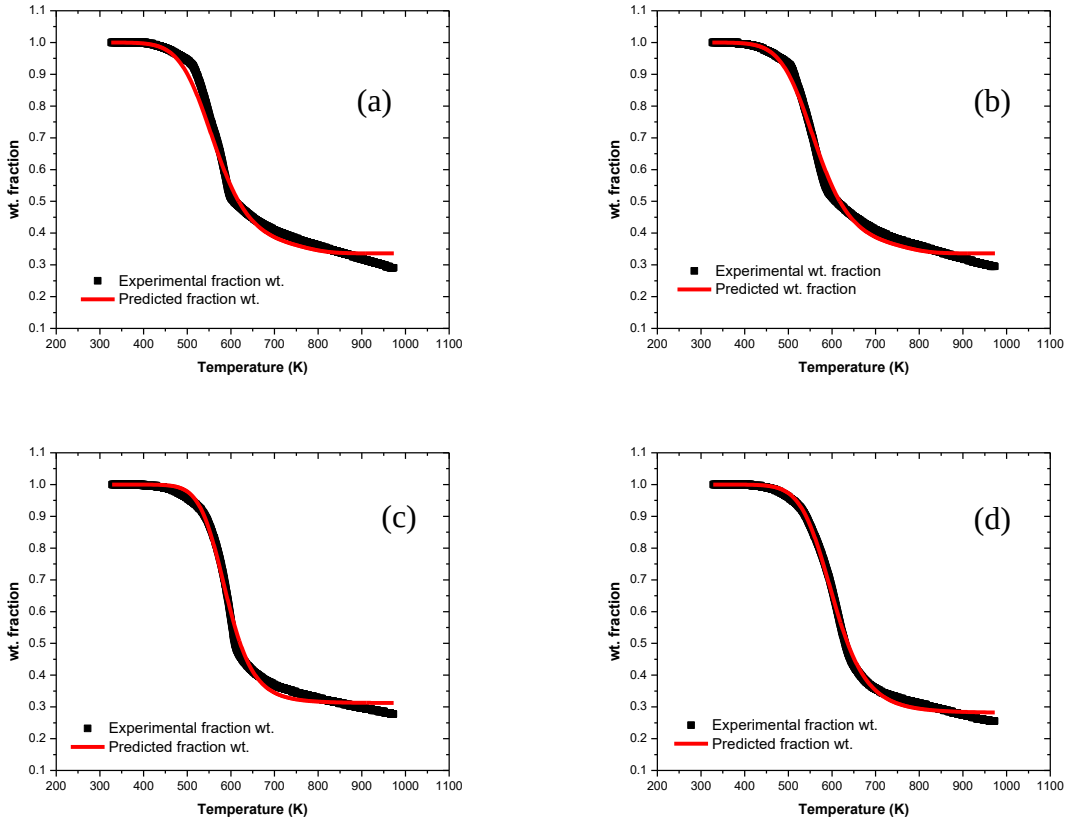

Fig. 5.28 Comparison of Experimental and simulated residual weight fraction at 700 ˚C temperature for particle size (a)1 inch (b) 0.5 inch (c) 10-14 mesh (1.4 to 2.0 mm) (d) 52-60 mesh (0.25 to 0.3 mm)

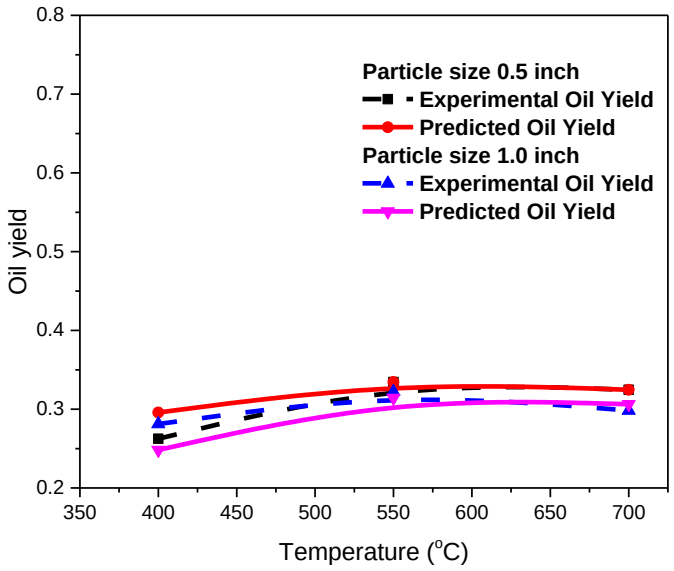

Figure 5.29 Comparison of Experimental and simulated oil yield at different reactor temperatures for particle size 0.5 inch and 1 inch

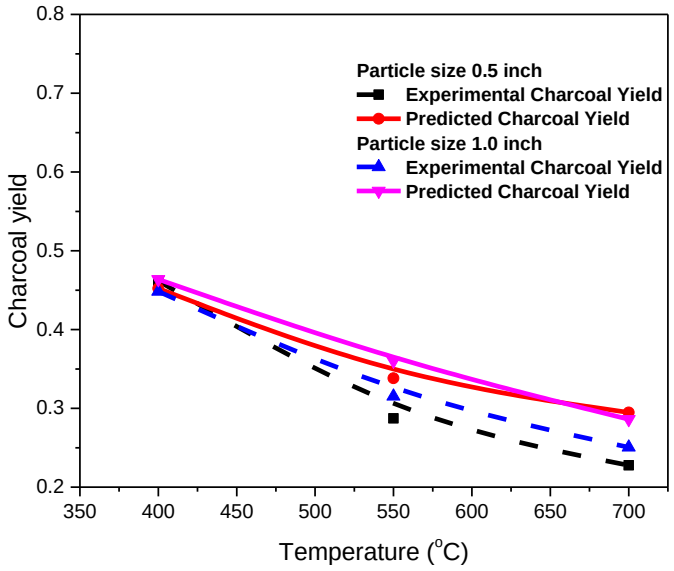

Figure 5.30 Comparison of Experimental and simulated char yield at different reactor temperatures for particle size 0.5 inch and 1 inch

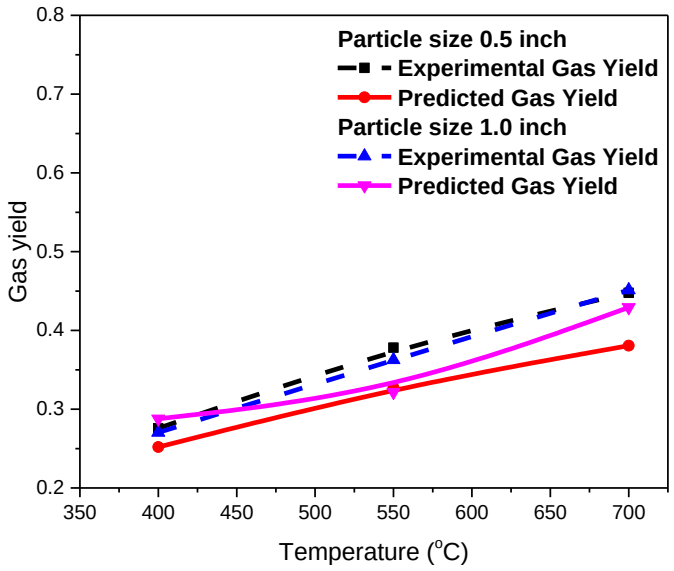

Figure 5.31 Comparison of Experimental and simulated gas yield at different reactor temperatures for particle size 0.5 inch and 1 inch

Figures 5.29- 5.31 show the comparison of experimental and simulated product yield at different reactor temperatures for particle size ranges from 0.5 inch and 1 inch respectively. It is observed that the experimental bio oil yield varied from 26.25 wt % to 33.5 wt % for 0.5 inch particle and 28.1 wt % to 32.2 wt % for 1 inch particle as the pyrolysis temperatures rise from 400 ˚C to 700 ˚C. The maximum bio oil yield is 33.5 wt % and 32.2 wt % at 550 ˚C for 0.5 inch and 1 inch particle respectively. However, the predicted or simulated bio oil yield varies from 29.5 wt % to 33.5 wt % and 24.82 wt % to 31.42 wt % respectively as the pyrolysis temperatures rise from 400 ˚C to 700 ˚C. The maximum bio oil yield is achieved at 550 ˚C. The experimental char yield gradually decreases from 46.17 wt % to 22.76 wt% with the increase in temperature. However the predicted or simulated char yield decreases from 45.22 wt % to 29.47 wt %. The experimental gas yield gradually increases from 27.57 wt % to 44.77 wt % with the increase in temperature. However the predicted or simulated gas yield increases from 25.2 wt % to 38.1 wt %.

5.2.2 Modeling and simulation of Fixed bed model

In present study, a 2D (*r*, *z*) unsteady state combined transport and kinetic model for the cylindrical fixed bed pyrolyzer is developed. The assumptions taken while developing the model are: (1) volatile transport in pyrolysis is only via diffusion, (2) by heating, volatile emission takes place in *z*-direction only, (3) biomass and char velocity is zero, (4) biomass, char and volatiles are at same temperature. The properties of the biomass along with other modeling parameters are tabulated in Table 5.11. The dynamic profiles of temperature, concentration of biomass and porosity is presented. Volatile flux with time is also plotted.

5.2.2.1 Temperature profiles in the bed at different time intervals

Temperature profiles in the bed on heating are illustrated in Figures 5.32 to 5.37 for reactor final temperature of 550 ˚C. The biomass bed is being heated indirectly by radiation mode of heat transfer at the top and cylindrical surface of the bed and bottom of the bed heated via conduction. Figure 5.32 has shown the temperature profile along axial and radial direction in which Figure 5.32 (a) shown the initial condition that is 30 ˚C temperature everywhere (plot at above is projection of the below one). As heating starts after 1 s (shown in Figure 5.32 (b) with the specifications given above (in particular case heating rate was 7.83 ˚C/min), at the bottom of the bed temperature started increasing because of conduction but the temperature at top and sides is still at lower temperatures because radiation is negligible.

Table 5.11 Nominal values of parameters

S. No	Parameters	Correlation/value	Unit
1.	P_1	1.5	Dimensionless
2.	P_2	1	Dimensionless
3.	Stefan–Boltzmann constant (σ)	5.67×10^{8}	W m^{-2} $^{\circ}C^{-4}$
4.	Initial Temperature (T_0)	33	˚C
5.	Final Temperature (T_f)	800	˚C
6.	Initial density of biomass (C_{B0})	601.2	kg/m^3
7.	Reaction progress variable (η)	$\eta = \frac{\rho_b}{\rho_b + \rho_c}$	Dimensionless
8.	Dimensionless temperature(θ)	$\theta = \frac{T_f - T}{T_f - T_0}$	Dimensionless
9.	Thermal diffusivity of wood(α)	$\alpha = \frac{k_{eff}}{\rho C_p}$	m^2/s
10.	Holder surface temperature(T_{hs})	In the range of 125-475	˚C
11.	Reactor surface Temperature(T_{rs})	T_{rs}+50	˚C
12.	Absolute density of biomass(ρ_{abb})	700	kg/m^3
13.	Absolute density of char(ρ_{abc})	700	kg/m^3
14.	Bed porosity(ϕ)	$\varphi = 1 - \frac{\rho_b}{\rho_{abb}} - \frac{\rho_c}{\rho_{abc}}$	Dimensionless
15.	Effective heat capacity	$C_{eff} = \eta C_{pb} + (1-\eta) C_{pc}$	J kg^{-1} $^{\circ}C^{-1}$
16.	Empirical co-efficient in porosity equation	a = 0.9839	Dimensionless
17.	Empirical co-efficient in porosity equation	b = -1.25× 10^{-3}	Dimensionless
18	Length of cylinder biomass bed	L= 10	mm
19	Radius of the biomass bed	R= 60	mm

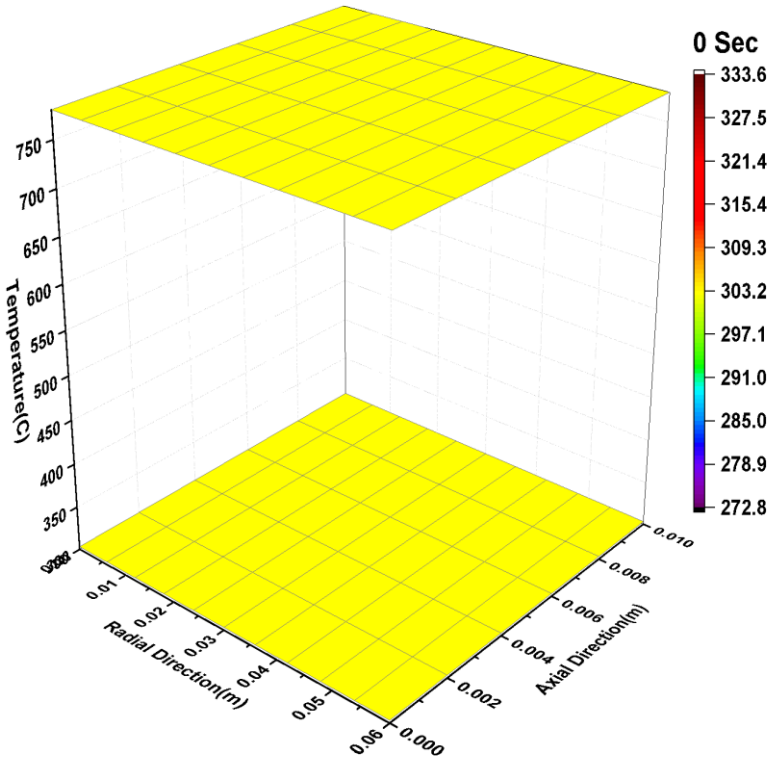

(a)

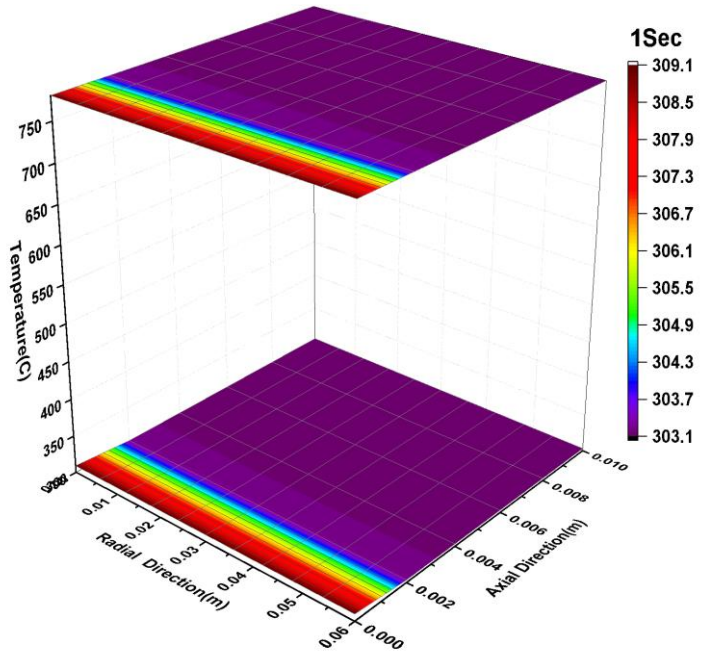

(b)

Figure 5.32 Temperature profiles plotted against radial and axial direction at initial time and *t*=1 s.

Figure 5.33 shows the temperature profiles after 10 s and 60 s, here we can see that the temperature is increasing slowly at the bottom (in axial direction at 0 mm) which is progressing in axial direction that is along the height of the bed. The temperature has increased to 27 $^{\circ}$C in Figures 5.33 (a) and (b) after 60 s temperature has reached to 40 $^{\circ}$C and is slowly progressing in upward direction.

Figures 5.34 (a) and (b) shows temperature profiles at 180 s and 600 s, where we can see that temperature is progressing in axial direction and has increased to 115 $^{\circ}$C and at top and sides also temperature has started increasing which is via radiation and is progressing towards center (in Figure 5.32(b)).

Figure 5.35 (a) and (b) shows temperature profiles at 1200 s and 1500 s, where we can see that temperature contour formation started towards center with the highest temperature at the bottom which is 192 $^{\circ}$C in Figure 5.35 (a) and 298 °C in Figure 5.35 (b).

Figures 5.36 (a) and (b) shows temperature profiles at 2400 s and 2700 s, where we can see that temperature at the bottom has increased to 450 $^{\circ}$C Figure 5.36 (a) and 390 $^{\circ}$C Figure 5.36 (b) whereas at the top the temperature is 10 $^{\circ}$C lesser then that of the bottom for both the Figures.

Figures 5.37 (a) and (b) shows temperature profiles at 3500 s and 3600 s, where we can see that temperature at the bottom in Figure 5.37 (a) is 490 $^{\circ}$C and in Figure 5.37 (b) throughout the bed temperature has increased to final temperature which is 550 $^{\circ}$C.

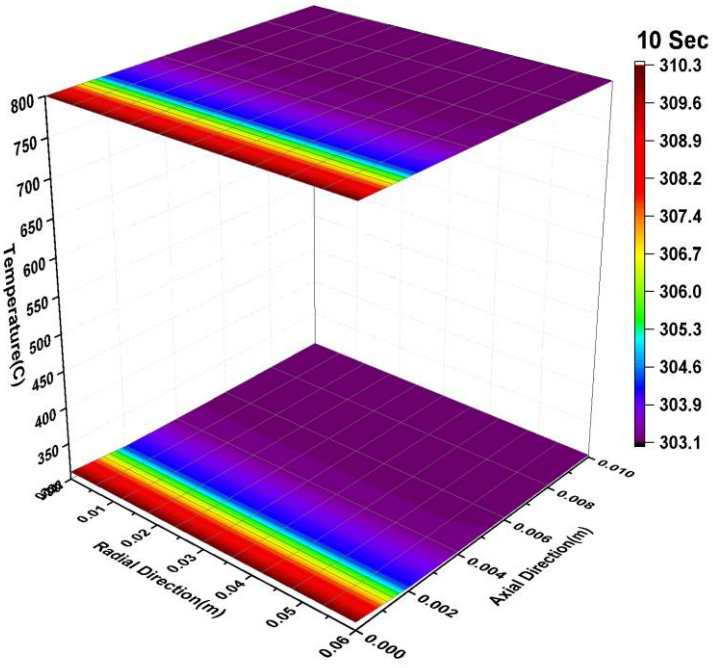

(a)

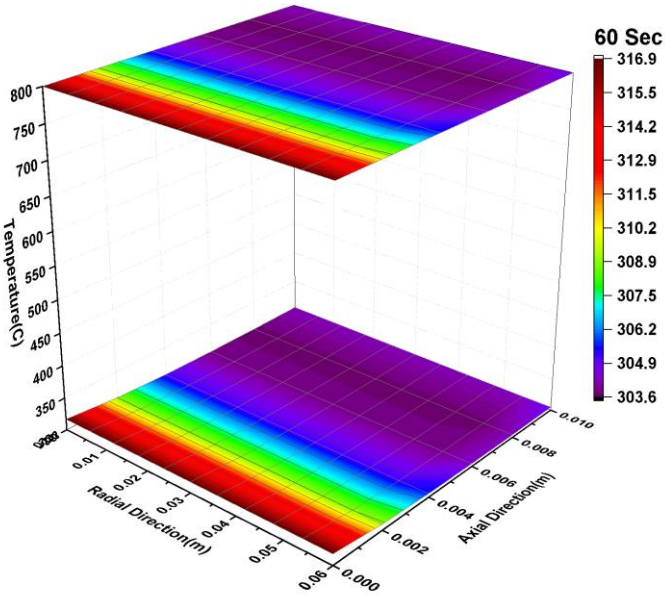

(b)

Figure 5.33 Temperature profiles plotted against radial and axial direction at *t*=10 and *t*=60 s.

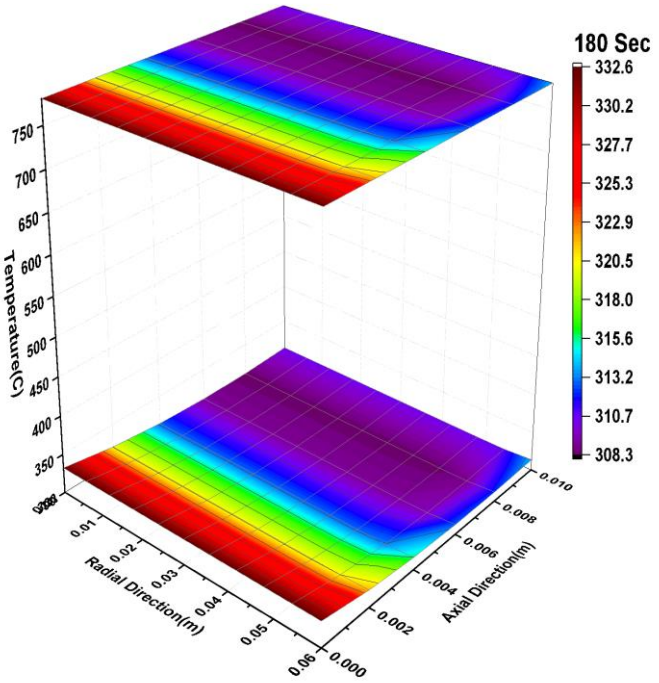

(a)

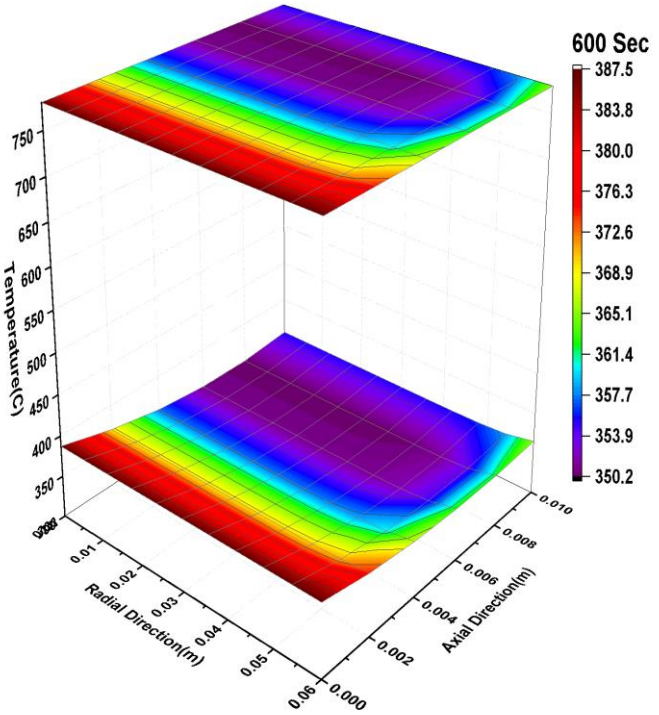

(b)

Figure 5.34 Temperature profiles plotted against radial and axial direction at *t*=180 s and *t*=600 s.

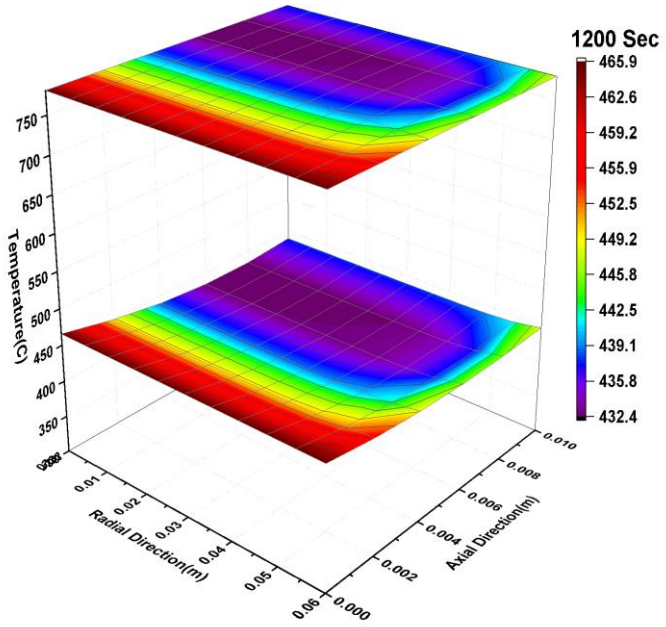

(a)

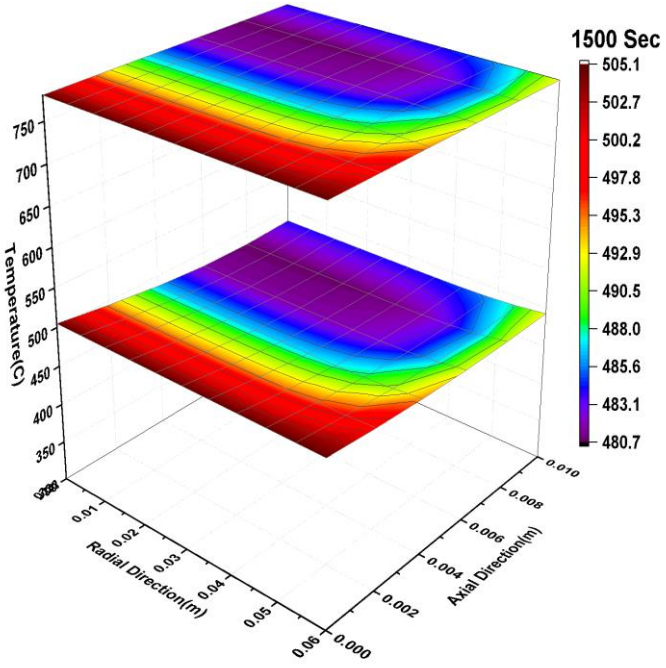

(b)

Figure 5.35 Temperature profiles plotted against radial and axial direction at *t*=1200 s and *t*=1500 s.

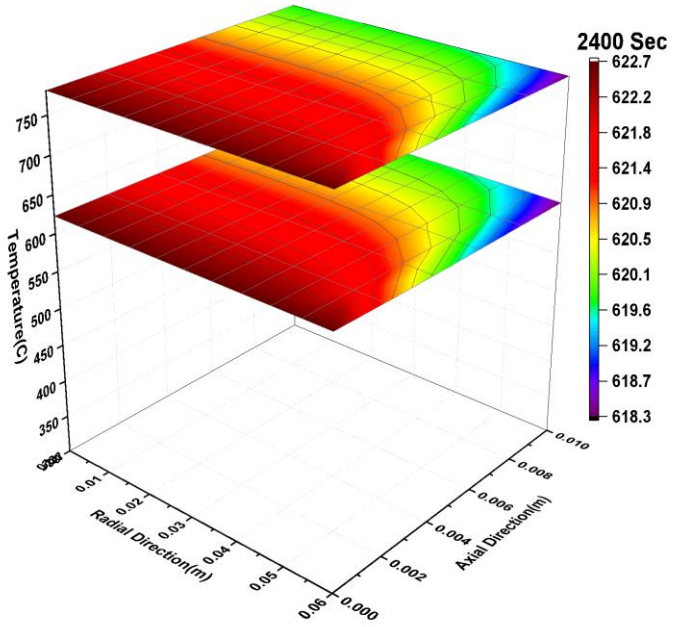

(a)

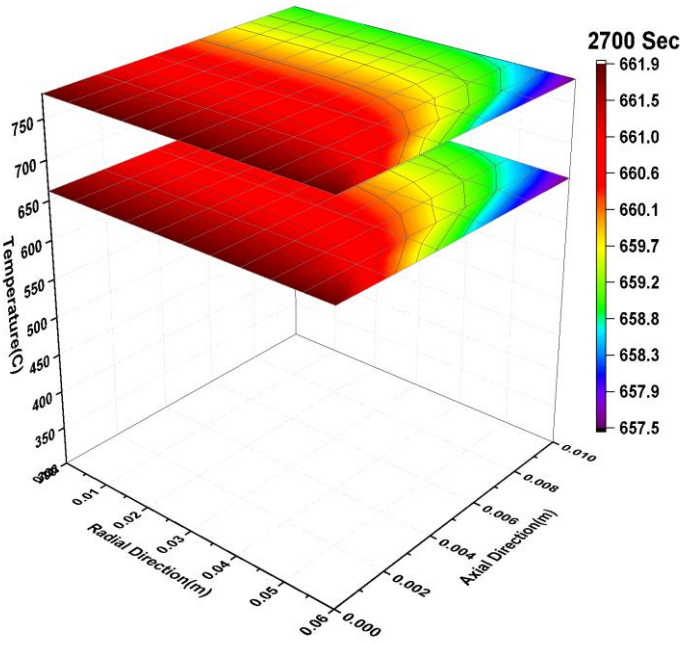

(b)

Figure 5.36 Temperature profiles plotted against radial and axial direction at *t*=2400 s and *t*=2700 s.

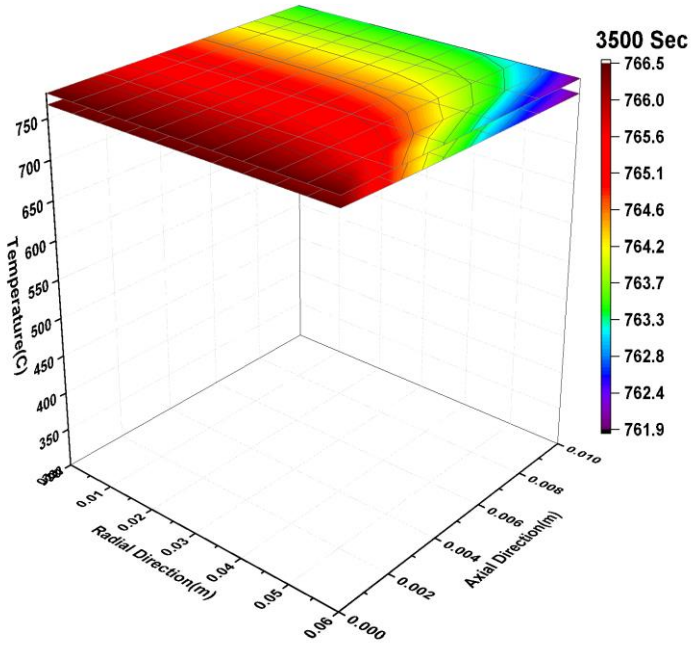

(a)

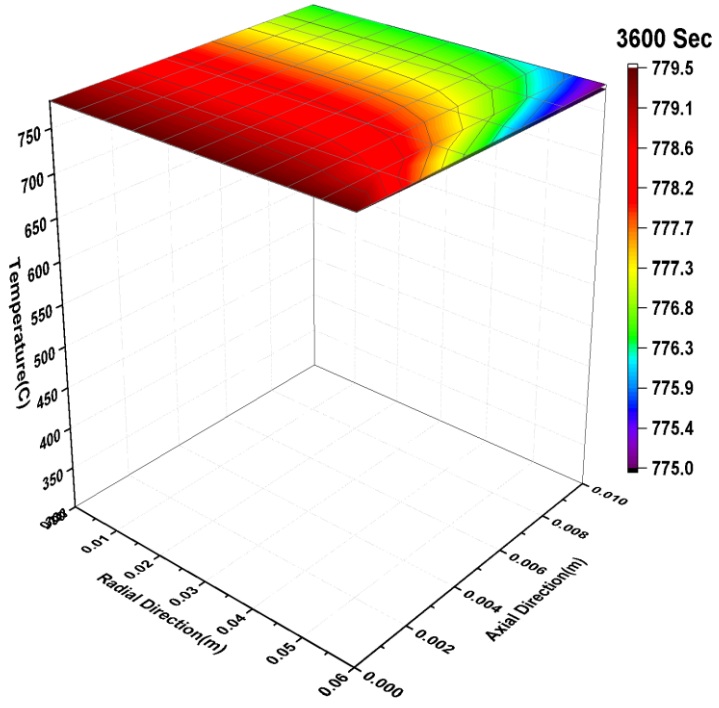

(b)

Figure 5.37 Temperature profiles plotted against radial and axial direction at *t*=3500 s and *t*=3600 s.

5.2.2.2 Biomass decomposition profiles in the bed at different time intervals

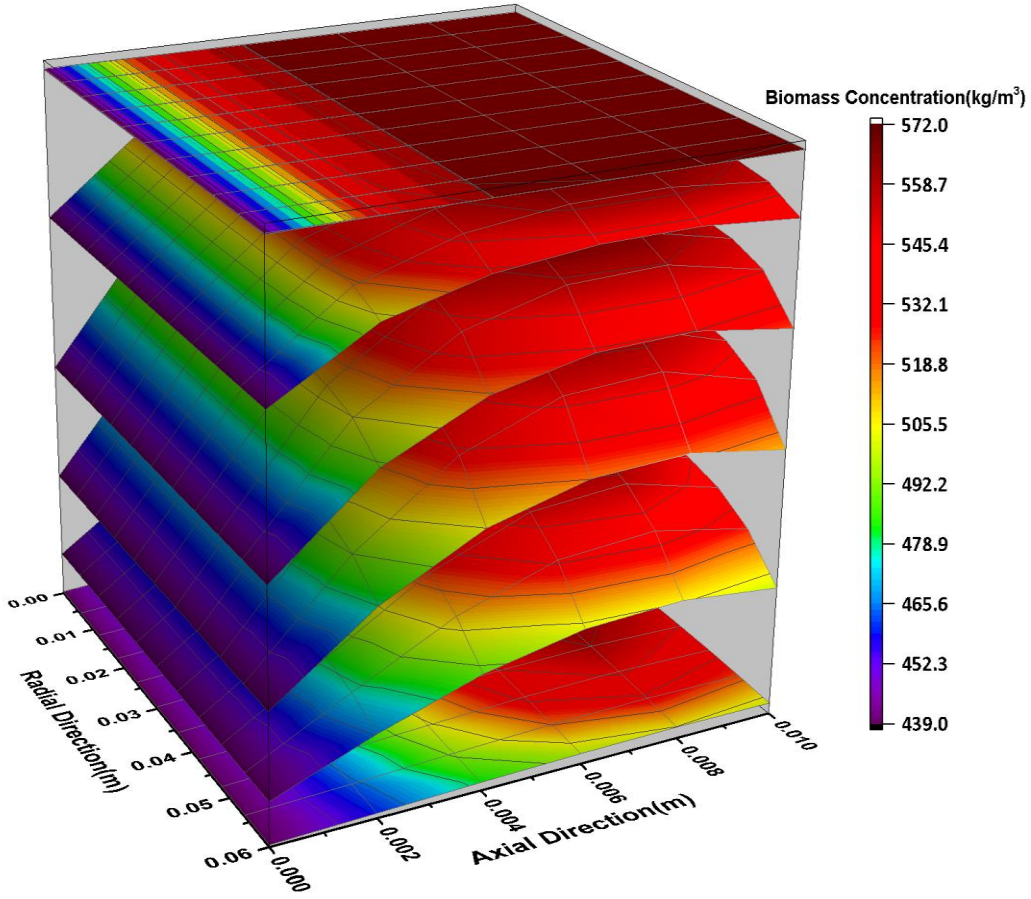

Figure 5.38 Biomass decomposition profiles plotted against radial and axial direction at different time.

Figure 5.38 shows biomass concentration profiles in the fixed bed for final temperature of 550 ˚C at different time that is from top to bottom 60 s, 1250 s, 1400 s, 1500 s and 1750 s, respectively. Hence here we see that how biomass concentration is varying in the bed as well as with time. At particular time the concentration is maximum at top where we have lesser temperature and vice versa. The profiles with time has almost same trend but different values which are shown in the plot.

5.2.2.3 Porosity profiles in the bed at different time intervals

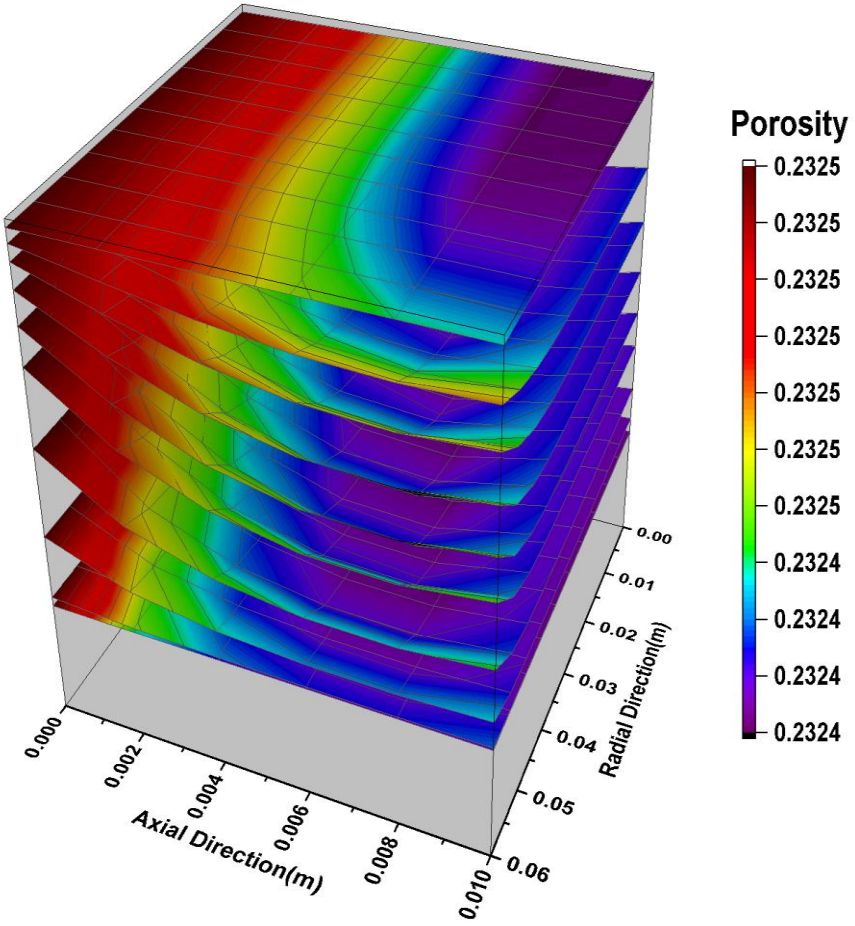

Figure 5.39 Porosity profiles plotted against radial and axial direction at different time.

Figure 5.39 shows the porosity variation in the fixed bed for final temperature of 550 $^{\circ}$C at different time those are 60 s, 180 s, 600 s, 1200 s, 1400 s, 1500 s, 2400 s, 3200 s and 3600 s, respectively from bottom to top. As the temperature in the bed increases biomass reacts to form char and volatiles, volatiles will leave the bed and the rate depends on the diffusion coefficient, whereas the char which is in solid phase stays in place. The porosity depends on how much biomass has converted into char, as reaction precedes porosity increases which are shown in the plot.

5.2.2.4 Char profiles in the bed at different time intervals

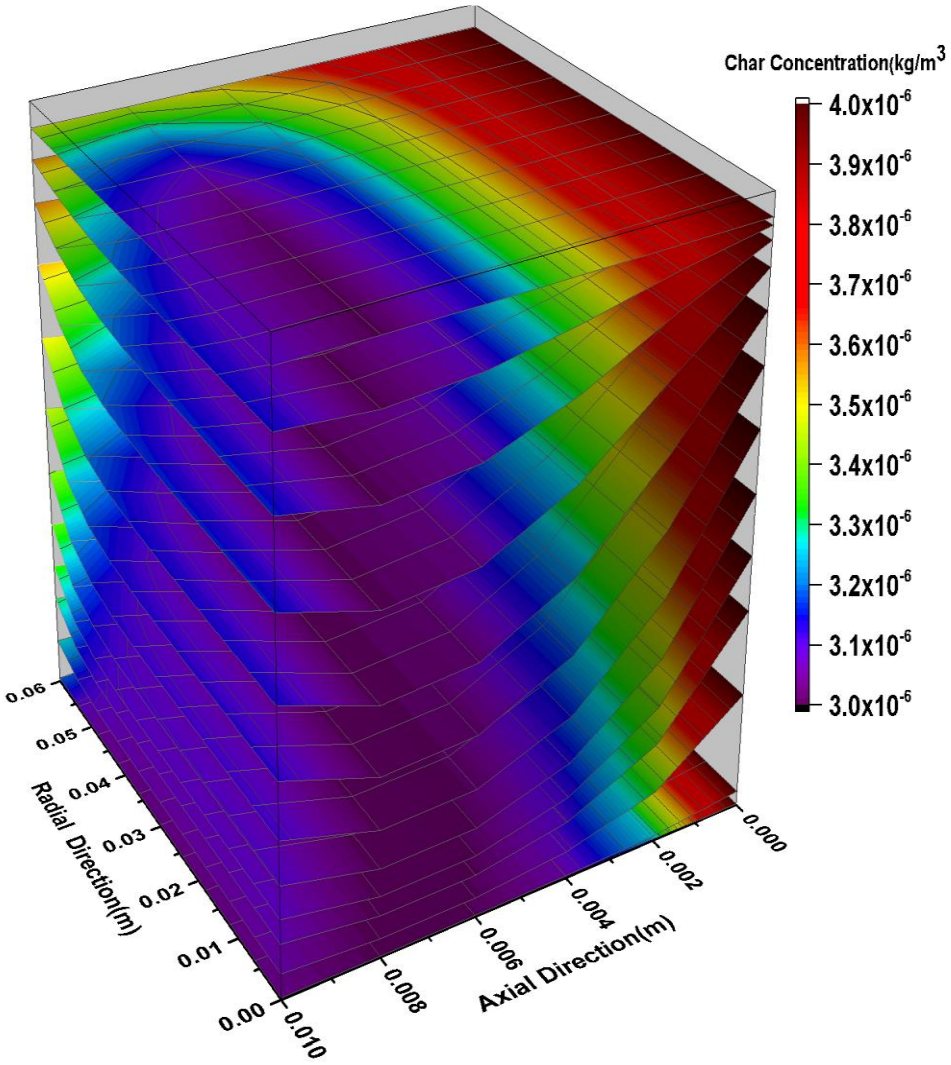

Figure 5.40 Char profiles plotted against radial and axial direction at different time.

Figure 5.40 shows the char concentration variation in the bed along the fixed bed for final temperature of 550 ˚C and variation with time also. The profiles are plotted at time 60 s, 120 s, 180 s, 600 s, 900 s, 1200 s, 1500 s, 1800 s, 2100 s, 2400 s, 2700 s, 3500 s and 3600 s. The variation of char along the bed shows the trend same as porosity that is as temperature increases reaction proceeds and char concentration increases which also increases with time as char we are taking cumulatively.

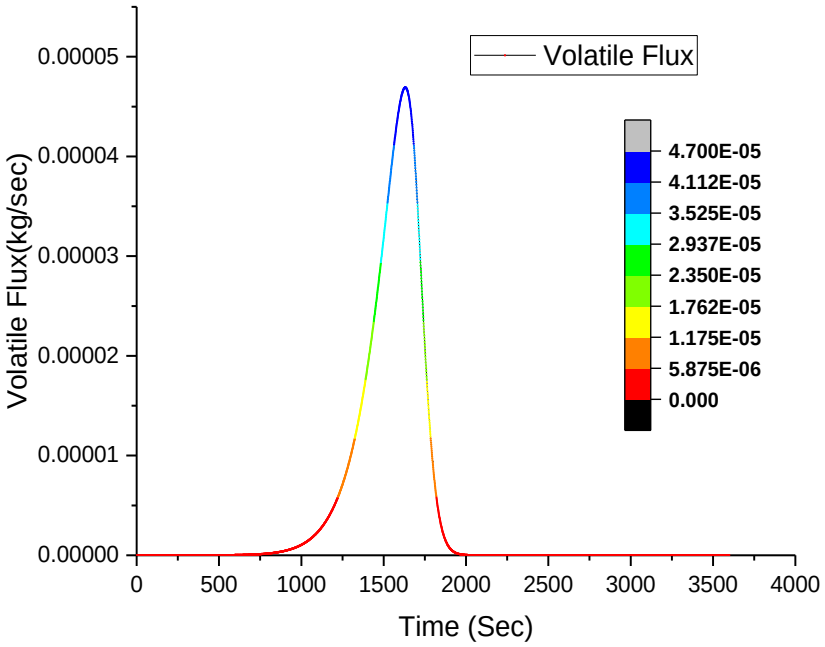

Figure 5.41 Volatile flux with pyrolysis time

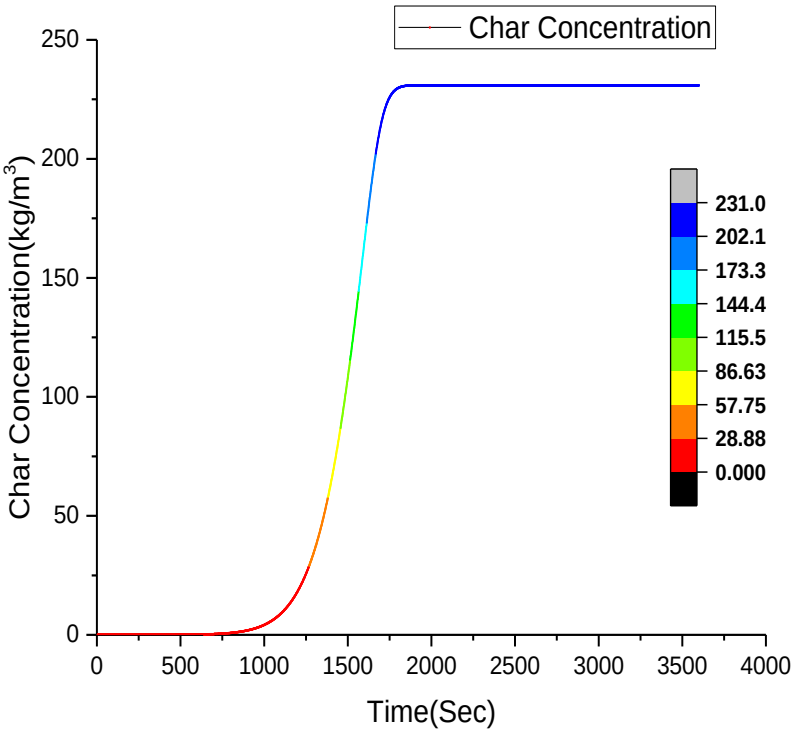

Figure 5.42 Char average concentration in the bed with time

Figure 5.41 demonstrates concentartion of volatiles passing through the bed top crossection per sec and plotted for each sec to take the area under the curve and calculate the total concentration of volailes. The plot trend tells that the flux increses, reaches to the maximum value of 0.000045 kg/s and again decreases to the zero value. Figure 5.42 shows the concentartion of char plotted againest time the char concentartion value average has taken for the whole bed to plot. The concentration increases as reaction starts reaches to the maximum value of the char concentartion 231 kg/m^3 and becomes constant.

CHAPTER – 6

CONCLUDING REMARKS

In the present study, two different kinetic models of biomass pyrolysis and one transport and kinetic model of fixed bed was developed and simulated. The first kinetic model involved multi reaction individual biomass constituent (*i.e.* cellulose, hemicellulose and lignin) decomposition based kinetic scheme with incorporation of moisture release phenomena for thermal decomposition. Apart from this, one step multi reaction apparent kinetic model was also proposed. The combined transport and kinetic model is 2D and dynamic in nature. It takes into account kinetics of chemical reactions, heat and mass transfer between solid and gaseous phases and transport of volatiles produced. It was developed to understand the dynamic temperature variation and porosity variation in the fixed bed. As far experimental study is concerned, biomass pyrolysis experiments were carried out covering a wide range of operating parameters using TGA and fixed bed pyrolyzer to estimate kinetic parameters. The fixed bed reactor is having facility to monitor the weight reduction with time same as TGA but at a macro level. Hence, the term "macro-TGA" was used for this kind of pyrolysis reactor. TGA of the biomass at different heating rates was performed. Experimental study with macro TGA was carried out using *jatropha curcas* de-oiled cake as biomass to generate bio-oil, char and non-condensable gases. The bio-oil produced was characterized using FTIR, TGA and GC-MS. This chapter presents a

brief summary of the present work followed by conclusions, major contributions and future scope for research in this area.

6.1 Summary

6.1.1 Introduction

The world relies heavily on conventional or traditional fuels to meet industrial and domestic needs. Before the industrial revolution, the energy requirements were fulfilled from the natural resources and forest produce. With the discovery of crude oil in 1860, the world has shifted to an unsustainable energy consumption pattern based on petroleum-based fuels as energy. This, combined with the issue of low availability of fossil fuels and gradually increasing awareness about the environmental degradation, suggests that the renewable sources of energy would be a major supplier of energy in the future. The extensive research is going on to replace a sizeable portion of conservative fuels with alternative fuels. Not only, the depletion of fossil fuel reserves, but also the CO_2 emissions released from the combustion of fossil fuels results in a net increase of CO_2 in the environment. The use of the biofuels is the most effective way of halting the increase of the CO_2 concentration. Biomass fuels make no net contribution to atmospheric CO_2 if used in a sustainable manner to allow re-growth. Biomass is an important source of energy and the most important fuel worldwide after coal, oil and natural gas. Biomass includes a wide range of fuels such as wood; agricultural crops, forest, farming residues and peat. Most biomasses are living or dead plants, which use the process of photosynthesis to create stored chemical energy. The industrial usage of biomass is becoming more and more technologically and economically attractive. Biomass can be processed into numerous ways depending upon the characteristics of raw materials, and the type of energy

desired. The conversion of biomass to energy is performed using two main process technologies: thermo-chemical and biochemical/biological. Pyrolysis is one of the primary thermo-chemical treatments to convert biomass into valuable products: solid products (char), liquid products (bio- oil) and gas products (non-condensable gases). Biochemical treatments proceed at mild operating conditions. However, slow productivity, the requirement of pre-treatment to biomass and process wastes poses a problem for implementing it on a large scale. Bio-oil is an unstable mixture of a large number of oxygenated molecules. The heating value of bio oil is significantly less in comparison to petroleum due to the high oxygen content. Bio-oil needs to be upgraded before use as a liquid fuel. Biomass pyrolysis is one of the promising routes amongst the renewable energy options of future energy. The pyrolytic products are more versatile than the original solid biomass. In view of the considerable interest in the pyrolysis process, it is essential to model and predict the performance of a pyrolyzer. There is a necessity to develop a model, which can predict the yield of pyrolysis products under particular operating conditions. After developing the mathematical model, it is important to validate the same using experimental data. To perform the experimental study, the fixed bed pyrolyzer is used for biomass pyrolysis.

6.1.2 Gaps in literature

The kinetics of thermal decomposition of biomass material is complicated, as it involves a large number of reactions in parallel and series. Different classes of mechanisms are reported for the pyrolysis of wood and other ligno-cellulosic materials. The models are classified into three categories: one-step global models; one-stage multi-reaction models; and two-stage semi-global models. The second category of models discuss those mechanisms, which consider simultaneous and competing first order reactions in which virgin biomass decomposes into different

constitutes of pyrolysis products, namely, tar, char, and volatile gases. The third class of models consider pyrolysis to be a two-stage reaction, in which the products of the first stage break up further in the presence of each other to produce secondary pyrolysis products. These reported kinetic studies are limited to use for certain species of biomass only for which kinetic data is available. Limited work has been done to describe the pyrolysis process by the independent parallel first order reactions model. Also, the degradation of biomass is described as the decomposition of its components *i.e.* cellulose, hemicelluloses and lignin. Biomass constituent's decomposition with moisture release phenomena is not reported in the literature yet. It is also observed that the applicability of kinetic of model is limited and used only for small size (less than 1 mm) particles. The pyrolysis of large size particles is controlled by heat and mass transport within the particle. To predict the rate of devolatilization and yield of products for the pyrolysis of large size particles there is a need to develop the particle model and incorporate it into the reactor model which is not reported in literature yet. To understand the dynamic temperature variation and porosity variation in the fixed bed one has to develop the fixed bed model which is not reported in literature yet.

Many of the researchers worked on characterization of bio-oil generated from the pyrolysis of various biomass resources such as wood, rice husk, mustard cake and other de-oiled cakes. However, very limited work has been done on the effect of various operating parameters such as reactor temperature and particle size on the bio-oil composition. It has been observed that the characterization of whole bio-oil leads to difficulty in identifying the exact components even with GC-MS. Very few researchers have used liquid column chromatographic technique to separate out the aliphatic, aromatic and polar compounds followed by GC-MS to determine different constituents of each fraction.

6.1.3 Scope of work

The use of abundant biomass waste is a big concern to the society. Thermo-chemical conversion is most prominent route to produce valuables from the biomass. There is a need of biomass pyrolysis is to be carried out to produce the bio-oil. To understand the pyrolysis of biomass a generalized mathematical model for fixed bed pyrolyzer (macro TGA) is to be developed which takes into account of the limitations of the earlier studies. For the successful operation of the pyrolyzer, prediction of the rate of biomass devolatilization and yield of pyrolysis products is crucial. In general, the kinetics of biomass pyrolysis is developed by conducting the thermo-gravimetric analysis (TGA) experiments but still limited work is done on prediction of order of degradation of biomass constituents with incorporation moisture release phenomena. Hence there is need to develop a kinetic model with moisture release inclusion to predict the order of degradation of biomass constituents as well as yield of products. To validate this type of model TGA experiments is to be carried out.

The applicability of this kinetic of model is limited and can be used only for small size particles, which controlled by kinetically devolatilization. For large size particles the heat and mass transport within the particle played an important role. To predict the rate of devolatilization and yield of products for the pyrolysis of large size particles, there is a need of development of apparent kinetic model for fixed bed pyrolyzer. This developed model could be an important contribution in the scientific literature to predict the pyrolysis process behavior and their product yields either for an independent operation or as a step/zone in the pyrolysis process operation. It can be further utilized for dynamic optimization for improving the performance of the system on a continuous basis. To validate this, pyrolysis experiments of large particle size biomass is to be carried out in laboratory fixed bed pyrolyzer.

For maximum utilization of the bio-oil by extracting the valuable chemical compounds presents in bio-oil, it is necessary to understand its composition and properties. Based on the gaps in literature, it is suggested to separate the bio-oil compounds in aliphatic, aromatic and polar compounds using liquid column chromatography. The analysis of oil requires various spectroscopic and chromatographic methods due to the limitations of the individual analytical techniques. The functional groups of bio-oil can be detected by Fourier transform infrared (FTIR) spectroscopy and components is identified by Gas chromatography and mass spectroscopy (GC-MS).

6.1.4 Mathematical modeling and simulation

The modeling and simulation of the pyrolysis process involves the development and simulation of two different kinetic models and one transport and kinetic model of fixed bed.

6.1.4.1 Component based decomposition kinetic model development

Different classes of mechanisms were proposed for the pyrolysis of wood and other cellulosic materials. The models are classified into three categories: one-step global models, one-stage multi-reaction models, and two-stage semi-global models. The decomposition of biomass can also be described by three independent parallel reactions, each analogous to the decomposition of the constituent hemicellulose, cellulose and lignin. The multi reaction individual biomass constituent (*i.e.* cellulose, hemicellulose and lignin) decomposition based kinetic model with incorporation of moisture release phenomena is proposed for pyrolysis of biomass. The kinetic parameter estimation is carried out by minimizing the sum of the square of the error between experimental and simulated values. However, previous researchers have not incorporated individual biomass constituent's decomposition in their kinetic model. In

the present study, the kinetic model based on biomass constituent's decomposition with moisture evaporation is proposed. Each biomass constituent, i.e. cellulose, hemi-cellulose and lignin get decomposed by two parallel independent n^{th} order reaction producing volatiles & gases and char. The volatiles and gases may further react with char to produce different types of volatiles, gases and char where the compositions are distinct.

6.1.4.2 Apparent kinetic model development

The applicability of kinetic model (based on TGA results) is limited and can be used only for small size (less than 1 mm) particles, which are undergoing kinetically controlled devolatilization. The pyrolysis of large size particles is controlled by heat and mass transport within the particle. To predict the rate of devolatilization and yield of products for the pyrolysis of large size particles, there is a need to develop the particle model and incorporate it into the reactor model. The alternative to this approach is to develop the apparent kinetic model for the pyrolysis process. The limitations of one step global kinetic model is the wrong prediction of the product yields. The model predicted that liquid, gas and char yield are continuously increases as the rate of reaction increases but actually the yield of liquid increases as the temperature increase till 550 ˚C and after that it decreases as the cracking of liquid product takes place. Hence, to predict the correct value of yield for various products, one or more step multi reaction global kinetic model is must. In the present study, the thermal degradation of biomass is proposed by one step multi reaction global model. The degradation of biomass is expressed as parallel production of volatiles, gases and char. Macro thermo-gravimetric analysis (TGA) of *Jatropha* de-oiled cake (biomass used in the present study) is performed using laboratory macro TGA. The weight loss of the biomass, product yields and composition of non-condensable gases are

measured. These results are used to develop the apparent kinetic model. The model is simulated and corresponding global kinetic parameters are found. The developed model could be an important contribution in the scientific literature to predict the pyrolysis process behavior and their product yields either for an independent operation or as a step/zone in the gasification process operation. It can be further utilized for dynamic optimization for improving the performance of the system on a continuous basis.

6.1.4.3 Fixed bed model development

A 2D (*r, z*) dynamic combined transport and kinetic model for the cylindrical fixed bed pyrolyzer. It is developed to understand the dynamic temperature variation and porosity variation in the fixed bed. The model consists of two partial differential equations (heat and volatile transport) and two ordinary differential equations (biomass decomposition and char generation). The heat transport equation includes the conductive heat transport in both directions along with accumulation term. The volatile transport equation includes the molecular diffusion of volatiles only in z-direction along with accumulation term. The model includes heat transfer from the reactor wall to biomass bed both by radiation as well as convection mode. In order to solve the nonlinear energy and mass transport equations, finite difference method is used for the spatial discretization and implicit method has been adopted for solving the temporal terms. Due to radiation effect model equations become nonlinear; hence Jacobian iterative method is utilized to solve the set of nonlinear algebraic equations.

6.1.5 Experimental studies

The pyrolysis of biomass experiments are conducted in the macro TGA for different reactor with variation in particle size. The experimental set up consists of mainly in six parts: furnace, pyrolysis reactor, condensers, sample holder, weighing balance,

and inert gas supply system. The temperature controller unit (M/N: FY 400-301000) is connected to the furnace, which controls the reactor temperature and also the heating rate. To provide the inert environment inside the reactor, nitrogen gas is purged continuously inside the reactor from two different positions. The biomass is placed on the sample holder, which is resting above the digital weighing balance which is resting in closed air tight chamber to avoid the contact of air. Upon increasing the temperature, the biomass sample gets pyrolyzed and releases the volatiles. The volatiles along with inert nitrogen exits from the top of the reactor and are cooled in a two-stage condenser assembly followed by an ice trap. The collected bio-oil are separated in to aliphatic, aromatic and polar fractions. These fractions are analyzed by FTIR and GC-MS.

6.1.6 Results and discussion

In these sections, the experimental results achieved in the present study are summarized. The section also described the simulation results which are obtained by validating the proposed mathematical model using the experimental data.

6.1.6.1 Mathematical modeling and simulation

6.1.6.1.1 Kinetic parameters estimation for kinetic model

The kinetic parameters are found by minimizing the square of the error between experimental and theoretical residual weight fractions at heating rate of 10 $^{\circ}$C/min to 60 $^{\circ}$C /min using logarithmic differential evolution (LDE). LDE gives set of optimum kinetic parameters with minimum value of the objective function. Kinetic parameters are estimated for reaction 1 (A_1 and E_1), reaction 2 and reaction 3 (A_{2i}, E_{2i} and A_{3i}, E_{3i}) of decomposition of biomass constituents, and reaction orders for the heating rate of 10 $^{\circ}$C/min to 60 $^{\circ}$C/min. We observed the model predicted values of residual weight fractions are matching very well with the TGA experimental data for all heating rates.

We also predicted the order of degradation of biomass constituents. It has been observed that first hemicellulose is decomposed followed by cellulose and finally lignin is decomposed.

6.1.6.1.2 Global kinetic parameters estimated for apparent kinetic model

The global kinetic parameters are established by minimizing the square of the error between experimental and theoretical residual weight fractions at different reactor temperature. Global kinetics parameters are found and the yields of products is predicted. We observed predicted yield of bio-oil, non-condensable gases and char have good agreement with experimental product yields for large particle of biomass (0.5 inch and 1.0 inch particle size) and good agreement is found with experimental product yield data.

6.1.6.1.3 Modeling and simulation of fixed bed model

In present study, a 2D (r, z) unsteady state combined transport and kinetic model for the cylindrical fixed bed pyrolyzer is developed. The assumptions taken while developing the model are: (1) volatile transport in pyrolysis is only via diffusion, (2) by heating, volatile emission takes place in z-direction only, (3) biomass and char velocity is zero, (4) biomass, char and volatiles are at same temperature. The dynamic temperature variation profile and porosity variation profile in the fixed bed are obtained.

6.1.6.2 Experimental studies

Biomass pyrolysis experiments are performed with *Jatropha curcas* de-oiled cake as biomass covering a wide range of reactor temperature and biomass particle size. The bio-oil obtained has a reddish-brown colour with an irritant odour. The maximum liquid yield is 31.2 wt % at 500 ˚C, which further decreases with an increase in temperature. The char yield gradually decreases from 48.25 wt % to 31.8 wt % with

the increase in temperature. The gas yield increases with an increase in temperature. This may be certainly due to the secondary cracking of the pyrolysis vapours and char at high temperatures, which may also lead to formation of some non-condensable gaseous products. The FTIR analysis of bio-oil observed the presence of O-H vibrations between 3050 cm^{-1} and 3600 cm^{-1}, together with the presence of C=O stretching vibrations between 1650 cm^{-1} and 1850 cm^{-1} indicates the presence of carboxylic acids and their derivatives. Monocyclic, polycyclic and substituted aromatic groups are indicated by the absorption peaks between 800 $cm^{-1}$and 1000 cm^{-1} and 1550 cm^{-1} and 1700 cm^{-1}. Single ring aromatic compounds and polycyclic compounds are also present in the pyrolysis oil. The presence of the C=O stretching vibrations between 1650 cm^{-1} and 1850 cm^{-1} may also indicate the presence of ketones and aldehydes.

The major compounds characterized by GC-MS are normal alkanes, alkenes, phenols, saturated fatty acids and their derivatives: esters, amides and nitriles were identified. Three major compounds are observed at 28.142, 28.672 and 27.656 retention times with area percent of 19.03, 6.91 and 9.12 respectively. These compounds were identified as 12-Nonadecatriene-5, 14-diol, Octadecanoic acid, methyl ester and (E)-9-Octadecenoic acid respectively. Gas chromatography of the gas sample (final temperature 700 ˚C) has been done and is plotted for different temperatures in Figure 6. The GC analysis of non-condensable gas are observed the presence of H_2, N_2, CH_4, CO and CO_2. Here we found that in non-condensable gases the maximum composition is CO_2 (70 vol %) and minimum is CH_4 varies from 2 vol % to 5 vol %. The composition of CO_2 is decreasing with temperature till 500 ˚C and then slightly increased till maximum at 600 ˚C. H_2 concentration is also almost constant. CO is almost following the decreasing trend as temperature increases.

6.2 Conclusions

Based on the results obtained in the present study, the following conclusions are drawn:

1. The multi reaction individual biomass constituent (*i.e.* cellulose, hemicellulose and lignin) decomposition based kinetic model with incorporation of moisture release phenomena was proposed for pyrolysis of biomass.
2. The kinetic parameters were found by minimization of sum of the square of the error method using non-traditional optimization technique logarithmic differential evolution (LDE). The proposed kinetic model was successfully validated with the experimental data reported in the literature and those obtained in the present experimental study.
3. The apparent kinetic model was developed considering one step multi reaction apparent kinetic scheme to represent the thermal degradation of biomass.
4. The global kinetic parameters were found by minimization of sum of the square error & was performed using non-traditional optimization technique logarithmic differential evolution (LDE).
5. The model predicted composition of pyrolysis products matches very well with the experimental data reported in the literature and those obtained in the present study.
6. The 2D (*r*, *z*) dynamic combined transport and kinetic model for the cylindrical fixed bed pyrolyzer was developed to understand the dynamic temperature variation and porosity variation in the fixed bed.
7. The model predicted dynamic temperature variation profile and porosity variation profile in the fixed bed were obtained.

8. *Jatropha curcas* de-oiled cake has been successfully converted to generate the bio-oil using a fixed bed pyrolyzer.
9. Effect of reactor temperature on yield on pyrolysis product has been studied and the maximum bio-oil yield was found to be 31.2 wt % at the final reactor temperature of 500 $^{\circ}$C, which further decreased with an increase in temperature**.** The char yield gradually decreased from 48.25 wt % to 31.8 wt % with the increase in temperature.
10. Effect of particle size of biomass on yield on pyrolysis product has been studied and the char yield was more for large size particle than the smaller size particles for the same final temperature of reactor and vice versa for bio-oil.
11. Residual weight fraction with time was observed for pyrolysis of *Jatropha curcas* de-oiled cake using TGA.
12. Residual weight fraction with time and the yield of pyrolysis products are observed for pyrolysis of *Jatropha curcas* de-oiled cake using macro TGA for different reactor temperature.
13. GC analysis of non-condensable gases were performed and found maximum composition of CO_2 and minimum composition of CH_4.
14. Bio-oil was analyzed using FTIR and found the presence of single bond with hydrogen that is (C-H, N-H etc), double bond with carbon (C=C, C=N, C=O etc) and single bond with carbon (C-O, C-H, C-N, C-X).
15. FTIR analysis performed for bio-oil collected at different reactor temperature and observed no significant difference in the presence of functional group.
16. TGA and DTG analysis were performed for bio-oil.
17. Bio-oil was separated in aliphatic, aromatic and polar fraction using liquid column chromatography.

18. Bio-oil and its fractions (aliphatic, aromatic and polar fraction) were analyzed and found the presence of acids, alkanes, aromatics, aldehydes and ketones.

6.3 Future scope of research

The future scope of this work is described below:

1. The developed mathematical model can be modified or used for other biomass feedstocks.
2. It is assumed in the fixed bed model that biomass is heated only by radiation from reactor surface and all the volatiles produced flow upwards in the reactor. It can be relaxed or further modeled.
3. Bio-oil produced from pyrolysis of *Jatropha curcas* de-oiled cake can be refined and used as a fuel for vehicles and compared with the other fuels.
4. Fraction of valuable chemical compound can be extracted form bio-oil pyrolysis of *Jatropha curcas* de-oiled cake.
5. The bio-oil production unit could be started with help of recent research.
6. To improve the bio-oil yield one can use the catalyst in pyrolyzer or modify the pyrolyzer.
7. Fraction of exhaust non-condensable gases can be separated by using inline gas separator.
8. Design a fixed bed pyrolyzer based on the analysis to achieve maximum bio-oil yield.

REFERENCES

1. Kothari, R., V.V. Tyagi, and A. Pathak, *Waste-to-energy: A way from renewable energy sources to sustainable development.* Renewable and Sustainable Energy Reviews, 2010. **14**(9): p. 3164-3170.
2. Angira, R. and B.V. Babu, *Optimization of process synthesis and design problems: A modified differential evolution approach.* Chemical Engineering Science, 2006. **61**(14): p. 4707-4721.
3. Sheth, P.N. and B.V. Babu, *Experimental studies on producer gas generation from wood waste in a downdraft biomass gasifier.* Bioresource Technology, 2009. **100**(12): p. 3127-3133.
4. Sheth, P.N. and B.V. Babu, *Production of hydrogen energy through biomass (waste wood) gasification.* International Journal of Hydrogen Energy, 2010. **35**(19): p. 10803-10810.
5. Bai, M., Z. Zhang, and X. Fu, *A review on well integrity issues for CO2 geological storage and enhanced gas recovery.* Renewable and Sustainable Energy Reviews, 2016. **59**(Supplement C): p. 920-926.
6. Sharma, R., P.N. Sheth, and A.M. Gujrathi, *Kinetic modeling and simulation: Pyrolysis of Jatropha residue de-oiled cake.* Renewable Energy, 2016. **86**: p. 554-562.
7. Balat, M. and M. Balat, *Political, economic and environmental impacts of biomass-based hydrogen.* International Journal of Hydrogen Energy, 2009. **34**(9): p. 3589-3603.
8. Keleş, S., K. Kaygusuz, and M. Akgün, *Pyrolysis of Woody Biomass for Sustainable Bio-oil.* Energy Sources, Part A: Recovery, Utilization, and Environmental Effects, 2011. **33**(9): p. 879-889.
9. Nicholas Canabarro, J.F.S., Chayene G Anchieta, Camila S Kelling and Marcio A Mazutti*, *Thermochemical processes for biofuels production from biomass.* 2013.
10. Viswanathan, B., *Chapter 15 - Biochemical Routes for Energy Conversion*, in *Energy Sources*, B. Viswanathan, Editor. 2017, Elsevier: Amsterdam. p. 357-368.
11. Demirbas, A., *Biomass resource facilities and biomass conversion processing for fuels and chemicals.* Energy Conversion and Management, 2001. **42**(11): p. 1357-1378.
12. Bhaskar, T. and P.H. Steele, *Thermo-chemical Conversion of Biomass.* Bioresource Technology, 2015. **178**(0): p. 1.
13. Bridgwater, A.V., *Review of fast pyrolysis of biomass and product upgrading.* Biomass and Bioenergy, 2012. **38**(0): p. 68-94.
14. Pereira, H., *Chapter 3 - The chemical composition of cork*, in *Cork*, H. Pereira, Editor. 2007, Elsevier Science B.V.: Amsterdam. p. 55-99.
15. Hayes, M.H.B., R. Mylotte, and R.S. Swift, *Chapter Two - Humin: Its Composition and Importance in Soil Organic Matter*, in *Advances in Agronomy*, D.L. Sparks, Editor. 2017, Academic Press. p. 47-138.

16. Saha, B.C., *Hemicellulose bioconversion.* Journal of Industrial Microbiology and Biotechnology, 2003. **30**(5): p. 279-291.
17. Rao, T.R. and A. Sharma, *Pyrolysis rates of biomass materials.* Energy, 1998. **23**(11): p. 973-978.
18. Velmurugan, R. and A. Incharoensakdi, *Chapter 18 - Nanoparticles and Organic Matter: Process and Impact*, in *Nanomaterials in Plants, Algae, and Microorganisms*, D.K. Tripathi, et al., Editors. 2018, Academic Press. p. 407-428.
19. Ntaganda1, J. and A.N. , *, Oscar Benimana1, *Characterization of physical and chemical properties of biodiesel produced from Jatropha curcas seeds oil cultivated in Rwanda.* Science Journal of Energy Engineering, 2014.
20. Khalil, H.P.S.A., N.A.S. Aprilia, A.H. Bhat, M. Jawaid, M.T. Paridah, and D. Rudi, *A Jatropha biomass as renewable materials for biocomposites and its applications.* Renewable and Sustainable Energy Reviews, 2013. **22**(0): p. 667-685.
21. Elshaarani, T., Z. Yaakob, M.D.K. Zaman, M. Mohammad, and S.R.S. Abdullah, *Mechanical properties, morphology, flammability, and thermokinetic investigation of high-density polyethylene/Jatropha deoiled cake composites.* Journal of Applied Polymer Science, 2012. **126**(S2): p. E78-E88.
22. Becker, K. and H.P.S. Makkar, *Jatropha curcas: A potential source for tomorrow' s oil and biodiesel.* Lipid Technology, 2008. **20**(5): p. 104-107.
23. Singh, R.N., D.K. Vyas, N.S.L. Srivastava, and M. Narra, *SPRERI experience on holistic approach to utilize all parts of Jatropha curcas fruit for energy.* Renewable Energy, 2008. **33**(8): p. 1868-1873.
24. Gottipati, R. and S. Mishra, *A kinetic study on pyrolysis and combustion characteristics of oil cakes: Effect of cellulose and lignin content.* Journal of Fuel Chemistry and Technology, 2011. **39**(4): p. 265-270.
25. Sricharoenchaikul, V. and D. Atong, *Thermal decomposition study on Jatropha curcas L. waste using TGA and fixed bed reactor.* Journal of Analytical and Applied Pyrolysis, 2009. **85**(1-2): p. 155-162.
26. Rakshit, K.D., J. Darukeshwara, K. Rathina Raj, K. Narasimhamurthy, P. Saibaba, and S. Bhagya, *Toxicity studies of detoxified Jatropha meal (Jatropha curcas) in rats.* Food and Chemical Toxicology, 2008. **46**(12): p. 3621-3625.
27. Makkar, H.P.S., A.O. Aderibigbe, and K. Becker, *Comparative evaluation of non-toxic and toxic varieties of Jatropha curcas for chemical composition, digestibility, protein degradability and toxic factors.* Food Chemistry, 1998. **62**(2): p. 207-215.
28. Babu, B.V., *Biomass pyrolysis: a state-of-the-art review.* Biofuels, Bioproducts and Biorefining, 2008. **2**(5): p. 393-414.
29. Demirbas, A., *Mechanisms of liquefaction and pyrolysis reactions of biomass.* Energy Conversion and Management, 2000. **41**(6): p. 633-646.
30. Mohammad I. Jahirul 1, Mohammad G. Rasul 1,*, Ashfaque Ahmed Chowdhury 1 and and N. Ashwath, *Biofuels Production through Biomass Pyrolysis*
—*A Technological Review.* energies, 2012.
31. Bridgwater, A.V., D. Meier, and D. Radlein, *An overview of fast pyrolysis of biomass.* Organic Geochemistry, 1999. **30**(12): p. 1479-1493.

32. Neves, D., H. Thunman, A. Matos, L. Tarelho, and A. Gómez-Barea, *Characterization and prediction of biomass pyrolysis products.* Progress in Energy and Combustion Science, 2011. **37**(5): p. 611-630.
33. Demirbaş, A., *Analysis of Liquid Products from Biomass via Flash Pyrolysis.* Energy Sources, 2002. **24**(4): p. 337-345.
34. Uzun, B.B., E. Apaydin-Varol, F. Ateş, N. Özbay, and A.E. Pütün, *Synthetic fuel production from tea waste: Characterisation of bio-oil and bio-char.* Fuel, 2010. **89**(1): p. 176-184.
35. Tripathi, M., J.N. Sahu, and P. Ganesan, *Effect of process parameters on production of biochar from biomass waste through pyrolysis: A review.* Renewable and Sustainable Energy Reviews, 2016. **55**: p. 467-481.
36. McHenry, M.P., *Agricultural bio-char production, renewable energy generation and farm carbon sequestration in Western Australia: Certainty, uncertainty and risk.* Agriculture, Ecosystems & Environment, 2009. **129**(1): p. 1-7.
37. Mohan, D., S. Rajput, V.K. Singh, P.H. Steele, and C.U. Pittman, *Modeling and evaluation of chromium remediation from water using low cost bio-char, a green adsorbent.* Journal of Hazardous Materials, 2011. **188**(1): p. 319-333.
38. Mohan, D., H. Kumar, A. Sarswat, M. Alexandre-Franco, and C.U. Pittman, *Cadmium and lead remediation using magnetic oak wood and oak bark fast pyrolysis bio-chars.* Chemical Engineering Journal, 2014. **236**: p. 513-528.
39. Kılıç, M., Ç. Kırbıyık, Ö. Çepelioğullar, and A.E. Pütün, *Adsorption of heavy metal ions from aqueous solutions by bio-char, a by-product of pyrolysis.* Applied Surface Science, 2013. **283**: p. 856-862.
40. De, M., R. Azargohar, A.K. Dalai, and S.R. Shewchuk, *Mercury removal by bio-char based modified activated carbons.* Fuel, 2013. **103**: p. 570-578.
41. Mohan, D., C.U. Pittman, M. Bricka, F. Smith, B. Yancey, J. Mohammad, P.H. Steele, M.F. Alexandre-Franco, V. Gómez-Serrano, and H. Gong, *Sorption of arsenic, cadmium, and lead by chars produced from fast pyrolysis of wood and bark during bio-oil production.* Journal of Colloid and Interface Science, 2007. **310**(1): p. 57-73.
42. Liu, P., W.-J. Liu, H. Jiang, J.-J. Chen, W.-W. Li, and H.-Q. Yu, *Modification of bio-char derived from fast pyrolysis of biomass and its application in removal of tetracycline from aqueous solution.* Bioresource Technology, 2012. **121**: p. 235-240.
43. Liu, W.-J., F.-X. Zeng, H. Jiang, and X.-S. Zhang, *Preparation of high adsorption capacity bio-chars from waste biomass.* Bioresource Technology, 2011. **102**(17): p. 8247-8252.
44. Ates, F. and U. Tezcan Un, *Production of char from hornbeam sawdust and its performance evaluation in the dye removal.* Journal of Analytical and Applied Pyrolysis, 2013. **103**: p. 159-166.
45. Koufopanos, C.A., A. Lucchesi, and G. Maschio, *Kinetic modelling of the pyrolysis of biomass and biomass components.* The Canadian Journal of Chemical Engineering, 1989. **67**(1): p. 75-84.
46. Di Blasi, C. and C. Branca, *Modeling a stratified downdraft wood gasifier with primary and secondary air entry.* Fuel, 2013. **104**(Supplement C): p. 847-860.
47. Zhou, H., Y. Long, A. Meng, S. Chen, Q. Li, and Y. Zhang, *A novel method for kinetics analysis of pyrolysis of hemicellulose, cellulose, and lignin in TGA and macro-TGA.* RSC Advances, 2015. **5**(34): p. 26509-26516.

48. Koufopanos, C.A., N. Papayannakos, G. Maschio, and A. Lucchesi, *Modelling of the pyrolysis of biomass particles. Studies on kinetics, thermal and heat transfer effects.* The Canadian Journal of Chemical Engineering, 1991. **69**(4): p. 907-915.
49. Babu, B.V. and A.S. Chaurasia, *Modeling for pyrolysis of solid particle: kinetics and heat transfer effects.* Energy Conversion and Management, 2003. **44**(14): p. 2251-2275.
50. Babu, B.V. and A.S. Chaurasia, *Modeling, simulation and estimation of optimum parameters in pyrolysis of biomass.* Energy Conversion and Management, 2003. **44**(13): p. 2135-2158.
51. Babu, B.V. and A.S. Chaurasia, *Dominant design variables in pyrolysis of biomass particles of different geometries in thermally thick regime.* Chemical Engineering Science, 2004. **59**(3): p. 611-622.
52. Babu, B.V. and A.S. Chaurasia, *Heat transfer and kinetics in the pyrolysis of shrinking biomass particle.* Chemical Engineering Science, 2004. **59**(10): p. 1999-2012.
53. Babu, B.V. and A.S. Chaurasia, *Pyrolysis of biomass: improved models for simultaneous kinetics and transport of heat, mass and momentum.* Energy Conversion and Management, 2004. **45**(9-10): p. 1297-1327.
54. Babu, B.V. and A.S. Chaurasia, *Parametric study of thermal and thermodynamic properties on pyrolysis of biomass in thermally thick regime.* Energy Conversion and Management, 2004. **45**(1): p. 53-72.
55. Bamford, C.H., J. Crank, and D.H. Malan, *The combustion of wood. Part I.* Mathematical Proceedings of the Cambridge Philosophical Society, 2008. **42**(2): p. 166-182.
56. Fan, L.T., Liang-Shih, K. Miyanami, T.Y. Chen, and W.P. Walawender, *A mathematical model for pyrolysis of a solid particle: Effects of the lewis number.* The Canadian Journal of Chemical Engineering, 1977. **55**(1): p. 47-53.
57. Miyanami, K., L.-S. Fan, L.T. Fan, and W.P. Walawender, *A mathematical model for pyrolysis of a solid particle — effects of the heat of reaction.* The Canadian Journal of Chemical Engineering, 1977. **55**(3): p. 317-325.
58. Bamford, C. C.H., and J.a.M. D.H. *The Combustion of Wood*. in *Proceedings Cambridge Philosophical Society*. 1946.
59. Tinney, E.R., *Modelling of Pyrolysis process* 1965.
60. Roberts, A.F.a.G.C. *degradation of wood in an inert atmosphere*. proceedings of the 9th International Symposium on Combustion, 1963.
61. Kung, H.C., *A mathematical model of wood pyrolysis.* Combust. Flame, 1972. **185-195**.
62. Kansa, E.J., H.E. Perlee, and R.F. Chaiken, *Mathematical model of wood pyrolysis including internal forced convection.* Combustion and Flame, 1977. **29**(0): p. 311-324.
63. Blasi, C.D., *Physico-chemical processes occurring inside a degrading two-dimensional anisotropic porous medium.* International Journal of Heat and Mass Transfer, 1998. **41**(24): p. 4139-4150.
64. Di Blasi, C., *Heat, momentum and mass transport through a shrinking biomass particle exposed to thermal radiation.* Chemical Engineering Science, 1996. **51**(7): p. 1121-1132.

65. Jalan, R.K. and V.K. Srivastava, *Studies on pyrolysis of a single biomass cylindrical pellet—kinetic and heat transfer effects.* Energy Conversion and Management, 1999. **40**(5): p. 467-494.
66. Srivastava, V.K., Sushil, and R.K. Jalan, *Prediction of concentration in the pyrolysis of biomass material—II.* Energy Conversion and Management, 1996. **37**(4): p. 473-483.
67. Pyle, D.L. and C.A. Zaror, *Heat transfer and kinetics in the low temperature pyrolysis of solids.* Chemical Engineering Science, 1984. **39**(1): p. 147-158.
68. Zaror, C.A., I.S. Hutchings, D.L. Pyle, H.N. Stiles, and R. Kandiyoti, *Secondary char formation in the catalytic pyrolysis of biomass.* Fuel, 1985. **64**(7): p. 990-994.
69. Roberts, A.F., *A review of kinetics data for the pyrolysis of wood and related substances.* Combustion and Flame, 1970. **14**(2): p. 261-272.
70. Shafizadeh, F. and P.P.S. Chin, *Thermal Deterioration of Wood*, in *Wood Technology: Chemical Aspects*. 1977, AMERICAN CHEMICAL SOCIETY. p. 57-81.
71. Thurner, F. and U. Mann, *Kinetic investigation of wood pyrolysis.* Industrial & Engineering Chemistry Process Design and Development, 1981. **20**(3): p. 482-488.
72. Chan, W.-C.R., M. Kelbon, and B.B. Krieger, *Modelling and experimental verification of physical and chemical processes during pyrolysis of a large biomass particle.* Fuel, 1985. **64**(11): p. 1505-1513.
73. Di Blasi, C., *Analysis of Convection and Secondary Reaction Effects Within Porous Solid Fuels Undergoing Pyrolysis.* Combustion Science and Technology, 1993. **90**(5-6): p. 315-340.
74. Di Blasi, C., *Modeling and simulation of combustion processes of charring and non-charring solid fuels.* Progress in Energy and Combustion Science, 1993. **19**(1): p. 71-104.
75. Di Blasi, C., *Comparison of semi-global mechanisms for primary pyrolysis of lignocellulosic fuels.* Journal of Analytical and Applied Pyrolysis, 1998. **47**(1): p. 43-64.
76. Liliedahl, T. and K. Sjöström, *Heat transfer controlled pyrolysis kinetics of a biomass slab, rod or sphere.* Biomass and Bioenergy, 1998. **15**(6): p. 503-509.
77. Di Blasi, C., *Modeling chemical and physical processes of wood and biomass pyrolysis.* Progress in Energy and Combustion Science, 2008. **34**(1): p. 47-90.
78. Chen, G. and D.Y.C. Leung, *Experimental Investigation of Biomass Waste, (Rice Straw, Cotton Stalk, and Pine Sawdust), Pyrolysis Characteristics.* Energy Sources, 2003. **25**(4): p. 331-337.
79. Williams, P.T. and S. Besler, *The influence of temperature and heating rate on the slow pyrolysis of biomass.* Renewable Energy, 1996. **7**(3): p. 233-250.
80. Miller, R.S.a.J.B., *A generalized biomass pyrolysis model based on superimposed cellulose, hemicellulose and lignin kinetics.* Combust. Sci. Technol., 1997.
81. Di Blasi, C. and M. Lanzetta, *Intrinsic kinetics of isothermal xylan degradation in inert atmosphere.* Journal of Analytical and Applied Pyrolysis, 1997. **40–41**(0): p. 287-303.
82. Bryden, K.M., K.W. Ragland, and C.J. Rutland, *Modeling thermally thick pyrolysis of wood.* Biomass and Bioenergy, 2002. **22**(1): p. 41-53.

83. Hagge, M.J. and K.M. Bryden, *Modeling the impact of shrinkage on the pyrolysis of dry biomass.* Chemical Engineering Science, 2002. **57**(14): p. 2811-2823.
84. Onwubolu, G.C. and B.V. Babu, *New Optimization Techniques in Engineering*. 2004, Berlin Heidelberg Germany: Springer.
85. Pettersson, L.J. and R. Westerholm, *State of the art of multi-fuel reformers for fuel cell vehicles: problem identification and research needs.* International Journal of Hydrogen Energy, 2001. **26**(3): p. 243-264.
86. Thunman, H. and B. Leckner, *Influence of size and density of fuel on combustion in a packed bed.* Proceedings of the Combustion Institute, 2005. **30**(2): p. 2939-2946.
87. Marias, F., H. Roustan, and A. Pichat, *Modelling of a rotary kiln for the pyrolysis of aluminium waste.* Chemical Engineering Science, 2005. **60**(16): p. 4609-4622.
88. Tabarés, J.L.M., L. Ortiz, E. Granada, and F.P. Viar, *Feasibility study of energy use for densificated lignocellulosic material (briquettes).* Fuel, 2000. **79**(10): p. 1229-1237.
89. Sadhukhan, A.K., P. Gupta, and R.K. Saha, *Modelling and experimental studies on pyrolysis of biomass particles.* Journal of Analytical and Applied Pyrolysis, 2008. **81**(2): p. 183-192.
90. Sadhukhan, A.K., P. Gupta, and R.K. Saha, *Modelling of pyrolysis of large wood particles.* Bioresource Technology, 2009. **100**(12): p. 3134-3139.
91. Park, W.C., A. Atreya, and H.R. Baum, *Experimental and theoretical investigation of heat and mass transfer processes during wood pyrolysis.* Combustion and Flame, 2010. **157**(3): p. 481-494.
92. Sun, S., H. Tian, Y. Zhao, R. Sun, and H. Zhou, *Experimental and numerical study of biomass flash pyrolysis in an entrained flow reactor.* Bioresource Technology, 2010. **101**(10): p. 3678-3684.
93. Csukás, B., M. Varga, N. Miskolczi, S. Balogh, A. Angyal, and L. Bartha, *Simplified dynamic simulation model of plastic waste pyrolysis in laboratory and pilot scale tubular reactor.* Fuel Processing Technology, 2012(0).
94. Meng, Q. and X. Chen, *Numerical Modeling of Pyrolysis of Sawdust in a Packed Bed*, in *Cleaner Combustion and Sustainable World*, H. Qi and B. Zhao, Editors. 2013, Springer Berlin Heidelberg: Berlin, Heidelberg. p. 209-215.
95. Olaleye, A.K., K.J. Adedayo, C. Wu, M.A. Nahil, M. Wang, and P.T. Williams, *Experimental study, dynamic modelling, validation and analysis of hydrogen production from biomass pyrolysis/gasification of biomass in a two-stage fixed bed reaction system.* Fuel, 2014. **137**(Supplement C): p. 364-374.
96. Chowdhury, R., S. Poddar, and S. De, *Kinetic modelling of non-catalytic pyrolysis of waste jute in a fixed bed pyrolyzer.* APCBEE Procedia, 2014. **9**: p. 18-24.
97. Chen, D., J. Zhou, and Q. Zhang, *Effects of heating rate on slow pyrolysis behavior, kinetic parameters and products properties of moso bamboo.* Bioresource Technology, 2014. **169**(Supplement C): p. 313-319.
98. Pozzobon, V., S. Salvador, J.J. Bézian, M. El-Hafi, Y. Le Maoult, and G. Flamant, *Radiative pyrolysis of wet wood under intermediate heat flux: Experiments and modelling.* Fuel Processing Technology, 2014. **128**(Supplement C): p. 319-330.

99. Boriouchkine, A., V. Sharifi, J. Swithenbank, and S.-L. Jämsä-Jounela, *Experiments and modeling of fixed-bed debarking residue pyrolysis: The effect of fuel bed properties on product yields.* Chemical Engineering Science, 2015. **138**: p. 581-591.
100. Nelson, L.S. and N.A. Kuebler, *Heterogeneous flash pyrolysis of hydrocarbon polymers.* Planetary and Space Science, 1961. **3**(0): p. 61-67.
101. Fujimaki, M., S. Kato, and T. Kurata, *Pyrolysis of Sulfur-containing Amino Acids.* Agricultural and Biological Chemistry, 1969. **33**(8): p. 1144-1151.
102. Tran, D.Q. and C. Rai, *A kinetic model for pyrolysis of Douglas fir bark.* Fuel, 1978. **57**(5): p. 293-298.
103. Bilbao, R., J.F. Mastral, J. Ceamanos, and M.E. Aldea, *Modelling of the pyrolysis of wet wood.* Journal of Analytical and Applied Pyrolysis, 1996. **36**(1): p. 81-97.
104. Di Blasi, C., *Kinetic and Heat Transfer Control in the Slow and Flash Pyrolysis of Solids.* Industrial & Engineering Chemistry Research, 1996. **35**(1): p. 37-46.
105. Blasi, C.D., *Dynamic behaviour of stratified downdraft gasifiers.* Chemical Engineering Science, 2000. **55**(15): p. 2931-2944.
106. Patra, T.K., K.R. Nimisha, and P.N. Sheth, *A comprehensive dynamic model for downdraft gasifier using heat and mass transport coupled with reaction kinetics.* Energy, 2016. **116**(Part 1): p. 1230-1242.
107. Bonnefoy, F., P. Gilot, and G. Prado, *A three-dimensional model for the determination of kinetic data from the pyrolysis of beech wood.* Journal of Analytical and Applied Pyrolysis, 1993. **25**(Supplement C): p. 387-394.
108. Sakuma, H., S. Munakata, and S. Sugawara, *Volatile Products of Cellulose Pyrolysis.* Agricultural and Biological Chemistry, 1981. **45**(2): p. 443-451.
109. Shafizadeh, F., *Introduction to pyrolysis of biomass.* Journal of Analytical and Applied Pyrolysis, 1982. **3**(4): p. 283-305.
110. Corte, P., C. Lacoste, and J.P. Traverse, *Gasification and catalytic conversion of biomass by flash pyrolysis.* Journal of Analytical and Applied Pyrolysis, 1985. **7**(4): p. 323-335.
111. Beaumont, O., *Flash Pyrolysis Products From Beech Wood.* Wood and Fiber Science, 1985. **17**(2): p. 228-239.
112. Rocha, J.D., S.D. Brown, G.D. Love, and C.E. Snape, *Hydropyrolysis: a versatile technique for solid fuel liquefaction, sulphur speciation and biomarker release.* Journal of Analytical and Applied Pyrolysis, 1997. **40–41**(0): p. 91-103.
113. Barth, T., *Similarities and differences in hydrous pyrolysis of biomass and source rocks.* Organic Geochemistry, 1999. **30**(12): p. 1495-1507.
114. Degroot, W.F., W.-P. Pan, M.D. Rahman, and G.N. Richards, *First chemical events in pyrolysis of wood.* Journal of Analytical and Applied Pyrolysis, 1988. **13**(3): p. 221-231.
115. Avenell, C.S., A.S. Arshad, A.J. Griffiths, and N. Syred. *The development of a 200 kW pyrolyser and its environmental impact*. in *Renewable Energy - Clean Power 2001, 1993., International Conference on*. 1993.
116. Sipilä, K., E. Kuoppala, L. Fagernäs, and A. Oasmaa, *Characterization of biomass-based flash pyrolysis oils.* Biomass and Bioenergy, 1998. **14**(2): p. 103-113.

117. Şensöz, S., D. Angın, and S. Yorgun, *Influence of particle size on the pyrolysis of rapeseed (Brassica napus L.): fuel properties of bio-oil.* Biomass and Bioenergy, 2000. **19**(4): p. 271-279.
118. Williams, P.T. and N. Nugranad, *Comparison of products from the pyrolysis and catalytic pyrolysis of rice husks.* Energy, 2000. **25**(6): p. 493-513.
119. Kockar, O.M., O. Onay, A.E. Putun, and E. Putun, *Fixed-Bed Pyrolysis of Hazelnut Shell: A Study on Mass Transfer Limitations on Product Yields and Characterization of the Pyrolysis Oil.* Energy Sources, 2000. **22**(10): p. 913-924.
120. Yorgun, S., S. Şensöz, and Ö.M. Koçkar, *Flash pyrolysis of sunflower oil cake for production of liquid fuels.* Journal of Analytical and Applied Pyrolysis, 2001. **60**(1): p. 1-12.
121. Şensöz, S. and M. Can, *Pyrolysis of Pine (Pinus Brutia Ten.) Chips: 1. Effect of Pyrolysis Temperature and Heating Rate on the Product Yields.* Energy Sources, 2002. **24**(4): p. 347-355.
122. Demirbas, A. and G. Arin, *An Overview of Biomass Pyrolysis.* Energy Sources, 2002. **24**(5): p. 471-482.
123. Demirbas, A., *Determination of calorific values of bio-chars and pyro-oils from pyrolysis of beech trunkbarks.* Journal of Analytical and Applied Pyrolysis, 2004. **72**(2): p. 215-219.
124. Miao, X. and Q. Wu, *High yield bio-oil production from fast pyrolysis by metabolic controlling of Chlorella protothecoides.* Journal of Biotechnology, 2004. **110**(1): p. 85-93.
125. Tuncel, F. and H.F. Gercel, *Production and Characterization of Pyrolysis Oils from Euphorbia Macroclada.* Energy Sources, 2004. **26**(8): p. 761-770.
126. Onay, O., S. Beis, and O.M. Kockar, *Pyrolysis of Walnut Shell in a Well-Swept Fixed-Bed Reactor*. Energy Sources, 2004. **26**(8): p. 771-782.
127. Li, L.I.N. and H. Zhang, *Production and Characterization of Pyrolysis Oil from Herbaceous Biomass (Achnatherum Splendens).* Energy Sources, 2005. **27**(4): p. 319-326.
128. Pütün, A., N. Özbay, and E. Pütün, *Effect of Steam on the Pyrolysis of Biomass.* Energy Sources, Part A: Recovery, Utilization, and Environmental Effects, 2006. **28**(3): p. 253-262.
129. Demiral, İ. and S. Şensöz, *Fixed-Bed Pyrolysis of Hazelnut (Corylus Avellana L.) Bagasse: Influence of Pyrolysis Parameters on Product Yields.* Energy Sources, Part A: Recovery, Utilization, and Environmental Effects, 2006. **28**(12): p. 1149-1158.
130. Tian, S., W. Luo, Y. Jing, and H. Xue. *Experimental Research on the Pyrolysis of Cornstalk of a Thermoelectric Station*. in *Electronic Measurement and Instruments, 2007. ICEMI '07. 8th International Conference on*. 2007.
131. Xiaoya, G., Z. Yong, and Z. Bo. *Influence of Absorption Medium on Microwave Pyrolysis of Fir Sawdust*. in *Bioinformatics and Biomedical Engineering, 2008. ICBBE 2008. The 2nd International Conference on*. 2008.
132. Xiaoya, G., Z. Bo, and Z. Yong. *Study on microwave radiation pyrolysis of biomass*. in *Sustainable Energy Technologies, 2008. ICSET 2008. IEEE International Conference on*. 2008.
133. Bologa, A., A. Hornung, H. Seifert, K. Woletz, and H.R. Paur. *Application of space-charge electrostatic precipitator for collection of oil mist from pyrolysis gases*. in *Dielectric Liquids, 2008. ICDL 2008. IEEE International Conference on*. 2008.

134. Aho, A., N. Kumar, K. Eränen, B. Holmbom, M. Hupa, T. Salmi, and D.Y. Murzin, *Pyrolysis of Softwood Carbohydrates in a Fluidized Bed Reactor.* International Journal of Molecular Sciences, 2008. **9**(9): p. 1665-1675.
135. Ateş, F. and M.j.A. Işıkdağ, *Evaluation of the Role of the Pyrolysis Temperature in Straw Biomass Samples and Characterization of the Oils by GC/MS.* Energy & Fuels, 2008. **22**(3): p. 1936-1943.
136. Garcia-Perez, M., S. Wang, J. Shen, M. Rhodes, W.J. Lee, and C.-Z. Li, *Effects of Temperature on the Formation of Lignin-Derived Oligomers during the Fast Pyrolysis of Mallee Woody Biomass.* Energy & Fuels, 2008. **22**(3): p. 2022-2032.
137. Mullen, C.A., A.A. Boateng, K.B. Hicks, N.M. Goldberg, and R.A. Moreau, *Analysis and Comparison of Bio-Oil Produced by Fast Pyrolysis from Three Barley Biomass/Byproduct Streams.* Energy & Fuels, 2009. **24**(1): p. 699-706.
138. Qiang, M., W. Qinhui, H. Long, Y. Chunjiang, and L. Zhongyang. *TG-FTIR Analysis on Sawdust Catalytic Pyrolysis with CaO*. in *Energy and Environment Technology, 2009. ICEET '09. International Conference on*. 2009.
139. Demirbas, A., *Pyrolysis Mechanisms of Biomass Materials.* Energy Sources, Part A: Recovery, Utilization, and Environmental Effects, 2009. **31**(13): p. 1186-1193.
140. Haykiri-Acma, H. and S. Yaman, *Thermogravimetric Investigation on the Thermal Reactivity of Biomass During Slow Pyrolysis.* International Journal of Green Energy, 2009. **6**(4): p. 333-342.
141. de Oliveira, J.S., P.M. Leite, L.B. de Souza, V.M. Mello, E.C. Silva, J.C. Rubim, S.M.P. Meneghetti, and P.A.Z. Suarez, *Characteristics and composition of Jatropha gossypiifoliaand Jatropha curcas L. oils and application for biodiesel production.* Biomass and Bioenergy, 2009. **33**(3): p. 449-453.
142. Zhanlong, S., Z. Xiqiang, M. Chunyuan, W. Tao, and L. Longzhi. *Kinetics of Pyrolysis of Straw Bales by Microwave Heating*. in *Power and Energy Engineering Conference, 2009. APPEEC 2009. Asia-Pacific*. 2009.
143. Xinbao, L., W. Shurong, W. Kaige, and W. Qi. *Experimental Study of the Effect of Spray Medium on the Collection of Bio-Oil Produced from Biomass Fast Pyrolysis*. in *Energy and Environment Technology, 2009. ICEET '09. International Conference on*. 2009.
144. Wu, W.-g., Y. Chen, L.-Y. Hu, and Y.-H. Luo. *Isothermal Pyrolysis of Biomass by Macro-TG*. in *Power and Energy Engineering Conference, 2009. APPEEC 2009. Asia-Pacific*. 2009.
145. Demirbas, A., *Pyrolysis of Biomass for Fuels and Chemicals.* Energy Sources, Part A: Recovery, Utilization, and Environmental Effects, 2009. **31**(12): p. 1028-1037.
146. Liu, R., C. Deng, and J. Wang, *Fast Pyrolysis of Corn Straw for Bio-oil Production in a Bench-scale Fluidized Bed Reactor.* Energy Sources, Part A: Recovery, Utilization, and Environmental Effects, 2009. **32**(1): p. 10-19.
147. Li, J. *The Optimal of Pyrolysis Process in the Rotating Cone Reactor and Pyrolysis Product Analysis*. in *Challenges in Environmental Science and Computer Engineering (CESCE), 2010 International Conference on*. 2010.
148. Li, J. *Study on the Maize Straw Process of Fast Pyrolysis in the Rotating Cone Reactor and Process*. in *Challenges in Environmental Science and Computer Engineering (CESCE), 2010 International Conference on*. 2010.

149. Bahri, S., E. Saputra, I. Detrina, Yusnitawati, and Muhdarina. *Bio oil from palm oil industry solid waste*. in *Energy and Sustainable Development: Issues and Strategies (ESD), 2010 Proceedings of the International Conference on*. 2010.
150. Xinbao, L., G. Xiujuan, W. Shurong, W. Kaige, L. Zhongyang, and W. Qi. *Characterization and Analysis of Char Produced by Biomass Fast Pyrolysis*. in *Power and Energy Engineering Conference (APPEEC), 2010 Asia-Pacific*. 2010.
151. Demirbas, A., *Competitive liquid biofuels from biomass.* Applied Energy, 2011. **88**(1): p. 17-28.
152. Duman, G., C. Okutucu, S. Ucar, R. Stahl, and J. Yanik, *The slow and fast pyrolysis of cherry seed.* Bioresource Technology, 2011. **102**(2): p. 1869-1878.
153. J.M. Montes1, M.R.A., J. Vaca Chávez1, C. Guzmán2 and E. Calandri2, *Characterization of jatropha curcas l. seed and its oil from Argentina and Paraguay.* The Journal of the Argentine Chemical Society, 2011.
154. Amutio, M., G. Lopez, R. Aguado, M. Artetxe, J. Bilbao, and M. Olazar, *Effect of Vacuum on Lignocellulosic Biomass Flash Pyrolysis in a Conical Spouted Bed Reactor.* Energy & Fuels, 2011. **25**(9): p. 3950-3960.
155. Dengxiang, J., G. Minghui, Y. Fengwen, A. Ning, J. Hongtao, J. Jianbing, and Y. Ping. *Conversion of sawdust to bio-fuels by pyrolysis within molten sodium hydroxide*. in *Biobase Material Science and Engineering (BMSE), 2012 International Conference on*. 2012.
156. Li, X., Y. Xu, L. He, X. Deng, and R. Li. *Analytical study on liquid products from populus tomentosa black liquor pyrolysis*. in *Biobase Material Science and Engineering (BMSE), 2012 International Conference on*. 2012.
157. Longchao, G., Y. Fengwen, and J. Jianbing. *The production of diesel-like fuel from catalytic pyrolysis of soybean oil*. in *Biobase Material Science and Engineering (BMSE), 2012 International Conference on*. 2012.
158. Sijin, L., C. Shihua, and M. Jun. *Influence of UF resin on pyrolysis characteristics of biomass components: A thermogravimetric study*. in *Biobase Material Science and Engineering (BMSE), 2012 International Conference on*. 2012.
159. Engr. FarrukhJamil, E.M.A., Engr. AwaisBokhari, *PRODUCTION OF BIOFUEL AND ACTIVATED CARBON FROM PYROLYSIS OF SEEDS OF WHEAT CROP WEEDS.* COMSATS, 2013.
160. AYSAL, G.Ö.A.Ö.S., *PYROLYSIS OF BEECH WOOD CATALYSED BY FeCl3: PRODUCTION AND CHARACTERISATION OF BIO-OIL.* PRO LIGNO, 2013.
161. Punsuwan, N. and C. Tangsathitkulchai, *Product Characterization and Kinetics of Biomass Pyrolysis in a Three-Zone Free-Fall Reactor.* International Journal of Chemical Engineering, 2014. **2014**: p. 10.
162. Poddar, S., R. Biswas, R. Chowdhury, and S. De. *Product characterization and kinetic study of co-pyrolysis of waste jute sacks and sesame oil cake*. in *Power and Energy Systems Conference: Towards Sustainable Energy, 2014*. 2014.
163. Jeong, H.M., M.W. Seo, S.M. Jeong, B.K. Na, S.J. Yoon, J.G. Lee, and W.J. Lee, *Pyrolysis kinetics of coking coal mixed with biomass under non-isothermal and isothermal conditions.* Bioresource Technology, 2014. **155**(0): p. 442-445.

164. Xie, X.-P., X.-D. Zhang, L. Chen, L.-Z. Sun, and H.-Y. Si, *Characterization of Rice Husk by Pyrolysis–Gas Chromatography–Mass Spectrometry.* Instrumentation Science & Technology, 2014. **43**(1): p. 65-73.
165. Ates, F., S. Tophanecioglu, and A.E. Putun, *The Evaluation of Mesoporous Materials as Catalyst in Fast Pyrolysis of Wheat Straw.* International Journal of Green Energy, 2014. **12**(1): p. 57-64.
166. Murugan, S. and S. Gu, *Research and development activities in pyrolysis – Contributions from Indian scientific community – A review.* Renewable and Sustainable Energy Reviews, 2015. **46**(0): p. 282-295.
167. Gorlitsky, L.E., A. Sadeghpour, M. Hashemi, F. Etemadi, and S.J. Herbert, *Biomass vs. quality tradeoffs for switchgrass in response to fall harvesting period.* Industrial Crops and Products, 2015. **63**(0): p. 311-315.
168. Sheth, P.N. and B.V. Babu, *Differential Evolution Approach for Obtaining Kinetic Parameters in Nonisothermal Pyrolysis of Biomass.* Materials and Manufacturing Processes, 2008. **24**(1): p. 47-52.
169. Babu, B.V. and S.A. Munawar, *Differential evolution strategies for optimal design of shell-and-tube heat exchangers.* Chemical Engineering Science, 2007. **62**(14): p. 3720-3739.
170. Sheth, P.N. and B.V. Babu. *Logarithmic Differential Evolution (LDE) for Optimization of Kinetic Parameters in Pyrolysis of Biomass*. in *Genetic and Evolutionary Computation Conference (GECCO-2008)*. 2008. Atlanta, Georgia, USA.
171. Gerald, C.F. and P.O. Wheatley, *Applied Numerical Analysis*. 1994, MA: Addison-Wesley Press.
172. Meng, A., S. Chen, Y. Long, H. Zhou, Y. Zhang, and Q. Li, *Pyrolysis and gasification of typical components in wastes with macro-TGA.* Waste Management, 2015. **46**: p. 247-256.
173. Meng, A., S. Chen, H. Zhou, Y. Long, Y. Zhang, and Q. Li, *Pyrolysis and simulation of typical components in wastes with macro-TGA.* Fuel, 2015. **157**: p. 1-8.
174. Sharma, R. and P.N. Sheth, *Multi reaction apparent kinetic scheme for the pyrolysis of large size biomass particles using macro-TGA.* Energy, 2018.
175. Skreiberg, A., Ø. Skreiberg, J. Sandquist, and L. Sørum, *TGA and macro-TGA characterisation of biomass fuels and fuel mixtures.* Fuel, 2011. **90**(6): p. 2182-2197.
176. Seo, D.K., S.S. Park, J. Hwang, and T.-U. Yu, *Study of the pyrolysis of biomass using thermo-gravimetric analysis (TGA) and concentration measurements of the evolved species.* Journal of Analytical and Applied Pyrolysis, 2010. **89**(1): p. 66-73.
177. Basu, P., *Chapter 3 - Pyrolysis and Torrefaction*, in *Biomass Gasification and Pyrolysis*, P. Basu, Editor. 2010, Academic Press: Boston. p. 65-96.
178. Volli, V. and R.K. Singh, *Production of bio-oil from de-oiled cakes by thermal pyrolysis.* Fuel, 2012. **96**(0): p. 579-585.
179. El-Sayed, S.A. and M. Khairy, *Effect of heating rate on the chemical kinetics of different biomass pyrolysis materials.* Biofuels, 2015. **6**(3-4): p. 157-170.
180. Pütün, A.E., B.B. Uzun, E. Apaydin, and E. Pütün, *Bio-oil from olive oil industry wastes: Pyrolysis of olive residue under different conditions.* Fuel Processing Technology, 2005. **87**(1): p. 25-32.

181. Nayan, N.K., S. Kumar, and R.K. Singh, *Characterization of the liquid product obtained by pyrolysis of karanja seed.* Bioresource Technology, 2012. **124**(0): p. 186-189.
182. Zhang, L., C. Xu, and P. Champagne, *Overview of recent advances in thermo-chemical conversion of biomass.* Energy Conversion and Management, 2010. **51**(5): p. 969-982.
183. Williams, P.T. and P.A. Horne, *Characterisation of oils from the fluidised bed pyrolysis of biomass with zeolite catalyst upgrading.* Biomass and Bioenergy, 1994. **7**(1-6): p. 223-236.
184. Tran, K.-Q., Q.-V. Bach, T.T. Trinh, and G. Seisenbaeva, *Non-isothermal pyrolysis of torrefied stump – A comparative kinetic evaluation.* Applied Energy, 2014. **136**: p. 759-766.
185. Vamvuka, D., E. Kakaras, E. Kastanaki, and P. Grammelis, *Pyrolysis characteristics and kinetics of biomass residuals mixtures with lignite ☆.* Fuel, 2003. **82**(15–17): p. 1949-1960.

LIST OF PUBLICATIONS

International Journals

1. Rajeev Sharma and Pratik N Sheth, “Multi reaction apparent kinetic scheme for the pyrolysis of large size biomass particles using macro-TGA" **Energy**, Vol. 151, pp. 1007-1017, 2018.
2. Sharma, R., Sheth, P.N., and Gujarathi, A.M., “Kinetic modeling and simulation: Pyrolysis of *Jatropha* residue de-oiled cake”, **Renewable Energy**, Vol. 86, pp. 554-562, 2016.
3. Sharma, R. and Sheth, P.N., "Thermo-Chemical Conversion and of *Jatropha* Deoiled Cake: Pyrolysis vs. Gasification" **International Journal of Chemical Engineering and Applications.** Vol. 6 (No 5), pp 376-380, 2015

International conference Proceedings

1. Rajeev Sharma and P N Sheth, " Green Energy for Green Future: Biofuels", Proceedings of International Symposium & 70 th Annual Session of IIChE in association with International Partners (CHEMCON-2017), Jointly organized by Haldia Regional Centre (HRC) of the IIChE in association with the Department of Chemical Engineering and supported by Department of Biotechnology & Food technology of Haldia Institute of Technology, from December 27 to 30th 2017 at Haldia, West Bengal.
2. Anuragmani Tripathi, Md Raihan and Rajeev Sharma, " Production of renewable diesel through the hydro-processing of ligno-cellulosic biomass-derived bio-oil and Microwave-assisted waste cooking oil ", Proceedings of International Symposium & 70 th Annual Session of IIChE in association with International Partners (CHEMCON-2017), Jointly organized by Haldia Regional Centre (HRC) of the IIChE in association with the Department of Chemical Engineering and

supported by Department of Biotechnology & Food technology of Haldia Institute of Technology, from December 27 to 30th 2017 at Haldia, West Bengal.

3. Rajeev Sharma, Divya Agarwal, Abhishek Sharma, & P N Sheth, " Future possibilities: Bio-oil produced from thermochemical conversion of biomass ", Proceedings of International Symposium & 68 th Annual Session of IIChE in association with International Partners (CHEMCON-2015), Jointly organized by Institute of Chemical Engineering & IIT Guwahati, India, December 27-30, 2015.
4. Deepak Sharma, Rajeev Sharma and Dr P N Sheth, " A step to bio energy: review of modelling and simulation of thermal degradation of deoiled cake", Proceedings of International Symposium & 67 th Annual Session of IIChE in association with International Partners (CHEMCON-2014), Jointly organized by Institute of Chemical Engineering & Dr. SSB University Institute of Chemical Engineering & Technology Panjab University, Chandigarh (India), December 27-30, 2014.
5. Rajeev Sharma and Dr P N Sheth, " Experimental Investigations of Thermal decomposition of *Jatropha* residue cake ", Proceedings of International Symposium & 66 th Annual Session of IIChE in association with International Partners (CHEMCON-2013), Jointly organized by Institute of Chemical Engineering & ICT Mumbai (India), December 27-30, 2013.
6. Rajeev Sharma and P N Sheth " Gasification Potential of *Jatropha* De-Oiled Resiude Cake", Proceedings of AIChE Annual Meeting 2012, Pittsburgh Convention Center, Pittsburgh (PA), USA, October 28-November 2, 2012.
7. B V Babu, Rajeev Sharma and P N Sheth " Kinetic Modeling & Simulation of Thermo-Chemical Conversion of *Jatropha* De-Oiled Cake", ", Proceedings of AIChE Annual Meeting 2012, Pittsburgh Convention Center, Pittsburgh (PA), USA, October 28-November 2, 2012.

BIOGRAPHY

Biography of the candidate

Rajeev Sharma completed his B.E. Degree in Chemical Engineering from Malaviya National Institute of Technology Jaipur in 2002. He obtained his master's degree in Chemical Engineering from BITS, PILANI in the year 2011. He joined BITS Pilani as a research associate in Chemical Engineering Group in January 2012 and currently he is working as an Assistant Professor in Amity University Rajasthan. He has 6 years of teaching experience and has guided around 40 project students. He taught courses such as Chemical Reaction Engineering-I, Chemical Reaction Engineering-II, Chemical Process Calculation, Thermodynamics, Modeling & Simulation, Engineering economics, Mass Transfer, Advanced separation process, Process Instrumentation and Process Equipment Design, and involved in the chemical laboratories of Chemical Reaction Engineering and Mass Transfer Operations. His research interests include biomass pyrolysis and modeling and simulation.

Biography of supervisor

Dr Pratik N Sheth is currently working as an Associate Professor in the Chemical Engineering Department at Birla Institute of Technology and Science, Pilani, Pilani Campus, Rajasthan. He has over 15 years of teaching, research and academic administration experience. He did his BE (Chemical Engineering) from Government Engineering College, Gandhinagar, Gujarat University , ME (Chemical Engineering) and PhD from Birla Institute of Technology and Science, Pilani, Pilani Campus, Rajasthan.

His current research interests include Pyrolysis, Biomass Gasification, Modeling and Simulation, Computational Fluid Dynamics, and Renewable Energy Sources. He has around 48 research publications including conference proceedings and book chapters to his credit which have been published over the years in various International and National

Journals and Conference Proceedings. Dr Sheth has completed four research projects (one funded from Department of Science and Technology, New Delhi; one from Birla Cellulosic, Kharach and two from BITS Pilani). The research publications of Dr Sheth have received the total number of citation of 975 as per Google scholar website (https://scholar.google.co.in/citations?hl=en&user=S6Im2SYAAAAJ) as on June 10, 2019.

Dr Sheth is guiding two PhD students in the area of hydrogen production from biomass and biomass pyrolysis. Dr Sheth has reviewed several research articles of various international journals such as Biomass and Bioenergy, Renewable Energy, Energy, Chemical Engineering Science, Case studies in thermal engineering, Fuel, Energy Conversion and Management, Renewable and Sustainable Energy Reviews, Separation Science and Technology, Journal of water process engineering, Journal of Petroleum technology, Journal of Engineering Tribology, Applied thermal engineering, Waste and Biomass Valorization and African Journal of Agricultural Research.

Dr Sheth is a Life Member of Indian Institute of Chemical Engineers (IIChE) and Institution of Engineers, India. Dr Sheth was Chairman - IIChE - Pilani Regional Centre and has held various positions. He organized a Workshop on Analytical Instruments for Chemical and Environmental Engineers (WAICEE - 2013) during March 22 – 23, 2013. He was the joint organizing secretary for the 8th Annual Session of Students' Chemical Engineering Congress (SCHEMCON - 2012) during September 21 – 22, 2012. Recently, Dr Sheth has organized a Workshop on Analytical Instruments for Chemical and Environmental Engineers (WAICEE - 2017) during Feb 10-11, 2017.

APPENDIX I

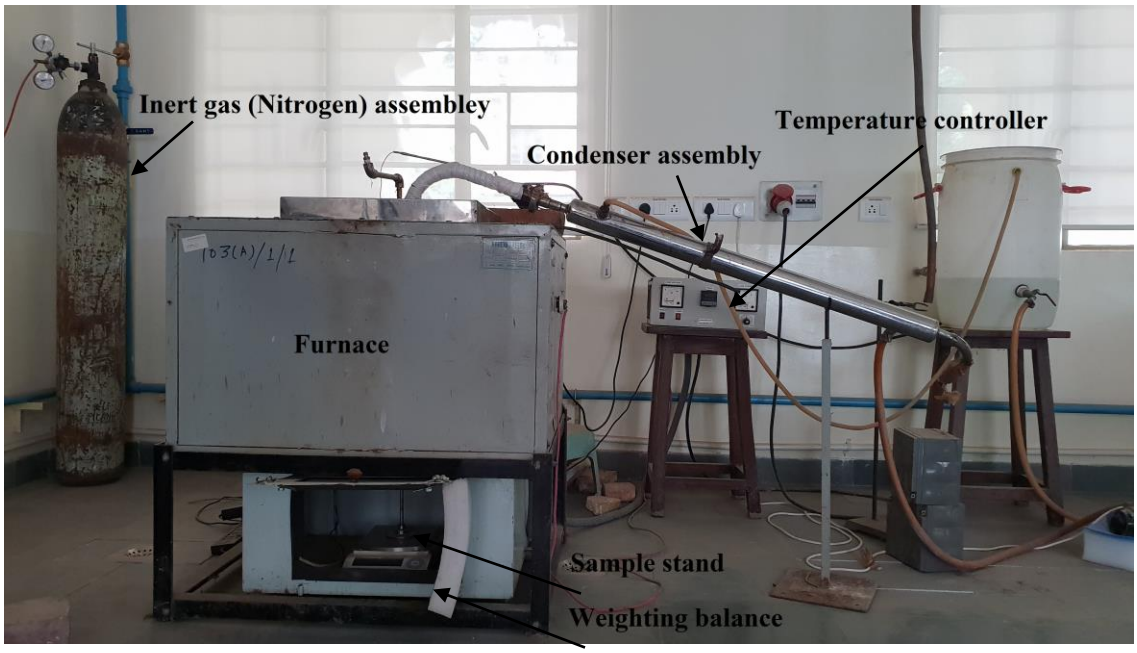

Figure I.1 Photograph of laboratory pyrolyzer setup

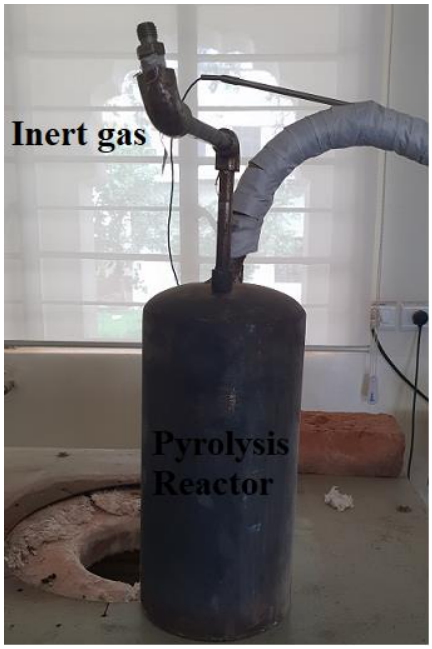

Figure I.2 Photograph of pyrolysis reactor

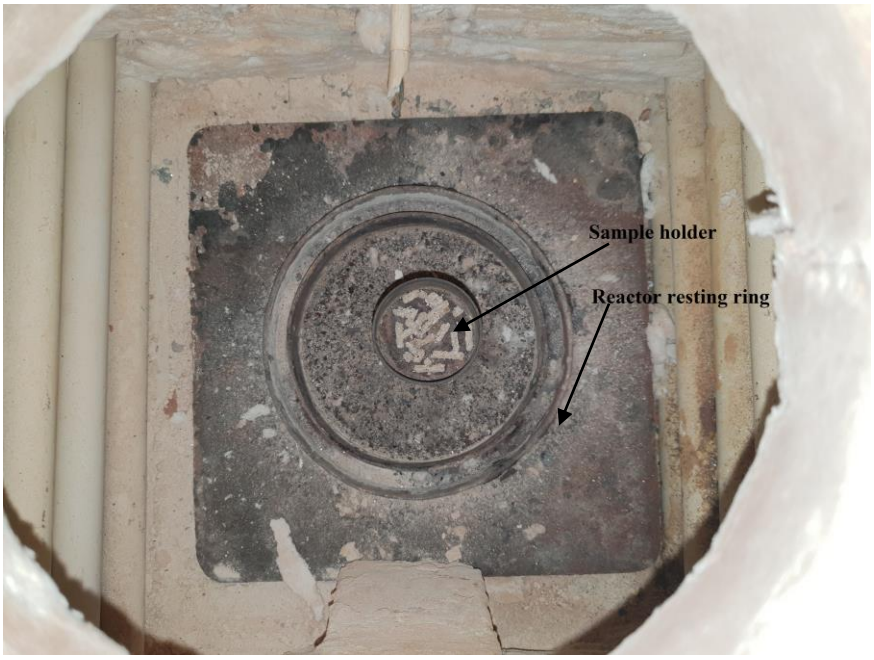

Figure I.3 Photograph of sample holder and inside view of reactor

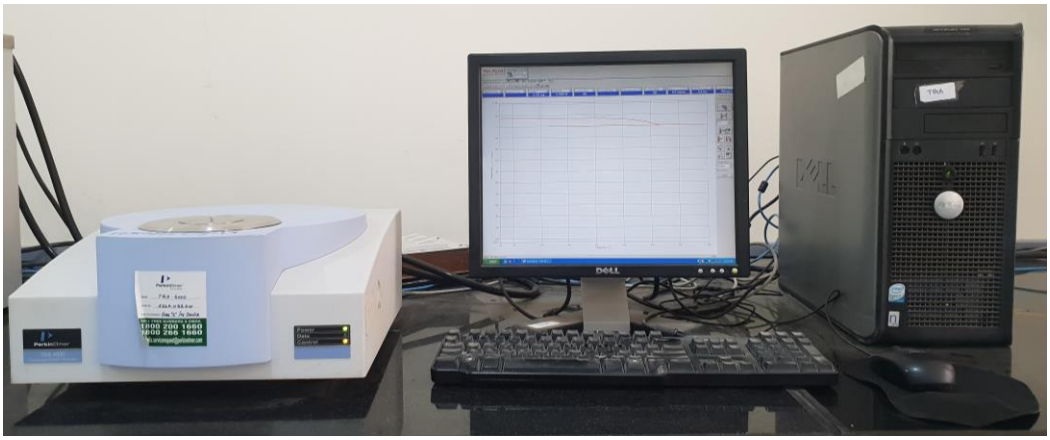

Figure I.4 Thermo-Gravimetric Analyzer (TGA) setup

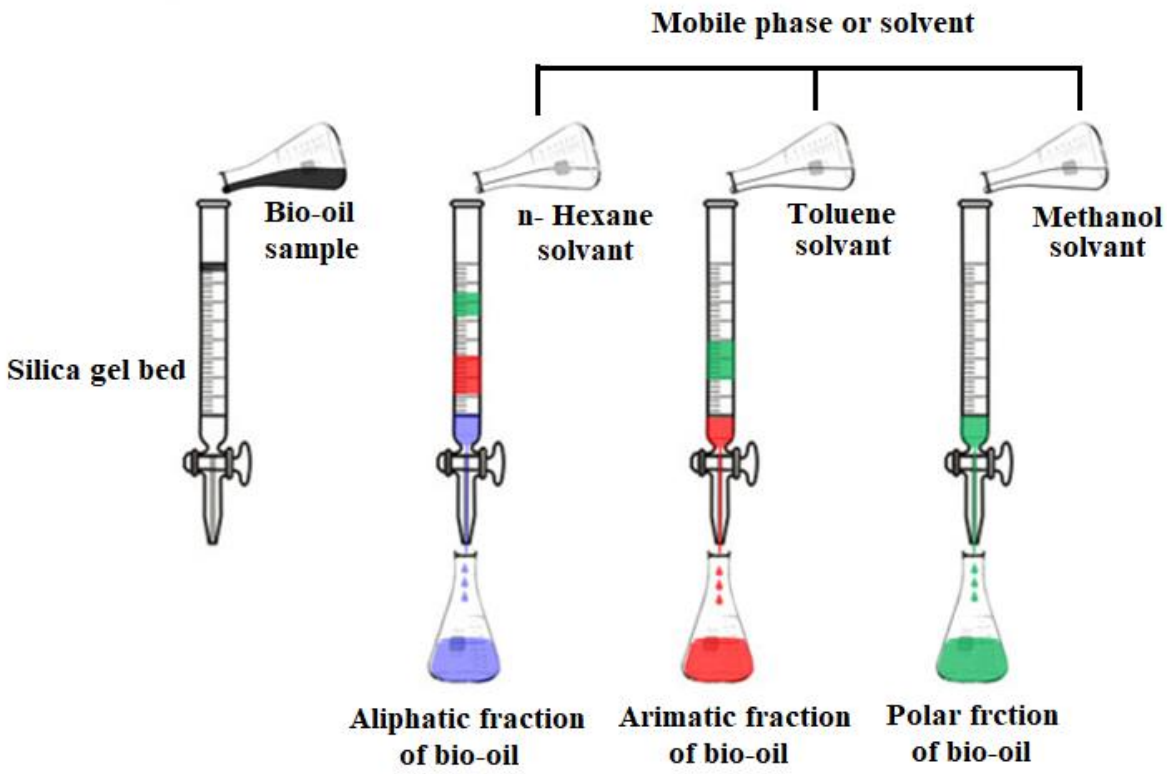

Figure I.5 Liquid column Chromatography setup

Figure I.6 Rotary evaporator setup

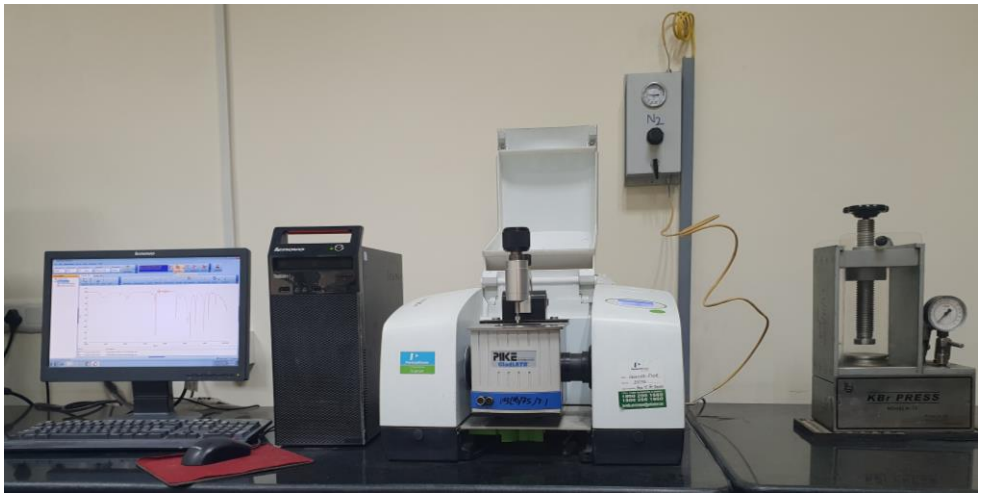

Figure I.7 Fourier Transform Infra-Red Spectroscopy (FTIR) setup

Figure I.8 Gas chromatography setup

Figure I.9 Gas chromatography mass spectrometry (GC-MS) setup

APPENDIX II

Code in 'C' Language for estimation of kinetic parameters for kinetic model of biomass pyrolysis

```
#include<conio.h>
#include<iostream.h>
#include<math.h>
#include<ctype.h>
#include<time.h>
#include<stdlib.h>
#include<stdio.h>
#define NP 200
#define D 14
#define genmax 100000
#define F 0.5
#define CR 0.9
FILE *fp;
FILE *fp1;
double funvalue(double aef[],double hr,double Wexp[],double Texp[],double texp[],int
k);
#define IM1 2147483563
#define IM2 2147483399
#define AM (1.0/IM1)
#define IMM1 (IM1-1)
#define IA1 40014
#define IA2 40692
#define IQ1 53668
#define IQ2 52774
#define IR1 12211
#define IR2 3791
#define NTAB 32
#define NDIV (1+ IMM1/NTAB)
#define EPS1 1.2e-7
int q,q11;
#define RNMX (1.0-EPS1)
//Random Number Generator Function
double rand_uni(double * );
double rand_uni(long *idum)
{
  long j,k;
  static long idum2=123456789;
  static long iy=0;
```

```
  static long iv[NTAB];
  double temp;
  if(*idum<=0)
    {
        if(-(*idum)<1)
                *idum=1;
        else
        *idum=-(*idum);
        idum2=(*idum);
        for (j=NTAB+7;j>=0;j--)
        {
          k=(*idum)/IQ1;
          *idum=IA1 * (*idum-k*IQ1)-k*IR1;
          if (*idum<0)
            *idum+=IM1;
          if(j<NTAB)
          iv[j]=*idum;
        }          //End of For loop for j
        iy=iv[0];
}
k=(*idum)/IQ1;
*idum=IA1*(*idum-k-IQ1)-k*IR1;
if(*idum<0)
*idum+=IM1;
k=idum2/IQ2;
idum2=IA2*(idum2-k*IQ2)-k*IR2;
if(idum2<0)
idum2+=IM2;
 j=iy/NDIV;
iy=iv[j]-idum2;
iv[j]=*idum;
if(iy<1)
iy+=IMM1;
if((temp=AM*iy)>RNMX)  {
            return RNMX;
  printf(" The Random Number is RNMX %4.4f \n ",RNMX); getchar();}
  else
  {
  return temp;
  printf(" The Random Number is %4.4f \n ",temp); getchar();
  }
} //End Rand Function
main()
{
```

```
double
ae[NP][D],ae1[D],aet[D],aeo[D],check,aef[D],newae[NP][D],Wexp[500],Texp[500],texp
[500];
int       i,j,k,a,b,c,seed;
double
sbv,hr,sbvhr,R,w1,w2,w3,w4,w5,w6,w7,y1,Ft,Fi,logmini,logmaxi,temp,l,LS=0.5,temp1;
float a1[4600],b1[4600],c1[4600],d1[4600];
static float ael[14] =
{1.0e+10,1.0e+5,1.0e+10,1.0e+5,1.0e+10,1.0e+5,1.0e+10,1.0e+5,1.0e+10,1.0e+5,1.0e+1
0,1.0e+5,1.0e+10,1.0e+5};
static float aeu[14] =
{1.0e+18,2.5e+5,1.0e+18,2.5e+5,1.0e+18,2.5e+5,1.0e+18,2.5e+5,1.0e+18,2.5e+5,1.0e+1
8,2.5e+5,1.0e+18,2.5e+5};
hr = 10.0/60.0 ;//C/sec
R = 8.3140;//J/ mol K
fp = fopen("D:\\Rajeev\\TGA results JAT\\simulation\\sim
10\\result_10\\jat_10.txt","a+");
fp1 = fopen("D:\\Rajeev\\TGA results JAT\\simulation\\sim
10\\result_10\\temp_10.txt","a+");
j=0;
for(i=0;i<4600;i=i+1)
        {
        fscanf(fp1,"%f%f%f%f",&a1[i],&b1[i],&c1[i],&d1[i]);
        if(i%10==0)
                {
                texp[j]= a1[i];
                Texp[j] = c1[i];
                Wexp[j] = d1[i];
                j = j+1;
                }
        }
printf("Enter the seed for random number\n");
scanf("%d",&seed);
long rand_uni_init=seed;
for(i=0;i<NP;i++)
        {
                for(j=0;j<D;j++)
                        {
                        ae[i][j] = 0.0;
                        logmini = log10(ael[j]); logmaxi = log10(aeu[j]);
                        temp = logmini +
                         (rand_uni(&rand_uni_init))*(logmaxi-logmini);
                        ae[i][j] = pow(10.0,temp);
                        printf("ae[%d][%d]=%e\n",i,j,ae[i][j]);
                        }
        }
```

```
for(k=0;k<genmax;k++)
        {
        if ((k%100)==0)
                {
                fprintf("k=%d\n",k);
                fprintf(fp,"k=%d\n",k);
                }
        for(i=0;i<NP;i++)
                {
                do a=(int)((NP)*rand_uni(&rand_uni_init));
                while(a==i);
                do b=(int)((NP)*rand_uni(&rand_uni_init));
                while(b==i || b==a);
                do c=(int)((NP)*rand_uni(&rand_uni_init));
                while( c==i || c==a || c==b);
                for(j=0;j<D;j++)
                        {
                        ae1[j] = 0.0;
                        aet[j] = 0.0;
                        l = rand_uni(&rand_uni_init);
                        temp1= log10(ae[c][j]) + F * (log10(ae[a][j]) –
                                        log10(ae[b][j]));
                        ae1[j] = pow(10.0,temp1);
                        }
                y1 = (rand_uni(&rand_uni_init));
                if ((ae1[j] > aeu[j]) || (ae1[j] < ael[j]))
                        {
                        logmini = log10(ael[j]); logmaxi = log10(aeu[j]);
                        temp = logmini +
                                (rand_uni(&rand_uni_init))*(logmaxi-logmini);
                        ae1[j] = pow(10.0,temp);
                        }
                if(y1>CR)
                        aet[j] = ae[i][j];
                else
                        aet[j] = ae1[j];
                if ((k%100)==0)
                        {
                        fprintf(fp,"%12.9le ",ae[i][j]);
                        fprintf(fp,",");
                        }
                if(aet[j] <0.0)
                aet[j] = aet[j] * (-1.0);
                }
        for(j=0;j<D;j++)
        aef[j] = ae[i][j];
```

```
        Fi = funvalue(aef,hr,Wexp,Texp,texp,k);
        for(j=0;j<D;j++)
        aef[j] = aet[j];
        Ft = funvalue(aef,hr,Wexp,Texp,texp,k);
        if ((k%100)==0)
                {
                fprintf(fp,"Fi = %12.9le\n",Fi);
                }
        if (Ft<Fi)
                {
                for (j=0;j<D;j++)
                newae[i][j]=aet[j];
                }
        }
for(i=0;i<NP;i++)
        {
        for(j=0;j<D;j++)
        ae[i][j]=newae[i][j];
        }
}
double funvalue(double aef[],double hr,double Wexp[],double Texp[],double texp[],int k)
{
int j;
double
B[6000],C[6000],W[6000],T[6000],ti,R,Fun,Funhalf,Fun10,Fun25,Fun40,Bhemi[600],C
hemi[600],Whemi[600],Bcel[600],Ccel[600],Wcel[600],Blig[600],Clig[600],Wlig[600],
Bm[600],Cm[600],Wm[600];
R = 8.314;
T[0] = Texp[0]+273.15;
B[0] = 1.0;
C[0] = 0.0;
W[0] = 1.0;
Bhemi[0]= 0.166;
Chemi[0]=0.0;
Whemi[0]=     0.166;
Bcel[0]= 0.535;
Ccel[0]=0.0;
Wcel[0]=0.535;
Blig[0]= 0.249;
Clig[0]=0.0;
Wlig[0]=0.249;
Bm[0]= 0.05;
Cm[0]=0.0;
Wm[0]=0.05;
Fun = 0.0;
for(j=0;j<458;j++)
```

```
{
ti = (Texp[j+1]-Texp[j]);
if (ti == 0.0)
ti=0.01;
T[j+1] = ti + T[j];
Bhemi[j+1]=Bhemi[j]-ti*(aef[0]*exp((-1.0)*aef[1]/(R* T[j]))
                + aef[2] * exp((-1.0)*aef[3]/(R * T[j]))) *
                Bhemi[j] * (1.0/hr);
Whemi[j+1]  = Whemi[j] - ti * aef[0] * exp((-1.0)*aef[1]/(R
                        * T[j])) * Bhemi[j] * (1.0/hr);
if (Whemi[j+1] < 0.0)
        Whemi[j+1] = Whemi[j];
if (Whemi[j+1] > 1.0)
        Whemi[j+1] = Whemi[j];
if (Bhemi[j+1] < 0.0)
        Bhemi[j+1] = 0.0;
Bcel[j+1]=Bcel[j] - ti*(aef[4]*exp((-1.0)*aef[5]/(R* T[j]))
                + aef[6] * exp((-1.0)*aef[7]/(R * T[j]))) * Bcel[j] * (1.0/hr);
Wcel[j+1]= Wcel[j] - ti * aef[4] * exp((-1.0)*aef[5]/(R *
                T[j])) * Bcel[j] * (1.0/hr);
if (Wcel[j+1] < 0.0)
        Wcel[j+1] = Wcel[j];
if (Wcel[j+1] > 1.0)
        Wcel[j+1] = Wcel[j];
if (Bcel[j+1] < 0.0)
        Bcel[j+1] = 0.0;
        Blig[j+1]  = Blig[j] - ti * ( aef[8] * exp((-
                        1.0)*aef[9]/(R * T[j]))+ aef[10] * exp((-1.0)*aef[11]/(R *
                        T[j]))) * Blig[j] * (1.0/hr);
        Wlig[j+1]  = Wlig[j] - ti * aef[8] * exp((-
                        1.0)*aef[9]/(R * T[j])) * Blig[j] * (1.0/hr);
if (Wlig[j+1] < 0.0)
        Wlig[j+1] = Wlig[j];
if (Wlig[j+1] > 1.0)
        Wlig[j+1] = Wlig[j];
if (Blig[j+1] < 0.0)
        Blig[j+1] = 0.0;
        Bm[j+1]  = Bm[j] - ti * ( aef[12] *exp((-1.0)*aef[13]/
                        (R * T[j]))) * Bm[j] * (1.0/hr);
        Wm[j+1]  = Bm[j+1];
if (Wm[j+1] < 0.0)
        Wm[j+1] = Wm[j];
if (Wm[j+1] > 1.0)
        Wm[j+1] = Wm[j];
if (Bm[j+1] < 0.0)
        Bm[j+1] = 0.0;
```

```
        if (W[j+1] < 0.0)
                W[j+1] = W[j];
        if (W[j+1] > 1.0)
                W[j+1] = W[j];
        if (B[j+1] < 0.0)
                B[j+1] = 0.0;
                W[j+1] = Whemi[j+1] +Wcel[j+1] + Wlig[j+1]+Wm[j+1];
        Fun =Fun + pow((Wexp[j+1]-W[j+1]),2.0);
        }
        return(Fun);
}
```

APPENDIX III

Code in 'C' Language for weight loss prediction for kinetic model of biomass pyrolysis

```
#include<conio.h>
#include<iostream.h>
#include<math.h>
#include<ctype.h>
#include<time.h>
#include<stdlib.h>
#include<stdio.h>
FILE *fp;
FILE *fp1;

void main()
{
double Wexp[500],Texp[500],texp[500];
int       i,j;
float a1[4600],b1[4600],c1[4600],d1[4600];
double
B[6000],hr,C[6000],W[6000],T[6000],ti,R,Fun,Funhalf,Fun10,Fun25,Fun40,Bhemi[600]
,Chemi[600],Whemi[600],Bcel[600],Ccel[600],Wcel[600],Blig[600],Clig[600],Wlig[600
];

static float aef[12] = {1.000000000e+010 ,2.009970299e+005 ,1.000000000e+010
,2.500000000e+005 ,1.000000000e+010 ,1.485846634e+005 ,1.000000000e+010
,1.516849901e+005 ,1.000000000e+010 ,1.220559776e+005 ,1.000000000e+010
,1.292044936e+005};
hr = 10.0/60.0 ;//C/sec
R = 8.3140;//J/ mol K
fp = fopen("D:\\Rajeev\\TGA results JAT\\simulation\\sim 10
          \\result_10\\w_simulated.txt","a+");
fp1 = fopen("D:\\Rajeev\\TGA results JAT\\simulation\\sim 10
          \\result_10\\temp_10.txt","a+");
j=0;
          for(i=0;i<4600;i=i+1)
          {
          fscanf(fp1,"%f%f%f%f",&a1[i],&b1[i],&c1[i],&d1[i]);
          if(i%10==0)
                    {
                    texp[j]= a1[i];
                    Texp[j] = c1[i];
```

```
        Wexp[j] = d1[i];
        j = j+1;
        }
}
for(j=0;j<458;j++)
{
R = 8.314;
T[0] = Texp[0]+273.15;
B[0] = 1.0;
C[0] = 0.0;
W[0] = 1.0;
Bhemi[0]= 0.1747;
Chemi[0]= 0.0;
Whemi[0]= 0.1747;
Bcel[0]= 0.5631;
Ccel[0]= 0.0;
Wcel[0]= 0.5631;
Blig[0]= 0.2622;
Clig[0]= 0.0;
Wlig[0]= 0.2622;
ti = (Texp[j+1]-Texp[j]);
if (ti == 0.0)
        ti=0.01;
T[j+1] = ti + T[j];
Bhemi[j+1]  = Bhemi[j] - ti * ( aef[0] * exp((-1.0)*aef[1]/(R * T[j]))+ aef[2] *
                        exp((-1.0)*aef[3]/(R * T[j]))) * Bhemi[j] *
                (1.0/hr);
Whemi[j+1]  = Whemi[j] - ti * aef[0] * exp((-1.0)*aef[1]/(R
                        * T[j])) * Bhemi[j] * (1.0/hr);
if (Whemi[j+1] < 0.0)
        Whemi[j+1] = Whemi[j];
if (Whemi[j+1] > 1.0)
        Whemi[j+1] = Whemi[j];
if (Bhemi[j+1] < 0.0)
        Bhemi[j+1] = 0.0;
Bcel[j+1]  = Bcel[j] - ti * ( aef[4] * exp((-1.0)*aef[5]/(R
                * T[j]))+ aef[6] * exp((-1.0)*aef[7]/(R *
        T[j]))) * Bcel[j] * (1.0/hr);
Wcel[j+1]  = Wcel[j] - ti * aef[4] * exp((-1.0)*aef[5]/(R *
                        T[j])) * Bcel[j] * (1.0/hr);
if (Wcel[j+1] < 0.0)
        Wcel[j+1] = Wcel[j];
if (Wcel[j+1] > 1.0)
        Wcel[j+1] = Wcel[j];
if (Bcel[j+1] < 0.0)
        Bcel[j+1] = 0.0;
```

```
        Blig[j+1]  = Blig[j] - ti * ( aef[8] * exp((-1.0)*aef[9]/(R
                                * T[j]))+ aef[10] * exp((-1.0)*aef[11]/(R *
        T[j]))) * Blig[j] * (1.0/hr);
        Wlig[j+1]  = Wlig[j] - ti * aef[8] * exp((-1.0)*aef[9]/(R *
                                T[j])) * Blig[j] * (1.0/hr);
        if (Wlig[j+1] < 0.0)
                Wlig[j+1] = Wlig[j];
        if (Wlig[j+1] > 1.0)
                Wlig[j+1] = Wlig[j];
        if (Blig[j+1] < 0.0)
                Blig[j+1] = 0.0;
        if (W[j+1] < 0.0)
                W[j+1] = W[j];
        if (W[j+1] > 1.0)
                W[j+1] = W[j];
        if (B[j+1] < 0.0)
                B[j+1] = 0.0;
        W[j+1] = Whemi[j+1] +Wcel[j+1] + Wlig[j+1];
        fprintf(fp,"%f\t%f\t%f\n ",Wexp[j+1],W[j+1],T[j+1]);
        }
}
```

APPENDIX IV

Code in 'C' Language for global kinetic parameter estimation for apparent kinetic model of biomass pyrolysis

```
#include<conio.h>
#include<iostream>
#include<math.h>
#include<ctype.h>
#include<time.h>
#include<stdlib.h>
#include<stdio.h>
#define NP 400
#define D 7
#define genmax 100000
#define F 0.5
#define CR 0.9
FILE *fp;
FILE *fp1;
FILE *fp2;
FILE *fp3;
FILE *fp4;
FILE *fp5;
FILE *fp6;
FILE *AG;
double funvalue(double aef[],double hr,double Wexp[],double Texp[],double texp[],int
k,int N, double Vexp, double Gexp);
#define IM1 2147483563
#define IM2 2147483399
#define AM (1.0/IM1)
#define IMM1 (IM1-1)
#define IA1 40014
#define IA2 40692
#define IQ1 53668
#define IQ2 52774
#define IR1 12211
#define IR2 3791
#define NTAB 32
#define NDIV (1+ IMM1/NTAB)
#define EPS1 1.2e-7
int q,q11;
#define RNMX (1.0-EPS1)
//Random Number Generator Function
```

```
double rand_uni(double * );
double simpson(double value[], int N, double a, double b);
double rand_uni(long *idum)
{
  long j,k;
  static long idum2=123456789;
  static long iy=0;
  static long iv[NTAB];
  double temp;
  if(*idum<=0)
    {
        if(-(*idum)<1)
                *idum=1;
        else
        *idum=-(*idum);
        idum2=(*idum);
        for (j=NTAB+7;j>=0;j--)
        {
          k=(*idum)/IQ1;
          *idum=IA1 * (*idum-k*IQ1)-k*IR1;
          if (*idum<0)
            *idum+=IM1;
          if(j<NTAB)
          iv[j]=*idum;
        }          //End of For loop for j
        iy=iv[0];

}       //End of if
k=(*idum)/IQ1;
*idum=IA1*(*idum-k-IQ1)-k*IR1;
if(*idum<0)
  *idum+=IM1;
  k=idum2/IQ2;
  idum2=IA2*(idum2-k*IQ2)-k*IR2;
  if(idum2<0)
  idum2+=IM2;
  j=iy/NDIV;
  iy=iv[j]-idum2;
  iv[j]=*idum;
  if(iy<1)
    iy+=IMM1;
  if((temp=AM*iy)>RNMX)  {
          return RNMX;
  printf(" The Random Number is RNMX %4.4f \n ",RNMX); getchar();}
  else
  {
```

```
  return temp;
  printf(" The Random Number is %4.4f \n ",temp); getchar();
  }
} //End Rand Function

int main(void)
{
double
ae[NP][D],ae1[D],aet[D],aeo[D],check,aef[D],newae[NP][D],Wexp1[2000],Texp1[2000]
,texp1[2000],Wexp2[2000],Texp2[2000],texp2[2000],Wexp3[2000],Texp3[2000],texp3[
2000];
int       i,j,k,a,b,c,seed,ij;
double
sbv,hr,sbvhr,R,w1,w2,w3,w4,w5,w6,w7,y1,Ft,Fi,logmini,logmaxi,temp,l,LS=0.5,temp1,
Gcal,Vcal;
float a1[16000],b1[16000],c1[16000],d1[16000];
float a2[16000],b2[16000],c2[16000],d2[16000];
float a3[16000],b3[16000],c3[16000],d3[16000];
float Vexp1, Gexp1, Cexp1;
float Vexp2, Gexp2, Cexp2;
float Vexp3, Gexp3, Cexp3;
static float ael[7] = {1.0e+2,0.40e+5,1.0e+2,0.40e+5,1.0e+2,0.4e+5,0.5};
static float aeu[7] = {1.0e+18,2.50e+5,1.0e+18,2.5e+5,1.0e+18,2.5e+5, 2.0};
hr = 5.0/60.0 ;// Heating rate in C/sec
R = 8.3140;//J/ mol K
fp = fopen("E:\\Rajeev\\data\\jat_macro.txt","a+");
fp1 = fopen("E:\\Rajeev\\data\\temp_400.txt","a+");
fp2 = fopen("E:\\Rajeev\\data\\temp_550.txt","a+");
fp3 = fopen("E:\\Rajeev\\data\\temp_700.txt","a+");
fp4 = fopen("E:\\Rajeev\\data\\yield_400.txt","a+");
fp5 = fopen("E:\\Rajeev\\data\\yield_550.txt","a+");
fp6 = fopen("E:\\Rajeev\\data\\yield_700.txt","a+");
fscanf(fp4,"%f%f%f%f",&Vexp1,&Gexp1,&Cexp1);
fscanf(fp5,"%f%f%f%f",&Vexp2,&Gexp2,&Cexp2);
fscanf(fp6,"%f%f%f%f",&Vexp3,&Gexp3,&Cexp3);
j=0;
        for(i=0;i<8496;i=i+1)
        {
                fscanf(fp1,"%f%f%f%f",&a1[i],&b1[i],&c1[i],&d1[i]);
                if(i%10==0)
                        {
                        texp1[j]= a1[i];
                        Texp1[j] = c1[i];
                        Wexp1[j] = d1[i];
                        j = j+1;
                        }
```

```
        }
j=0;
        for(i=0;i<12194;i=i+1)
        {
                fscanf(fp2,"%f%f%f%f",&a2[i],&b2[i],&c2[i],&d2[i]);
                if(i%10==0)
                        {
                        texp2[j]= a2[i];
                        Texp2[j] = c2[i];
                        Wexp2[j] = d2[i];
                        j = j+1;
                        }
        }
j=0;
        for(i=0;i<15794;i=i+1)
        {
                fscanf(fp3,"%f%f%f%f",&a3[i],&b3[i],&c3[i],&d3[i]);
                if(i%10==0)
                        {
                        texp3[j]= a3[i];
                        Texp3[j] = c3[i];
                        Wexp3[j] = d3[i];
                        j = j+1;
                        }
        }
printf("Enter the seed for random number\n");
scanf("%d",&seed);
long rand_uni_init=seed;
for(i=0;i<NP;i++)
        {
        for(j=0;j<D;j++)
                {
                ae[i][j] = 0.0;
                logmini = log10(ael[j]); logmaxi = log10(aeu[j]);
                temp = logmini + (rand_uni(&rand_uni_init))*(logmaxi-
                                logmini);
                ae[i][j] = pow(10.0,temp);
                printf("ae[%d][%d]=%e\n",i,j,ae[i][j]);
                }
        }
for(k=0;k<genmax;k++)
        {
        if ((k%100)==0)
                {
                printf("k=%d\n",k);
                fprintf(fp,"k=%d\n",k);
```

```
        }
for(i=0;i<NP;i++)
        {
        do a=(int)((NP)*rand_uni(&rand_uni_init));
        while(a==i);
        do b=(int)((NP)*rand_uni(&rand_uni_init));
        while(b==i || b==a);
        do c=(int)((NP)*rand_uni(&rand_uni_init));
        while( c==i || c==a || c==b);
        for(j=0;j<D;j++)
                {
                ae1[j] = 0.0;
                aet[j] = 0.0;
                l = rand_uni(&rand_uni_init);
                temp1= log10(ae[c][j]) + F * (log10(ae[a][j]) -
                log10(ae[b][j]));
                ae1[j] = pow(10.0,temp1);
                //Cross over
                y1 = (rand_uni(&rand_uni_init));
                if ((ae1[j] > aeu[j]) || (ae1[j] < ael[j]))
                        {
                        logmini = log10(ael[j]); logmaxi =
                        log10(aeu[j]);
                        temp = logmini +        (rand_uni(&rand_uni_init))
                                *(logmaxi-logmini);
                        ae1[j] = pow(10.0,temp);
                        }
                if(y1>CR)
                aet[j] = ae[i][j];
                else
                aet[j] = ae1[j];
                if ((k%100)==0)
                        {
                        fprintf(fp,"%12.9le ",ae[i][j]);
                        fprintf(fp,",");
                        }
                if(aet[j] <0.0)
                aet[j] = aet[j] * (-1.0);
                }
        for(j=0;j<D;j++)
        aef[j] = ae[i][j];
Fi = funvalue(aef,hr,Wexp1,Texp1,texp1,k,850,Vexp1,Gexp1);
        for(j=0;j<D;j++)
        aef[j] = aet[j];
Ft = funvalue(aef,hr,Wexp1,Texp1,texp1,k,850,Vexp1,Gexp1);
        if ((k%100)==0)
```

```
                fprintf(fp,"Fi = %12.9le\tFt = %12.9le\n",Fi,Ft);
                if (Ft<Fi)
                        {
                        for (j=0;j<D;j++)
                        newae[i][j]=aet[j];
                        }
                else
                        {
                        for (j=0;j<D;j++)
                        newae[i][j]=ae[i][j];
                        }
                }
        for(i=0;i<NP;i++)
                {
                for(j=0;j<D;j++)
                ae[i][j]=newae[i][j];
                }
        }
}
double funvalue(double aef[],double hr,double Wexp[],double Texp[],double texp[],int k,
int N, double Vexp, double Gexp)
{
// L_temp = Lower Temp
// H_temp = Higher Temp
// N = Number of sample point taken
int j;
double B[6000],G[6000],V[6000],C[6000],W[6000],T[6000],ti,R,Fun,Gexp3,Vexp3;
R = 8.314;
T[0] = Texp[0]+273.15;
B[0] = 1.0;
G[0] = 0.0;
V[0] = 0.0;
C[0] = 0.0;
W[0] = 1.0;
Fun = 0.0;
for(j=0;j<N-1;j++) /* Earlier it was 458 instead of N */
        {
        ti = (Texp[j+1]-Texp[j]);
        T[j+1] = ti + T[j];
        B[j+1]  = B[j] - ti * ( aef[0] * exp((-1.0)*aef[1]/(R *
        T[j]))+ aef[2] * exp((-1.0)*aef[3]/(R *
        T[j]))+aef[4] * exp((-1.0)*aef[5]/(R * T[j]))) *
        pow((B[j]),aef[6]) * (1.0/hr);
        G[j+1]  = G[j] + ti * aef[0] * exp(-aef[1]/(R * T[j])) *
        pow((B[j]),aef[6]) * (1.0/hr);
```

```
        V[j+1]  = V[j] + ti * aef[2] * exp(-aef[3]/(R * T[j])) *
        pow((B[j]),aef[6]) * (1.0/hr);
        C[j+1]  = C[j] + ti * aef[4] * exp(-aef[5]/(R * T[j])) *
        pow((B[j]),aef[6]) * (1.0/hr);
        W[j+1]  =       B[j+1] +        C[j+1];
        if (W[j+1] < 0.0)
                W[j+1] = W[j];
        if (W[j+1] > 1.0)
                W[j+1] = W[j];
        if (B[j+1] < 0.0)
                {
                B[j+1] = 0.0;
                G[j+1]  = G[j];
                V[j+1]  = V[j];
                C[j+1]  = C[j];
                }
        if (G[j+1] < 0.0)
                G[j+1] = G[j];
        if (G[j+1] > 1.0)
                G[j+1] = G[j];
        if (V[j+1] < 0.0)
                V[j+1] = V[j];
        if (V[j+1] > 1.0)
                V[j+1] = V[j];
        if (C[j+1] < 0.0)
                C[j+1] = C[j];
        if (C[j+1] > 1.0)
                C[j+1] = C[j];
/* integate the G and V will give the value of Gcal & Vcal */
        Fun =Fun + (pow((Wexp[j+1]-W[j+1]),2.0));
        }
        Fun = Fun  + pow((Gexp-G[N-1]),2.0)+pow((Vexp-V[N-1]),2.0);
        return(Fun);
}
```

APPENDIX V

Code in 'C' Language for product yield prediction for apparent kinetic model of biomass pyrolysis

```
#include<conio.h>
#include<iostream.h>
#include<math.h>
#include<ctype.h>
#include<time.h>
#include<stdlib.h>
#include<stdio.h>
FILE *fp;
FILE *fp1;
FILE *fp2;
void main()
{
double Wexp[1600],Texp[1600],texp[1600];
int       i,j;
float a1[16000],b1[16000],c1[16000],d1[16000];
double B[6000],hr,C[6000],W[6000],T[6000],G[6000],V[6000],                ti,R,Fun;
static float aef[7] = {1.018199168e+017 ,2.091901846e+     005 ,1.000000000e+002
,5.274381425e+004 ,7.157176580e+ 010 ,1.407289656e+005 ,2.000000000e+000};
hr = 5.0/60.0 ;//C/sec
R = 8.3140;//J/ mol K
fp = fopen("E:\\Rajeev\\data\\result\\w_simulated_400.txt","a+");
fp1 = fopen("E:\\Rajeev\\data\\temp_400.txt","a+");
fp2 = fopen("E:\\Rajeev\\data\\result\\G_V_simulated_                        400.txt","a+");
j=0;
for(i=0;i<8496;i=i+1)
          {
          fscanf(fp1,"%f%f%f%f",&a1[i],&b1[i],&c1[i],&d1[i]);
          if(i%10==0)
                    {
                    texp[j]= a1[i];
                    Texp[j]= c1[i];
                    Wexp[j]= d1[i];
                    j = j+1;
                    }}
for(j=0;j<849;j++)
          {
          R = 8.314;
          T[0] = Texp[0]+273.15;
          B[0] = 1.0;
```

```
        C[0] = 0.0;
        W[0] = 1.0;
        G[0] = 0.0;
        V[0] = 0.0;
        ti = (Texp[j+1]-Texp[j]);
        if (ti == 0.0)
        ti=0.01;
        T[j+1] = ti + T[j];
        B[j+1]  = B[j] - ti * ( aef[0] * exp((-1.0)*aef[1]/(R *
        T[j]))+ aef[2] * exp((-1.0)*aef[3]/(R *
        T[j]))+aef[4] * exp((-1.0)*aef[5]/(R * T[j]))) *
        pow((B[j]),aef[6]) * (1.0/hr);
        G[j+1]  = G[j] + ti * aef[0] * exp(-aef[1]/(R * T[j])) *
        pow((B[j]),aef[6]) * (1.0/hr);
        V[j+1]  = V[j] + ti * aef[2] * exp(-aef[3]/(R * T[j])) *
        pow((B[j]),aef[6]) * (1.0/hr);
        C[j+1]  = C[j] + ti * aef[4] * exp(-aef[5]/(R * T[j])) *
        pow((B[j]),aef[6]) * (1.0/hr);
        W[j+1]  =       B[j+1] +        C[j+1];
        if (W[j+1] < 0.0)
                W[j+1] = W[j];
        if (W[j+1] > 1.0)
                W[j+1] = W[j];
        if (B[j+1] < 0.0)
                {
                B[j+1] = 0.0;
                G[j+1]  = G[j];
                V[j+1]  = V[j];
                C[j+1]  = C[j];
                }
        if (G[j+1] < 0.0)
                G[j+1] = G[j];
        if (G[j+1] > 1.0)
                G[j+1] = G[j];
        if (V[j+1] < 0.0)
                V[j+1] = V[j];
        if (V[j+1] > 1.0)
                V[j+1] = V[j];
        if (C[j+1] < 0.0)
                C[j+1] = C[j];
        if (C[j+1] > 1.0)
                C[j+1] = C[j];
        fprintf(fp,"%f\t%f\t%f\n ",Wexp[j+1],W[j+1],T[j+1]);
        }
fprintf(fp2,"%f\t%f\t\%f\n ",G[j],V[j],C[j]);
}
```

APPENDIX VI

Code in 'C' Language for simulation of fixed bed model of biomass pyrolysis

```
// Code for single step global kinetics
// Implicit discretization scheme has adopted for both spatial and temporal discretization
in mass and energy balance equations.
// Non linear terms has calulated at previous time only (i.e. not pure implicit)
// Equations have solved using jacobian iteration method
#include <stdio.h>
#include <math.h>
#include <ctype.h>
#include <stdlib.h>
#include <conio.h>
#define M 50  //M is no of grid points in radial direction
#define N 25  //N is no of grid points in axial direction
main()
{
        double
rhobavg,s3,s4,Tavg,s1,s2,AH[M+1][N+1],AD[M+1][N+1],AE[M+1][N+1],AF[M+1][N
+1],AG[M+1][N+1],AC[M+1][N+1],H,BB[M+1][N+1],HR,Trsu,G[M+1][N+1],E[M+1]
[N+1],F[M+1][N+1],kb[M+1][N+1],kc[M+1][N+1],Cpb[M+1][N+1],Cpc[M+1][N+1],C
psolid[M+1][N+1],eta[M+1][N+1],R,delH,AA[M+1][N+1],AB[M+1][N+1],s,m,
FluxAVG,rhovAVG[M+1][N+1],v[M+1][N+1],FluxvAVG,rhovolatiles,
rhochar,pi,rhocAVG, rhocN_22, rhocN1_22, rhovN_22, rhovN1_22, rhovAVGN_22,
rhocAVGN_22,av21,ac21,rhocN_21, rhocN1_21, rhovN_21, rhovN1_21,
rhovAVGN_21, rhocAVGN_21,rhocN_20, rhocN1_20, rhovN_20, rhovN1_20,
rhovAVGN_20, rhocAVGN_20,rhocN_3, rhocN1_3, rhovN_3, rhovN1_3,
rhovAVGN_3, rhocAVGN_3, rhocN_4, rhocN1_4, rhovN_4, rhovN1_4, rhovAVGN_4,
rhocAVGN_4,rhocN_5, rhocN1_5, rhovN_5, rhovN1_5, rhovAVGN_5,
rhocAVGN_5,rhocN_6, rhocN1_6, rhovN_6, rhovN1_6, rhovAVGN_6,
rhocAVGN_6,rhocN_7, rhocN1_7, rhovN_7, rhovN1_7, rhovAVGN_7,
rhocAVGN_7,rhocN_8, rhocN1_8, rhovN_8, rhovN1_8, rhovAVGN_8,
rhocAVGN_8,rhocN_9, rhocN1_9, rhovN_9, rhovN1_9, rhovAVGN_9,
rhocAVGN_9,rhocN_10, rhocN1_10, rhovN_10, rhovN1_10, rhovAVGN_10,
rhocAVGN_10,rhocN_11, rhocN1_11, rhovN_11, rhovN1_11, rhovAVGN_11,
rhocAVGN_11,rhocN_12, rhocN1_12, rhovN_12, rhovN1_12, rhovAVGN_12,
rhocAVGN_12,rhocN_13, rhocN1_13, rhovN_13, rhovN1_13, rhovAVGN_13,
rhocAVGN_13,rhocN_14, rhocN1_14, rhovN_14, rhovN1_14, rhovAVGN_14,
rhocAVGN_14,rhocN_15, rhocN1_15, rhovN_15, rhovN1_15, rhovAVGN_15,
rhocAVGN_15,rhocN_16, rhocN1_16, rhovN_16, rhovN1_16, rhovAVGN_16,
rhocAVGN_16,rhocN_17, rhocN1_17, rhovN_17, rhovN1_17, rhovAVGN_17,
rhocAVGN_17,rhocN_18, rhocN1_18, rhovN_18, rhovN1_18, rhovAVGN_18,
rhocAVGN_18,rhocN_19, rhocN1_19, rhovN_19,
```

```
rhovN1_19,rhovAVGN_19,rhocAVGN_19,av1,av2,av3,av4,av5,av6,av7,av8,av9,av10,a
v11,av12,av13,av14,av15,av16,av17,av18,av19,ac1,ac2,ac3,ac4,ac5,ac6,ac7,ac8,ac9,
ac10,ac11,ac12,ac13,ac14,ac15,ac16,ac17,av20,ac20,ac18,ac19,T[M+1][N+1],Tp[M+1][
N+1],Tnew[M+1][N+1],a,b,e,k0[M+1][N+1],rho,phi[M+1][N+1],cp,k10,keff[M+1][N+1
],delr,delz,alpha[M+1][N+1],sigma,delt,Trs,Ths,A[M+1][N+1],B[M+1][N+1],C[M+1][N
+1],D[M+1][N+1],rhoc[M+1][N+1],rhov[M+1][N+1],rhob[M+1][N+1],rhocp[M+1][N+
1],rhovp[M+1][N+1],rhobp[M+1][N+1],rhocnew[M+1][N+1],rhobnew[M+1][N+1]
,rhovnew[M+1][N+1],Ap,Ep,Dab,Rg,Fluxc,Fluxv[M+1][N+1],rhovN,rhovN1,rhovN_1,r
hovN1_1,rhocN,rhocN1,rhocN_1,rhocN1_1,rhovAVGN,rhovAVGN_2,rhocAVGN_2,rh
ovAVGN_1,rhocAVGN,rhocAVGN_1,rhocN1_2,rhovN_2,rhovN1_2,rhocN_2,areav,are
ac,pdctYv,pdctYc,fv,fc[1501],p,q,rhocN_23, rhocN1_23, rhovN_23, rhovN1_23,
rhovAVGN_23, rhocAVGN_23,av22,ac22,rhocN_24, rhocN1_24, rhovN_24,
rhovN1_24, rhovAVGN_24, rhocAVGN_24,av23,ac23, rhocN_25, rhocN1_25,
rhovN_25, rhovN1_25, rhovAVGN_25, rhocAVGN_25,av24,ac24, rhocN_26,
rhocN1_26, rhovN_26, rhovN1_26, rhovAVGN_26, rhocAVGN_26,av25,ac25;
int r;                  //  Radial direction variable
int z;                  //  Axial direction variable
int t;                  //  Time variable
int i,j,k1;             //  i, j, k1 are loop counter variables
a=0.9839;               //      Dimensionless constant used to calculate porosity in the
                        bed taken from Chan W. C. R. et al.1985
b=-1.25*pow(10,-3);     //      Dimensionless constant used to calculate porosity in the
                        bed taken from Chan W. C. R. et al.1985
Rg= 8.314;                  //  J/mol.K
Dab=3.0*pow(10,-5.0);       //  Mass transfer diffusivity in m2/s taken from Di-Blasi
                            2000.
cp=2800.0;                  //  Constant Heat Capacity in J/kg.K
sigma=5.67*pow(10,-8.0);    //  Stefan Boltzmann's constant in
                        J/m2.s.K4
delr =(0.06/M);             //  Step size in r direction
delz =(0.01/N);             //  Step size in z direction
delt =1;                    //  Time step in sec
e=0.95;                     //  Emmisivity
pi=3.14;                    //  Pi a constant
delH=-255000;               //  Heat of reaction in J/kg
char filename[]="AC1.dat";  //  All the constants are defined below.
//      1, 2,3 stores the value of particular constant (in .dat format) till defined limit(e.g.
in the code AC1 stores value of AC from t=0 to=1200, AC2 from t=1200 to t=2400, and
AC3 from t=2400 to t=3600)
char filename1[]="AC2.dat";
char filename2[]="AC3.dat";
char filename3[]="kc4.dat";
char filename6[]="AA1.dat";
char filename7[]="AA2.dat";
char filename8[]="AA3.dat";
char filename4[]="AA4.dat";
```

```
char filename9[]="A1.dat";
char filename10[]="A2.dat";
char filename11[]="A3.dat";
char filename5[]="A4.dat";
char filename12[]="AB1.dat";
char filename13[]="AB2.dat";
char filename14[]="AB3.dat";
char filename54[]="AG1.dat";
char filename15[]="B1.dat";
char filename16[]="B2.dat";
char filename17[]="B3.dat";
char filename55[]="AG2.dat";
char filename18[]="C1.dat";
char filename19[]="C2.dat";
char filename20[]="C3.dat";
char filename56[]="AG3.dat";
char filename21[]="D1.dat";
char filename22[]="D2.dat";
char filename23[]="D3.dat";
char filename57[]="D4.dat";
char filename24[]="E1.dat";
char filename25[]="E2.dat";
char filename26[]="E3.dat";
char filename58[]="E4.dat";
char filename27[]="F1.dat";
char filename28[]="F2.dat";
char filename29[]="F3.dat";
char filename59[]="F4.dat";
char filename30[]="cpsolid1.dat";     // Stores heat capacity vales (J/kg.K) in .dat file
char filename31[]="cpsolid2.dat";
char filename32[]="cpsolid3.dat";
char filename60[]="cpsolid4.dat";
char filename33[]="keff1.dat";         // Stores thermal conductivity vales (J/s.m.K) in .dat
                                       file
char filename34[]="keff2.dat";
char filename35[]="keff3.dat";
char filename61[]="keff4.dat";
char filename36[]="alpha1.dat";        // Stores thermal difffusivity vales (m2/s) in .dat file
char filename37[]="alpha2.dat";
char filename38[]="alpha3.dat";
char filename62[]="alpha4.dat";
char filename39[]="outputtemp1.dat";          // Stores temperature values in K
char filename40[]="outputrhob.dat";
char filename41[]="outputrhoc.dat";
char filename42[]="outputrhov.dat";
char filename43[]="outputtemp2.dat";
```

```
char filename44[]="outputtemp3.dat";
char filename45[]="AD1.dat";
char filename46[]="AD2.dat";
char filename47[]="AD3.dat";
char filename48[]="AE1.dat";
char filename49[]="AE2.dat";
char filename50[]="AE3.dat";
char filename51[]="AF1.dat";
char filename52[]="AF2.dat";
char filename53[]="AF3.dat";
char filename63[]="fluxv.dat";          // Stores flux of volatiles in kg/sec
char filename64[]="fluxc.dat";          // Stores char concentration in kg/m3.s
printf("Creating file %s \n",filename);
        FILE *fp;
        fp=fopen(filename,"w+");
        FILE *fp1;
        fp1=fopen(filename1,"w+");
        FILE *fp2;
        fp2=fopen(filename2,"w+");
        FILE *fp3;
        fp3=fopen(filename3,"w+");
        FILE *fp4;
        fp4=fopen(filename4,"w+");
        FILE *fp5;
        fp5=fopen(filename5,"w+");
        FILE *fp6;
        fp6=fopen(filename6,"w+");
        FILE *fp7;
        fp7=fopen(filename7,"w+");
        FILE *fp8;
        fp8=fopen(filename8,"w+");
        FILE *fp9;
        fp9=fopen(filename9,"w+");
        FILE *fp10;
        fp10=fopen(filename10,"w+");
        FILE *fp11;
        fp11=fopen(filename11,"w+");
        FILE *fp12;
        fp12=fopen(filename12,"w+");
        FILE *fp13;
        fp13=fopen(filename13,"w+");
        FILE *fp14;
        fp14=fopen(filename14,"w+");
        FILE *fp15;
        fp15=fopen(filename15,"w+");
        FILE *fp16;
```

```
fp16=fopen(filename16,"w+");
FILE *fp17;
fp17=fopen(filename17,"w+");
FILE *fp18;
fp18=fopen(filename18,"w+");
FILE *fp19;
fp19=fopen(filename19,"w+");
FILE *fp20;
fp20=fopen(filename20,"w+");
FILE *fp21;
fp21=fopen(filename21,"w+");
FILE *fp22;
fp22=fopen(filename22,"w+");
FILE *fp23;
fp23=fopen(filename23,"w+");
FILE *fp24;
fp24=fopen(filename24,"w+");
FILE *fp25;
fp25=fopen(filename25,"w+");
FILE *fp26;
fp26=fopen(filename26,"w+");
FILE *fp27;
fp27=fopen(filename27,"w+");
FILE *fp28;
fp28=fopen(filename28,"w+");
FILE *fp29;
fp29=fopen(filename29,"w+");
FILE *fp30;
fp30=fopen(filename30,"w+");
FILE *fp31;
fp31=fopen(filename31,"w+");
FILE *fp32;
fp32=fopen(filename32,"w+");
FILE *fp33;
fp33=fopen(filename33,"w+");
FILE *fp34;
fp34=fopen(filename34,"w+");
FILE *fp35;
fp35=fopen(filename35,"w+");
FILE *fp36;
fp36=fopen(filename36,"w+");
FILE *fp37;
fp37=fopen(filename37,"w+");
FILE *fp38;
fp38=fopen(filename38,"w+");
FILE *fp39;
```

```
fp39=fopen(filename39,"w+");
FILE *fp40;
fp40=fopen(filename40,"w+");
FILE *fp41;
fp41=fopen(filename41,"w+");
FILE *fp42;
fp42=fopen(filename42,"w+");
FILE *fp43;
fp43=fopen(filename43,"w+");
FILE *fp44;
fp44=fopen(filename44,"w+");
FILE *fp45;
fp45=fopen(filename45,"w+");
FILE *fp46;
fp46=fopen(filename46,"w+");
FILE *fp47;
fp47=fopen(filename47,"w+");
FILE *fp48;
fp48=fopen(filename48,"w+");
FILE *fp49;
fp49=fopen(filename49,"w+");
FILE *fp50;
fp50=fopen(filename50,"w+");
FILE *fp51;
fp51=fopen(filename51,"w+");
FILE *fp52;
fp52=fopen(filename52,"w+");
FILE *fp53;
fp53=fopen(filename53,"w+");
FILE *fp54;
fp54=fopen(filename54,"w+");
FILE *fp55;
fp55=fopen(filename55,"w+");
FILE *fp56;
fp56=fopen(filename56,"w+");
FILE *fp57;
fp57=fopen(filename57,"w+");
FILE *fp58;
fp58=fopen(filename58,"w+");
FILE *fp59;
fp59=fopen(filename59,"w+");
FILE *fp60;
fp60=fopen(filename60,"w+");
FILE *fp61;
fp61=fopen(filename61,"w+");
FILE *fp62;
```

```
fp62=fopen(filename62,"w+");
FILE *fp63;
fp63=fopen(filename63,"w+");
FILE *fp64;
fp64=fopen(filename64,"w+");
for(i=0;i<M+1;i++)
{
        for(j=0;j<N+1;j++)
        {
        Tp[i][j]=303.15;                // Initial condition for temperature
        T[i][j]=Tp[i][j]+1.0;           // Assumed temperature at time t=1 sec
        rhobp[i][j]=601.2;              // Biomass concentartion at time t=0 sec
                                        in kg/m3 (initial condition)
        rhocp[i][j]=0.0;                // Char concentartion in kg/m3  at time
                                        t=0 sec (initial condition)
        rhovp[i][j]=0.0;                // Volatile concentartion in kg/m3  at
                                        time t=0 sec (initial condition)
        rhob[i][j]=rhobp[i][j]-1.0;     // Assumed Biomass concentartion at
                                        time t=1sec in kg/m3
        rhoc[i][j]=rhocp[i][j]+1.0;     // Assumed char concentartion at time
                                        t=1sec in kg/m3
        rhov[i][j]=rhovp[i][j]+1.0;      // Assumed volatile concentartion at
                                        time t=1sec in kg/m3
        }
}
p=0.0;                  // Initiallization of the consatnt which stores volatile flux
k10=25.77*pow(10,-3.0);                 // Thermal conductivity of gas in J/s.m.K
for(t=0;t<=5000;t++)                // Time loop starts
{
printf("\n\nt=%d\n",t);
// Checks difference in succesive temperature values whether the difference is
under acceptable limit
for (k1=0;k1<50;k1++)   // k1 loop starts
        {
        for(r=0;r<=M;r++)
                {
                for(z=0;z<=N;z++)
                        {
                        Ap=23333.33;
// Frequency factor used in the kinetics taken from Di-Blasi 2008 in 1/sec
                        Ep=84200;
// Activation energy used in the kinetics taken from Di-Blasi 2008 in J/mol
                        H=Ep/Rg;
                        if(t<=4442)
        // t=4442 to achieve final temperature 673.15 K
                                {
```

```
                    Trs=303.15+(0.0833)*t;
                // Linear dependancy of temperature on heating rate
                    Ths=1.001101*Trs+12.50375;
// Relation b/w reactor surface temperature and sample holder surface temperature
derived from calibration curve experimentally
                    }
                    else
                    {
                    Trs=Tp[r][z];
                    Ths=Tp[r][z];
                    }
                phi[r][z]=a+b*rhobp[r][z];
// Porosity variation in the biomass bed as reaction proceeds taken from Chan W. C. R. et
al.1985
            k0[r][z]=0.0013+0.05*(Tp[r][z]/1000)+0.63*(pow((Tp[r][z]/1000),2));
        // Thermal conductivity biomass in J/s.m.K
            keff[r][z]=k0[r][z]/(1-
phi[r][z]+(1/((k10/(k0[r][z]*phi[r][z]))+((4*sigma*pow(Tp[r][z],3)*0.01)/(k0[r][z])))));
// Effective thermal conductivity in J/s.m.K taken from Di-Blasi-1996
            Cpb[r][z]=1112+4.85*(Tp[r][z]-273);
// Heat capacity of biomass in J/kg.K taken from Koufopanos C.A.1991

            Cpc[r][z]=1003.2+2.09*(Tp[r][z]-273);
// Heat capacity of char in J/kg.K taken from Koufopanos C.A.1991
            eta[r][z]=(rhobp[r][z]/(rhobp[r][z]+rhocp[r][z]));
// Reaction progress variable dimensioless taken from Koufopanos C.A.1991
            Cpsolid[r][z]=eta[r][z]*Cpb[r][z]+(1-eta[r][z])*Cpc[r][z];
// Effective heat capacity in J/kg.K taken from Koufopanos C.A.1991
            alpha[r][z]=(keff[r][z]/(rhobp[r][z]*Cpsolid[r][z]));
 // Thermal diffusivity in m2/s
// Varibles used in model equations
        B[r][z]=((exp((-Ep)/(Rg*Tp[r][z])))*Ap*delt);
        C[r][z]=(alpha[r][z]*delt/(pow(delr,2.0)));
        D[r][z]=(alpha[r][z]*delt/(pow(delz,2.0)));
        E[r][z]=((2.0*sigma*e*delr)/(keff[r][z]));
        F[r][z]=((2.0*sigma*e*delz)/(keff[r][z]));
        BB[r][z]=((delH)/(Cpsolid[r][z]));
        AA[r][z]=(1.0/(1.0+(2.0*C[r][z])+(2.0*D[r][z])+((B[r][z]*BB[r][z]*H)/(pow(
                    Tp[r][z],2.0)))-((B[r][z]*H)/(Tp[r][z]))-(B[r][z])));
        AB[r][z]=(1.0/(1.0+(4.0*C[r][z])+(2.0*D[r][z])+((B[r][z]*BB[r][z]*H)/(pow(
                    Tp[r][z],2.0)))-((B[r][z]*H)/(Tp[r][z]))-(B[r][z])));
        AC[r][z]=B[r][z]*(((BB[r][z]*H)/(Tp[r][z]))-(BB[r][z])-(H));
        AD[r][z]=(1.0/(1.0+(2.0*C[r][z])+(2.0*D[r][z])+((B[r][z]*BB[r][z]*H)/(pow(
                    Tp[r][z],2.0)))-((B[r][z]*H)/(Tp[r][z]))-
                    (B[r][z])+(4.0*D[r][z]*F[r][z]*(pow(Trs,3.0)))));
        AF[r][z]=(1.0/(1.0+(4.0*C[r][z])+(2.0*D[r][z])+((B[r][z]*BB[r][z]*H)/(pow(
```

```
                        Tp[r][z],2.0)))-((B[r][z]*H)/(Tp[r][z]))-
                        (B[r][z])+(4.0*D[r][z]*F[r][z]*(pow(Trs,3.0)))));
        AH[r][z]=((2.0*Dab*delt)/(pow(delz,2.0)));
        }
}
for(r=1;r<=M;r++)
        {
        for(z=1;z<=N;z++)
                {
                A[r][z]=((alpha[r][z]*delt)/(2.0*r*0.0012*delr));
                }
        }
for(r=1;r<=M;r++)
        {
        for(z=1;z<=N;z++)
                {
                AE[r][z]=(1.0/(1.0+(2.0*C[r][z])+(2.0*D[r][z])+((B[r][z]*BB[r][z]*H)
                                /(pow(Tp[r][z],2.0)))-((B[r][z]*H)/(Tp[r][z]))-
                                (B[r][z])+(4.0*(C[r][z]+A[r][z])*E[r][z]*(pow(Trs,3.0)))));
AG[r][z]=(1.0/(1.0+(2.0*C[r][z])+(2.0*D[r][z])+((B[r][z]*BB[r][z]*H)/(pow(Tp[r][z]
                ,2.0)))-((B[r][z]*H)/(Tp[r][z]))-
                (B[r][z])+(4.0*D[r][z]*F[r][z]*(pow(Trs,3.0)))+(4.0*(C[r][z]+A[r][z])*E[
                r][z]*(pow(Trs,3.0)))));
                                        }
                }
// Stores values of all the property and varibles every sec
if(k1==49 && t<=1200)
        {
        fprintf(fp,"t=%d\n",t);
        for(i=0;i<M+1;i++)
        {
        for(j=0;j<N+1;j++)
        {
        fprintf(fp,"%f\t",AC[i][j]);
        if(j==N)
        fprintf(fp,"\n");
        }}}
if(k1==49 && t>1200 && t<2400)
        {       fprintf(fp1,"%d\n",t);
        for(i=0;i<M+1;i++)
        {       for(j=0;j<N+1;j++)
        {       fprintf(fp1,"%f\t",AC[i][j]);
                if(j==N)
                fprintf(fp1,"\n");
        }}}
if(k1==49 && t>=2400 && t<=3600)
```

```
        {
        fprintf(fp2,"%d\n",t);
        for(i=0;i<M+1;i++)
        {       for(j=0;j<N+1;j++)
        {       fprintf(fp2,"%f\t",AC[i][j]);
                if(j==N)
                fprintf(fp2,"\n");
        }}}
if(k1==49 && t<=1200)
        {       fprintf(fp45,"t=%d\n",t);
                for(i=0;i<M+1;i++)
        {       for(j=0;j<N+1;j++)
        {       fprintf(fp45,"%f\t",AD[i][j]);
                if(j==N)
                fprintf(fp45,"\n");
        }}}
if(k1==49 && t>1200 && t<2400)
        {       fprintf(fp46,"%d\n",t);

                for(i=0;i<M+1;i++)
        {       for(j=0;j<N+1;j++)
        {       fprintf(fp46,"%f\t",AD[i][j]);
                if(j==N)
                fprintf(fp46,"\n");
        }}}
// Energy balance equations
if(t==0)                        // Initial condition
        {
        for(i=0;i<M+1;i++)
{
for(j=0;j<N+1;j++)
{
Tnew[i][j]=303.15;                      // Temperature to be calculated in K
}}}
else if(t<=4442)
        {
        or(r=1;r<=M-1;r++)  // Governing equations for interior points except boundaries
        {
        for(z=1;z<=N-1;z++)
        {
Tnew[r][z]=AA[r][z]*((Tp[r][z])+(T[r+1][z])*(A[r][z]+C[r][z])+(T[r-1][z])*(C[r][z]-
A[r][z])+(D[r][z])*(T[r][z-1]+T[r][z+1])+(AC[r][z]));
        }}
for(z=1;z<=N-1;z++) // Boundary conditions for r=0 and r=M
        {
```

```
                Tnew[0][z]=AB[0][z]*((Tp[0][z])+(4.0*C[0][z])*(T[1][z])+(D[0][z])*(T[
                0][z+1]+T[0][z-1])+(AC[0][z]));
                Tnew[M][z]=AE[M][z]*((Tp[M][z])+(C[M][z]+A[M][z])*(E[M][z])*(4*
        pow(Trs,4.0))+(2.0*C[M][z])*(T[M-1][z])+(D[M][z])*(T[M][z+1]+T[M][z-
        1])+(AC[M][z]));
        }
for(r=0;r<=M;r++) // Boundary condition at z=0
{
Tnew[r][0]=1.001101*Trs+12.50375;
}
for(r=1;r<=M-1;r++) // Boundary conditions for z=1 and r=N
{
Tnew[r][N]=AD[r][N]*((Tp[r][N])+(T[r+1][N])*(A[r][N]+C[r][N])+(T[r-
1][N])*(C[r][N]-A[r][N])+(D[r][N])*(2.0*T[r][N-
1]+(4*F[r][N]*pow(Trs,4.0)))+(AC[r][N]));
}
// Corner point (0,N)
Tnew[0][N]=AF[0][N]*((Tp[0][N])+(T[1][N])*(4.0*C[0][N])+(D[0][N])*(2.0*T[0][N-
1]+(F[0][N])*(4*pow(Trs,4.0)))+(AC[0][N]));
// C[r][z]orner point (M,N)
Tnew[M][N]=AG[M][N]*((Tp[M][N])+(T[M-
1][N])*(2.0*C[M][N])+(A[M][N]+C[M][N])*(E[M][N])*((4*pow(Trs,4.0)))+(D[M][N])
*(2.0*T[M][N-1]+(F[M][N])*(4*pow(Trs,4.0)))+(AC[M][N]));
}
else
        {
        for(r=0;r<=M;r++)  // Governing equations for interior points
                {
                for(z=0;z<=N;z++)
                        {
                        Tnew[r][z]=T[r][z];
                        }}}
for(i=0;i<M+1;i++) // Store Tnew values in T arry and print values of temperature after
first iteration
{
for(j=0;j<N+1;j++)
        {
        T[i][j] = Tnew[i][j];
        }
}
// Stores Temperature values in .dat files created above
if(k1==49 && t<=1200)
        {
        fprintf(fp39,"t=%d\n",t);
        for(i=0;i<M+1;i++)
                {
```

```
                for(j=0;j<N+1;j++)
                        {
                        fprintf(fp39,"%f\t",T[i][j]);
                        if(j==N)
                        fprintf(fp39,"\n");
                        }
                }
        }
if(k1==49 && t>1200 && t<2400)
        {
        fprintf(fp43,"%d\n",t);
        for(i=0;i<M+1;i++)
                {
                for(j=0;j<N+1;j++)
                        {
                        fprintf(fp43,"%f\t",T[i][j]);
                        if(j==N)
                        fprintf(fp43,"\n");
                        }
                }
        }
        if(k1==49 && t>=2400 && t<=3600)
                {
                fprintf(fp44,"%d\n",t);
                for(i=0;i<M+1;i++)
                        {
                        for(j=0;j<N+1;j++)
                                {
                                fprintf(fp44,"%f\t",T[i][j]);
                                if(j==N)
                                fprintf(fp44,"\n");
                                }
                        }
        }

// Mass balance equations
if(t==0) // Initial condition
        {
        for(i=0;i<M+1;i++)
                {
                for(j=0;j<N+1;j++)
                        {
                        rhobnew[i][j]=601.2;            // in kg/m3
                        rhocnew[i][j]=0.0;                 // in kg/m3
                        rhovnew[i][j]=0.0;                 // in kg/m3
                        }
```

```
                }
        }
else
        {
        for(r=0;r<M+1;r++)
                {
                for(z=0;z<N+1;z++)
                        {
                        // Biomass balance equation at each grid point
rhobnew[r][z]=rhobp[r][z]/(1.0+(((B[r][z]*H*T[r][z])/(Tp[r][z]))-
(B[r][z]*H)+(B[r][z]*T[r][z])));
                        // Char balance equation at each grid point
rhocnew[r][z]=rhocp[r][z]+0.32*(((B[r][z]*H*T[r][z])/(Tp[r][z]))-
(B[r][z]*H)+(B[r][z]*T[r][z]))*rhob[r][z];
                        }
                        for(z=1;z<=N-1;z++)
                                {
                        // Volatile balance equations at interior points
rhovnew[r][z]=(1.0/(1.0+AH[r][z]))*(rhovp[r][z]+0.5*AH[r][z]*(rhov[r][z-
1]+rhov[r][z+1])+0.525*rhob[r][z]*(((B[r][z]*H*T[r][z])/(Tp[r][z]))-
(B[r][z]*H)+(B[r][z]*T[r][z])));
                                }
                        // Volatile balance equations at z=0
rhovnew[r][0]=0.0;
                        // Volatile balance equations at z=N
rhovnew[r][N]=(1.0/(1+(AH[r][N])-
(2.0*0.00005*delz/Dab)))*(rhovp[r][N]+(0.5*AH[r][N])*(2*rhov[r][N-
1])+(0.525*(rhob[r][N])*(((B[r][N]*H*T[r][N])/(Tp[r][N]))-
(B[r][N]*H)+(B[r][N]*T[r][N]))));
                        }
        }
for(i=0;i<M+1;i++)
        {
        for(j=0;j<N+1;j++)
                {
                rhoc[i][j] = rhocnew[i][j];
                rhov[i][j] = rhovnew[i][j];
                rhob[i][j] = rhobnew[i][j];
                }
        }
} // k1 loop ends
printf("Trs\t");
printf(" %f\t ",Trs);
printf("\n\n");
printf("Ths\t");
printf(" %f\t ",Ths);
```

```
printf("\n\n");
// Copies temperature and concentartion array values calculated at time t+1 into array at time t, so that same can be used for next iteration
		for(i=0;i<M+1;i++)
		{
			for(j=0;j<N+1;j++)
			{
				Tp[i][j] = T[i][j];
				rhocp[i][j] = rhoc[i][j];
				rhovp[i][j] = rhov[i][j];
				rhobp[i][j] = rhob[i][j];
			}
		}
		// Stores concentartion values in .dat files
		fprintf(fp40,"\n t=%f sec \n",1*float(t));
		fprintf(fp41,"\n t=%f sec \n",1*float(t));
		fprintf(fp42,"\n t=%f sec \n",1*float(t));
		for(i=0;i<M+1;i++)
		{
			for(j=0;j<N+1;j++)
			{
				fprintf(fp40,"%f\t",rhob[i][j]);
				if(j==N)
				fprintf(fp40,"\n");
				fprintf(fp41,"%f\t",rhoc[i][j]);
				if(j==N)
				fprintf(fp41,"\n");
				fprintf(fp42,"%f\t",rhov[i][j]);
				if(j==N)
				fprintf(fp42,"\n");
			}
		}
		// Calculates avg volatile concentartion
		for(r=0;r<=M-1;r++)
		{
			for(z=0;z<=N;z++)
			{
				rhovAVG[r][z]=(((rhov[r][z])+(rhov[r+1][z]))/2.0);
			}
		}
	// Calculates avg volatile concentartion
		for(r=0;r<=M-1;r++)
		{
		for(z=N-1;z>=0;z--)
			{
			v[r][z]=(rhovAVG[r][N]-rhovAVG[r][z]);
```

```
        }
}
// Avg value of temperature
s1=0.0;
for(i=0;i<M+1;i++)
{
        for(j=0;j<N+1;j++)
        {
                s1=s1+T[i][j];
        }
}
s2=s1/((M+1)*(N+1));
printf("Tavg=%f\n\n",s2);
fprintf(fp,"%d\n",t);
// Avg value of biomass concentration
s3=0.0;
for(i=0;i<M+1;i++)
{
        for(j=0;j<N+1;j++)
        {
                s3=s3+rhob[i][j];
        }
}
s4=s3/((M+1)*(N+1));
printf("rhobavg=%f\n\n",s4);
// Calculates flux of volatiles in kg/sec
s=0.0;
for(r=0;r<=M-1;r++)
{
        for(z=N-1;z>=0;z--)
        {
                        if(v[r][z]>0.0)
                        {
                        m=r+1;
Fluxv[r][z]=(pi*(r+m)*delr*delr*Dab*v[r][z])/(delz);
                        s=s+Fluxv[r][z];
                        break;
                        }
                        else
                        {
                                continue;
                        }
        }
}
        printf("s=%e\n\n",s);
        fprintf(fp63,"%e\n",s);
```

```
// Summation of volatile concentration using simpson's 3/8 rule
                        if(t==0 || t==5000)
                        {
                                fv=s;
                        }
                        else if(t%3==0)
                        {
                                fv=2.0*s;
                        }
                        else
                        {
                                fv=3.0*s;
                        }
                        p=p+fv;
        } // t loop ends
// Avg value of char concentration
                rhocN=0.0;
                rhocN_1=0.0;
                rhocN_2=0.0;
                rhocN_3=0.0;
                rhocN_4=0.0;
                rhocN_5=0.0;
                rhocN_6=0.0;
                rhocN_7=0.0;
                rhocN_8=0.0;
                rhocN_9=0.0;
                rhocN_10=0.0;
                rhocN_11=0.0;
                rhocN_12=0.0;
                rhocN_13=0.0;
                rhocN_14=0.0;
                rhocN_15=0.0;
                rhocN_16=0.0;
                rhocN_17=0.0;
                rhocN_18=0.0;
                rhocN_19=0.0;
                rhocN_20=0.0;
                rhocN_21=0.0;
                rhocN_22=0.0;
                rhocN_23=0.0;
                rhocN_24=0.0;
                rhocN_25=0.0;
                rhocN_26=0.0;
        for(r=0;r<=M;r++)
                {
                        rhocN1=rhoc[r][N];
```

```
rhocN=rhocN+rhocN1;
rhocN1_1=rhoc[r][N-1];
rhocN_1=rhocN_1+rhocN1_1;
rhocN1_2=rhoc[r][N-2];
rhocN_2=rhocN_2+rhocN1_2;
rhocN1_3=rhoc[r][N-3];
rhocN_3=rhocN_3+rhocN1_3;
rhocN1_4=rhoc[r][N-4];
rhocN_4=rhocN_4+rhocN1_4;
rhocN1_5=rhoc[r][N-5];
rhocN_5=rhocN_5+rhocN1_5;
rhocN1_6=rhoc[r][N-6];
rhocN_6=rhocN_6+rhocN1_6;
rhocN1_7=rhoc[r][N-7];
rhocN_7=rhocN_7+rhocN1_7;
rhocN1_8=rhoc[r][N-8];
rhocN_8=rhocN_8+rhocN1_8;
rhocN1_9=rhoc[r][N-9];
rhocN_9=rhocN_9+rhocN1_9;
rhocN1_10=rhoc[r][N-10];
rhocN_10=rhocN_10+rhocN1_10;
rhocN1_11=rhoc[r][N-11];
rhocN_11=rhocN_11+rhocN1_11;
rhocN1_12=rhoc[r][N-12];
rhocN_12=rhocN_12+rhocN1_12;
rhocN1_13=rhoc[r][N-13];
rhocN_13=rhocN_13+rhocN1_13;
rhocN1_14=rhoc[r][N-14];
rhocN_14=rhocN_14+rhocN1_14;
rhocN1_15=rhoc[r][N-15];
rhocN_15=rhocN_14+rhocN1_15;
rhocN1_16=rhoc[r][N-16];
rhocN_16=rhocN_16+rhocN1_16;
rhocN1_17=rhoc[r][N-17];
rhocN_17=rhocN_17+rhocN1_17;
rhocN1_18=rhoc[r][N-18];
rhocN_18=rhocN_18+rhocN1_18;
rhocN1_19=rhoc[r][N-19];
rhocN_19=rhocN_19+rhocN1_19;
rhocN1_20=rhoc[r][N-20];
rhocN_20=rhocN_20+rhocN1_20;
rhocN1_21=rhoc[r][N-21];
rhocN_21=rhocN_21+rhocN1_21;
rhocN1_22=rhoc[r][N-22];
rhocN_22=rhocN_22+rhocN1_22;
rhocN1_23=rhoc[r][N-23];
```

```
        rhocN_23=rhocN_23+rhocN1_23;
        rhocN1_24=rhoc[r][N-24];
        rhocN_24=rhocN_24+rhocN1_24;
        rhocN1_25=rhoc[r][N-25];
        rhocN_25=rhocN_25+rhocN1_25;
        rhocN1_26=rhoc[r][N-26];
        rhocN_26=rhocN_26+rhocN1_26;
}
        rhocAVGN=(rhocN)/(M+1);
        rhocAVGN_1=(rhocN_1)/(M+1);
        rhocAVGN_2=(rhocN_2)/(M+1);
        rhocAVGN_3=(rhocN_3)/(M+1);
        rhocAVGN_4=(rhocN_4)/(M+1);
        rhocAVGN_5=(rhocN_5)/(M+1);
        rhocAVGN_6=(rhocN_6)/(M+1);
        rhocAVGN_7=(rhocN_7)/(M+1);
        rhocAVGN_8=(rhocN_8)/(M+1);
        rhocAVGN_9=(rhocN_9)/(M+1);
        rhocAVGN_10=(rhocN_10)/(M+1);
        rhocAVGN_11=(rhocN_11)/(M+1);
        rhocAVGN_12=(rhocN_12)/(M+1);
        rhocAVGN_13=(rhocN_13)/(M+1);
        rhocAVGN_14=(rhocN_14)/(M+1);
        rhocAVGN_15=(rhocN_15)/(M+1);
        rhocAVGN_16=(rhocN_16)/(M+1);
        rhocAVGN_17=(rhocN_17)/(M+1);
        rhocAVGN_18=(rhocN_18)/(M+1);
        rhocAVGN_19=(rhocN_19)/(M+1);
        rhocAVGN_20=(rhocN_20)/(M+1);
        rhocAVGN_21=(rhocN_21)/(M+1);
        rhocAVGN_22=(rhocN_22)/(M+1);
        rhocAVGN_23=(rhocN_23)/(M+1);
        rhocAVGN_24=(rhocN_24)/(M+1);
        rhocAVGN_25=(rhocN_25)/(M+1);
        rhocAVGN_26=(rhocN_26)/(M+1);
        printf("rhocAVGN=%e\t\n",rhocAVGN);
        printf("rhocAVGN_1=%e\t\n",rhocAVGN_1);
        printf("rhocAVGN_2=%e\t\n",rhocAVGN_2);
        printf("rhocAVGN_3=%e\t\n",rhocAVGN_3);
        printf("rhocAVGN_4=%e\t\n",rhocAVGN_4);
        printf("rhocAVGN_5=%e\t\n",rhocAVGN_5);
        printf("rhocAVGN_6=%e\t\n",rhocAVGN_6);
        printf("rhocAVGN_7=%e\t\n",rhocAVGN_7);
        printf("rhocAVGN_8=%e\t\n",rhocAVGN_8);
        printf("rhocAVGN_9=%e\t\n",rhocAVGN_9);
        printf("rhocAVGN_10=%e\t\n",rhocAVGN_10);
```

```
                        printf("rhocAVGN_11=%e\t\n",rhocAVGN_11);
                        printf("rhocAVGN_12=%e\t\n",rhocAVGN_12);
                        printf("rhocAVGN_13=%e\t\n",rhocAVGN_13);
                        printf("rhocAVGN_14=%e\t\n",rhocAVGN_14);
                        printf("rhocAVGN_15=%e\t\n",rhocAVGN_15);
                        printf("rhocAVGN_16=%e\t\n",rhocAVGN_16);
                        printf("rhocAVGN_17=%e\t\n",rhocAVGN_17);
                        printf("rhocAVGN_18=%e\t\n",rhocAVGN_18);
                        printf("rhocAVGN_19=%e\t\n",rhocAVGN_19);
                        printf("rhocAVGN_20=%e\t\n",rhocAVGN_20);
                        printf("rhocAVGN_21=%e\t\n",rhocAVGN_21);
                        printf("rhocAVGN_22=%e\t\n",rhocAVGN_22);
                        printf("rhocAVGN_23=%e\t\n",rhocAVGN_23);
                        printf("rhocAVGN_24=%e\t\n",rhocAVGN_24);
                        printf("rhocAVGN_25=%e\t\n",rhocAVGN_25);
                        printf("rhocAVGN_26=%e\t\n",rhocAVGN_26);
rhochar=((rhocAVGN+rhocAVGN_1+rhocAVGN_2+rhocAVGN_3+rhocAVGN_4+rho
cAVGN_5)/(N));
        printf("rhochar=%e\n",rhochar);
        fprintf(fp64,"%e\n",rhochar);
        printf("\np= %e\n",p);
        // Simpson's rule
        areav=((3.0*delt)/8)*(p);
        printf("\n area under the curve v = %f\n\n",areav);
        pdctYv=((areav)/(pi*pow(0.06,2.0)*0.01*601.2))*100;
        pdctYc=((rhochar)/601.2)*100;
        printf("\n percent product yield of volatiles =%f\n",pdctYv);
        printf("\n percent product yield of char =%f\n",pdctYc);
        fclose(fp);
return 0;
} // Main loop ends
```